THE INFLUENCE OF POCKETED ELASTIC JOURNAL LINERS ON HYDRODYNAMIC BEARING PERFORMANCE.

by

Timothy John Coates, B.Sc.(Eng.), A.C.G.I.

A thesis submitted for the degree of
DOCTOR OF PHILOSOPHY
of the University of London, and also for the
DIPLOMA OF IMPERIAL COLLEGE.

Lubrication Laboratory,
Mechanical Engineering Dept.,
Imperial College,
London SW7 2BX.

May 1982.

ABSTRACT.

It is conceivable that the fitting of various forms of pocketed elastic liner on the journal of hydrodynamic bearings could show significant increases in load carrying capacity for a given minimum film thickness when compared to plain bearings. This is due to the presence of varying volume pockets which provide a self contained, self pressurizing action in addition to the normal hydrodynamic mechanism.

The particular configuration of a bearing with a pocketed, elastic liner bonded to the journal is examined both theoretically and experimentally. The bearing is found to have a lower load carrying capacity than a plain bearing when comparison is made on both an eccentricity ratio and a friction basis. It is suggested that the elastohydrodynamic film shapes observed around the pocket edges have a substantial effect in lowering the performance.

A satisfactory explanation for the discrepancies between the present findings and the previous theoretical work of Alexandrov is given.

ACKNOWLEDGEMENTS.

It is necessary for me to record my thanks to the many people who were involved in this work.

Firstly, to my supervisor, Dr. C.M.M. Ettles, for his encouragement and many helpful and expert suggestions.

Secondly, to the Science Research Council for a two year studentship and an equipment grant for the test machine under contract no. G/RA/4369.

Thirdly, to Professor Cameron and the Lubrication Laboratory for their financial assistance during the first year and for their words of advice.

Fourthly, to Reg Dobson, Tony, Harold, Bill, Ken, and Pete Saunders for their technical help with the test machine, and to my colleague Rob Wordsworth for his advice and friendship.

Fifthly, to Mr. D. Hitchings of the Aeronautical Engineering Department for allowing me to use the finite element programme FINEL and for his help in its modification.

Sixthly, to my father and mother for their encouragement and financial support.

Finally, to my wife, Christine, who still thinks I am a good investment.

CONTENTS.

	Page
TITLE PAGE.	i
ABSTRACT.	ii
ACKNOWLEDGEMENTS.	iii
CONTENTS.	iv
LIST OF FIGURES, TABLES AND PLATES.	ix
CHAPTER 1 : THE ATTEMPT TO IMPROVE FLUID FILM BEARING PERFORMANCE.	1
1.1. The Plain Journal Bearing.	1
1.2. The Self Pressurizing Journal Bearing.	3
1.3. Project Aims.	5
1.4. Nomenclature.	6
Figures.	10
CHAPTER 2 : PRELIMINARY THEORY FOR AN INFINITELY LONG BEARING.	12
2.1. Introduction.	12
2.2. Film Pressure.	12
2.3. Liner Distortion.	14
2.4. Pocket Pressure.	15
2.5. Solution Procedure.	17
2.6. Numerical Results.	19
Figures.	24

Page

CHAPTER 3 : DEVELOPMENT OF THE TREATMENT OF DISTORTION FOR THE INFINITELY LONG BEARING. 38

3.1. Introduction. 38
3.2. The Finite Element Method. 38
3.3. Influence Matrix Generation. 41
3.4. Solution Procedure. 42
3.5. Numerical Results. 43
Figures and Table. 46

CHAPTER 4 : DEVELOPMENT OF THE THEORY FOR A FINITE LENGTH BEARING. 54

4.1. Introduction. 54
4.2. Theoretical Development. 54
4.3. Numerical Results. 57
Figures. 59

CHAPTER 5 : THE DESIGN AND COMMISSIONING OF THE EXPERIMENTAL APPARATUS. 64

5.1. Introduction. 64
5.2. Mechanical Design. 64
5.3. Instrumentation Design. 65
5.4. Bearing Load. 66
5.5. Journal Speed. 67

Page

5.6. Bearing Friction. 67

5.7. Oil Inlet And Film Temperature. 68

5.8. Film Pressure. 69

5.9. Eccentricity. 71

5.10. Film Thickness. 73

5.11. Commissioning Of The Experimental Apparatus. 75

5.12. The Plain Rigid Journal Bearing. 77

Plates and Figures. 80

CHAPTER 6 : THE HYDRODYNAMIC BEARING WITH POCKETED ELASTIC JOURNAL LINERS. 96

6.1. Introduction. 96

6.2. Journal Liner Material. 96

6.3. Experimental Procedure. 97

6.4. Test Series 1. 99

6.5. Test Series 2. 101

6.6. Test Series 3. 105

6.7. Test Series 4. 106

Table and Figures. 110

CHAPTER 7 : A REVIEW. 141

7.1. Considerations Of Oil Compressibility. 141

7.2. The Work Of Alexandrov. 143

Page

7.3. Conclusions. 147

7.4. Suggestions For Further Work. 151

APPENDIX A1 : LITERATURE REFERENCES. 153

APPENDIX A2 : THEORETICAL ANALYSIS NEGLECTING AXIAL FIELD VARIATION. 160

A2.1. Film Pressure. 160

A2.2. Distortion. 162

A2.3. Pocket Pressure. 164

A2.4. Load, Attitude Angle And Friction. 171

APPENDIX A3 : COMPUTER PROGRAMMES FOR AN INFINITELY LONG BEARING. 174

APPENDIX A4 : POCKET PRESSURE ANALYSIS INCLUDING FINITE ELEMENT DISTORTIONS. 190

APPENDIX A5 : COMPUTER PROGRAMME INCLUDING FINITE ELEMENT DISTORTIONS. 195

APPENDIX A6 : THEORETICAL ANALYSIS INCLUDING AXIAL FIELD VARIATION. 203

A6.1. Film Pressure. 203

A6.2. Pocket Pressure. 207

A6.3. Load, Attitude Angle, Friction And Flow. 217

APPENDIX A7 : COMPUTER PROGRAMMES FOR A FINITE LENGTH BEARING. 220

APPENDIX A8 : DETAIL ASSEMBLY DRAWING OF THE EXPERIMENTAL APPARATUS. back pocket

LIST OF FIGURES, TABLES AND PLATES.

		Page
Fig. 1.1.	The Plain Journal Bearing.	10
Fig. 1.2.	The Journal Bearing With A Pocketed Elastic Journal Liner.	11
Fig. 2.1.	The Influence Of The Elasticity Factor, K, On Sommerfeld Number For Plain And Pocketed Liners.	24
Fig. 2.2.	The Influence Of K On Friction For Plain And Pocketed Liners.	25
Fig. 2.3.	The Influence Of K On Attitude Angle For Plain And Pocketed Liners.	26
Fig. 2.4.	Film Shapes And Pressure Profiles For A Plain Elastic Liner With Varying K.	27
Fig. 2.5.	Film Shapes And Pressure Profiles For A Pocketed Elastic Liner With Varying K.	28
Fig. 2.6.	Sommerfeld Number Comparing The Two Methods Of Pocket Pressure Analysis.	29
Fig. 2.7.	Friction Comparing The Two Methods Of Pocket Pressure Analysis.	30
Fig. 2.8.	Attitude Angle Comparing The Two Methods Of Pocket Pressure Analysis.	31
Fig. 2.9.	The Effect Of Varying The Film Starting Position On Sommerfeld Number.	32

Page

Fig. 2.10. The Effect Of Varying The Film Starting Position On Friction. 33

Fig. 2.11. The Effect Of Varying The Film Starting Position On Attitude Angle. 34

Fig. 2.12. The Influence Of The Number Of Pockets On Sommerfeld Number. 35

Fig. 2.13. The Influence Of The Number Of Pockets On Friction. 36

Fig. 2.14. The Influence Of The Number Of Pockets On Attitude Angle. 37

Fig. 3.1. Finite Element Idealisation Of A Single Land With The Test Pressure Distribution. 46

Fig. 3.2. Distorted Land Shape Under The Test Pressure Distribution. 47

Table 3.3. The Effect Of Varying Element Density On Selected Surface Distortions. 48

Fig. 3.4. Diagram Of The Loading Used To Produce The Matrix Of Influence Coefficients. 49

Fig. 3.5. A Comparison Of The Distortion Theories For Sommerfeld Number. 50

Fig. 3.6. A Comparison Of The Distortion Theories For Friction. 51

Fig. 3.7. A Comparison Of The Distortion Theories For Attitude Angle. 52

Page

Fig. 3.8.	Film Shape And Pressure Profile For The Finite Element Distortion Theory.	53
Fig. 4.1.	Finite Difference Grid For A Finite Length Pocketed Liner.	59
Fig. 4.2.	A Comparison Of The Results Of Alexandrov And Coates For Sommerfeld Number.	60
Fig. 4.3.	A Comparison Of The Results Of Alexandrov And Coates For Friction.	61
Fig. 4.4.	A Comparison Of The Results Of Alexandrov And Coates For Attitude Angle.	62
Fig. 4.5.	A Comparison Of The Results Of Alexandrov And Coates For Side Flow.	63
Fig. 5.1.	Pressure Transducer Mounting.	70
Fig. 5.2.	Capacitance Transducer Mounting.	72
Fig. 5.3.	Film Thickness Transducer Mounting.	74
Fig. 5.4.	Bearing Lapping Tool.	77
Plate 5.5.	General View Of The Experimental Apparatus.	80
Plate 5.6.	Detail View Of The Journal And Test Bearing Assembly.	81
Fig. 5.7.	Schematic Diagram Of The Instrumentation.	82

Page

Fig. 5.8. The Variation Of Viscosity With Temperature For The Test Oil. 83

Fig. 5.9. Pressure In The Loading Cylinder Against Measured Load. 84

Fig. 5.10. Calibrating Load Against Beam Deflection For The Friction Measuring System. 85

Fig. 5.11. Bridge Output Voltage Against Film Thickness For The Capacitance Transducers Used In Measuring Eccentricity. 86

Fig. 5.12. Injected Capacitance Against Bridge Output Voltage For The Film Thickness Transducers. 87

Fig. 5.13. Pressure Profiles For The First Commissioning Test. 88

Fig. 5.14. Pressure Profiles With The Test Bearing At Two Different Angular Positions. First Commissioning Test. 89

Fig. 5.15. Pressure Profiles As In Fig. 5.14. After Lapping. 90

Fig. 5.16. Attitude Angle For The Commissioning Test With A Plain Rigid Journal Liner. 91

Fig. 5.17. Sommerfeld Number For The Commissioning Test With A Plain Rigid Journal Liner. 92

Page

Fig. 5.18. Friction For The Commissioning Test With A Plain Rigid Journal Liner. 93

Fig. 5.19. Maximum Film Pressure For The Commissioning Test With A Plain Rigid Journal Liner. 94

Fig. 5.20. Film Thickness For The Commissioning Test With A Plain Rigid Journal Liner. 95

Table 6.1. Physical Properties Of Conductive Silicone Rubber, Grade X1116B. 110

Fig. 6.2. Attitude Angle For A Plain Liner. Test Series 1. 111

Fig. 6.3. Sommerfeld Number For A Plain Liner. Test Series 1. 112

Fig. 6.4. Friction For A Plain Liner. Test Series 1. 113

Fig. 6.5. Film Thickness For A Plain Liner. Test Series 1. 114

Fig. 6.6. Pressure Profiles For A Plain Liner. Test Series 1. 115

Fig. 6.7. Attitude Angle For A Pocketed Liner. Test Series 1. 116

Fig. 6.8. Sommerfeld Number For A Pocketed Liner. Test Series 1. 117

Fig. 6.9. Friction For A Pocketed Liner. Test Series 1. 118

Page

Fig. 6.10. Attitude Angle For A Plain Liner. Test Series 2. 119

Fig. 6.11. Sommerfeld Number For A Plain Liner. Test Series 2. 120

Fig. 6.12. Friction For A Plain Liner. Test Series 2. 121

Fig. 6.13. Attitude Angle For A Pocketed Liner. Test Series 2. 122

Fig. 6.14. Sommerfeld Number For A Pocketed Liner. Test Series 2. 123

Fig. 6.15. Friction For A Pocketed Liner. Test Series 2. 124

Fig. 6.16. Maximum Film Pressure For A Pocketed Liner. Test Series 2. 125

Fig. 6.17. An Experimental Comparison Of Sommerfeld Number For Plain And Pocketed Liners. Test Series 2. 126

Fig. 6.18. An Experimental Comparison Of Friction For Plain And Pocketed Liners. Test Series 2. 127

Fig. 6.19. An Experimental Comparison Of Performance, ξ, For Plain And Pocketed Elastic Liners. Test Series 2. 128

Fig. 6.20. Pressure Profiles For A Pocketed Liner. Test Series 2. 129

Fig. 6.21. A Comparison Of Theoretical Pressure Profiles For An Infinitely Long Bearing. 130

Page

Fig. 6.22. Attitude Angle For A Pocketed Liner. Test Series 3. 131

Fig. 6.23. Sommerfeld Number For A Pocketed Liner. Test Series 3. 132

Fig. 6.24. Friction For A Pocketed Liner. Test Series 3. 133

Fig. 6.25. Attitude Angle For A Pocketed Liner. Test Series 4. 134

Fig. 6.26. Sommerfeld Number For A Pocketed Liner. Test Series 4. 135

Fig. 6.27. Friction For A Pocketed Liner. Test Series 4. 136

Fig. 6.28. Maximum Film Pressure For A Pocketed Liner. Test Series 4. 137

Fig. 6.29. An Experimental Comparison Of Performance, ξ, For Plain Rigid And Pocketed Elastic Liners. Test Series 4. 138

Fig. 6.30. Pressure Profiles For A Pocketed Liner. Test Series 4. 139

Fig. 6.31. Film Shapes For A Pocketed Liner. Test Series 4. 140

CHAPTER 1.

THE ATTEMPT TO IMPROVE FLUID FILM BEARING PERFORMANCE.

1.1. The Plain Journal Bearing.

Since the experimental discovery by Tower (1)* in 1883 that the moving surfaces in a journal bearing are separated by a pressurized fluid film, and the resultant theoretical analysis of the hydrodynamics of converging fluid films by Reynolds (2) in 1886, the basic concept of the journal bearing has remained largely unchanged.

While much work on journal bearings has been carried out in the century since these discoveries, the basic mode of operation is still that of a bearing and journal running with eccentric centres, forming a thin converging viscous film which generates a pressure field to support the load (Fig. 1.1.).

Rather than attempting to improve this fundamental mechanism, the majority of work has subsequently concentrated on refining the theoretical analyses involved.

Theoretical treatments have been extended to include temperature variation and its effect on viscosity, the influence of pressure on viscosity (3),

* Numbers in brackets denote references given in Appendix A1.

and of more relevance to this present work, elastohydrodynamic studies which consider distortions and their interaction with pressure and film shape (4-11).

Practical considerations have necessitated studies of turbulence, beginning with the work of Taylor (12) and its confirmation by Wilcock (13), oil whirl, dynamic loading and so on.

Innovations such as the foil bearing (14,15) remain as mathematical curiosities with few apparent practical advantages.

The principle of the hydrostatic bearing has been used in 'hybrid' bearings where oil under pressure is admitted to the pockets in the loaded region of the film (16), but this has been to improve starting under load and the stiffness of the assembly rather than the running performance. This requires costly external equipment to provide a high pressure supply and has not been used in general practice to improve the load carrying performance of plain journal bearings.

As demands on performance have increased and the limits of hydrodynamic action have been reached, other areas have had to be explored. For example, the very small film thicknesses encountered in internal combustion engines have prompted the development of material improvements such as overlay-plating (17).

An attempt to improve the load carrying capacity of journal bearings would therefore seem welcome.

1.2. The Self Pressurizing Journal Bearing.

Ettles (18) in 1969 proposed a new type of hybrid bearing relying on both hydrodynamic and self acting hydrostatic principles for its operation.

In considering the action of a vane pump with the outlet port closed so that it was operating in a stalled condition, he realised that if the resultant configuration was thought of in terms of a journal bearing, it showed some advantageous characteristics. The film under the vane tips would operate on hydrodynamic principles, and the variable volume pockets between the vanes (which are the principle on which the pump works) would provide a self pressurizing action as the pocket volumes decreased with the angular motion.

In (18) and (19) he described various methods of applying the basic principle to journal bearings, including those of a free ring on the journal and an elastic liner, all of which relied on some form of variable volume pockets to provide the self pressurizing effect.

Further descriptions of the various applications were given in (20) together with a theoretical analysis of the 'sealed-piston' configuration. This consisted of a free, pocketed ring driven via the pockets by plungers projecting from the journal. The normal hydrodynamic action was assumed to operate over the lands of the ring, and the self pressurizing effect

of the pockets was formed by the ring running eccentric to the journal.

The analysis was somewhat idealistic in that a zero clearance was assumed between the ring and plungers (which cannot be true in eccentric operation), and also no attempt was made to find the equilibrium position of the ring due to the action of film forces. However, the analysis was useful as a feasability study and showed an increase in the Sommerfeld number at a given eccentricity ratio, at the expense of increased flow and power consumption, and decreased bearing stiffness. Improvement in the Sommerfeld number of the order of 3-10 was thought possible and it was proposed that the bearing would exhibit approximately the same load carrying, flow and power loss characteristics as a larger plain journal bearing. The other significant advantage over the usual hybrid bearings appeared to be that the pressure sources travelling with the journal would operate automatically so that the self pressurization would be in proportion to the load applied. This suggested that the principle should work well under dynamic as well as steady state operating conditions.

Alexandrov (21,22) in 1977 considered one of the simplest practical configurations, that of a perforated, resilient liner bonded to the journal. In this case, the liner undergoes distortion due to the film pressure. This in turn produces a decrease in volume of the pockets as they move into the loaded

region due to the angular motion of the journal. The lubricant from these pockets is forced into the film, thus producing the self pressurizing effect. The theoretical analysis showed similar trends to the 'sealed-piston' configuration, with the difference that the pockets had a derating effect on the Sommerfeld number at low eccentricity ratios (less than 0.6 approximately). The Sommerfeld number was shown to be up to 3 times higher than a plain journal bearing without pockets, again at the expense of increased flow and power consumption.

1.3. Project Aims.

It was decided to study the same configuration as Alexandrov, that of a journal with a pocketed elastic liner (Fig. 1.2.), mainly because a valid theoretical analysis was easier to conceive than a free ring type, and also it was thought that manufacturing would be simpler.

It was proposed to extend the theoretical work of Alexandrov and also to undertake an experimental study to correlate with the theory.

1.4. Nomenclature.

A, A_δ, A_ε - coefficients.

c - radial clearance.

C - compressibility coefficient.

CE, CN, CP, CS, CW, C0, C1, C2 - computing coefficients.

D - bearing diameter.

e - eccentricity of bearing journal centres.

E - Young's modulus.

F - friction.

h - film thickness.

i - node number in the circumferential direction.

I - integral value.

j - node number in the axial direction.

k - element of stiffness matrix.

L - bearing axial length.

L_A - pocket axial half length.

n_p - number of pockets.

p - pressure.

P - load.

q - flow.

r - radius.

R_1 - journal radius.

R_2 - journal plus liner radius.

t - liner thickness.

u - translational velocity, displacement.

U - journal surface velocity.

V, V' - displaced pocket volume.

W - bearing load.

W_x - load component parallel to the line of centres.

W_y - load component perpendicular to the line of centres.

x, y, z - cartesian co-ordinates.

α - influence coefficient.

β_p - pressure relaxation factor.

β_δ - distortion relaxation factor.

γ - land side distortion.

δ - radial distortion.

Δ - increment.

η - viscosity.

θ - circumferential co-ordinate.

ν - Poisson's ratio.

σ - stress.

τ - shear stress.

ϕ - attitude angle.

ω - rotational velocity.

Dimensionless variables:

$\bar{h}$ - film thickness, $\bar{h} = \frac{h}{c}$.

$\bar{p}$ - pressure, $\bar{p} = \frac{c^2 p}{6\eta U R_2}$.

$\bar{y}$ - axial co-ordinate, $\bar{y} = \frac{2y}{L}$.

$\bar{z}$ - through film co-ordinate, $\bar{z} = \frac{z}{t}$.

$\bar{F}$ - friction, $\bar{F} = \frac{cF}{\eta U R_2 L}$.

K - Elasticity factor, $K = \frac{6\eta U R_2 t}{Ec^3}\left(1 - \frac{2\nu^2}{1-\nu}\right)$.

$\bar{Q}$ - flow, $\bar{Q} = \frac{-LQ}{2UcR_2^2}$.

S - Sommerfeld number, $S = \frac{W}{LU\eta}\left(\frac{c}{R_2}\right)^2$.

$\bar{V}$, $\bar{V}'$ - displaced pocket volume, $\bar{V} = \frac{2V}{\Delta\theta_{poc} L_A c R_2}$.

$\bar{\gamma}$ - land side distortion, $\bar{\gamma} = \frac{\gamma}{c}$.

$\bar{\delta}$ - distortion, $\bar{\delta} = \frac{\delta}{c}$.

ε - eccentricity ratio, $\varepsilon = \frac{e}{c}$.

λ - bearing diameter to length ratio squared, $\lambda = \left(\frac{D}{L}\right)^2$.

$\bar{\xi}$ - bearing performance, $\bar{\xi} = \frac{S}{\bar{F}} = \frac{Wc}{FR_2}$.

Subscripts:

cav - cavitation.

l - number of meshes across a pocket.

max - maximum.

min - minimum.

n - nett, pocket number.

new - new iterative value.

old - old iterative value.

poc - pocket.

pocl - pocket and land.

s - side (i.e. axial).

v - volumetric.

1
2 - film stations.

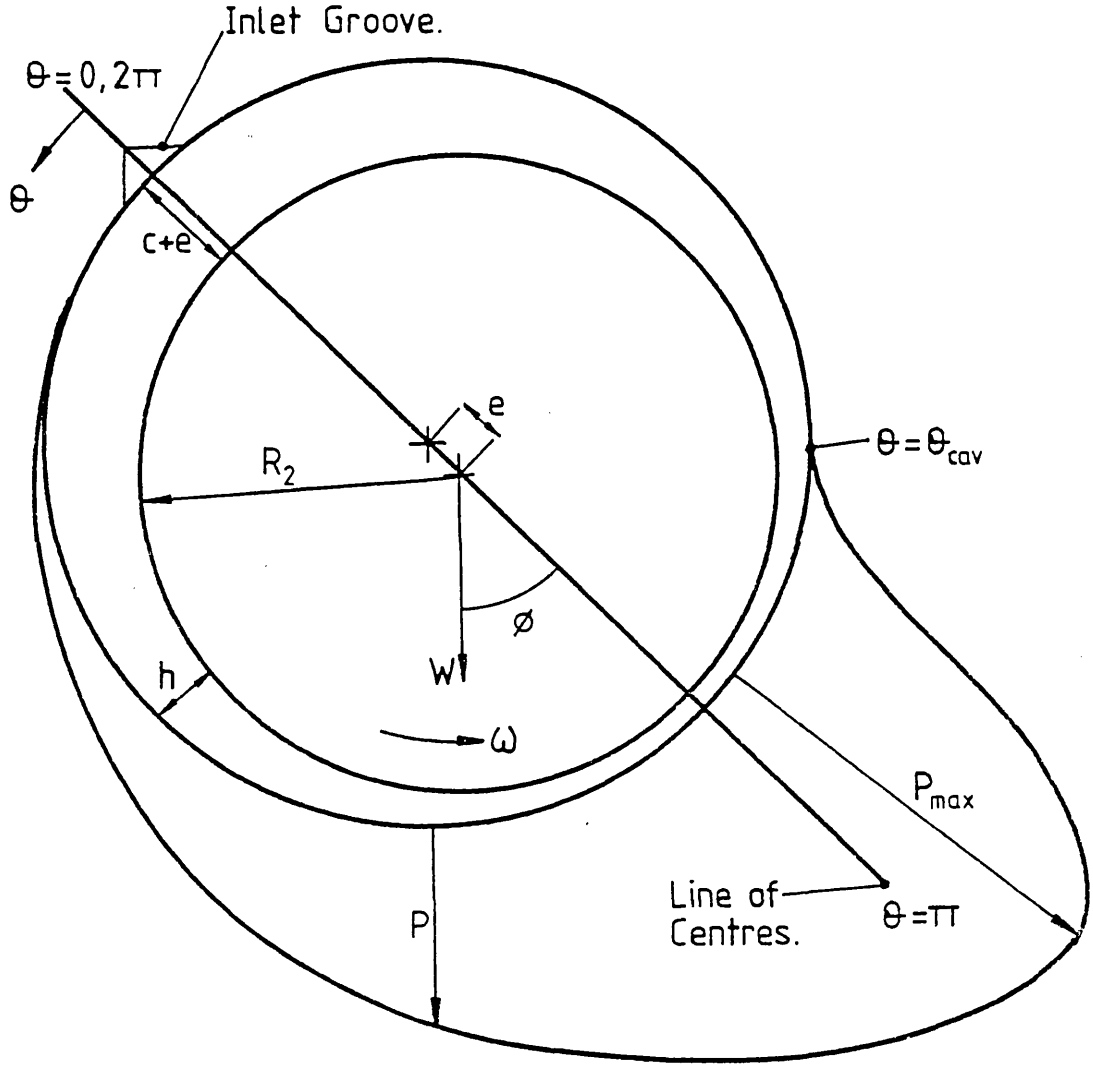


Figure 1.1. The Plain Journal Bearing.

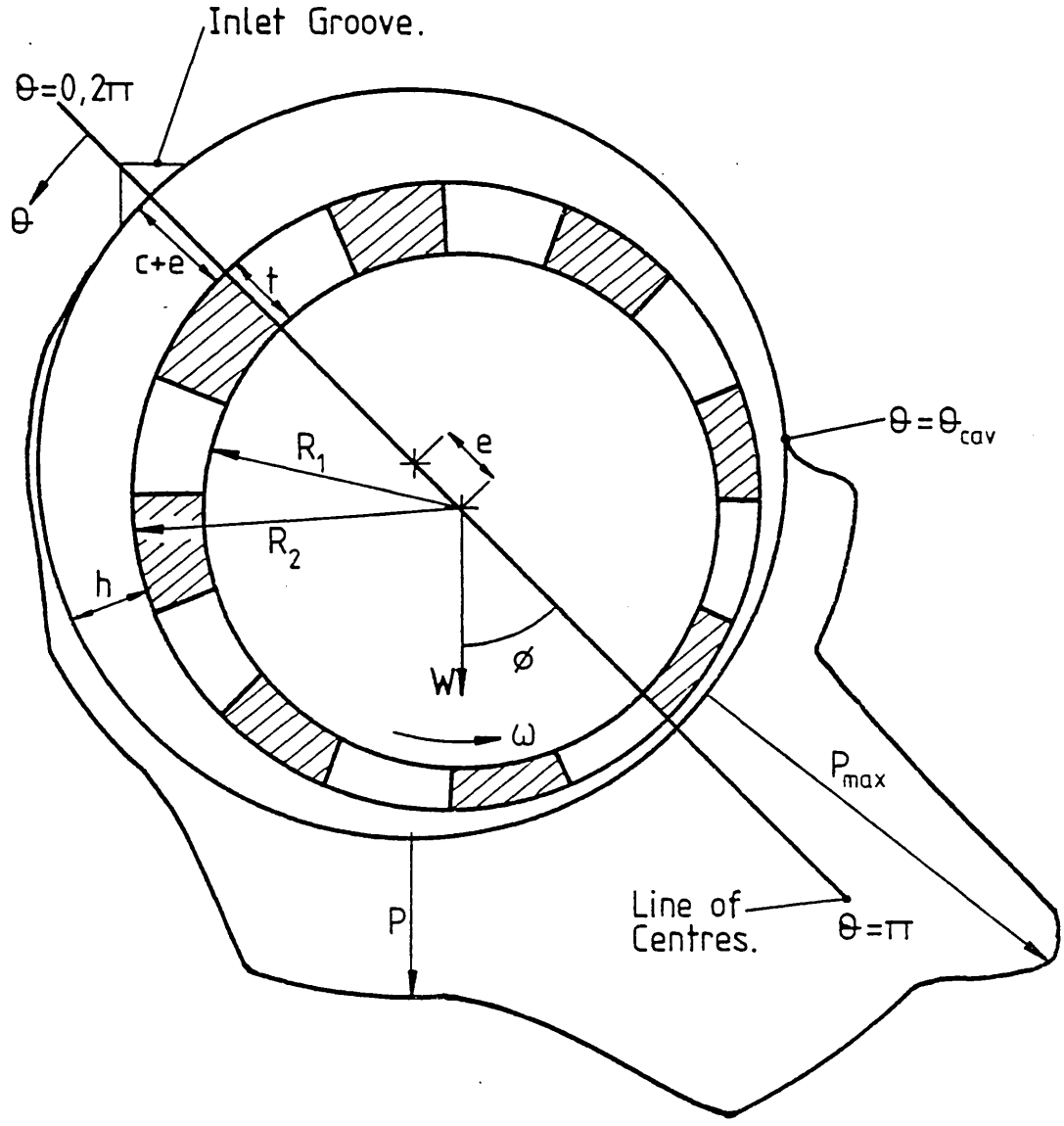


Figure 1.2. The Journal Bearing With A Pocketed Elastic Journal Liner.

CHAPTER 2.

PRELIMINARY THEORY FOR AN INFINITELY LONG BEARING.

2.1. Introduction.

In order to assess and develop the theory of Alexandrov (21,22), and to determine the influence of various parameters on the performance of the bearing, a treatment was set up for the one dimensional case of a bearing infinitely long in the axial direction.

Among changes to previous work (21,22) were a different method for calculating the pocket pressure and a more exact solution for liner distortion.

The configuration is as in Chapter 1 (Fig. 1.2.). Details of the method outlined in the following sections are given in Appendix A2.

2.2. Film Pressure.

For the film across the lands between the pockets, pressure was found using Reynold s' equation. Assuming steady, incompressible, isoviscous flow, this is;

$$\frac{d}{dx}\left(h^3\frac{dp}{dx}\right) = 6\eta U\frac{dh}{dx} \quad . \qquad (2.1.)$$

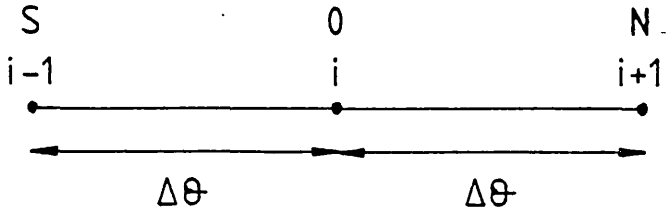
For convenience, the following dimensionless variables were defined;

$$h = c\bar{h}, \quad p = \frac{6\eta U R_2 \bar{p}}{c^2} .$$

Substituting these and $x = R_2\theta$ and expanding gives

$$\frac{d^2\bar{p}}{d\theta^2} + \frac{3}{\bar{h}} \frac{d\bar{h}}{d\theta} \frac{d\bar{p}}{d\theta} = \frac{1}{\bar{h}^3} \frac{d\bar{h}}{d\theta} . \qquad (2.2.)$$

A computing equation was set up by discretizing the fields and assuming a linear variation of pressure and film thickness between discrete points (nodes). This gives an equation for the pressure at node i in terms of the pressure at surrounding nodes.



$$\bar{p}_i = CN_i \bar{p}_{i+1} + CS_i \bar{p}_{i-1} + C0_i . \qquad (2.3.)$$

The coefficients CN, CS and C0 are functions of film thickness only. This forms a set of linear equations which can be solved for pressure given the film shape.

$$\left[CN, CS\right] \left[\bar{p}\right] = \left[C0\right] .$$

For the case where distortions are included, the film shape is given by

$$\bar{h}_i = 1 + \cos\theta - \bar{\delta}_i \quad . \tag{2.4.}$$

2.3. Liner Distortion.

Initially, results were obtained using a treatment for liner distortion which was the same as that of Alexandrov (21,22).

This assumes a linear elastic material for the liner which is rigidly bonded at the inner surface to the journal. The strain in the circumferential direction is thus taken to be negligible. As the bearing is infinitely long in the axial direction, the strain in that direction is also assumed to be zero, that is a plane strain condition. Using the Hookean stress--strain laws gives;

$$\bar{\delta} = -K\bar{p} \quad . \tag{2.5.}$$

where the Elasticity factor, K, is given by;

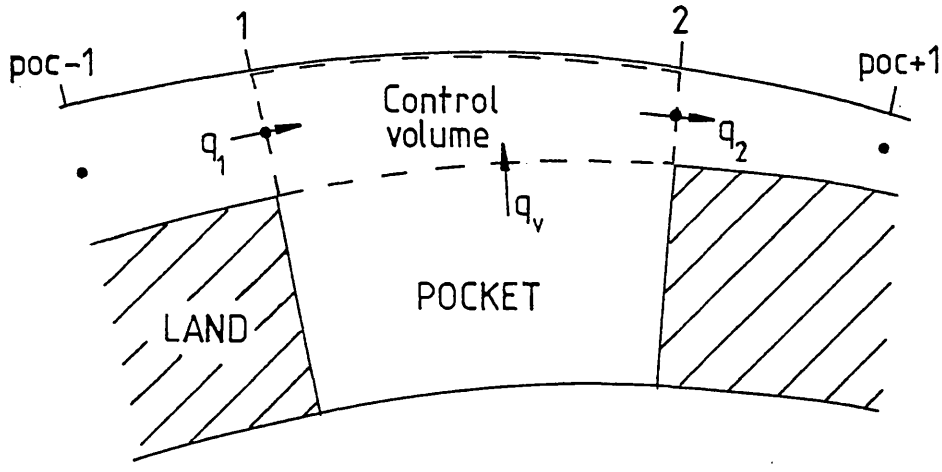
$$K = \frac{6\eta U R_2 t}{E c^3} \left(1 - \frac{2\nu^2}{1-\nu} \right) . \tag{2.6.}$$

This method is not as rigorous as that used

by others (23), but the presence of pockets is a complicating factor and the theory is valid for the thin liners used later in the experimental work.

Having obtained an expression for distortion in terms of pressure, a solution can be found for pressure by iteration between the distortion, film thickness and pressure fields.

2.4. Pocket Pressure.



An equation for pocket pressure was determined from flow continuity across the control volume shown above. The pocket depth is an order of magnitude greater than the film above the lands and hence the pocket pressure was considered uniform.

The film flows q_1 and q_2 are of the form

$$q = \frac{-h^3}{12\eta}\left(\frac{dp}{dx}\right) + \frac{Uh}{2},$$ and the nett film flow out

of the control volume is equal to the volumetric flow from the pocket due to the liner distortion at the edges.

$$q_2 - q_1 = q_v \ . \qquad (2.7.)$$

From this a computing equation was set up for the pocket pressure in terms of the film pressures at the sides of the pockets.

$$\bar{p}_{poc} = C1\bar{p}_{poc-1} + C2\bar{p}_{poc+1} + CP \ , \qquad (2.8.)$$

where $$\bar{P}_{poc} = \bar{p}_1 = \bar{p}_2 \ . \qquad (2.9.)$$

This can therefore be included in the computing equation for film pressure. Thus, the pressure field (for both film and pockets) can be solved for in total for a given film shape. This is different to the method Alexandrov used where the pocket pressures were calculated externally to the film pressure - distortion iteration, in a further level of iteration in which the pocket pressures were adjusted according to the difference between the volumetric flow, q_v, and the nett film flow, q_n, around each pocket. The present method reduces the number of iteration levels because the pocket pressure is calculated implicitly with the film pressure and hence results in a reduction in programme execution time. Convergence was also improved.

The expression used to calculate pocket

pressure yields a term containing the rate of change of displaced pocket volume, $\left(\frac{dV}{d\theta}\right)_{poc}$ (see Appendix A2), and this was evaluated in two different ways. Method 1 is crude but realistic and uses a backwards difference approximation.

$$\left(\frac{dV}{d\theta}\right)_{poc} = \frac{V_n - V_{n-1}}{\Delta\theta} . \qquad (2.10.)$$

Method 2 is the same as that used by Alexandrov. As $V = f(\bar{\delta})$ and $\bar{\delta} = -K\bar{p}$, then

$$\left(\frac{dV}{d\theta}\right)_{poc} = f\left(\frac{d\bar{p}}{d\theta}\right)_{poc} . \qquad (2.11.)$$

In the limit, the rate of change of pocket pressure with θ is assumed to be the same as the mean of the pressure gradients in the film at the edges of the pocket.

2.5. Solution Procedure.

The set of linear equations for pocket and film pressure was solved using a Gauss-Seidel iteration scheme with successive over relaxation in which the change in pressure in each iteration was modified

using a relaxation factor, β_p . Typical values for β_p were in the range of 1.7 to 1.9. Over relaxation ensured fast convergence which was typically of the order of 100 iterations. Cavitation of the film was allowed for by using the method first suggested by Christopherson (24) of setting any negative pressures to zero as they occurred. It is generally accepted that this gives the Reynolds' boundary condition,

$$\bar{p} = \frac{d\bar{p}}{d\theta} = 0 \qquad \text{at } \theta = \theta_{cav} \ .$$

The other boundary condition used was $\bar{p} = 0$ at $\theta = 0$ ($\bar{h} = \bar{h}_{max}$).

Distortions were then calculated at each node point using the converged pressure field. Under relaxation of the change in distortion was needed (i.e. $\beta_\delta < 1.0$), in order to obtain convergence. The under relaxed distortion field was then subtracted from the rigid film thickness field. New coefficients for the pressure equations were then calculated and the iterative scheme for solution of the pressure field was entered again. Thus, an overall iteration between pressure and distortion was performed until the two fields did not change significantly. Convergence was tested for interactively as the solution proceeded by inspecting mid-field values. Relevant values could be written to tape where they were used to restart subsequent runs. In this way, either more iterations could be performed for a given value of eccentricity

ratio, ε , or a solution for a slightly higher value of ε could be started. The latter procedure was particularly necessary at values of ε of 1.0 and above, where the rigid solution contains zero or negative film thicknesses.

Having obtained converged fields for a given value of ε, the pressure field was then integrated to give the Sommerfeld number, S, and the attitude angle, ϕ, and the elemental shear stresses were integrated to give the total dimensionless friction, $\bar{F}$. Integrations were performed using Simpson's rule.

Programme listings are given in Appendix A3 for a plain rigid bearing, a bearing with a plain elastic liner, and a bearing with a pocketed elastic journal liner for which there are two programmes corresponding to the two different methods used for analysing the pocket pressure. Unless otherwise stated, all results are presented for the first method of pocket pressure analysis.

2.6. Numerical Results.

In all cases the pockets took up half the available pitch in the circumferential direction, that is the pocket and land lengths were equal. Results were mainly calculated with a uniform finite difference grid of 64 nodes, although this was varied for convenience for runs with other than eight pockets.

Plain bearing results used a uniform grid of 100 nodes. For each set of conditions, Sommerfeld number, dimensionless friction and attitude angle are plotted against eccentricity ratio with Sommerfeld number being plotted on a logarithmic scale. Three parameters were varied; the Elasticity factor, K, the number of pockets, n_p, and the position of the maximum film thickness relative to the pocket-land configuration. Unless otherwise stated the values for these variables are K = 0.5, n_p = 8, and the maximum film thickness at the centre of a land.

Figs. 2.1. to 2.5. show the effect of varying the Elasticity factor for both plain and pocketed bearings.

For the plain bearing, the results follow established solutions. The Sommerfeld number is reduced from the rigid case with increasing eccentricity ratio as the effect of distortion on film thickness becomes pronounced. The larger film thickness also leads to a reduction in bearing friction. Fig. 2.4. shows this increase in film thickness which becomes greater with increasing Elasticity factor. A reduction in peak pressure accompanies this together with an increase in the angle at which the film cavitates, that is the pressure profile is flatter and operates over a wider arc. This is reflected in the change in attitude angle with eccentricity ratio.

For the pocketed bearing, the results are

surprising and do not follow the same trends as Alexandrov. As expected, the Sommerfeld number is reduced at low eccentricity ratios as the distortion is too low to produce any significant pumping effect from the pockets and so the pockets have a derating effect on the film. This effect is similar to that found in externally pressurized bearings with the pockets isolated from the pressure supply (25,26). The Sommerfeld number, however, is reduced over the whole eccentricity ratio range. This is in contrast to Alexandrov's results where the Sommerfeld number became greater than the plain rigid bearing at eccentricity ratios of approximately 0.7. The fact that for an infinitely long bearing, pocket pressure is not attenuated by side leakage, as it was in Alexandrov's case, makes the results less understandable. Bearing friction is also reduced over the whole eccentricity ratio range due to the fact that there is less film to be sheared. However, there is a sharp rise as ε approaches 1.0, and it was found that the programme could not be run at values of eccentricity ratio greater than 1.0, because negative film thicknesses were then generated. This was a rather surprising result for an elastic bearing. However, an examination of Fig. 2.5. provides some clues to the mechanism involved. The pressure field drops to zero at $\theta = 202.5^{\circ}$ and as a result the distortion at that point is zero. Hence the film thickness at that point is the same as the

rigid film thickness. This is somewhat artificial due to the simple distortion treatment used, as the influence of the other pressures on the land on the distortion at $\theta = 202.5^{\circ}$ is not taken into account. However, the mechanism involved is generally valid in that the pocket immediately after $\theta = 180^{\circ}$ in the diverging region of the film acts as a strong sink. This induces cavitation and this pocket pressure is therefore always zero, independent of the Elasticity factor. Thus, although the peak pressures are approximately the same as for the plain elastic bearing, the induction of early cavitation reduces the integral of the profile and hence the Sommerfeld number. The sharp rise in friction as ε approaches 1.0 is also explained due to the film thickness becoming the same as the rigid case very close to $\theta = 180^{\circ}$ (where the rigid minimum film thickness occurs).

Figs. 2.6. to 2.8. give a comparison between the two methods used for pocket pressure analysis. Although method 1 was thought to be a crude approximation, it can be seen that the two methods show close agreement.

Figs. 2.9. to 2.11. show the effect of varying the position of $\bar{h}_{max}$ (the start of the film). This produces a small variation in the dependent parameters which in practice would mean a small vibration of the journal centre for a given load. Friction tends to infinity at $\varepsilon = 1.0$ for position 3 and this confirms the previous argument. In this case the film cavitates at $\theta = 180^{\circ}$ and hence the minimum film thickness is

zero at $\xi = 1.0$.

Figs. 2.12. to 2.14. show that the influence of the number of pockets on the dependent variables is small. In particular, the Sommerfeld number is reduced with increasing numbers of pockets showing the derating effect of the pockets.

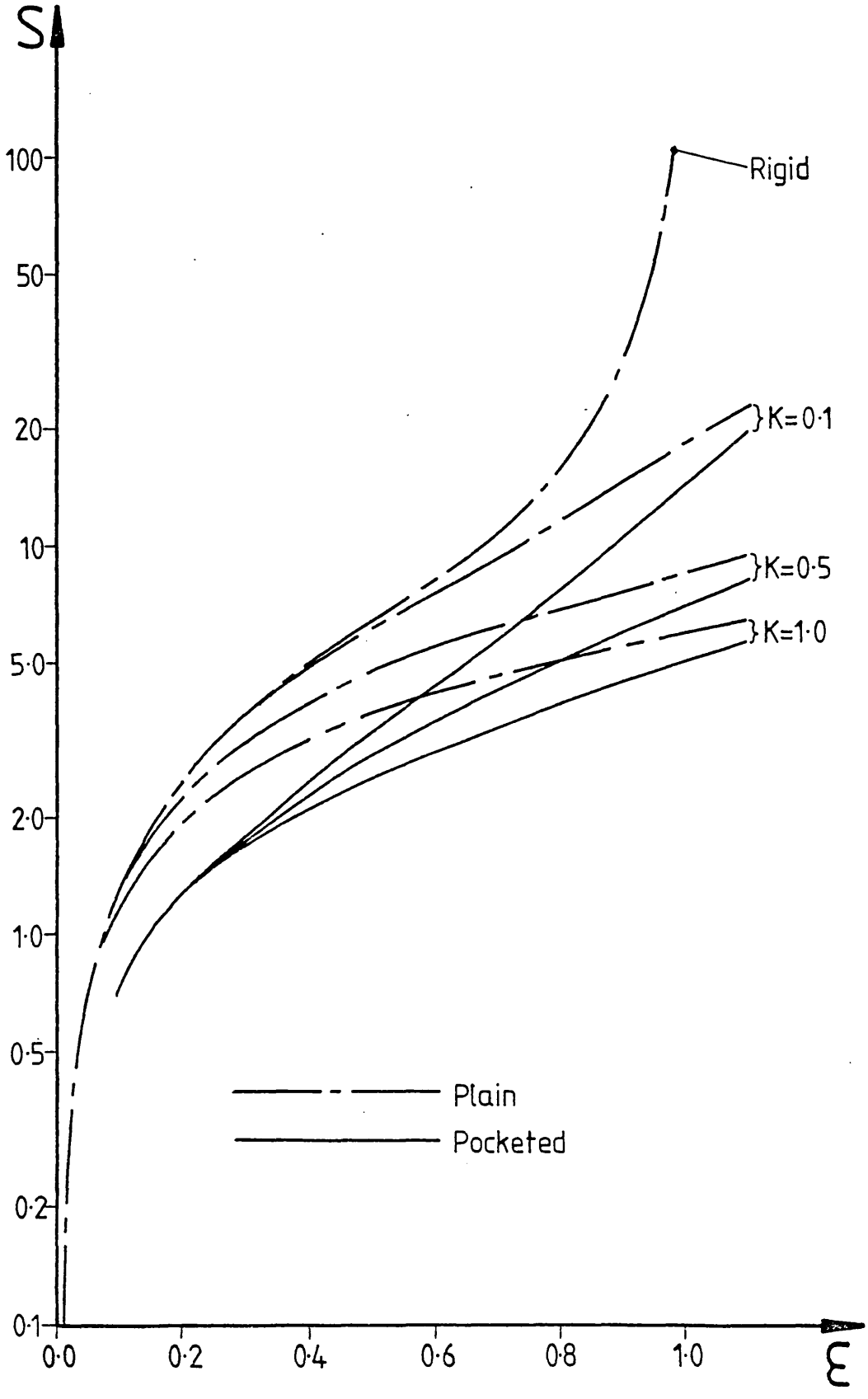


Figure 2.1. The Influence Of The Elasticity Factor, K, On Sommerfeld Number For Plain And Pocketed Liners.

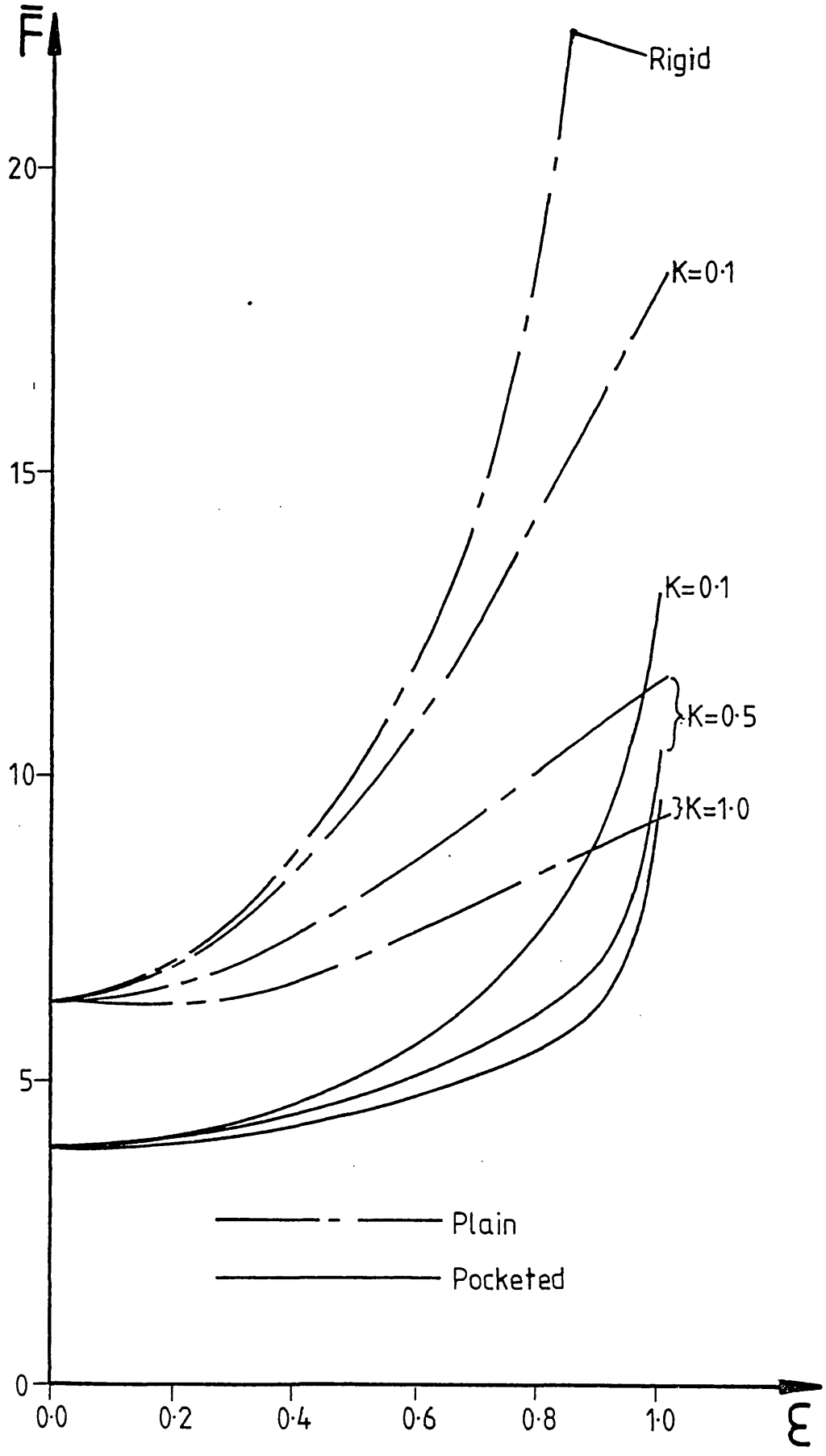


Figure 2.2. The Influence Of K On Friction For Plain And Pocketed Liners.

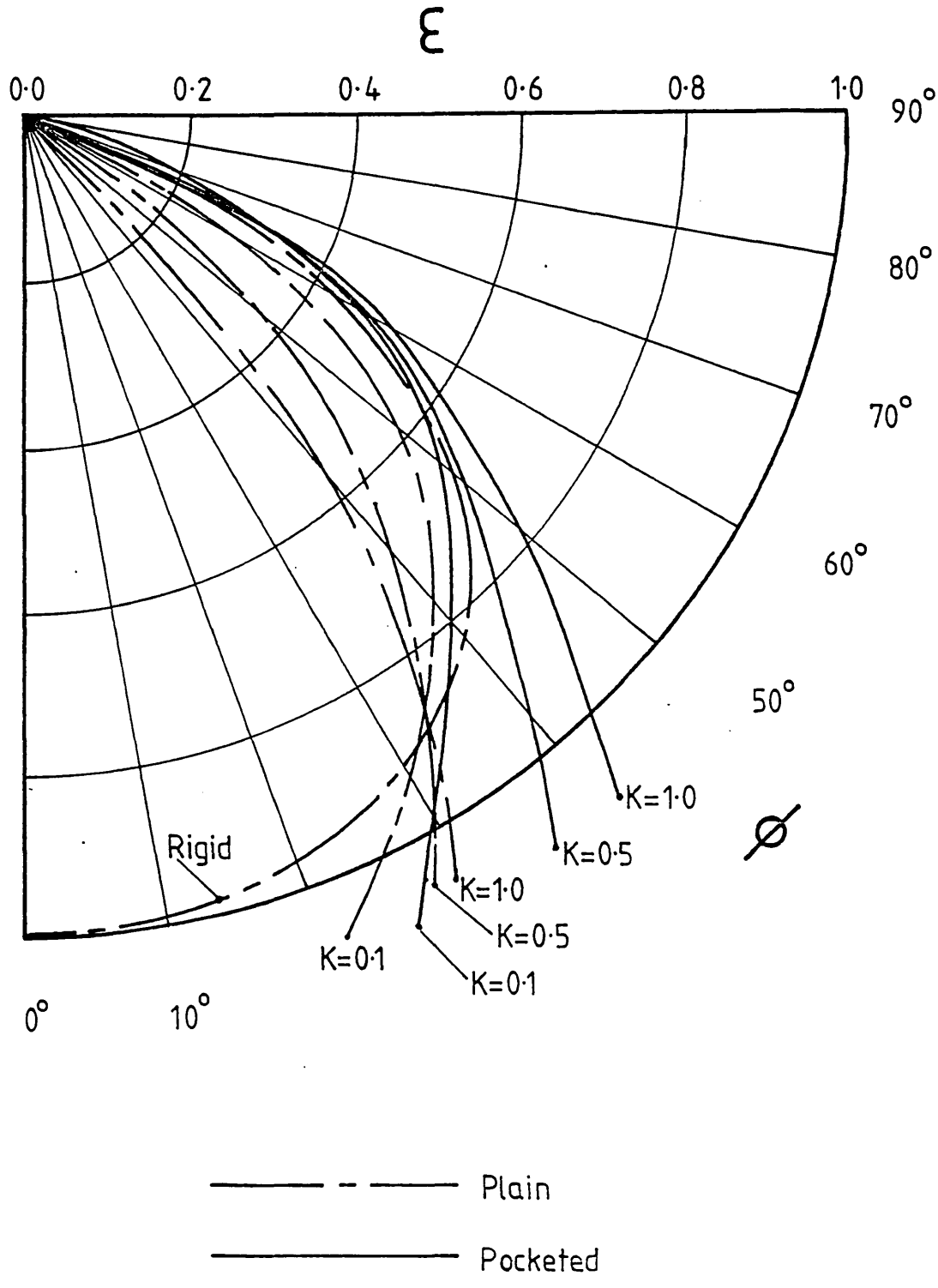


Figure 2.3. The Influence Of K On Attitude Angle For Plain And Pocketed Liners.

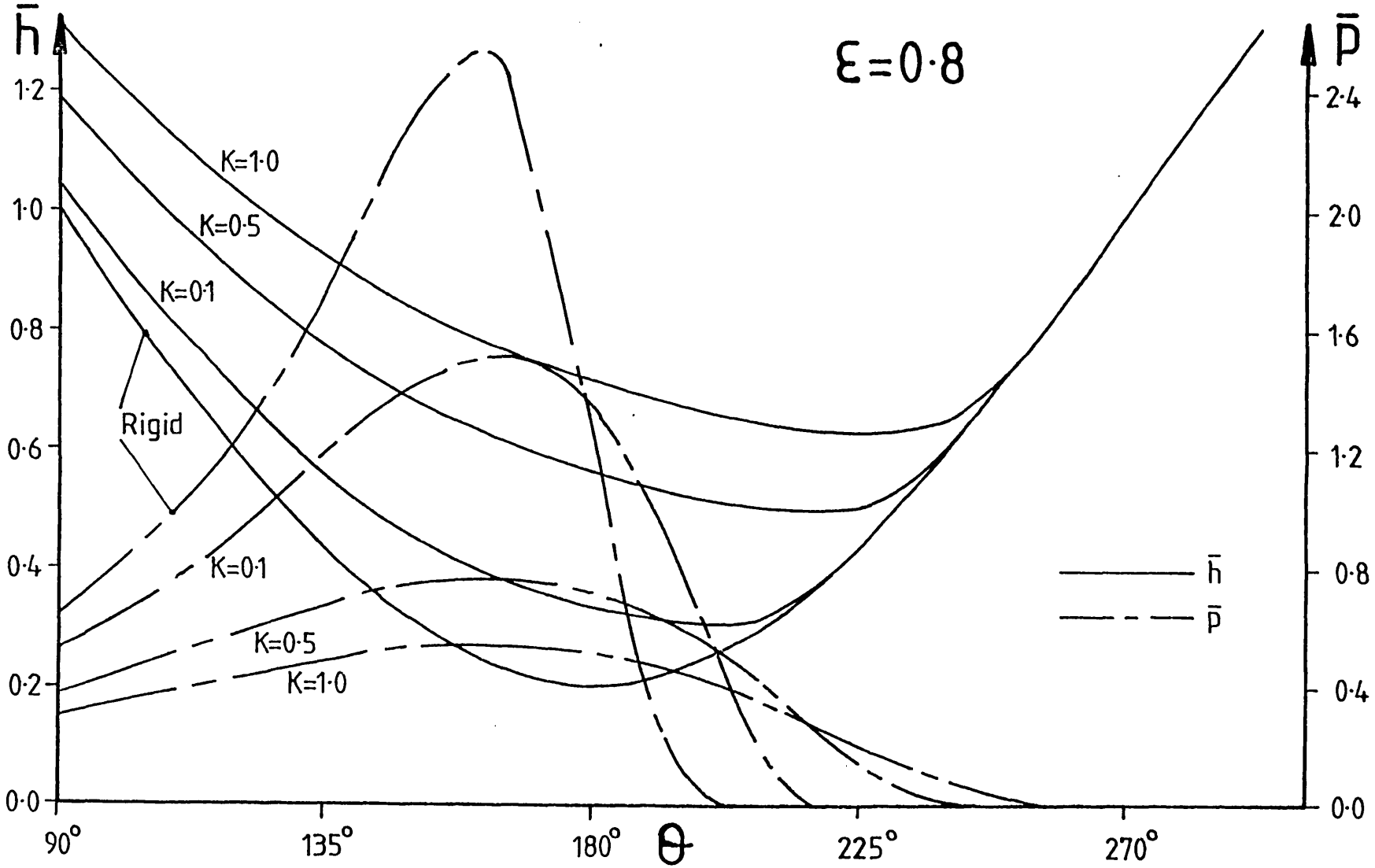


Figure 2.4. Film Shapes And Pressure Profiles For A Plain Elastic Liner With Varying K.

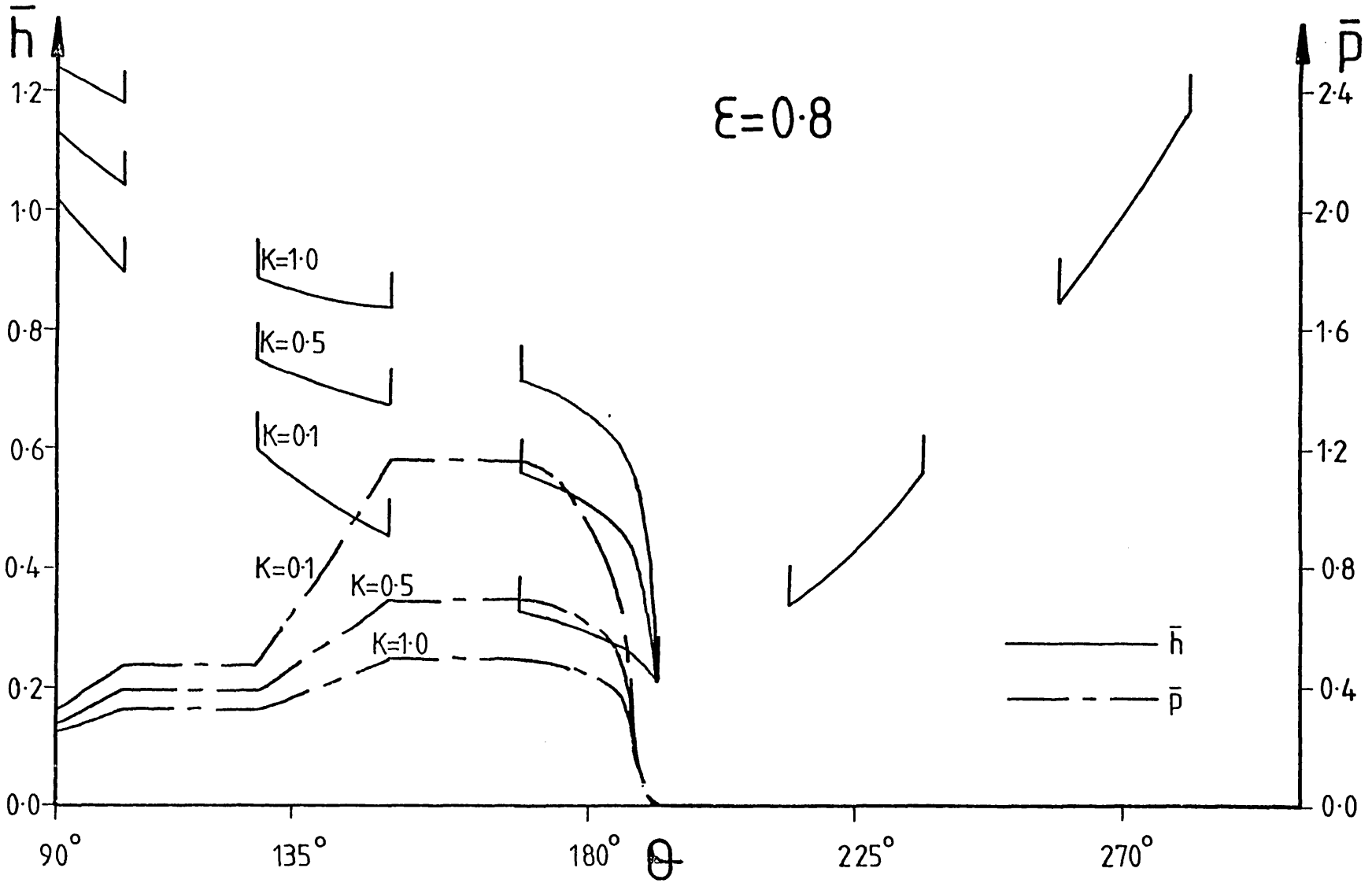


Figure 2.5. Film Shapes And Pressure Profiles For A Pocketed Elastic Liner With Varying K.

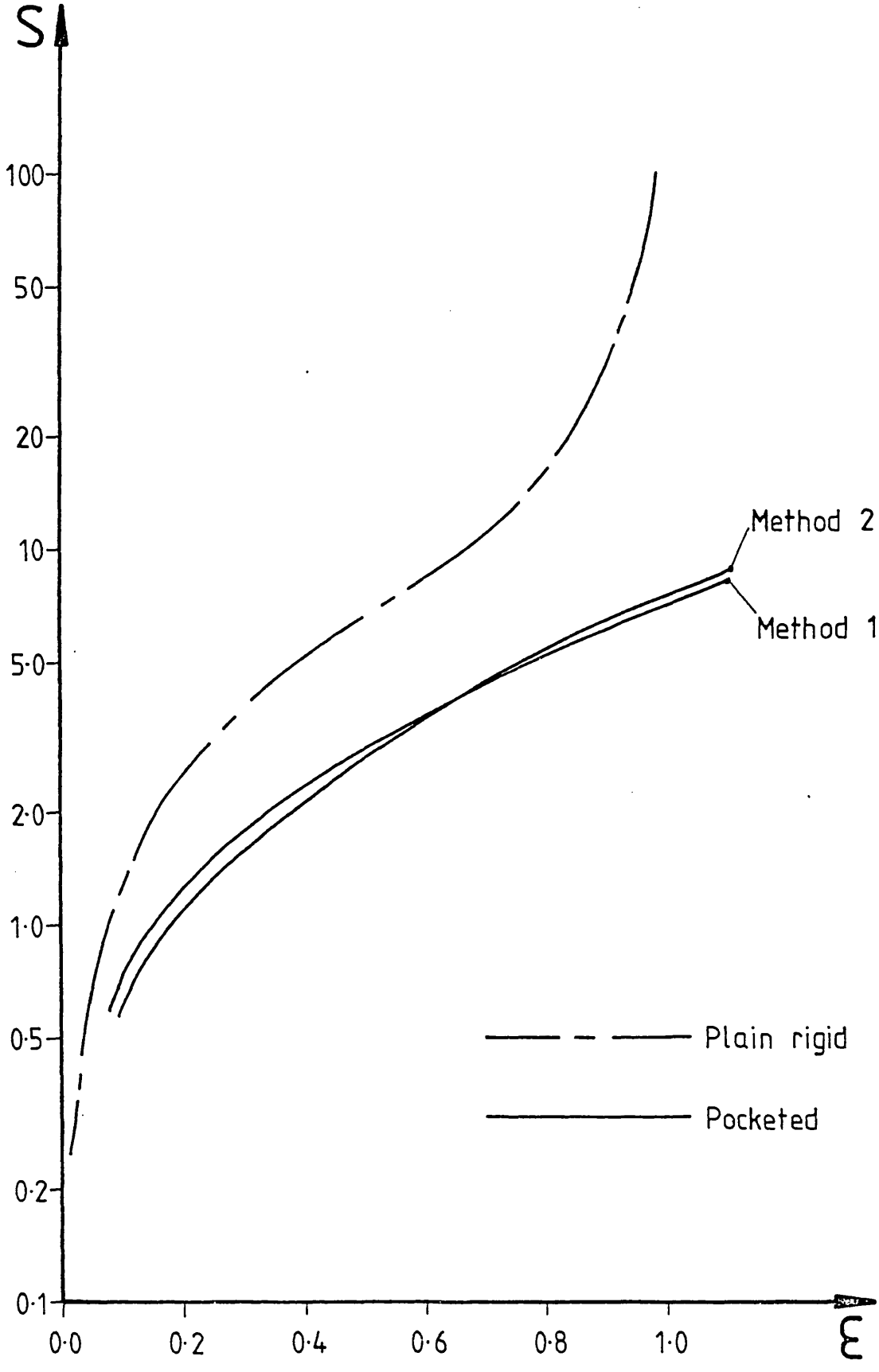


Figure 2.6. Sommerfeld Number Comparing The Two Methods Of Pocket Pressure Analysis.

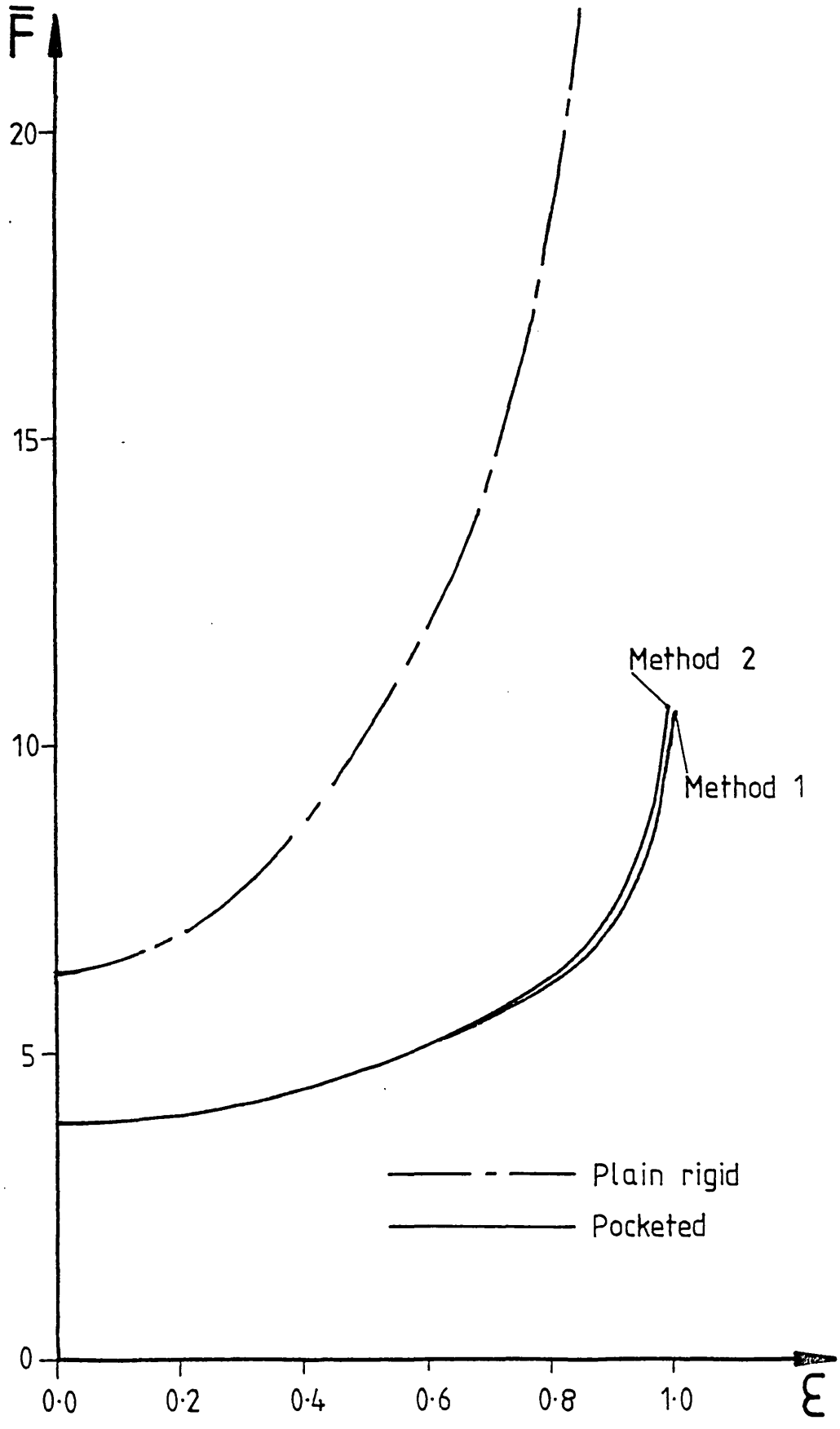


Figure 2.7. Friction Comparing The Two Methods Of Pocket Pressure Analysis.

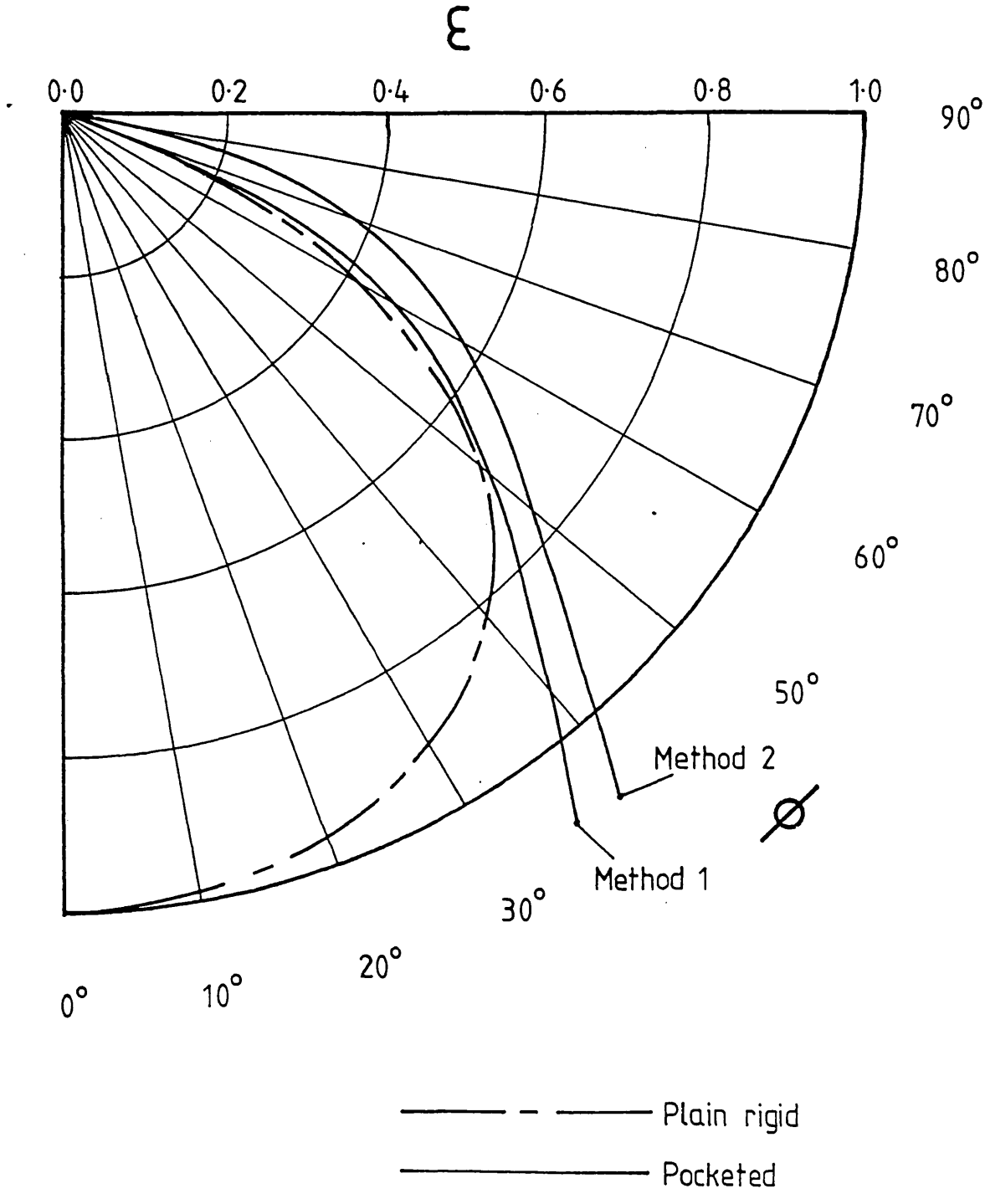


Figure 2.8. Attitude Angle Comparing The Two Methods Of Pocket Pressure Analysis.

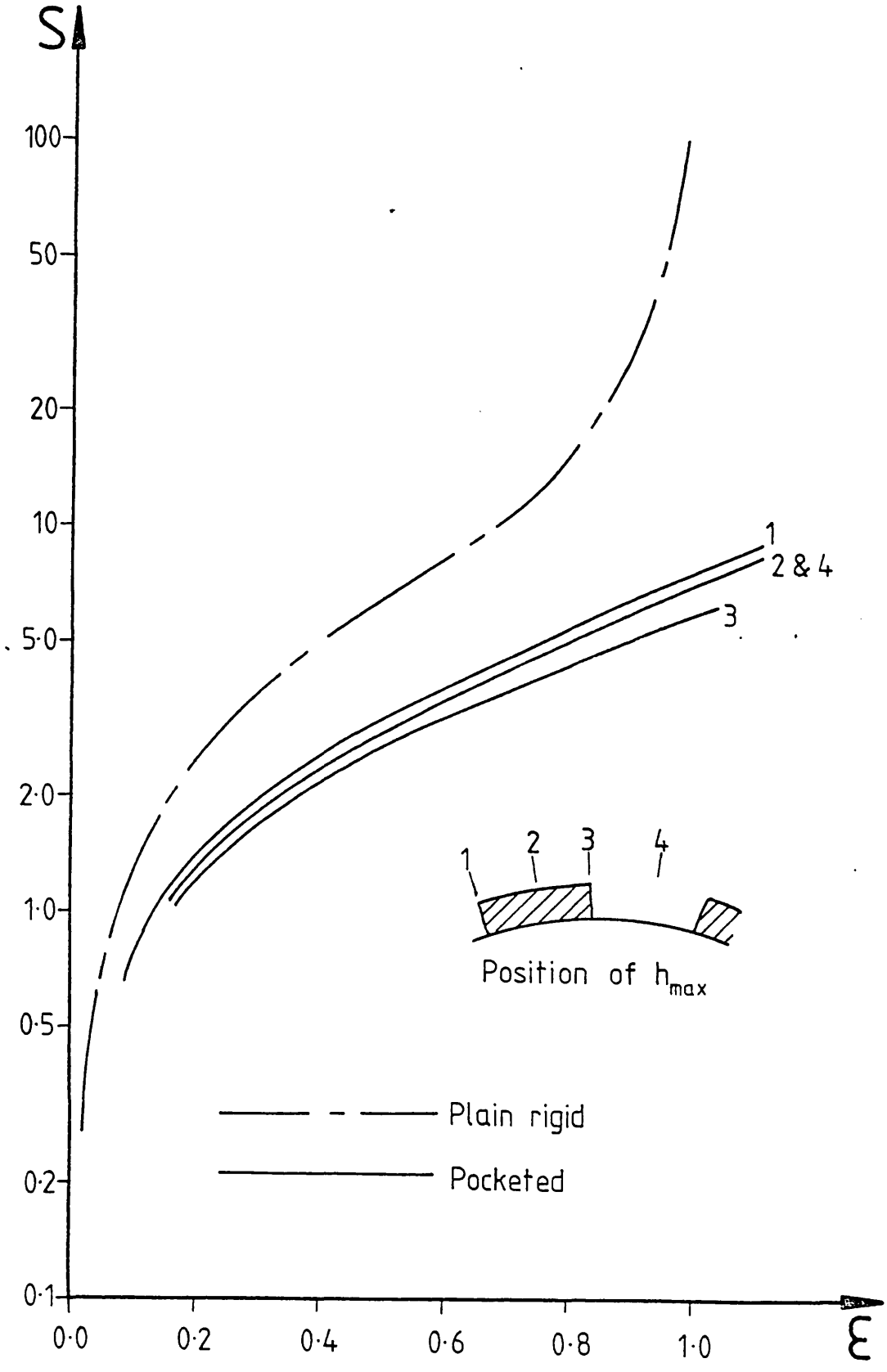


Figure 2.9. The Effect Of Varying The Film Starting Position On Sommerfeld Number.

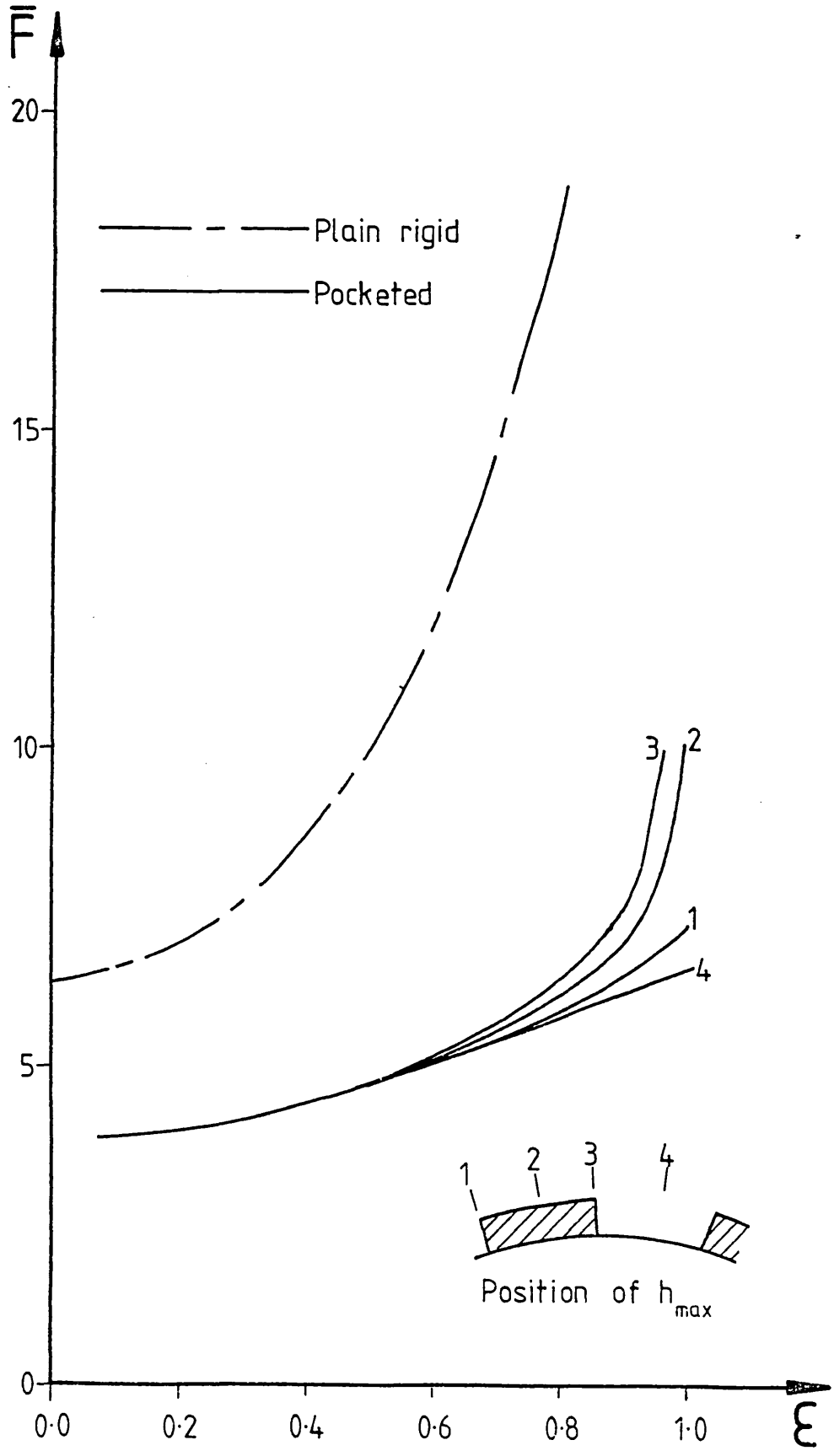


Figure 2.10. The Effect Of Varying The Film Starting Position On Friction.

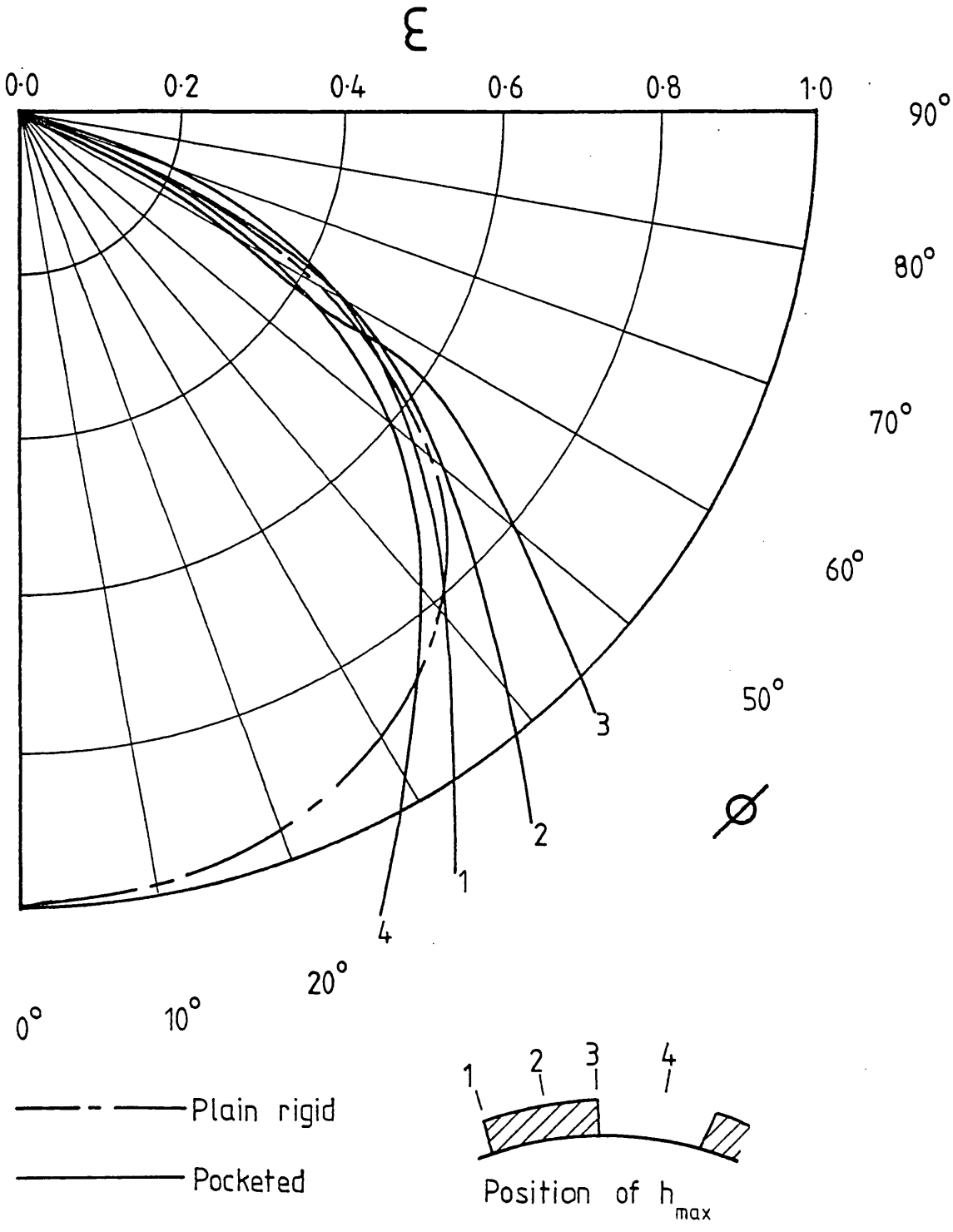


Figure 2.11. The Effect Of Varying The Film Starting Position On Attitude Angle.

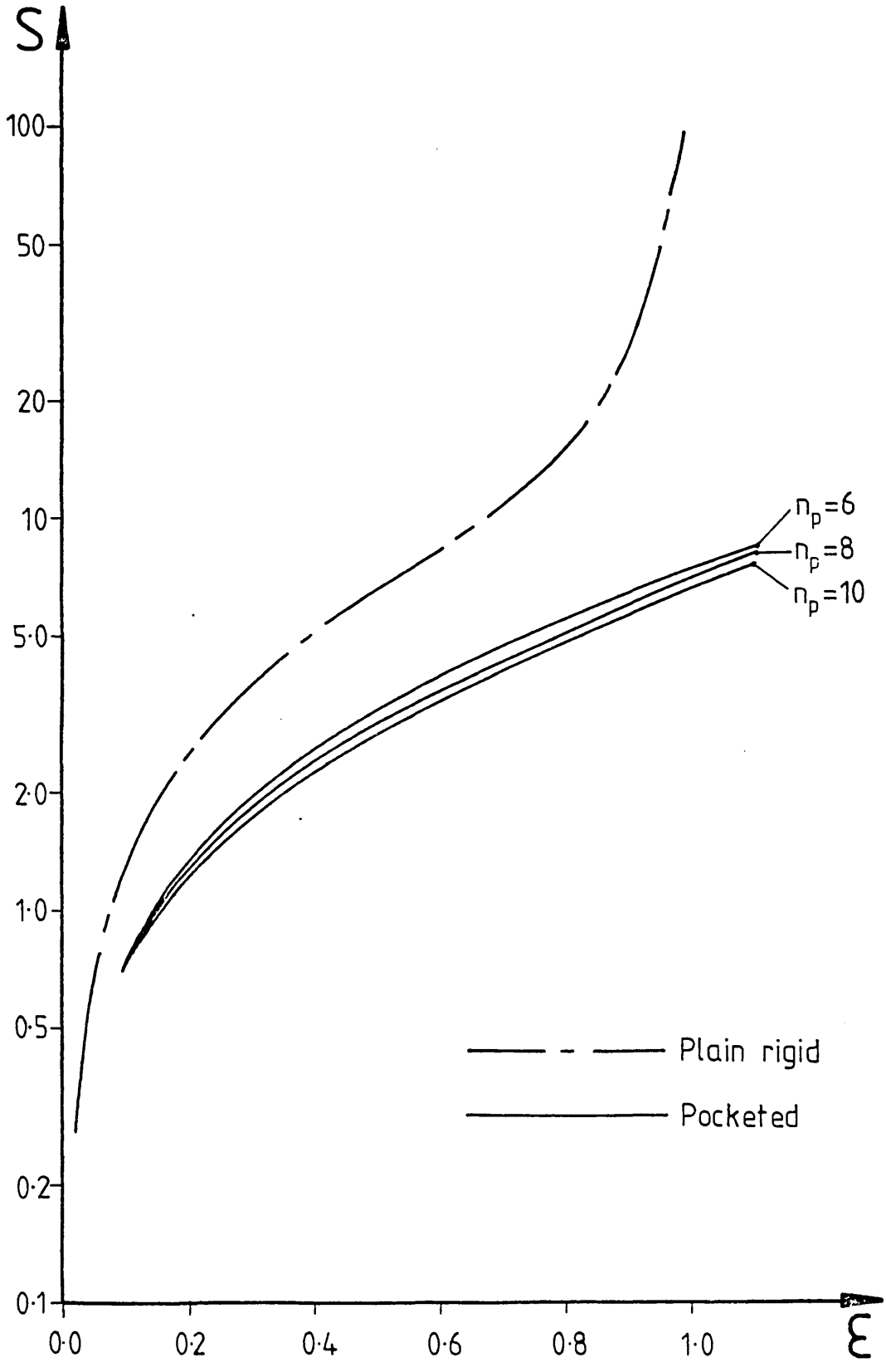


Figure 2.12. The Influence Of The Number Of Pockets On Sommerfeld Number.

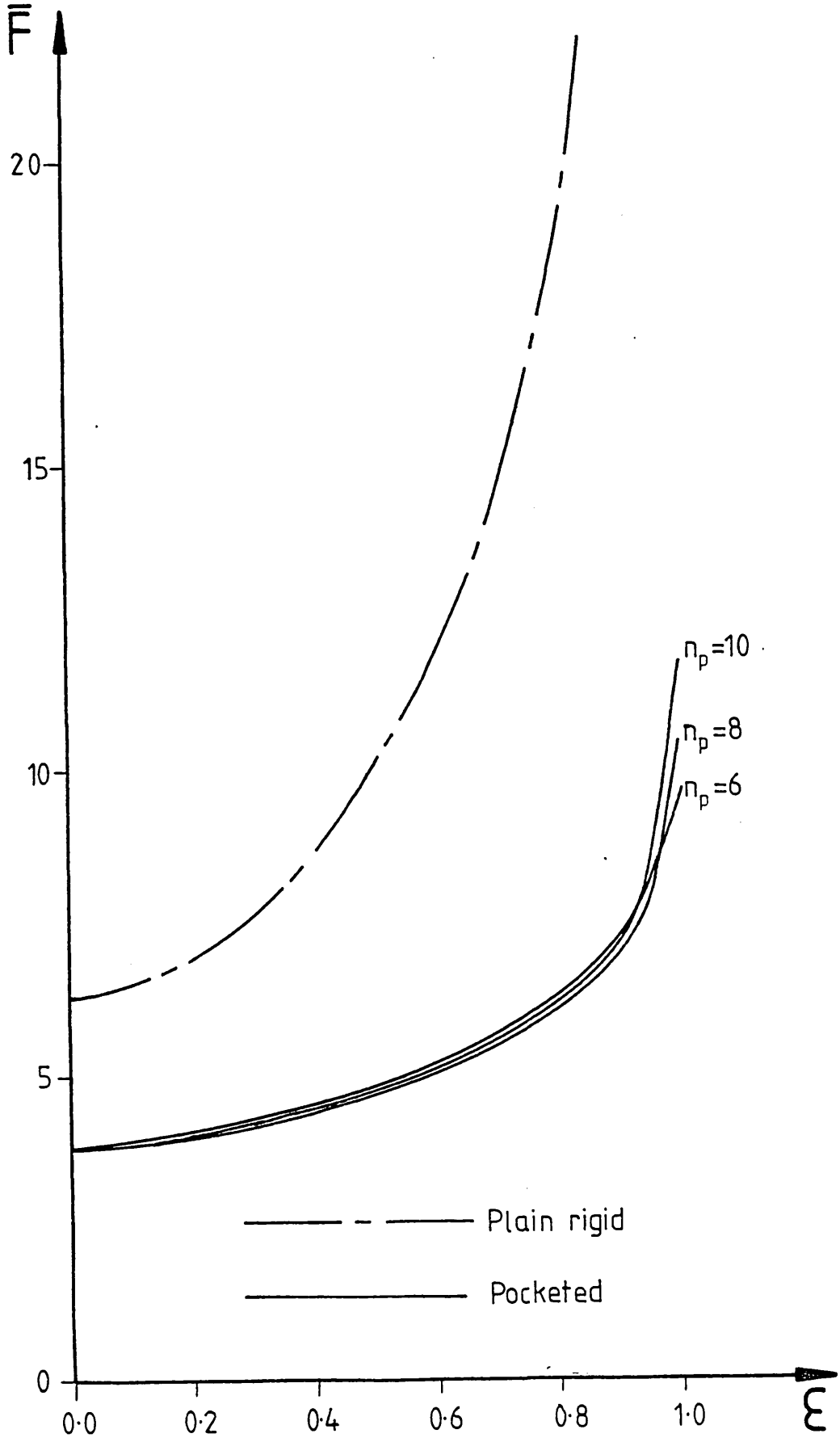


Figure 2.13. The Influence Of The Number Of Pockets On Friction.

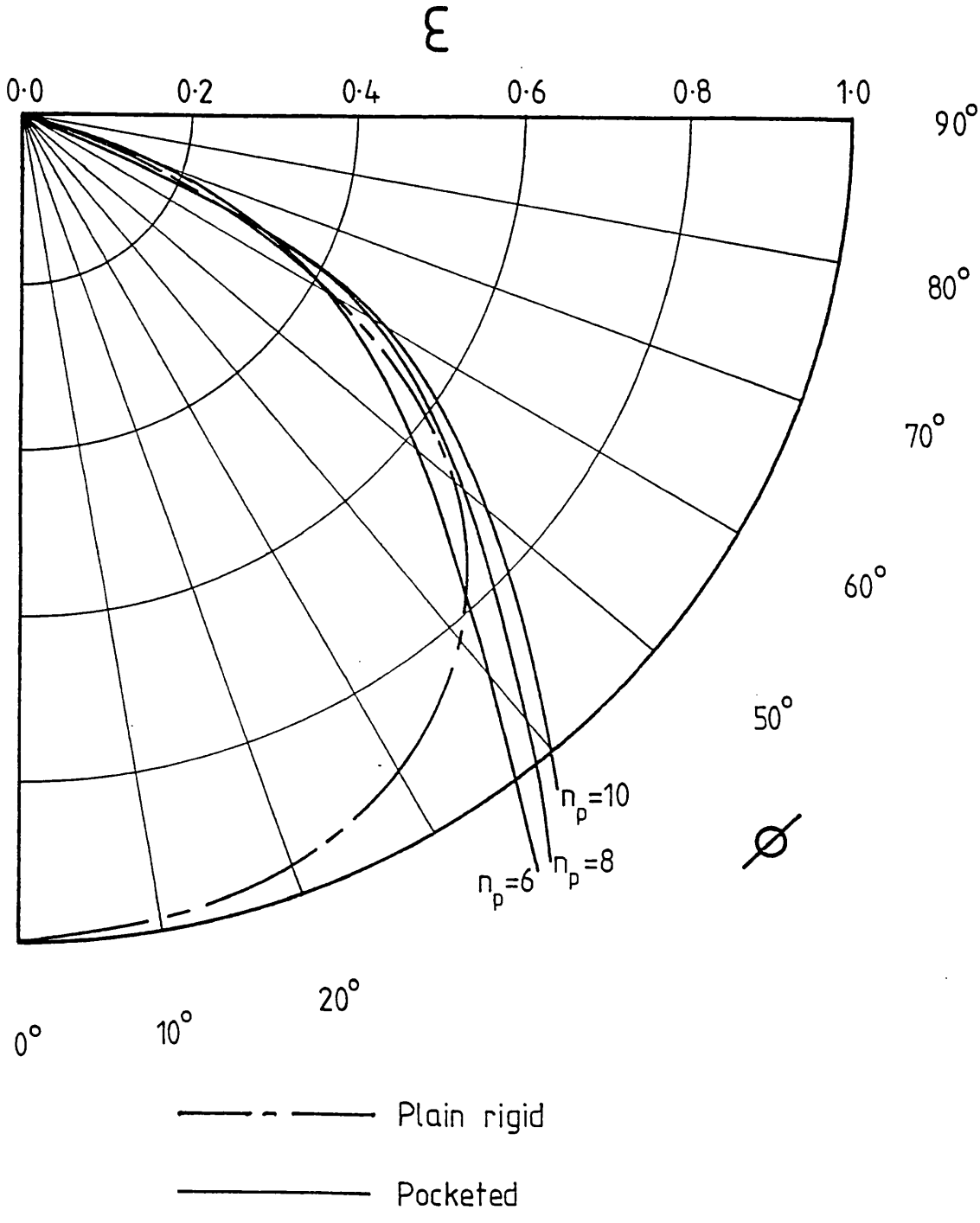


Figure 2.14. The Influence Of The Number Of Pockets On Attitude Angle.

CHAPTER 3.

DEVELOPMENT OF THE TREATMENT OF DISTORTION FOR THE INFINITELY LONG BEARING.

3.1. Introduction.

The coarseness of the method used for calculating distortions presented in Chapter 2 is evident. In an attempt to define whether the approximations used had a significant effect on the hydrodynamic characteristics of the bearing, finite element methods were considered.

Matrix methods of structural analysis, in which an elastic continuum is idealised as a series of finite elements, lend themselves to general purpose computer programmes. Fortunately, one such programme was available and nominally ready for use at Imperial College. FINEL, a programme written and maintained by Mr. D. Hitchings of the Aeronautical Engineering Department, was used to generate a matrix of influence coefficients for incorporation into the hydrodynamic programme after suitable modification.

3.2. The Finite Element Method.

FINEL uses the displacement method of structural analysis in which an elastic continuum

is defined in terms of the nodal displacements of a series of finite elements. Assumed functions are used to describe the variables (e.g. displacement) between the node points and each element has its stiffness defined in terms of its nodal displacements and applied loads. The assembly of this for the complete global structure of n nodes results in the equation;

$$\begin{bmatrix} k_{11} & k_{12} & k_{13} & \cdot & \cdot & \cdot & \cdot & k_{1n} \\ k_{21} & k_{22} & k_{23} & \cdot & \cdot & \cdot & \cdot & k_{2n} \\ k_{31} & k_{32} & k_{33} & \cdot & \cdot & \cdot & \cdot & k_{3n} \\ \cdot & \cdot & \cdot & \cdot & & & & \cdot \\ \cdot & \cdot & \cdot & & \cdot & & & \cdot \\ \cdot & \cdot & \cdot & & & \cdot & & \cdot \\ \cdot & \cdot & \cdot & & & & \cdot & \cdot \\ k_{n1} & k_{n2} & k_{n3} & \cdot & \cdot & \cdot & \cdot & k_{nn} \end{bmatrix} \begin{bmatrix} u_1 \\ u_2 \\ u_3 \\ \cdot \\ \cdot \\ \cdot \\ \cdot \\ u_n \end{bmatrix} = \begin{bmatrix} P_1 \\ P_2 \\ P_3 \\ \cdot \\ \cdot \\ \cdot \\ \cdot \\ P_n \end{bmatrix} \qquad (3.1.)$$

where $[k]$ is the global stiffness matrix, $[u]$ is the nodal displacement vector and $[P]$ is the nodal applied load vector. $[k]$ is then inverted, after suitable partitioning operations, to obtain a solution for the nodal displacements given the applied loading.

The main choice left to the user of the programme is the type and number of elements needed to idealise the structure to a reasonable accuracy. The nature of the present problem enabled the analysis of only a single land. Eight node, isoparametric, membrane elements were chosen as both the geometry and displacement along the edges of these elements are defined in terms of a second order polynomial.

This enabled an accurate representation to be made of the curved surfaces of the land.

The elements also assume a zero strain in the through thickness (axial) direction. The through thickness was chosen to be unity to ensure compatability with the hydrodynamic equations. The condition of the land being bonded to the journal was achieved by fully constraining the nodes on the inner edge of the land.

The further question of the number of elements to be used was resolved by performing a series of runs with a sample pressure distribution on the land, and varying the number of elements both in the radial and circumferential directions. As the finite element method cannot handle pressure loading along the edge of an element as such, the programme was modified as Zienkiewicz (27) describes by representing the pressure loads in terms of kinematically equivalent nodal loads.

Fig. 3.1. shows this sample loading, and as the loading is symmetric, Fig. 3.2. shows the resulting distortion field for half the land together with a comparison in Table 3.3. of varying the numbers of elements. The distortion at selected nodes is seen to change less as the number of elements increases and the solution approximates more closely to the exact solution. For this reason a final choice was made to use eight elements in the circumferential direction and four elements in the radial direction.

3.3. Influence Matrix Generation.

As the inclusion of the finite element programme as a whole in the hydrodynamic programme would be expensive in terms of computing time, requiring a separate execution of FINEL for each iteration between pressure and distortion, a flexibility matrix approach was adopted. Using the principle of superposition described by Timoshenko and Goodier (28), unit pressures were applied across the land producing a given distortion field. Factoring and combining the unit pressures enabled the distortion field of the land to be found for any given pressure field. The assumption of a linear variation of pressure between the nodes in the hydrodynamic theory was accommodated by using triangular pressure profiles of unit height, similar to the method used by Ranger et al (29).

The collection of applied unit loading is shown in Fig. 3.4. The matrix of flexibility coefficients, $[\alpha]$, for the five nodes on the top surface of the land, is defined by

$$\begin{bmatrix} \delta_1 \\ \delta_2 \\ \delta_3 \\ \delta_4 \\ \delta_5 \end{bmatrix} = \begin{bmatrix} \alpha_{11} & \alpha_{12} & \alpha_{13} & \alpha_{14} & \alpha_{15} & \alpha_{16} & \alpha_{17} \\ \alpha_{21} & \alpha_{22} & \alpha_{23} & \alpha_{24} & \alpha_{25} & \alpha_{26} & \alpha_{27} \\ \alpha_{31} & \alpha_{32} & \alpha_{33} & \alpha_{34} & \alpha_{35} & \alpha_{36} & \alpha_{37} \\ \alpha_{41} & \alpha_{42} & \alpha_{43} & \alpha_{44} & \alpha_{45} & \alpha_{46} & \alpha_{47} \\ \alpha_{51} & \alpha_{52} & \alpha_{53} & \alpha_{54} & \alpha_{55} & \alpha_{56} & \alpha_{57} \end{bmatrix} \begin{bmatrix} P_1 \\ P_2 \\ P_3 \\ P_4 \\ P_5 \\ P_6 \\ P_7 \end{bmatrix} \qquad (3.2.)$$

Applying each of the pressure loads P_1 to P_7 separately to the land, for example P_1, gives

$$\begin{bmatrix} P_1 \\ P_2 \\ P_3 \\ P_4 \\ P_5 \\ P_6 \\ P_7 \end{bmatrix} = \begin{bmatrix} 1 \\ 0 \\ 0 \\ 0 \\ 0 \\ 0 \\ 0 \end{bmatrix}$$

and substituting this in eq. 3.2. gives

$$\begin{bmatrix} \delta_1 \\ \delta_2 \\ \delta_3 \\ \delta_4 \\ \delta_5 \end{bmatrix} = \begin{bmatrix} \alpha_{11} \\ \alpha_{21} \\ \alpha_{31} \\ \alpha_{41} \\ \alpha_{51} \end{bmatrix} \qquad (3.3.)$$

Thus the flexibility matrix can be assembled from selected values of nodal distortions.

Three flexibility matrices were required, one (5x7) matrix for the top surface of the land and two (9x7) matrices for each of the sides of the land.

3.4. Solution Procedure.

The relevant nodal distortions from an execution of FINEL were selected and concatenated

via a separate programme to produce the three flexibility matrices. The matrices were also scalar multiplied by $\frac{6\eta U R_2}{c^3}$ to ensure compatibility with the dimensionless variables of pressure and distortion in the hydrodynamic theory. The matrices were then stored off-line for subsequent use.

The values for η, U, c, R_1 and R_2 were chosen for purposes of comparison with the simple distortion treatment to give an equivalent Elasticity factor, K, of 0.5. The land material was taken to be Nylon with $E = 2.758 \times 10^9$ N/m^2 and $\nu = 0.4$.

Apart from the calculation of distortion, the solution is broadly similar to that of Chapter 2 except for the changes in the computing equation for pocket pressure, details of which are given in Appendix A4. This includes the flow contribution from the deflections of the sides of the land, which introduces a further dimensionless variable $\frac{R_1}{R_2}$ whose value was taken to be 0.9. This added flow term could either be included or excluded in the programme. The programme listing is given in Appendix A5.

3.5. Numerical Results.

Results were calculated for a bearing with eight pockets taking up half the available pitch in

the circumferential direction. A uniform spacing of four meshes per land gave a finite difference grid of 64 nodes in total. The position of the start of the film, $\bar{h}_{max}$, was taken to be at the mid-point of a land.

Relevant results from Chapter 2 are plotted for comparison with the results for the finite element distortion treatment in Figs. 3.5. to 3.8.

In general, the results are surprisingly close to those presented in Chapter 2 considering the differences in method, and the trends previously described are confirmed.

The Sommerfeld number, shown in Fig. 3.5. is almost the same as for the simple distortion treatment up to an eccentricity ratio of 0.8. Beyond this point, results could not be produced due to the presence of negative film thicknesses in the programme. This is reflected in a sharp increase in friction in Fig. 3.6. Whereas in the simple distortion treatment this was due to an artificially low value of the minimum film thickness, caused by the plane strain assumption, in this case the more realistic film shape in Fig. 3.8. shows film thicknesses which are less than the rigid film thickness at two points, due to the lands exhibiting elastohydrodynamic type constrictions. Although generally in contacts such as balls and rollers, but particularly in this context in thrust pads (30), an elastohydrodynamic constriction

appears at the trailing edge of the contact, in this case there would appear to be one at the leading edge as well. The pressure field also operates over a wider arc with the film cavitating later than in the simple distortion treatment.

The exclusion from the programme of the effects of the distortion of the land sides on pocket volume, was found to have a negligible effect on all the dependent variables. This would suggest that the pumping effect of the pockets due to the displaced volume does not have a dominant effect on the hydrodynamic characteristics of the bearing. This is confirmed in that the effect of the land side distortions was to decrease the displaced volume of the pockets in the converging region of the film, and yet when these distortions were excluded the Sommerfeld number was only marginally higher than when they were included.

Despite the differences in film thickness and pressure fields due to a more realistic treatment of distortion, Sommerfeld number, friction and attitude angle are largely similar to the previous results for the simple distortion treatment.

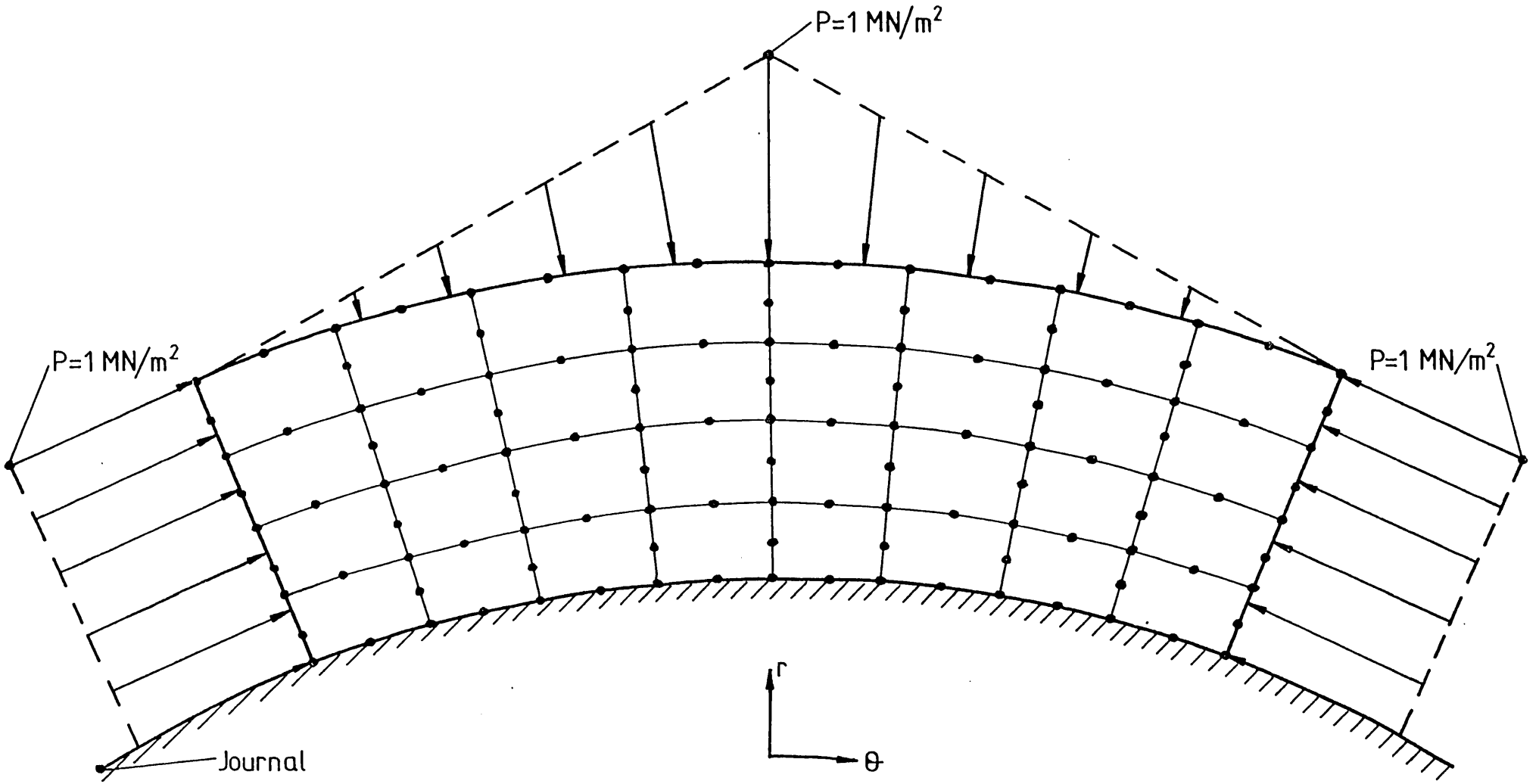


Figure 3.1. Finite Element Idealisation Of A Single Land With The Test Pressure Distribution.

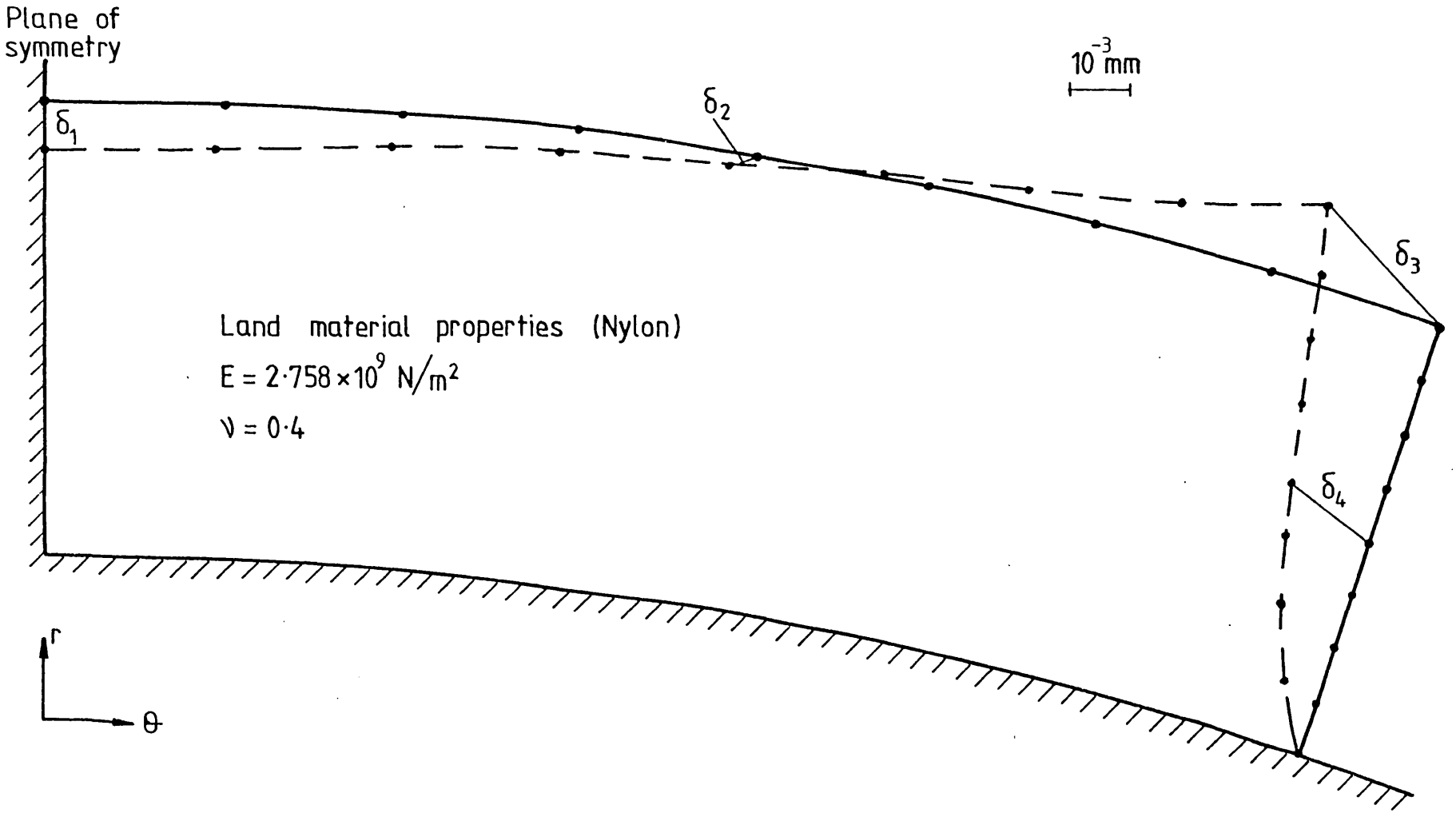


Figure 3.2. Distorted Land Shape Under The Test Pressure Distribution.

Surface Distortions 10^{-3} mm.	Number of Elements (circumferential x radial)			
	2x1	4x2	6x3	8x4
δ_1 (land centre)	0.674	0.828	0.813	0.810
δ_2 (mid-top)	0.383	0.458	0.473	0.483
δ_3 (corner)	2.390	2.498	2.666	2.715
δ_4 (mid-side)	1.276	1.642	1.694	1.714

Table 3.3. The Effect Of Varying Element Density On Selected Surface Distortions.

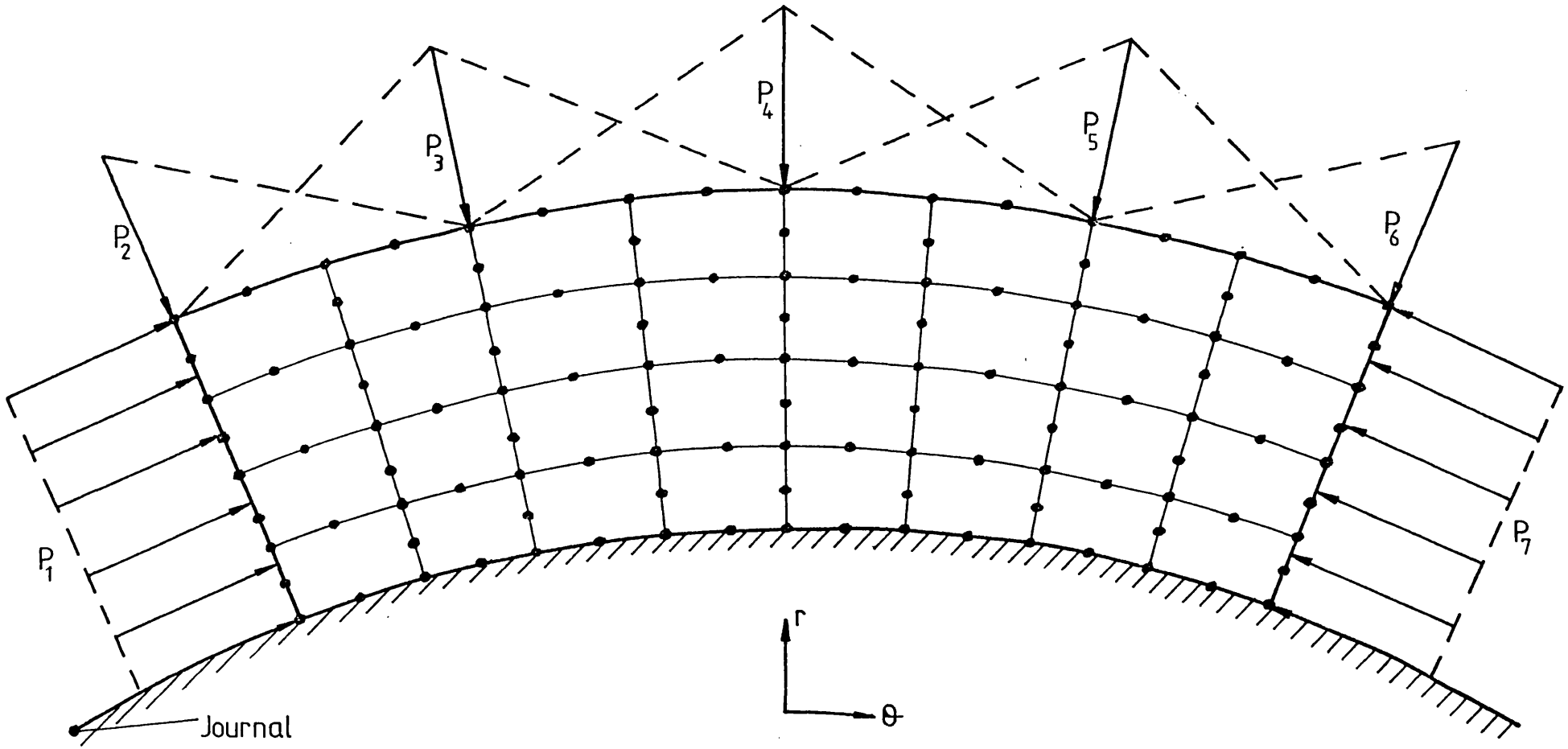


Figure 3.4. Diagram Of The Loading Used To Produce The Matrix Of Influence Coefficients.

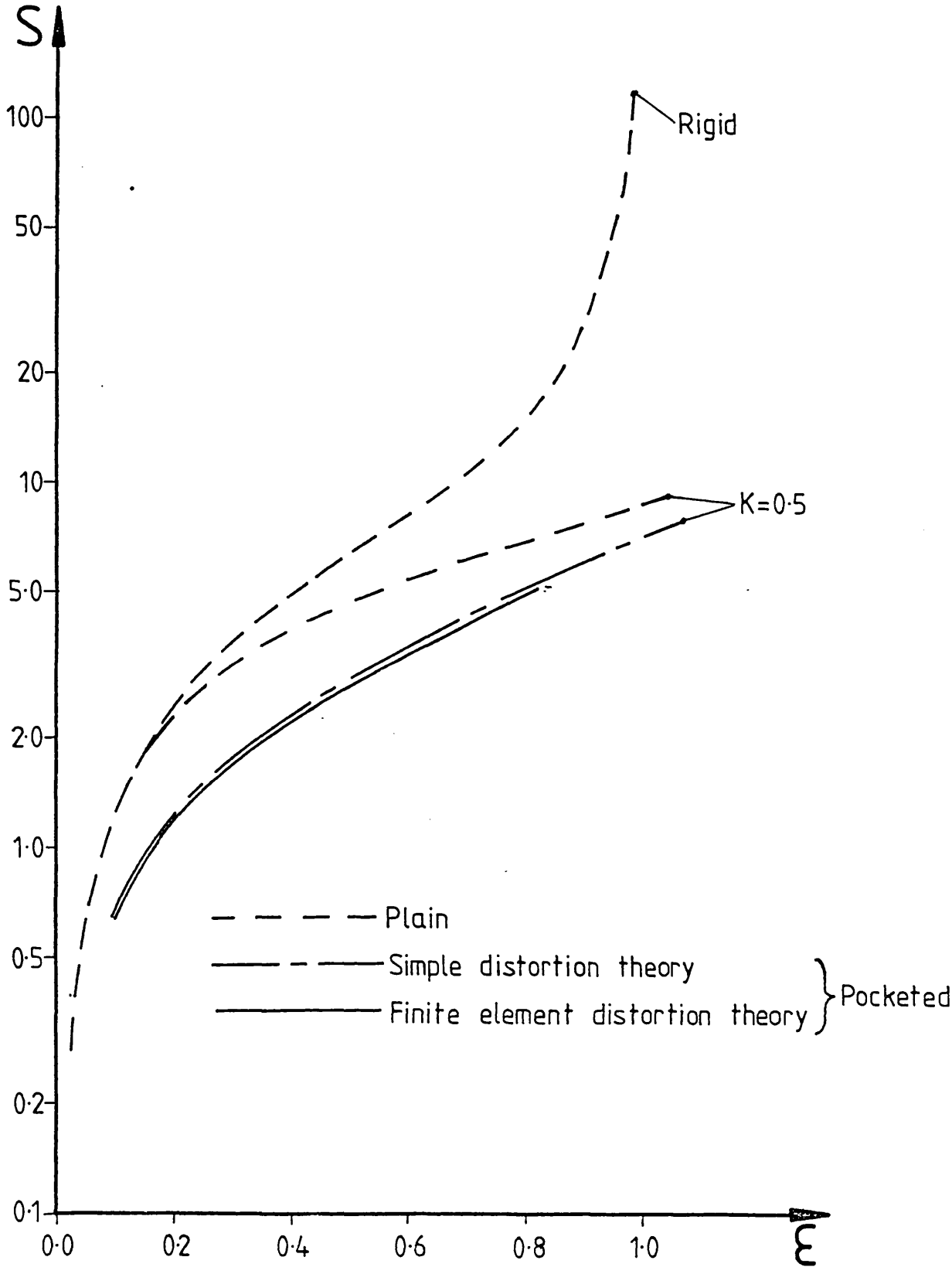


Figure 3.5. A Comparison Of The Distortion Theories For Sommerfeld Number.

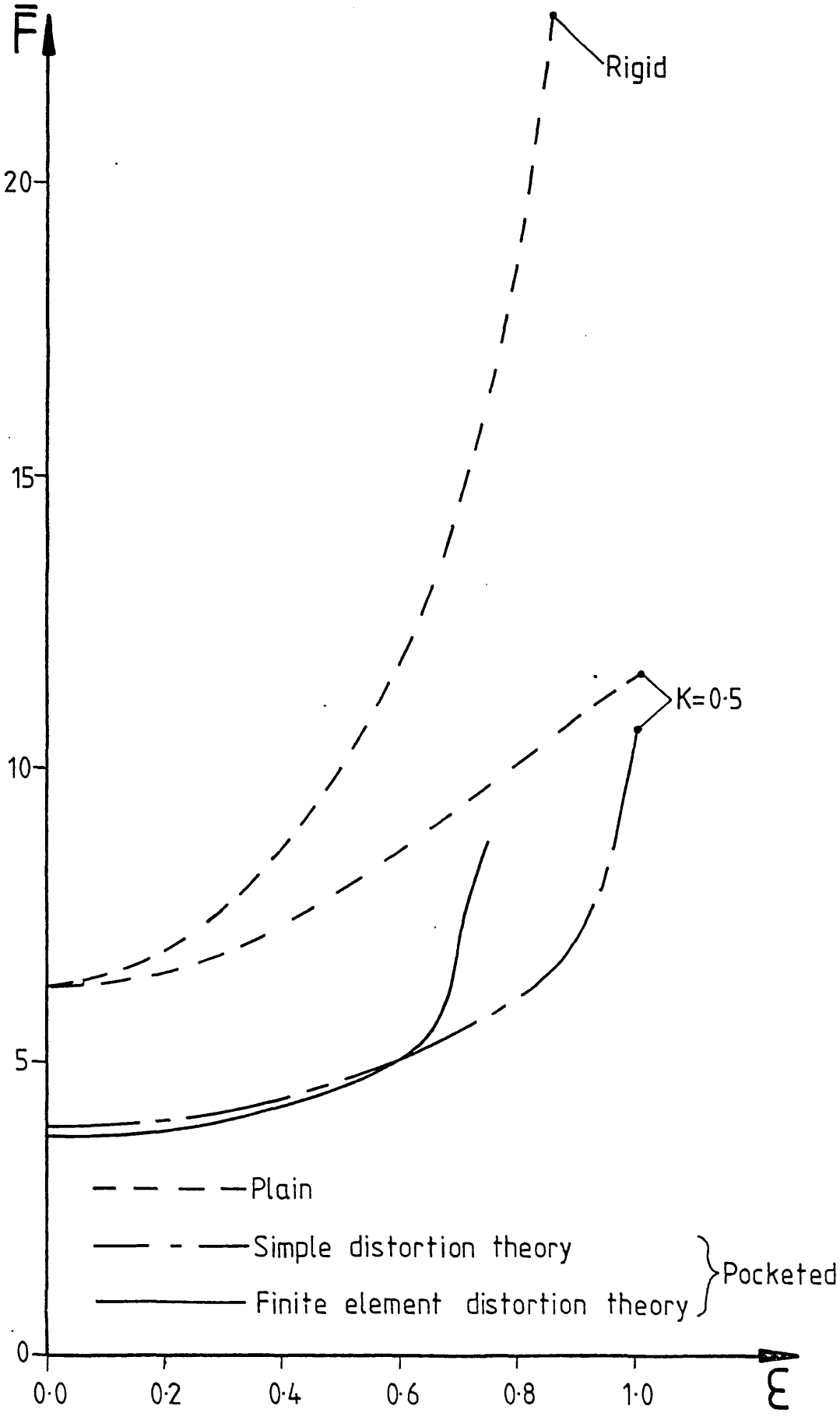


Figure 3.6. A Comparison Of The Distortion Theories For Friction.

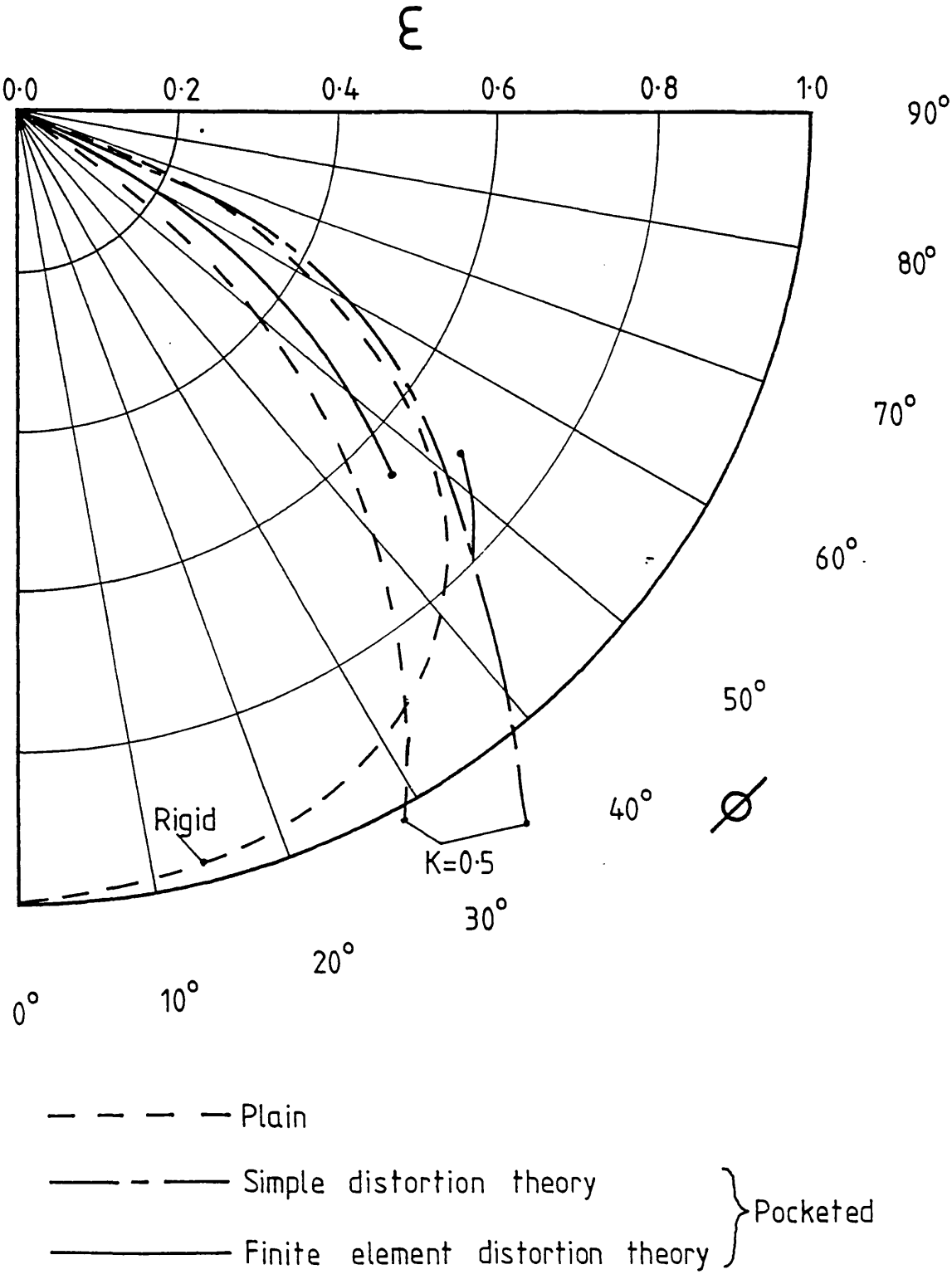


Figure 3.7. A Comparison Of The Distortion Theories For Attitude Angle.

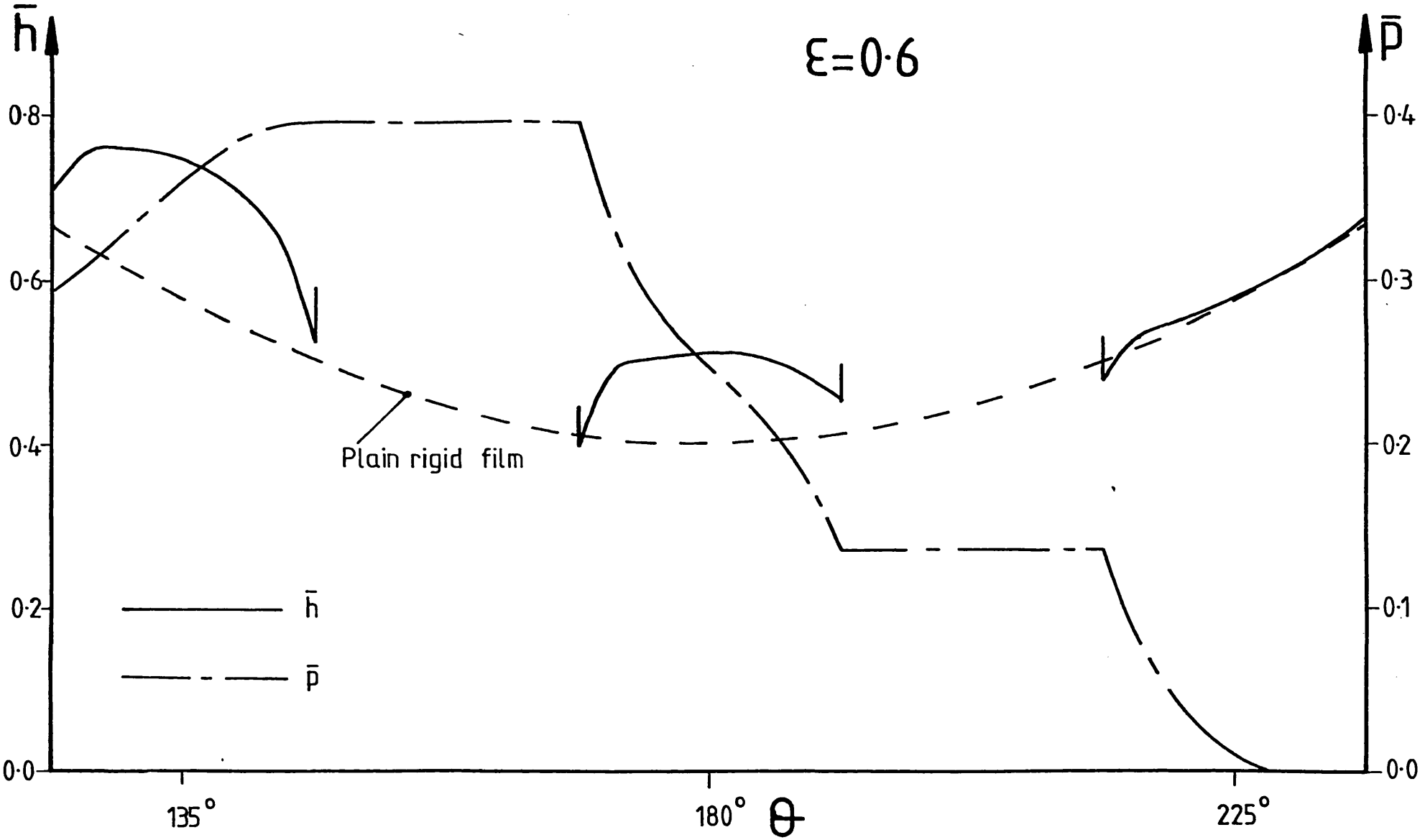


Figure 3.8. Film Shape And Pressure Profile For The Finite Element Distortion Theory.

CHAPTER 4.

DEVELOPMENT OF THE THEORY FOR A FINITE LENGTH BEARING.

4.1. Introduction.

An extension of the previous theoretical work to include variations of pressure in the axial direction was necessary to enable comparison to be made with the later experimental results for a finite length bearing.

At the same time, a direct comparison with the results of Alexandrov (21) could be made. Although a difference in trends between the present and Alexandrov's work was noted in Chapters 2 and 3, this could have been a peculiarity of the infinitely long bearing and a reproduction of Alexandrov's results was considered to be useful.

4.2. Theoretical Development.

The theoretical analysis of Chapter 2 was developed to include variations of the pressure, distortion and film thickness fields in the axial direction as follows.

Film pressure was found using Reynold s'

equation assuming two dimensional, steady incompressible, isoviscous flow, namely;

$$\frac{\partial}{\partial x}\left(h^3\frac{\partial p}{\partial x}\right) + \frac{\partial}{\partial y}\left(h^3\frac{\partial p}{\partial y}\right) = 6\eta U\frac{\partial h}{\partial x} \quad . \qquad (4.1.)$$

The simple distortion treatment was again used in which $\bar{\delta} = -K\bar{p}$. Although the assumption of plane strain used in the simple distortion treatment is not valid for the finite length liner, it was thought that this would have a small effect on the dependent variables of the bearing and their overall trends. As the omission of the circumferential strain assumption in Chapter 3 showed a negligible change with respect to the simple distortion treatment results, the approximation of zero circumferential strain was again considered to be valid. It was considered that the above assumptions would be acceptable for the thin liners used later in the experimental work, and so the complications involved in producing a three dimensional elasticity solution were thought to be unnecessary.

An equation for pocket pressure, in terms of integrated functions of the land and sill pressures around the pocket, was derived from a consideration of flow continuity. The pocket pressure was taken to be uniform, and the approximation for the rate of change of displaced pocket volume, $\frac{\partial V}{\partial \theta}$, was again performed in two ways using the methods presented

in Chapter 2. The second method of pocket pressure analysis, relating to Alexandrov's method, was used for all the results in this chapter.

The axial pressure gradient introduces side leakage from the edges of the bearing, and so in addition to the dependent variables of Sommerfeld number, dimensionless friction and attitude angle, the dimensionless flow, $\bar{Q}$, was calculated, where

$$\bar{Q} = \frac{-LQ}{2UcR_2^2} \quad . \tag{4.2.}$$

Details of the theoretical analysis are given in Appendix A6.

The equations were set up in finite difference form using the grid shown in Fig. 4.1. Cavitation of the film was allowed for by setting any negative pressures to zero as they appeared in the iterative solution for pressure. Advantage was taken of axial symmetry by considering only half the bearing, using the boundary condition

$$\frac{\partial \bar{p}}{\partial \bar{y}} = 0 \quad \text{at} \quad \bar{y} = 0 \ .$$

This was achieved by equating the pressures on a series of dummy nodes at $\bar{y} = -\Delta\bar{y}$ to the pressures at $\bar{y} = \Delta\bar{y}$ in the pressure iteration scheme. Listings of the computer programmes for rigid and elastic plain bearings, and the two programmes for a pocketed bearing corresponding to the two methods used for

pocket pressure analysis, are presented in Appendix A7.

4.3. Numerical Results.

A comparison with Alexandrov's results is shown in Figs. 4.2. to 4.5. A length to diameter ratio, $\frac{L}{D}$, of 0.5 and an Elasticity factor, K, of 0.7 were used. The number of pockets was eight, and these took up half the available pitch in the axial and circumferential directions. A uniform finite difference grid of five nodes per pocket, land and sill gave a total of 64 nodes in the circumferential direction and 9 nodes in the axial direction. The film was taken to start at the mid line of a land.

The results in general show disturbing differences. The Sommerfeld number for both Alexandrov and Coates are close up to an eccentricity ratio of 0.65, but after that they diverge rapidly with Alexandrov's rising above that for the plain rigid bearing. This is reflected in the larger dimensionless friction and flow for Alexandrov, due to a higher contribution to the shear stress from circumferential pressure gradients or possibly smaller film thicknesses, and a higher axial pressure gradient boosting the side flow.

At this stage in the work, the above discrepancies remained unresolved, but as they could

have been due to a logical or programme error in either case, a comparison with some experimental results was obviously needed.

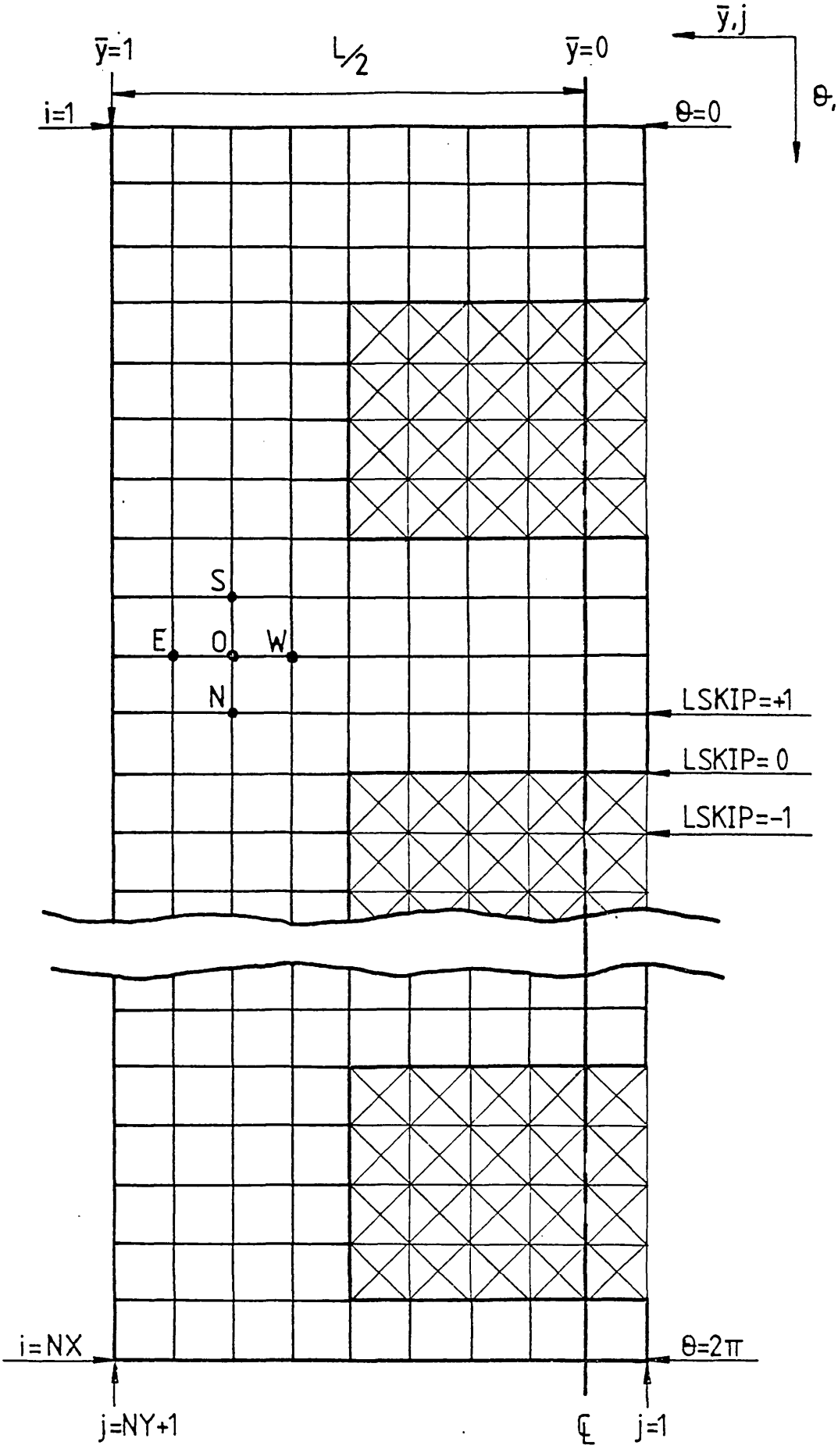


Figure 4.1. Finite Difference Grid For A Finite Length Pocketed Liner.

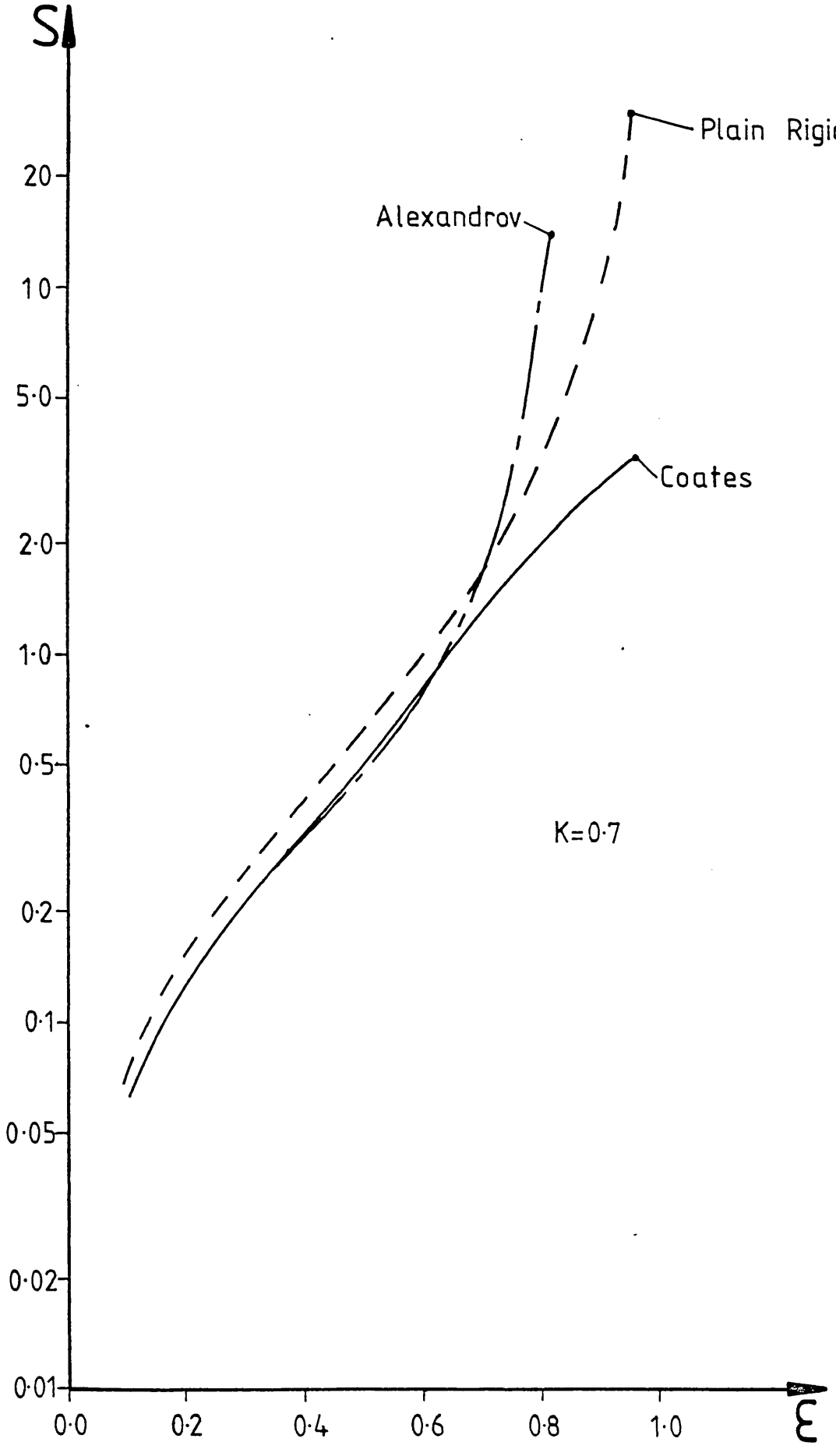


Figure 4.2. A Comparison Of The Results Of Alexandrov And Coates For Sommerfeld Number.

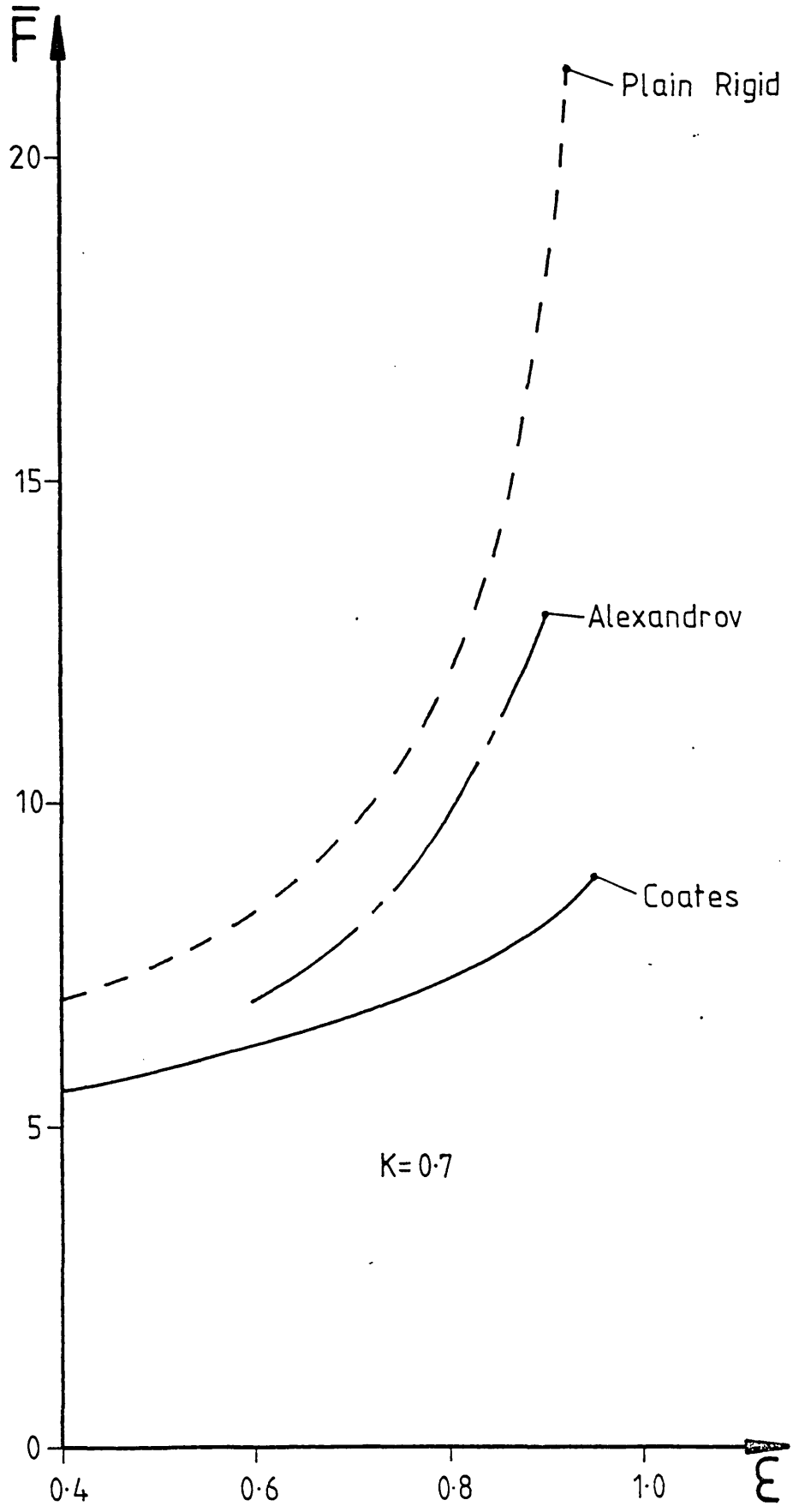


Figure 4.3. A Comparison Of The Results Of Alexandrov And Coates For Friction.

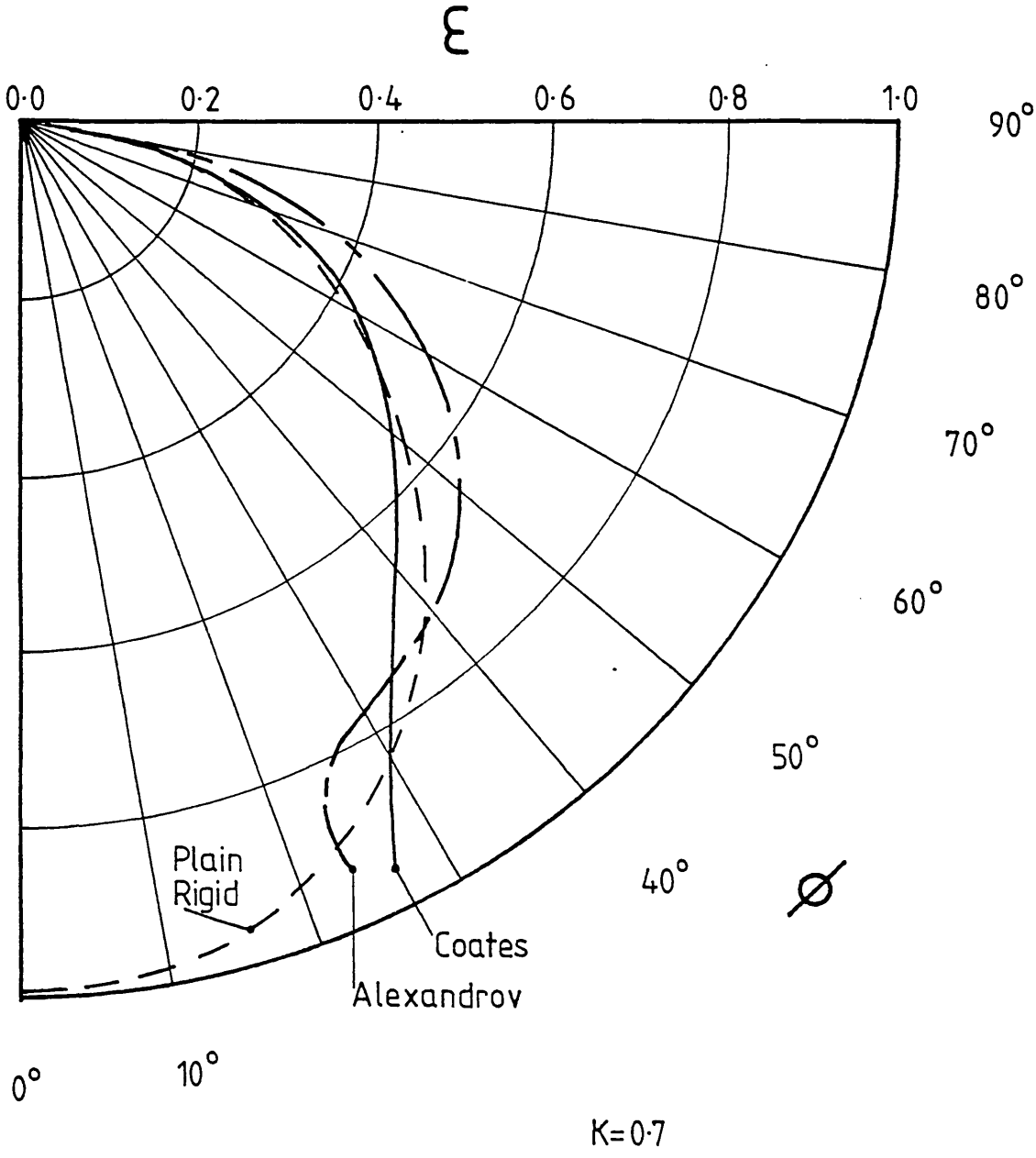


Figure 4.4. A Comparison Of The Results Of Alexandrov And Coates For Attitude Angle.

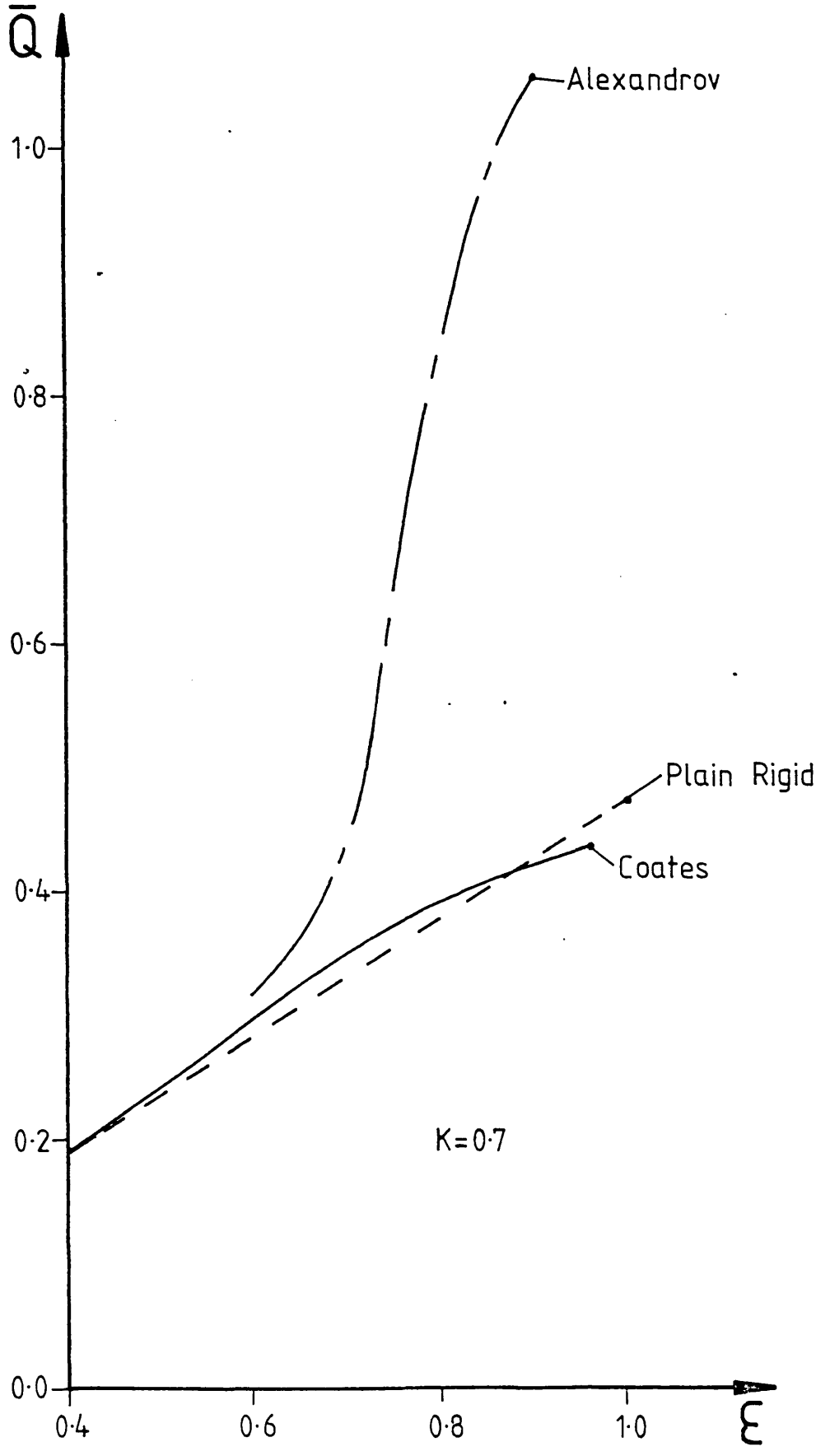


Figure 4.5. A Comparison Of The Results Of Alexandrov And Coates For Side Flow.

CHAPTER 5.

THE DESIGN AND COMMISSIONING OF THE EXPERIMENTAL APPARATUS.

5.1. Introduction.

As the validity of all theories depends on how closely they match physical measurements, so in this project experimental work was envisaged from the start. This was made even more necessary because of the differences in the theoretical results of Alexandrov and Coates presented in previous chapters. For this purpose a test machine was designed and commissioned.

5.2. Mechanical Design.

An overall view of the experimental apparatus with its ancillary equipment is shown in Plate 5.5., with a detailed view of the test head in Plate 5.6. An assembly drawing of the test head is given in Appendix A8.

The journal runs in a central fluid film test bearing supported by a slave roller bearing at either side. The journal was driven by an electric motor via pulleys through a torque limiter which

allowed for possible bearing seizure.

The test bearing was loaded using a commercial hydraulic cylinder and hand pump, acting through a pair of linkages and a hydrostatic bearing. Each linkage consisted of a pair of static spherical bearings to allow for load misalignment. The oil supply to the hydrostatic bearing was from a high pressure swash plate pump, and this was fed through a separate linear restrictor for each of the four bearing pockets to provide stiffness of the assembly under load.

A regulated supply from a gear pump fed the test bearing, the bearing inlet pressure being measured on a standard gauge, and the side leakage from the bearing splash lubricated the two slave roller bearings. These were sealed at their outer ends by flingers and labyrinth seals.

Provision was made for exchanging liners on the central part of the journal.

5.3. Instrumentation Design.

Various measuring systems were added to the basic mechanical apparatus. A schematic diagram of this instrumentation is shown in Fig. 5.7. A description of each system and its calibration is given in subsequent sections.

The electrical signals for film pressure

and film thickness were displayed on an oscilloscope. This was triggered once per revolution by a magnetic transducer opposing a steel pin on the journal. The trigger was set to start the trace when the pressure transducer was opposite the oil feed position, approximately the point of maximum film thickness.

An SAE 30 grade mineral oil was used in all the experiments. The variation of viscosity with temperature was measured using a Ferranti rotating cylinder viscometer, the results of which are shown in Fig. 5.8.

The nominal bearing diameter was 80 mm. and the nominal axial length of the liners used in all cases was 60 mm., giving a length to diameter ratio of 0.75.

5.4. Bearing Load.

The oil pressure in the loading cylinder was measured using a commercial gauge. The effective area of the cylinder (the ratio of load produced to cylinder pressure) was found by loading the plattens of a compression testing machine, the results of which are shown in Fig. 5.9. The calculated effective area (1776 mm^2.) was within 0.3% of the figure supplied by the manufacturers of 1781 mm^2. Hysteresis was noted on the unloading cycle, probably due to seal friction in the cylinder, and for this reason all experiments

were performed with increasing increments of load.

5.5. Journal Speed.

A magnetic transducer fixed to the machine frame opposed a 64 tooth gear wheel fixed to the journal. The transducer output was fed to a digital frequency meter. The angular velocity of the journal, ω, is given by $\omega = \frac{N}{64}$ r.p.s. where N is the measured frequency. The system was checked for a number of speeds against a Hasler contacting tachometer held on the end of the journal, and there was a difference of 1% at worst between the two sets of readings.

5.6. Bearing Friction.

The hydrostatic bearing separated the loading system from the test bearing assembly, thus allowing its free rotation. A torque arm, fixed to the test bearing, was constrained by a spring steel cantilever beam fixed to the machine frame. The end deflection of the beam was measured using a dial indicator with 0.0254 mm. divisions.

The variation of beam deflection with bearing friction was found by applying known forces to an arm of known length fixed to the test bearing opposite the torque arm. This was done in situ to allow for effects such as oil feed pipes. With zero calibrating

load, the dial indicator was zeroed with the journal running at low speed (approximately 0.5 r.p.s.) to overcome any dry friction. A calibrating load was then applied in 2.224 N increments and the beam deflection was measured giving the results shown in Fig. 5.10. Since the resultant curve was not linear, all test readings of beam deflection were converted to bearing friction by using linear interpolation between the calibration points.

The later addition of dial indicators to measure eccentricity ratio (section 5.9.) introduced a constant offset torque to the bearing. A counterweight was added to the torque arm to balance this, but there still remained a small resultant positive offset which changed due to small variations in the eccentricity dial indicator positions each time the apparatus was assembled. Therefore, at the start of each experiment, the beam dial indicator was zeroed with no load on the beam. The journal was then run at various speeds under no load, and the product of journal speed and film viscosity was plotted against beam deflection. Extrapolation of the results to zero speed then gave the beam deflection offset due to the residual torque which was then subtracted from all friction readings.

5.7. Oil Inlet And Film Temperature.

Oil film temperature was measured at four points of the bearing to allow an effective film

viscosity to be calculated. Holes were drilled to within 0.635 mm. of the bearing surface in the loaded region at $\pm$ 22.5^{o} to the vertical and 10 mm. either side of the centre plane. Copper-constantan thermocouples were then bonded in these holes with a conductive epoxy resin to give good thermal contact, and then the rest of the hole was filled with a plain epoxy resin (Araldite A.V.138/H.V.998) to strengthen the assembly. The wires were led out in grooves in the top surface of the bearing under the bearing cap. A fifth thermocouple was bonded into the oil feed pipe close to the bearing inlet to measure oil supply temperature. The signals from all five thermocouples were displayed on a Comark electronic thermometer. The system was checked by heating the bearing in a water bath and comparing readings with a mercury in glass thermometer known to be accurate to 0.2^{o}C. Both sets of readings were within 0.5^{o}C of each other.

5.8. Film Pressure.

Film pressure was measured using a commercial transducer, containing a semiconductor Wheatstone bridge. This had a range of 0 - 68.95 MN/m^{2} , a compensated temperature range of 15^{o}C - 71^{o}C , and required an excitation of 3.0 V D.C. which was supplied by two 1.5 V batteries in series.

The transducer was bonded into a bolt which

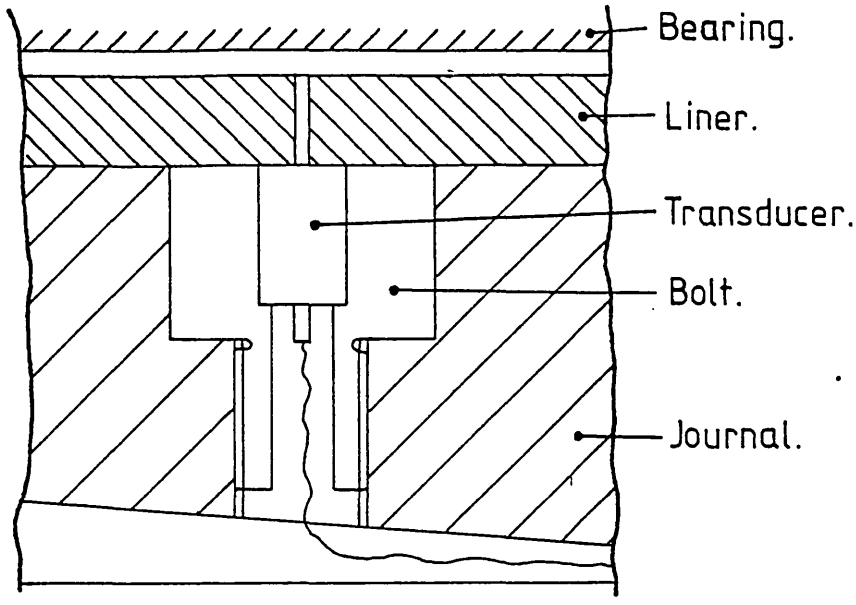


Figure 5.1. Pressure Transducer Mounting.

was screwed into the journal at the axial centre plane of the test bearing underneath the journal liner (Fig. 5.1.). Communication with the film was by means of a small hole in the case of a plain liner, and in the pocketed case the transducer was situated at the bottom of a pocket. Wires were taken out via a keyway and slip rings on the non-driven end of the journal. A calibration record was supplied by the manufacturers giving the following values for bridge output.

	% capacity	Output/mV
	0	0.00
ascending	50	97.38
	100	192.13
descending	50	96.52
	0	0.00

This was checked using a special bearing with an oilway machined through from a hole under one of the hydrostatic bearing pockets to the inside surface on the centre plane and good agreement was found up to pressures of 3.45 MN/m^2.

Applying a shunt resistance of 59 kΩ across the negative input and output of the bridge gave 3.2 mV output which corresponded to the manufacturer's figure of 3.17 mV. Hence, neglecting non-linearity, the manufacturer's figure of 192.13 mV for 68.95 MN/m^2 was used, giving the relationship $p = 0.1196 v_s V$ MN/m^2 where V is the supply voltage and v_s is the output signal in mV.

5.9. Eccentricity.

Initially, provisions were made to measure the eccentricity of journal and bearing centres using capacitance techniques. Probes of 3.175 mm. diameter were bonded using Araldite A.V.138/H.V.998 into rings rotating with the journal at either side of the liner (Fig. 5.2.). The probes were first thinly coated with the adhesive which was then cured to provide an insulating film. The probes were then bonded into the rings and the assembly was finish ground so that the probes were flush with the ring surface.

The probe formed part of a tuned circuit with a Southern Instruments oscillator in which changes

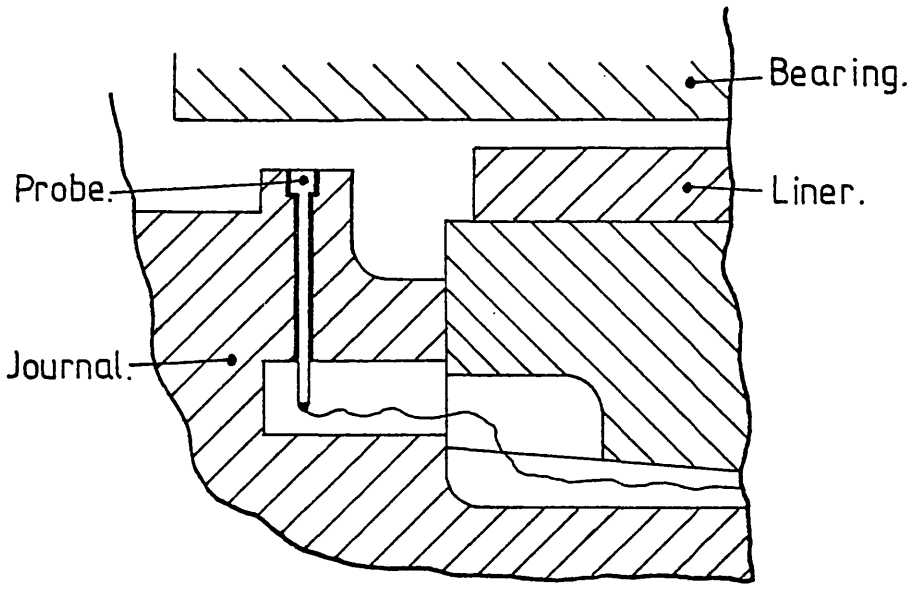


Figure 5.2. Capacitance Transducer Mounting.

in capacitance were detected by a change in bridge output voltage. Two methods of calibration were used.

Firstly, a direct method in which the bridge was balanced (i.e. the output voltage was zero) with the probe opposite a large film. The test bearing was then loaded against a rubber journal liner with the probe in the vertical position and the deflection of the bearing was measured with a dial indicator with divisions of 0.00254 mm. This deflection was then plotted against bridge output, taking the zero film to be when the bearing and probe touched.

Secondly, an indirect method was used in which known values of capacitance were injected in parallel with the probe while it was opposite a large film and the bridge output was measured. Use of the parallel plate capacitance law then gave a relationship between film thickness and bridge output.

The two methods gave fair agreement as can be seen from Fig. 5.11. However, early experiments with a rubber liner in place showed the probes to be unsuitable due to their small range. As a result, a new measuring system was devised with a greater range at the expense of a possible decrease in accuracy.

Four dial indicators with ranges of 12.7 mm. and divisions of 0.00254 mm. were fixed to the test bearing, one pair at each side to provide mean values. Each pair was set so that their measuring points touched the rings at the side of the liner, one in the vertical position, and one at 90^{o} to this. Special tips for the measuring points were machined from PTFE to allow for running on the journal. Thus, the deflection of the bearing centre relative to the journal centre in two orthogonal directions could be measured, so fixing the two centres in space.

The validity of this system was found by a commissioning test with a plain phosphor-bronze journal liner in place, so enabling comparison with established results for a plain, rigid bearing (section 5.12.).

5.10. Film Thickness.

Film thickness at nine discrete points in the loaded region of the bearing was measured using capacitance probes similar to those used initially

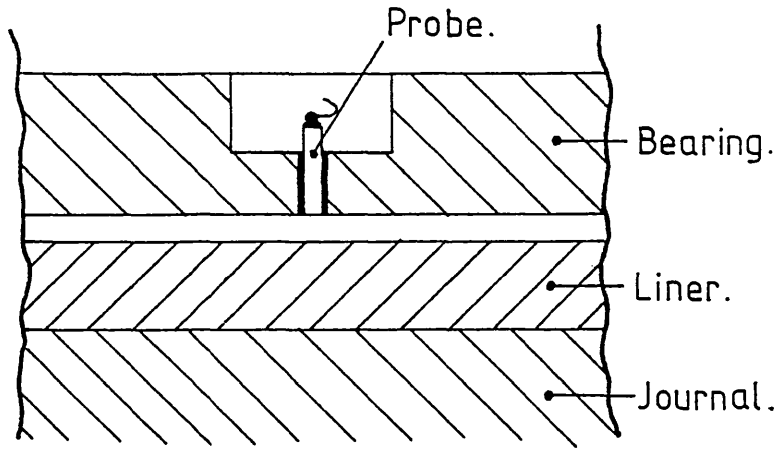


Figure 5.3. Film Thickness Transducer Mounting.

for eccentricity measurement (Fig. 5.3.). The nine probes were situated on the axial centre plane and $\pm$ 20 mm. to this, and at the vertical and $\pm$ 45^{o} to the vertical. The probes were 1.5875 mm. diameter and were mounted by first covering with an insulating film as before and then bonding into place. The wires were led out in grooves under the bearing cap and then through a nine way switch to the bridge circuit. On the inner surface of the test bearing, the probes were filed down close to the surface and then the bearing was finish honed.

As the two methods of calibration for the eccentricity probes gave good agreement, it was decided to rely on the indirect method, assuming the parallel plate capacitance law which is valid in this case as the diameter of the probe is large in relation to

the film thickness and hence edge effects are small.

The results of injected capacitance against bridge output voltage can be seen in Fig. 5.12. The bridge output is non-linear above approximately 19 pF and so excluding the two points above this the gradient is 6.77 pF/V.

The relative permittivity of the oil used in all experiments was found by measuring the capacitance of a Wayne Kerr dielectric cell firstly with air and then with oil between the plates. As the gap is the same in each case then $\frac{\varepsilon_{r,air}}{\varepsilon_{r,oil}} = \frac{C_{air}}{C_{oil}}$, and taking

$\varepsilon_{r,air} = 1.00006$ gave $\varepsilon_{r,oil} = 2.285$. Heating the cell in a water bath showed an increase of 0.079 %/^{o}C in the relative permittivity which was considered small enough to neglect in the calculation of film thickness. Taking the probe diameter as 1.5875 mm., and the permittivity of free space as $\frac{10^3}{36\pi}$ pF/m, gives

$h = \frac{5.91 \times 10^{-3}}{V}$ mm. where V is the bridge output voltage.

5.11. Commissioning Of The Experimental Apparatus.

Having calibrated all the measuring systems separately, a series of commissioning experiments were performed with a plain phosphor-bronze journal liner in place so that comparison with established

solutions could be made. The liner was fixed to the journal by four screws at the edges of the liner and at $\pm$ 90° to the pressure transducer. The liner was then finish turned in situ between centres to a diameter of 80.137 mm. giving a radial clearance of 44.45 μm.

The first test was distinctive in exhibiting pressure profiles which were not classical in shape (Fig. 5.13.). It was thought that this was due to non-circularity of the test bearing. In order to confirm this, the test bearing was rotated to positions of $\pm$ 20° from its normal circumferential position while under load. The resultant pressure traces are shown in Fig. 5.14. The two traces are not the same, which should be the case for a truly circular bearing neglecting the effect of changing the oil feed position. Measurement of the bearing with a bore gauge showed a circumferential variation in diameter greater than 0.01778 mm. and so a special lapping tool was made (Fig. 5.4.). By driving the cast iron sleeve up the taper the outside diameter of the lap could be increased. Lapping was performed with progressively decreasing grit sizes of silicon carbide (63 μm., 17 μm. grit size) and then aluminium oxide (17 μm., 13 μm., 9 μm. grit size).

Repeating the same test as before gave much closer pressure profiles (Fig. 5.15.). Measurement with a bore gauge showed a circumferential variation in diameter less than 0.00127 mm. The diameter of

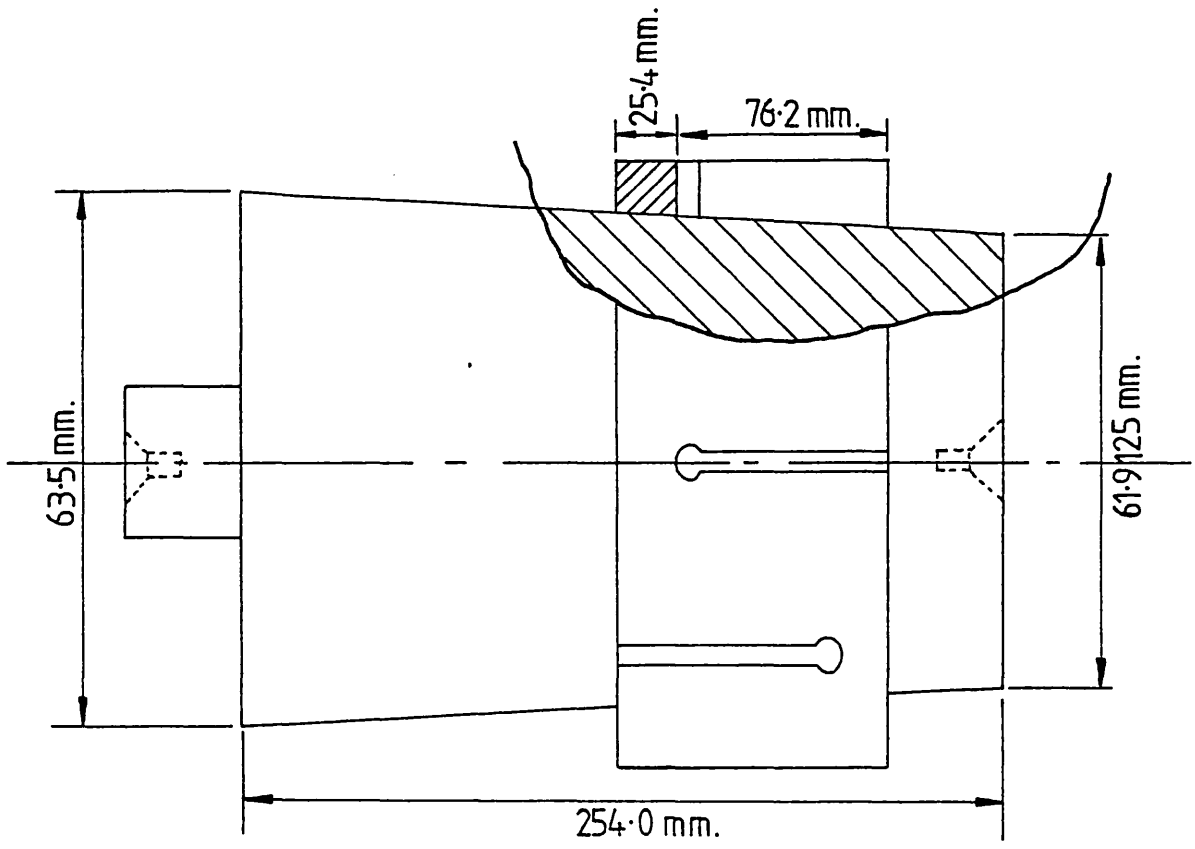


Figure 5.4. Bearing Lapping Tool.

the bearing was increased from 80.2259 mm. to 80.2767 mm. by these operations.

5.12. The Plain Rigid Journal Bearing.

Having been satisfied that the test bearing was now circular, a full test procedure was performed. A new phosphor-bronze journal liner was machined as before to a diameter of 80.0862 mm. giving a radial clearance of 95.25 μm. The results are shown in Figs. 5.16. to 5.20., together with the theoretical predictions using the analysis developed in Chapter 4.

For each condition of load and speed, the position of the journal centre relative to the bearing

centre was plotted directly from the mean values of each pair of dial indicators, giving values of both eccentricity ratio and attitude angle (Fig. 5.16.). The zero for the dial indicators was taken with the journal at rest and with the bearing resting on the journal under its own weight. This is the point $\varepsilon = 1.0$, $\phi = 0^{\circ}$.

In general, the results follow the classical solutions satisfactorily. The Sommerfeld number (Fig. 5.17.) and maximum film pressure (Fig. 5.19.) both show good agreement with theory. A small amount of distortion of the liner and bearing could explain the attenuation of these variables at high eccentricity ratios. Perhaps the least satisfactory result is that of friction (Fig. 5.18.). However, the theory of Chapter 4 does not include the effects of cavitation in its calculation. Assuming Couette flow in the cavitation region, then the sum of the streamer widths, L', is given by $L' = \frac{Lh_{cav}}{h}$ where h_{cav} is the film thickness at the point of cavitation. By multiplying each of the elemental shear stresses in the cavitation region by this reduced bearing width gives a better approximation to the bearing friction. The programme changes needed to include this were small, and the resultant curve shown as a dotted line in Fig. 5.18. gives better agreement with the experimental results. The values of film thickness (Fig. 5.20.) are

reasonably good despite being sensitive to the measurement of attitude angle.

On the whole, the results for a plain rigid bearing were considered sufficiently accurate and consistent to proceed to an examination of the trends involved in plain and pocketed elastic journal liners.

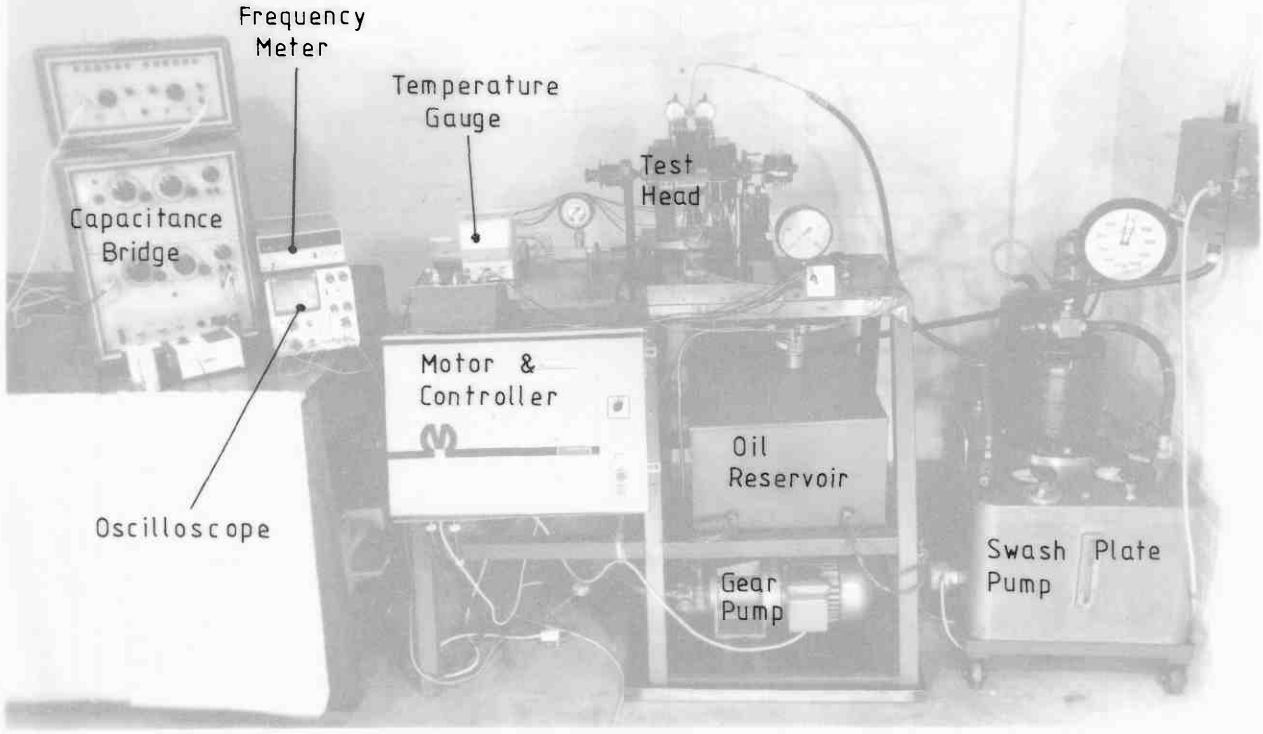


Plate 5.5. General View Of The Experimental Apparatus.

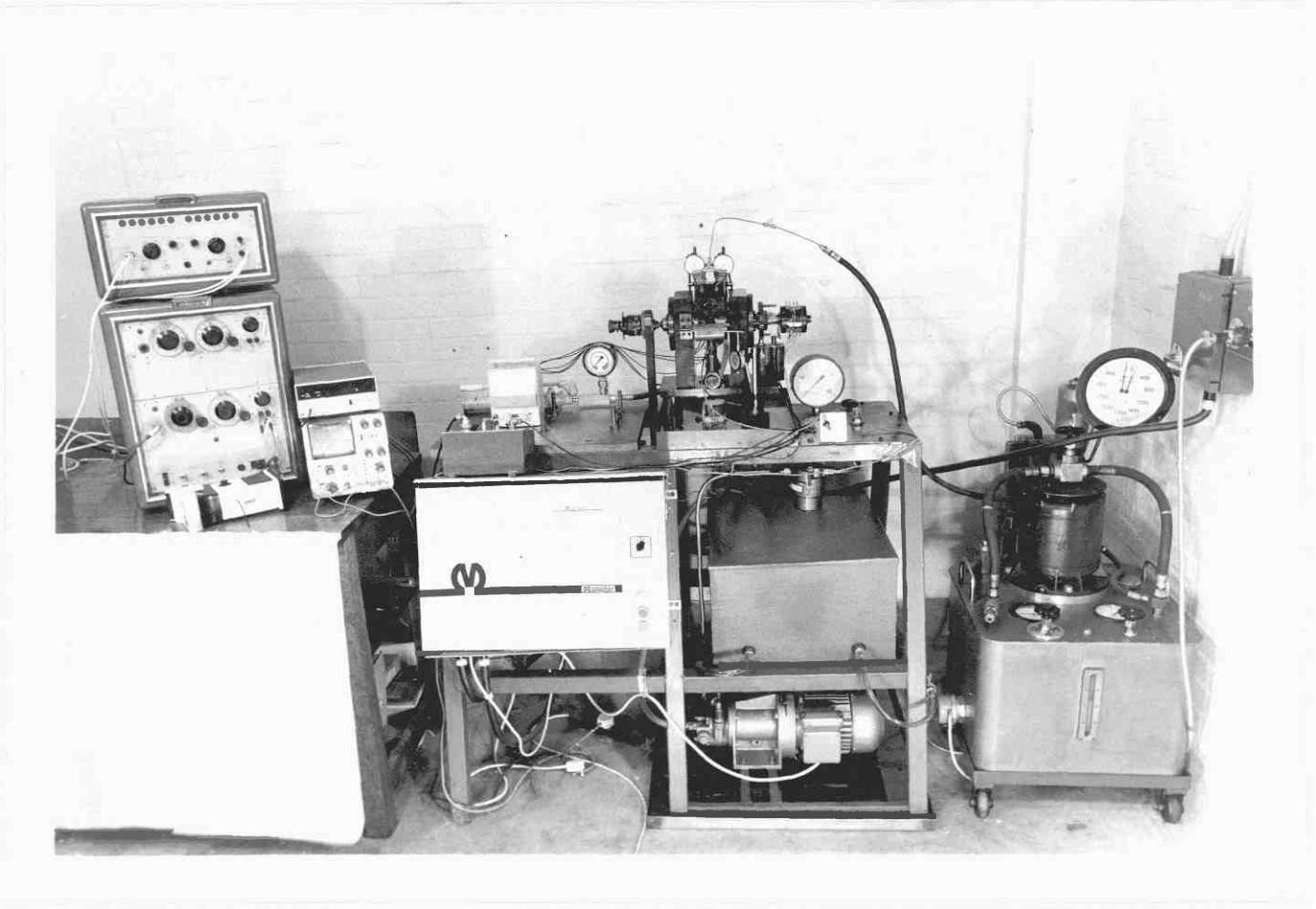


Plate 5.5. General View Of The Experimental Apparatus.

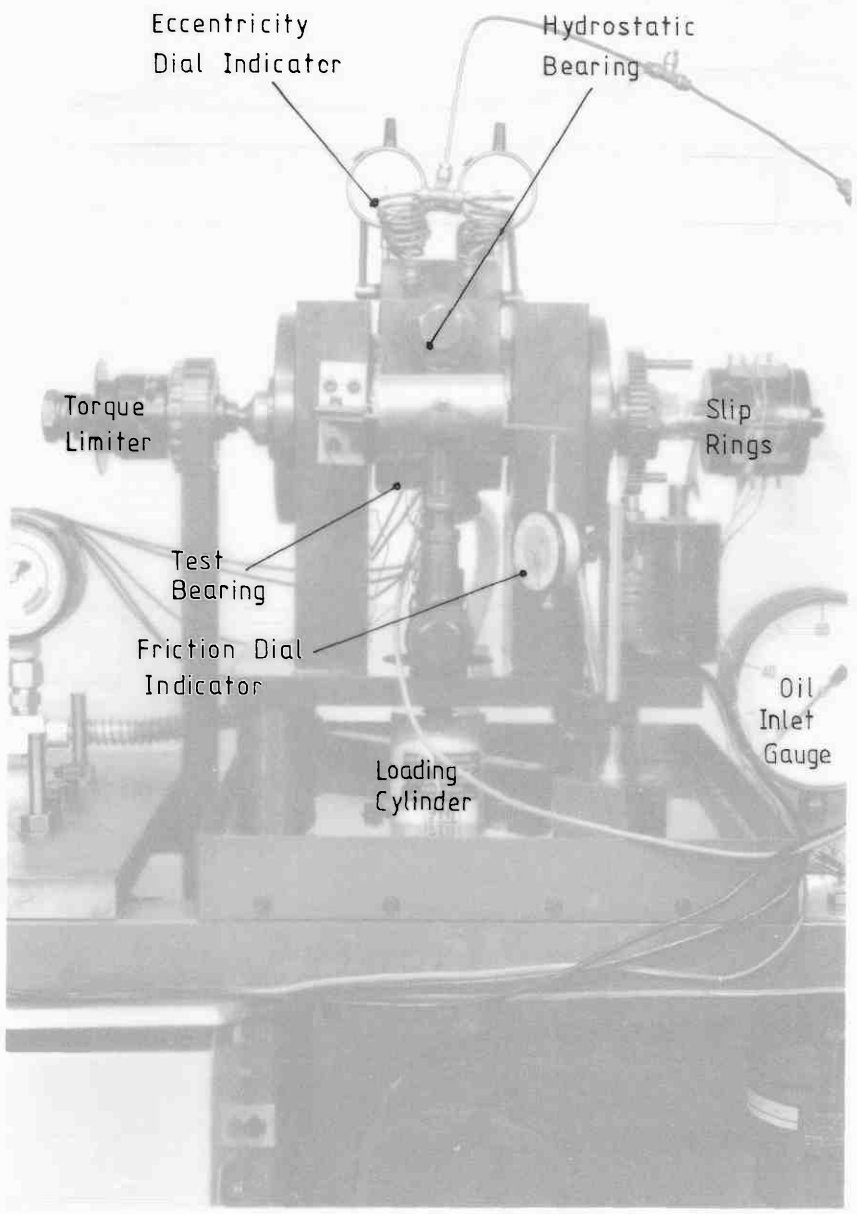


Plate 5.6. Detail View Of The Journal And Test Bearing Assembly.

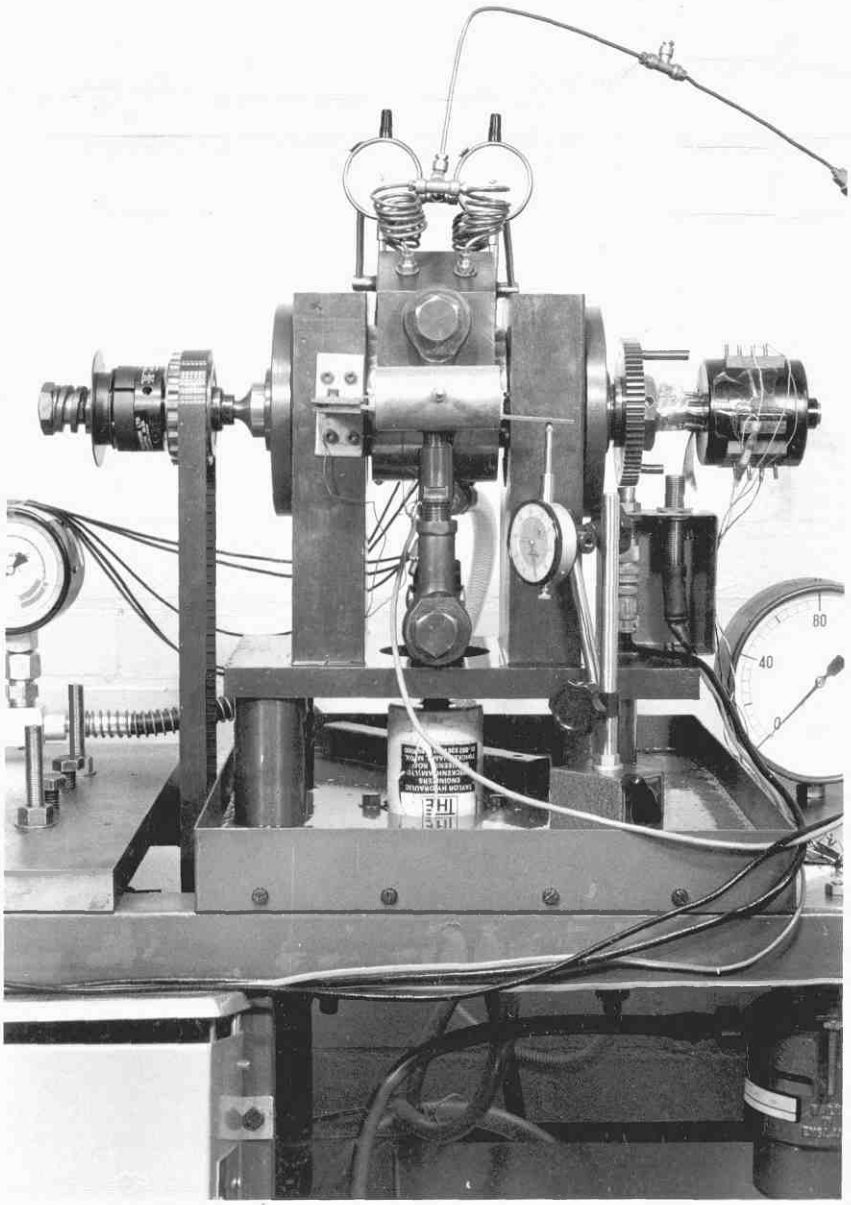


Plate 5.6. Detail View Of The Journal And Test Bearing Assembly.

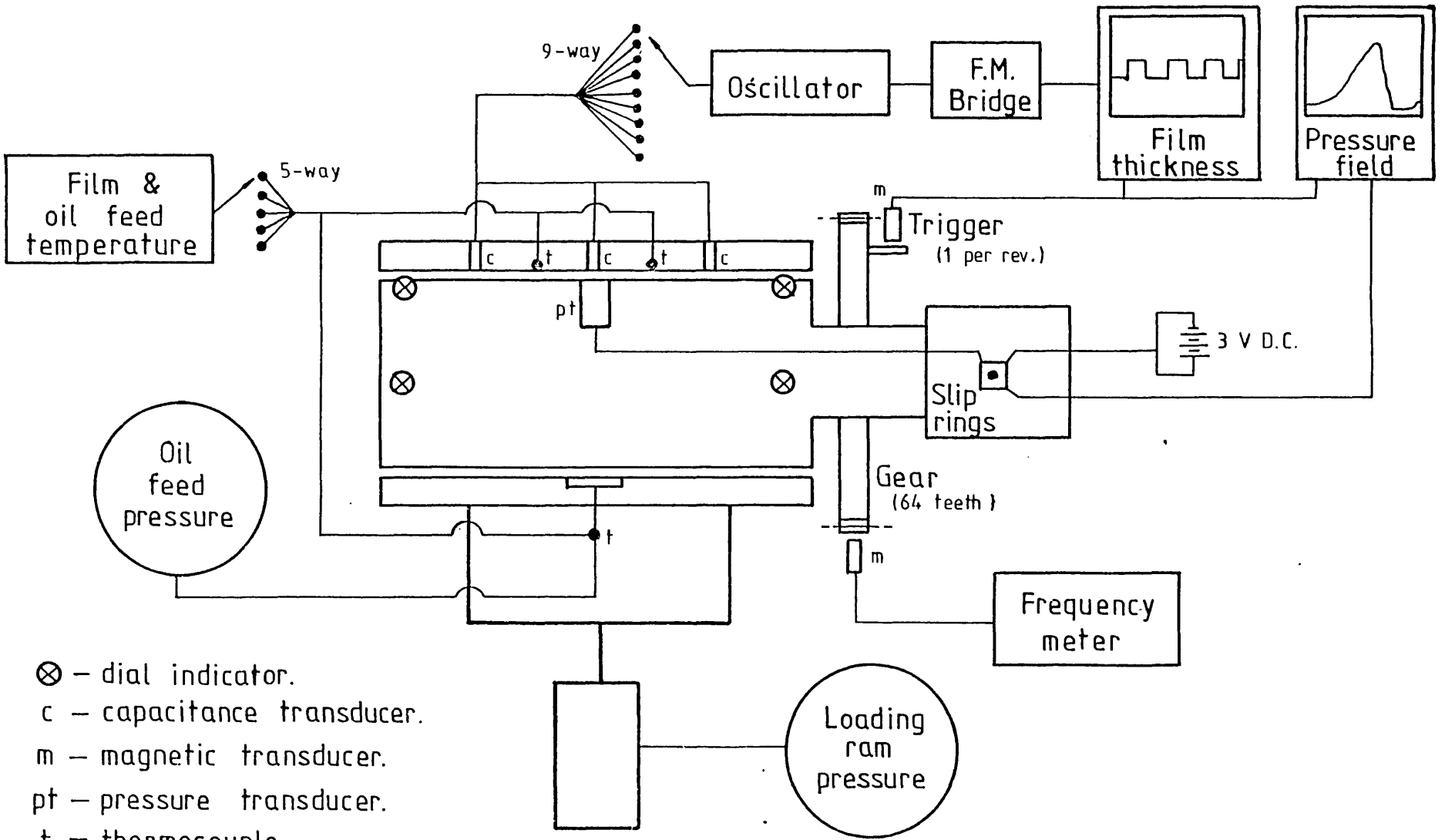


Figure 5.7. Schematic Diagram Of The Instrumentation.

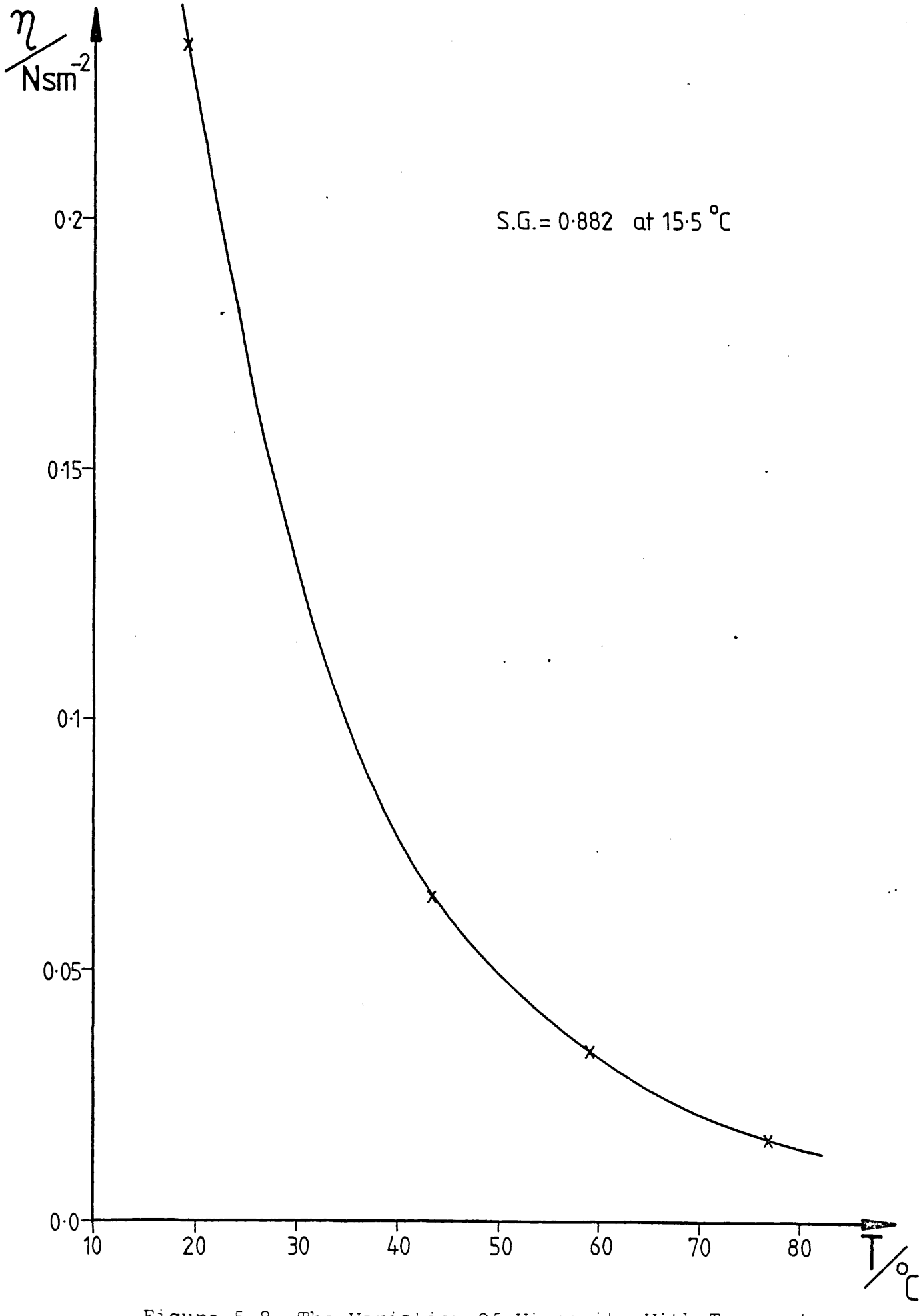


Figure 5.8. The Variation Of Viscosity With Temperature For The Test Oil.

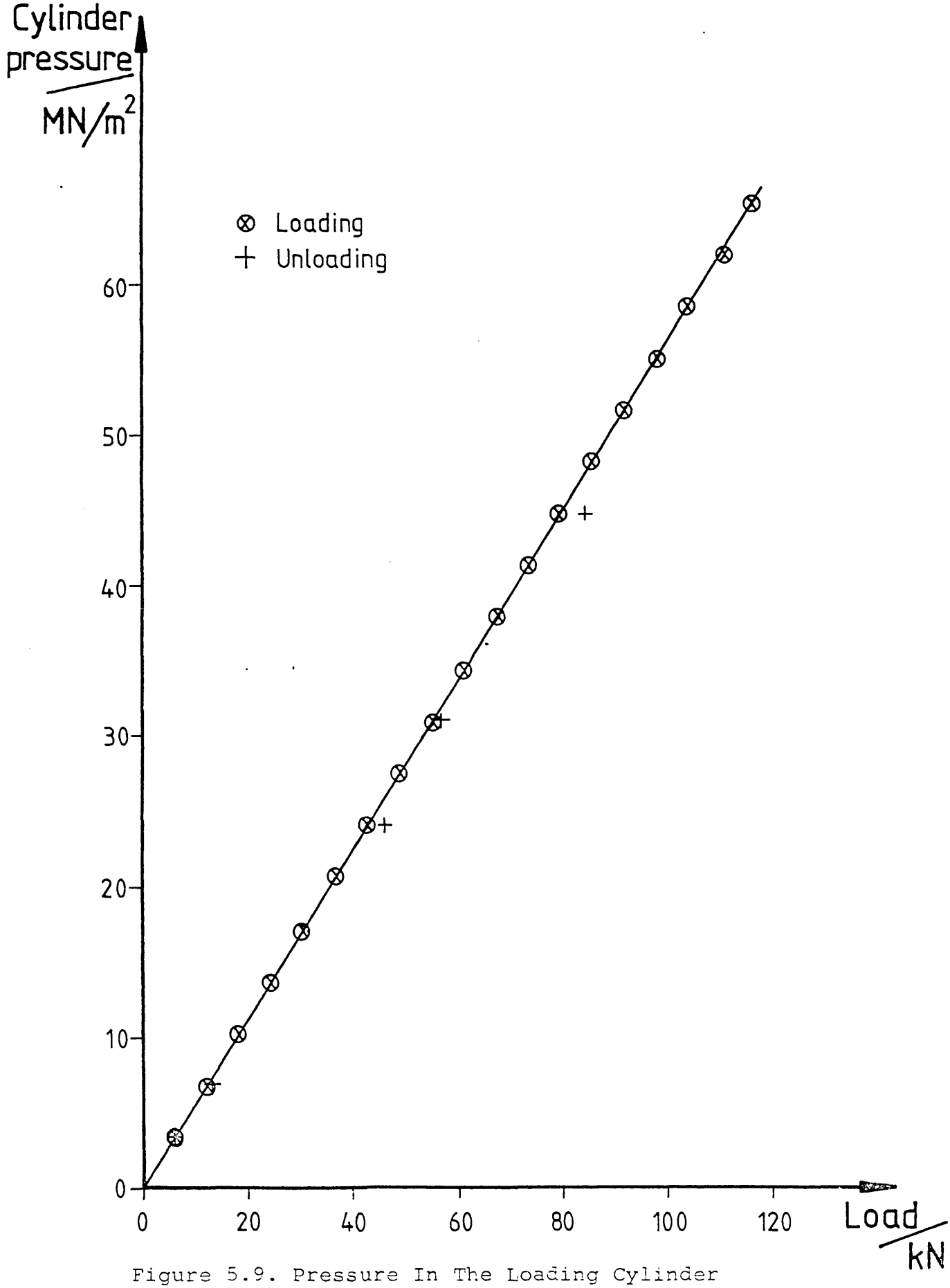


Figure 5.9. Pressure In The Loading Cylinder Against Measured Load.

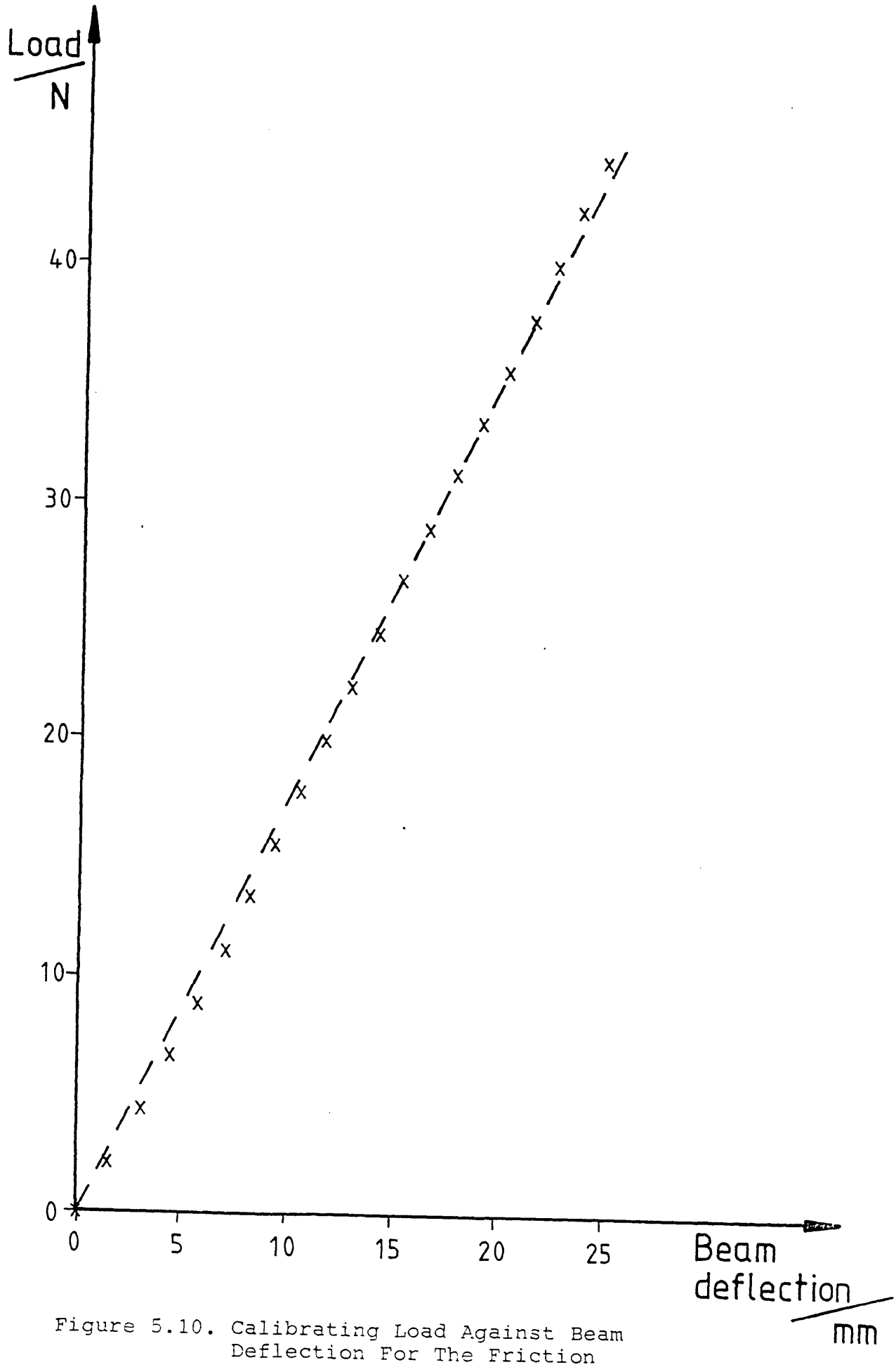


Figure 5.10. Calibrating Load Against Beam Deflection For The Friction Measuring System.

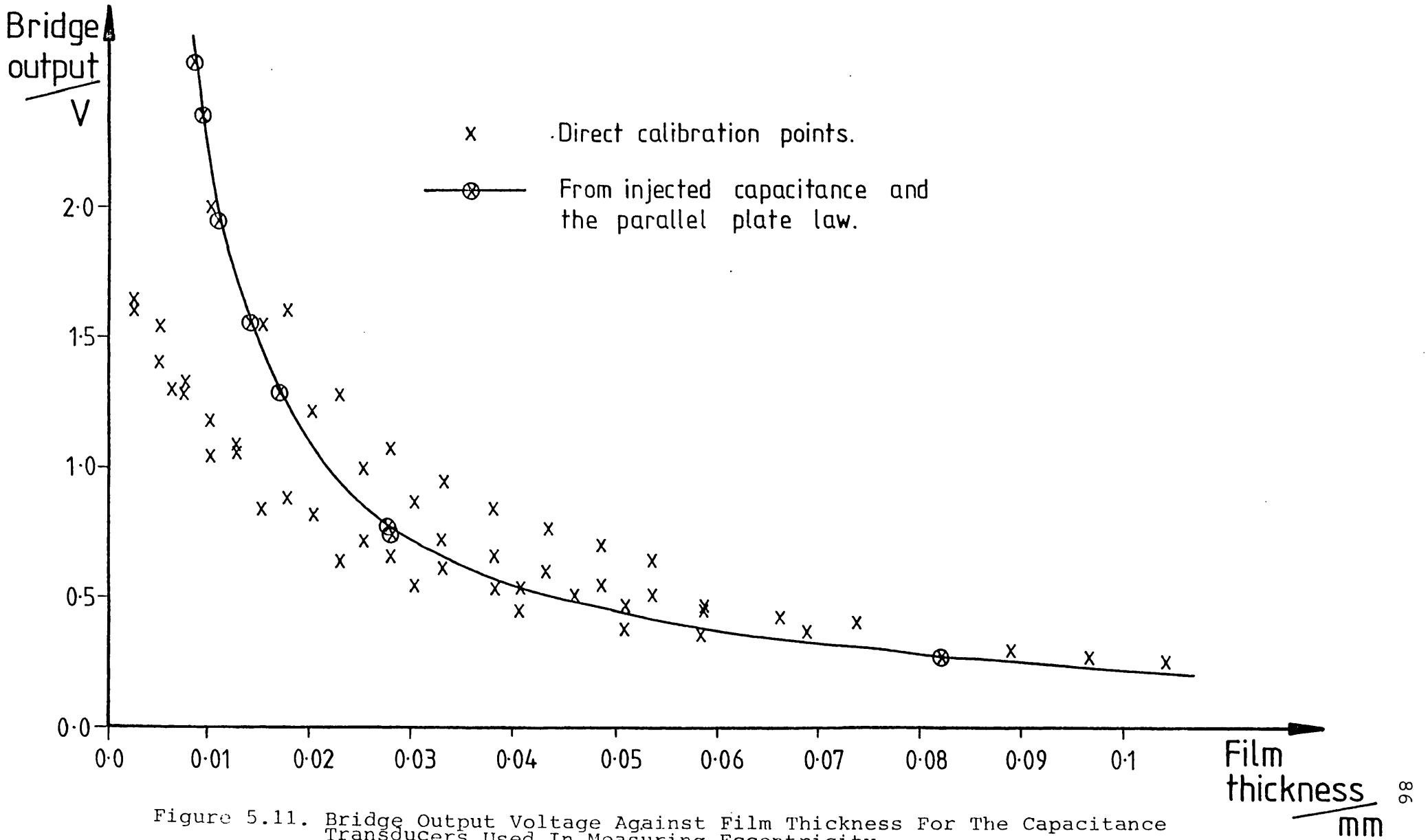


Figure 5.11. Bridge Output Voltage Against Film Thickness For The Capacitance Transducers Used In Measuring Eccentricity.

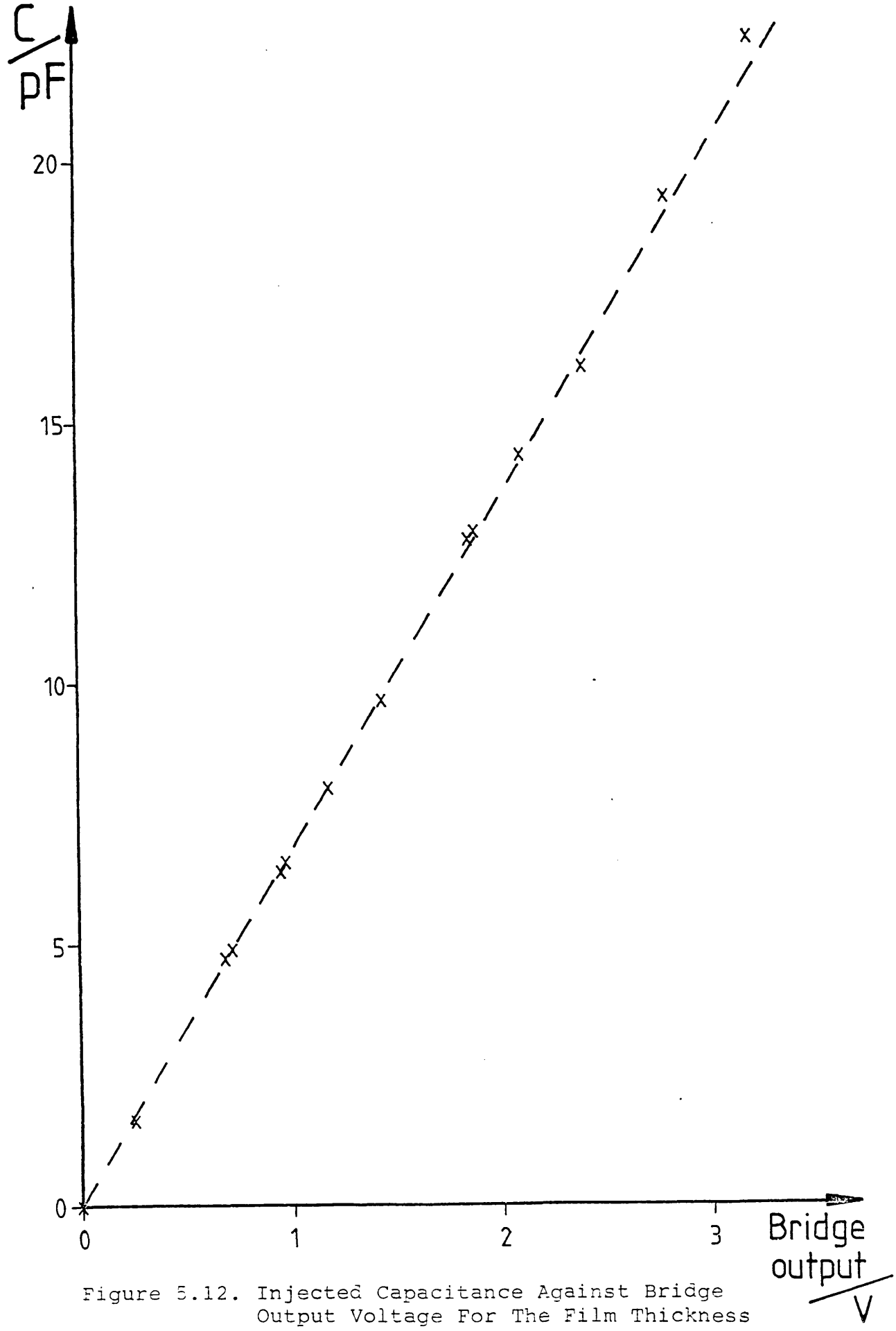


Figure 5.12. Injected Capacitance Against Bridge Output Voltage For The Film Thickness Transducers.

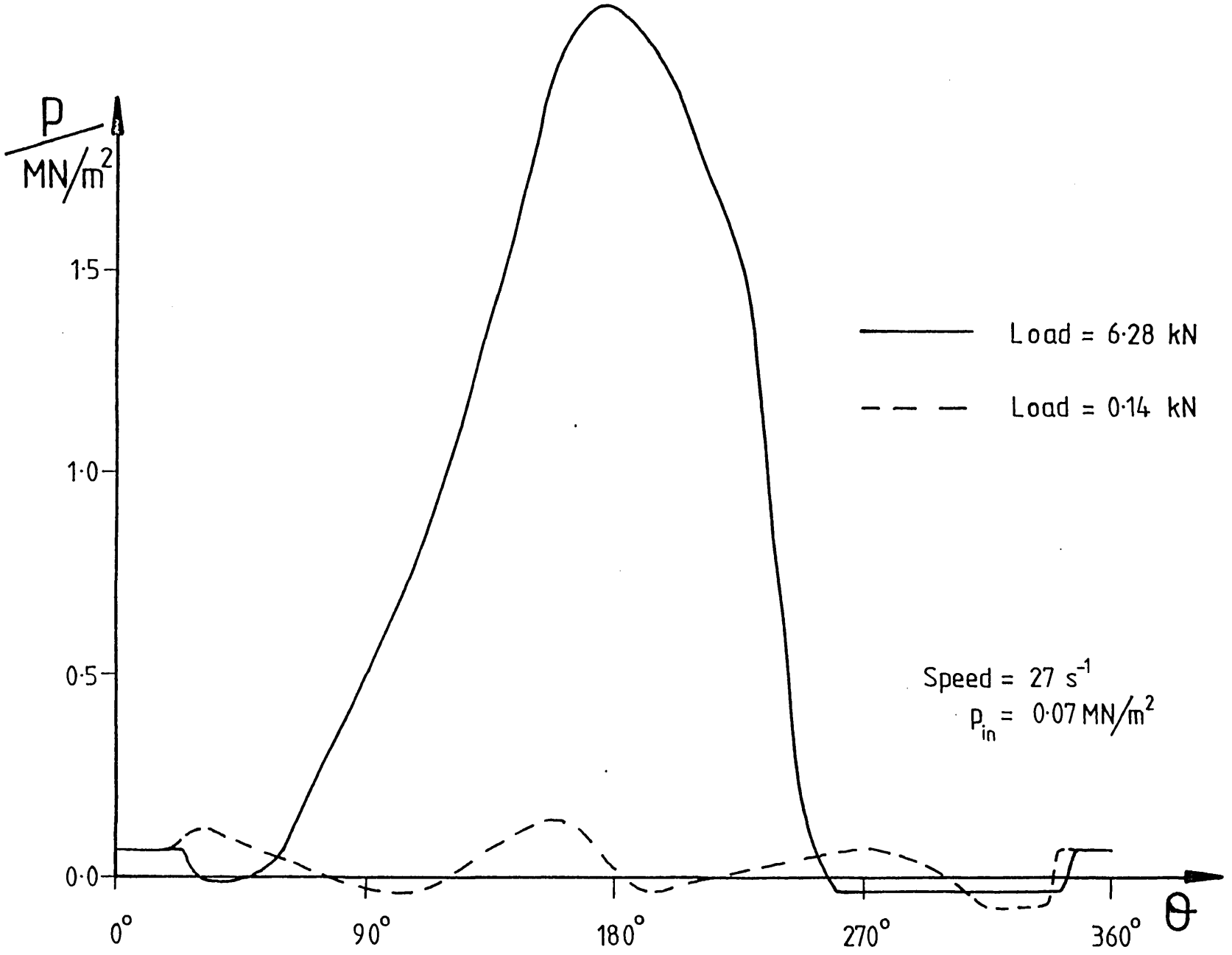


Figure 5.13. Pressure Profiles For The First Commissioning Test.

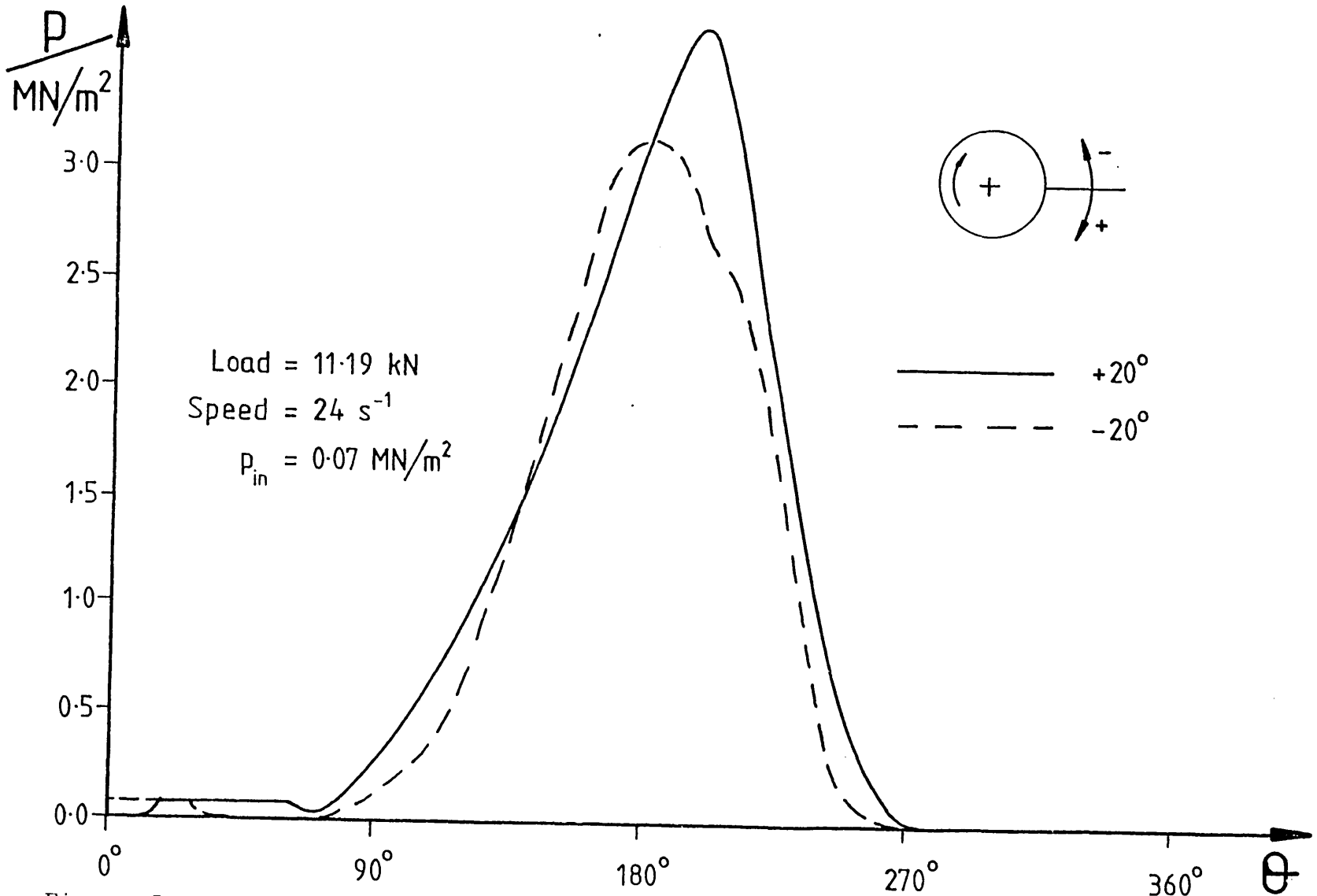


Figure 5.14. Pressure Profiles With The Test Bearing At Two Different Angular Positions. First Commissioning Test.

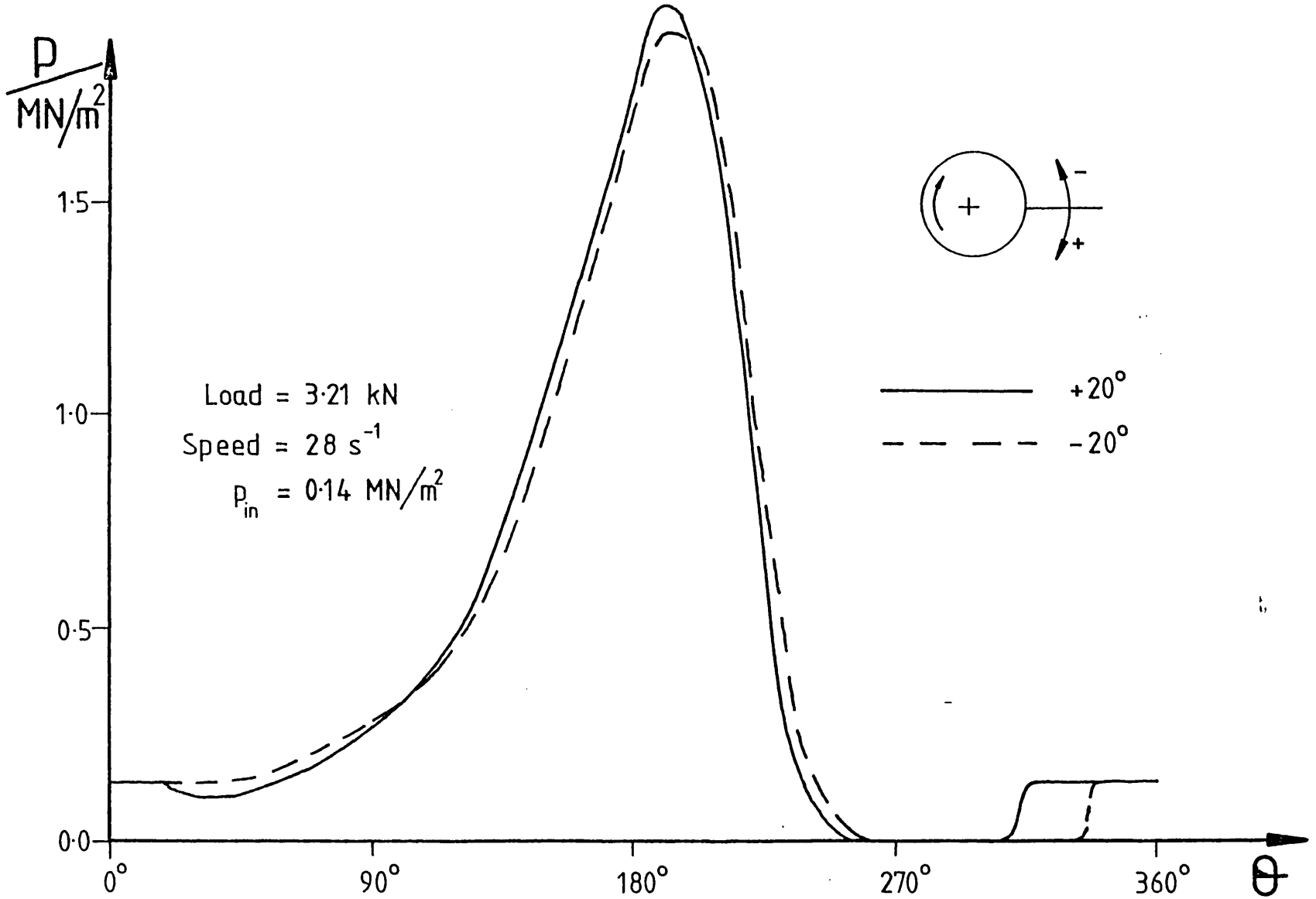


Figure 5.15. Pressure Profiles As In Fig. 5.14. After Lapping.

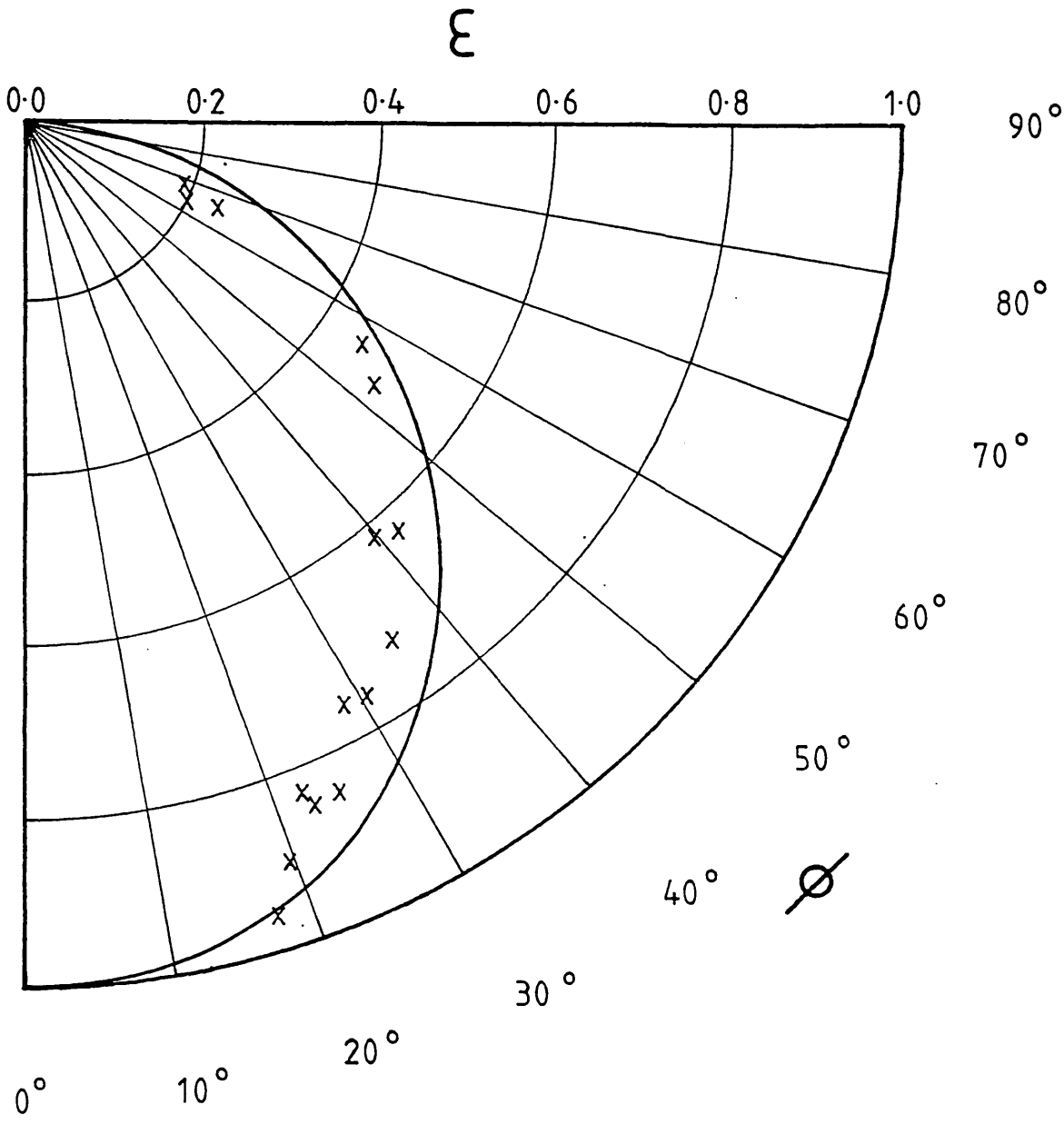


Figure 5.16. Attitude Angle For The Commissioning Test With A Plain Rigid Journal Liner.

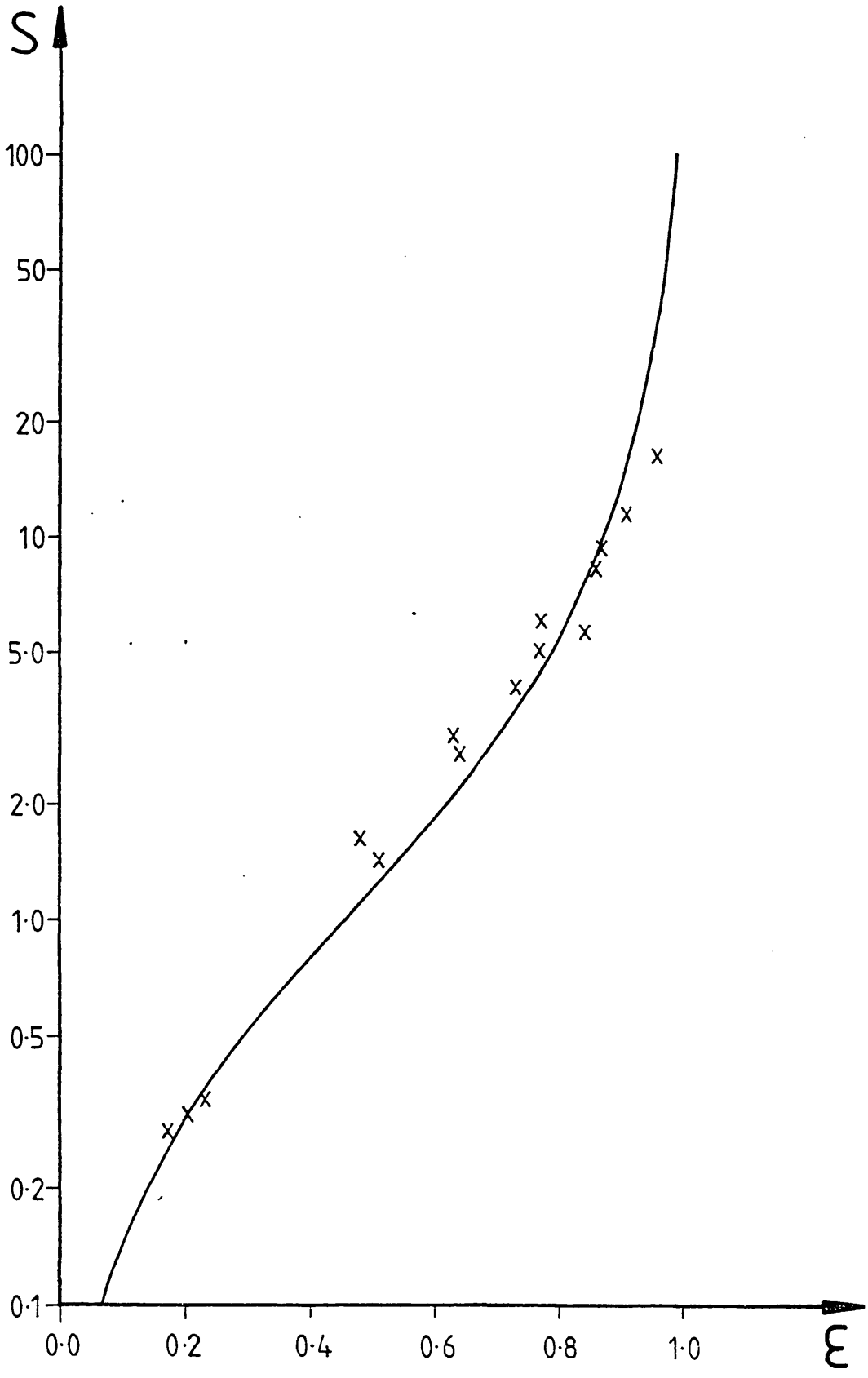


Figure 5.17. Sommerfeld Number For The Commissioning Test With A Plain Rigid Journal Liner.

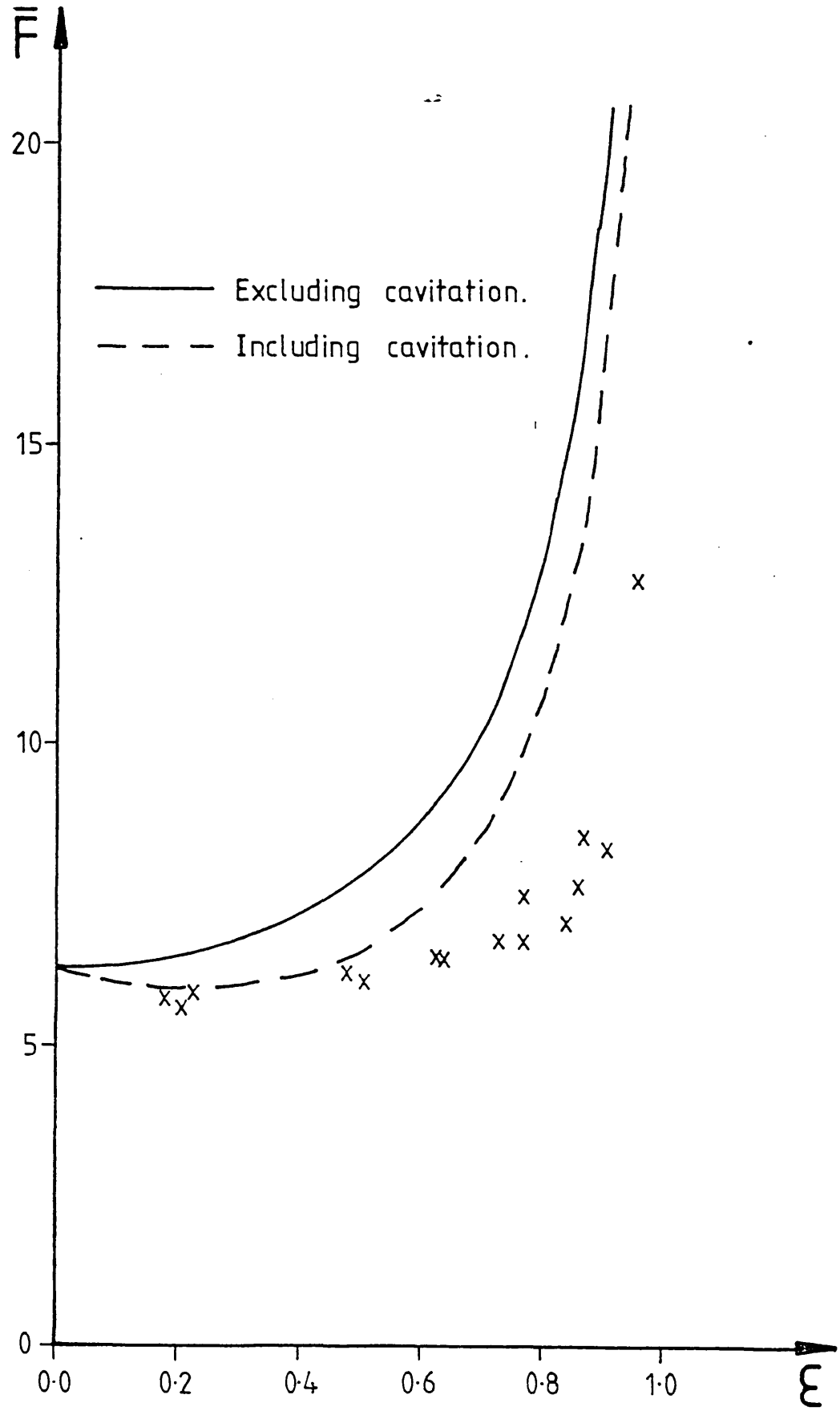


Figure 5.18. Friction For The Commissioning Test With A Plain Rigid Journal Liner.

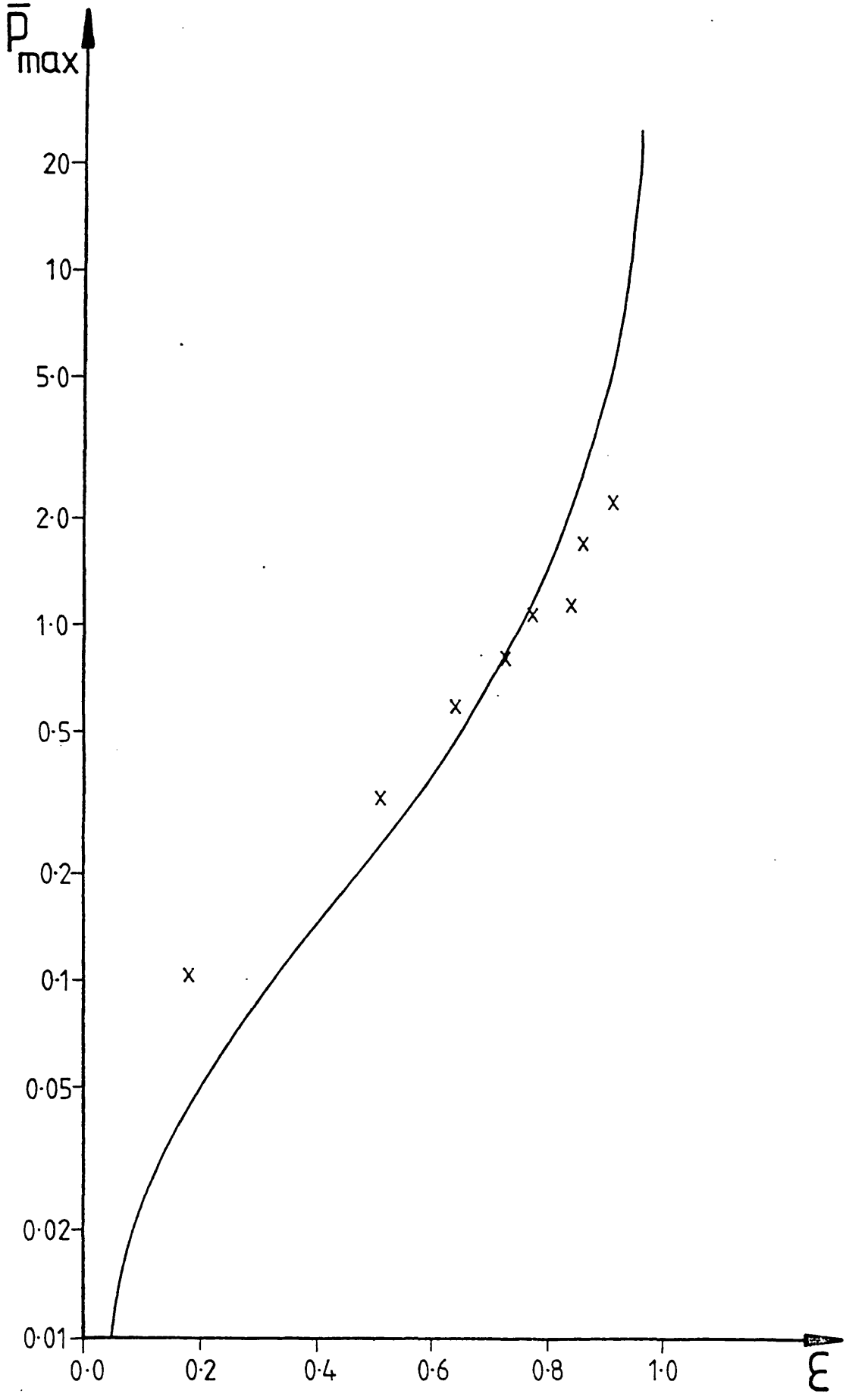


Figure 5.19. Maximum Film Pressure For The Commissioning Test With A Plain Rigid Journal Liner.

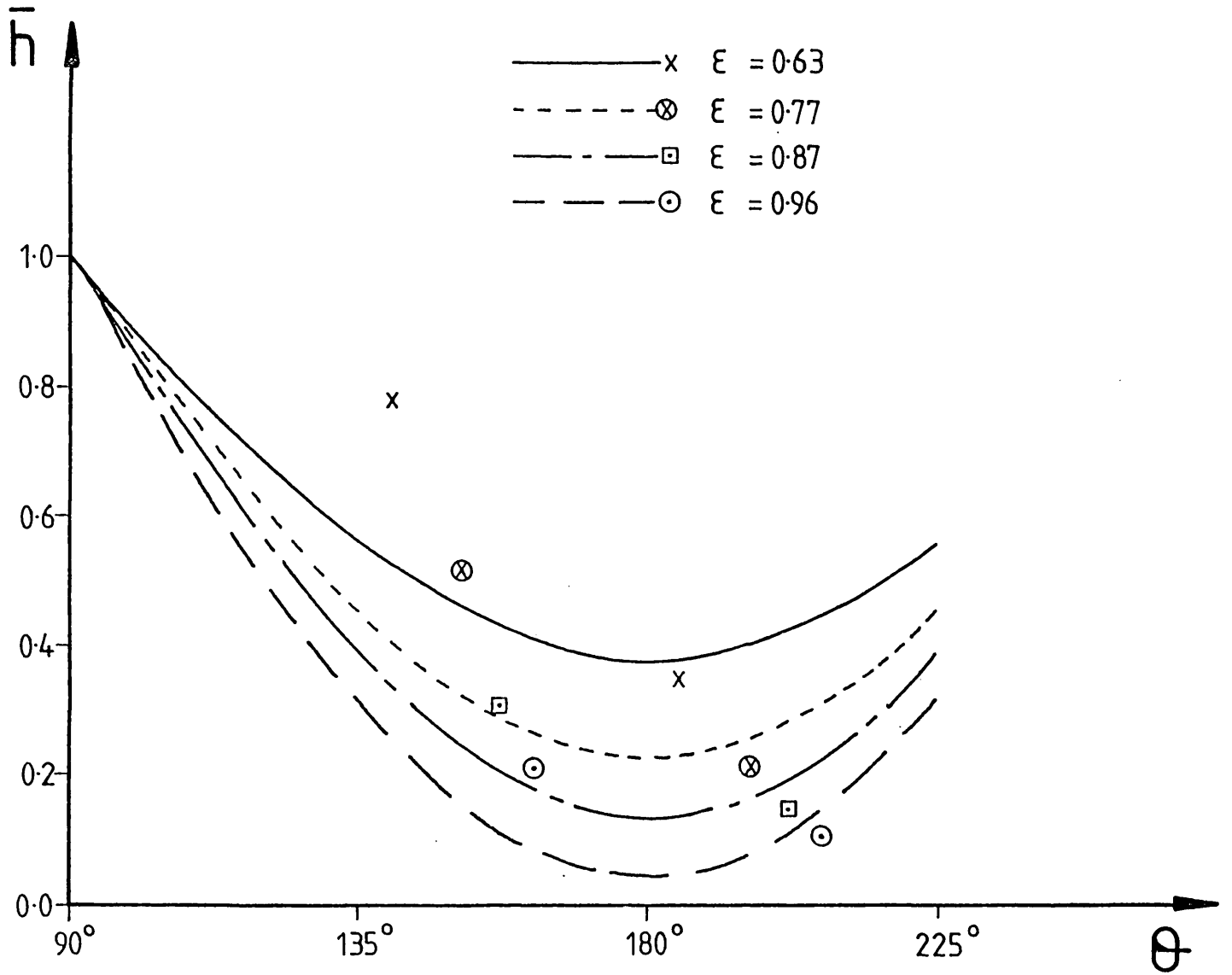


Figure 5.20. Film Thickness For The Commissioning Test With A Plain Rigid Journal Liner.

CHAPTER 6.

THE HYDRODYNAMIC BEARING WITH POCKETED ELASTIC JOURNAL LINERS.

6.1. Introduction.

Having obtained satisfactory results for a plain rigid bearing, the main part of the experimental work with rubber journal liners was performed in order to correlate with the theory and hopefully to resolve the differences between the results of Alexandrov and Coates outlined in Chapters 2, 3 and 4.

The four series of experiments are presented in chronological order in subsequent sections.

6.2. Journal Liner Material.

Although interferometry has successfully been used in the study of rubber/fluid/metal interfaces in the past (31,32), in this work its use was excluded due to the large film thicknesses involved. However, others have employed a capacitance method by rendering the rubber conductive with the addition of large amounts of carbon black (33), and this was the approach adopted in this case.

After discussions with a manufacturer, tubes

of a conductive silicone rubber were supplied whose properties are listed in Table 6.1. After cutting to length, the liner (which was an interference fit on the journal) was bonded on the inner surface to the journal using silicone room temperature vulcanising (RTV) adhesive. The outside diameter of the liner was then finished using normal grinding methods. Milling techniques for the pockets proved unsuccessful, but hand cutting the pockets with a sharp blade gave acceptable enough results.

The swelling of rubber in liquids is a well known phenomenon (34). In order to avoid problems such as clearances changing during a test series, a sample of the rubber 2.54 mm. thick was soaked in oil and the change in thickness was measured. The swelling of 76.2 μm. after 40 hours was recorded with no further change after 1 month and no visible signs of degradation. For this reason, the liners were soaked in oil for at least 2 days before mounting on the journal and finish grinding.

6.3. Experimental Procedure.

The experimental procedure followed was similar in all tests.

Each time the apparatus was assembled (for example, when a liner had been changed) a new offset was found for the friction measuring system (section 5.6.). Then, with the journal brought up to speed, increments

of increasing load were applied and readings of eccentricity, bearing friction, inlet and oil film temperature, film thickness and maximum pressure were taken. Pressure and film thickness traces were recorded on film from the oscilloscope for selected conditions of interest.

In order for comparison to be made with the theoretical predictions, a value for the Elasticity factor, K, needed to be found. Poisson's ratio for rubber is very close to 0.5, that is the material exhibits a near incompressible behaviour. In general, the stiffness of rubber structures is a function of the unloaded area into which the material can deform. In simple cases such as compression blocks of rectangular section, the compressive modulus of rubber is strongly influenced by the 'shape factor' (35), defined as the ratio of the cross sectional area to the total force free (side face) area. The situation in the case of the present pocketed journal liners is more complex, and as the value of the Elasticity factor is zero for a Poisson's ratio of 0.5 (due to the simplifying assumptions used in the distortion theory), it was considered better to estimate K from in situ experimental measurements as follows.

The liner distortion at the positions of the three film thickness transducers on the centre plane of the bearing was calculated as the difference between the measured (elastic) film thickness and the rigid film thickness at these points derived from the

measurement of eccentricity ratio and attitude angle. The pressure at these points was also known from the experimental pressure profiles. Thus, the stiffness of the liner could be calculated as the ratio of the measured liner distortion at a point to the measured pressure at that point. The method is approximate (for example, distortions are measured on the lands whereas the pressures are measured as the pocket passes through the same point), and fairly large local variations in K were found (up to 25% in some cases) for which a mean value was taken, but the method was considered satisfactory in producing a value of K for input to the theoretical analysis.

In all pocketed cases there were 8 pockets, taking half the pitch circumferentially and axially, and all tests except one were performed with an inlet pressure of 68.95 kN/m^2.

6.4. Test Series 1.

The first rubber journal liner was plain. It was ground to a diameter of 79.934 mm. giving a radial clearance of 171.5 μm. The Elasticity factor was measured to be 0.73.

The results for the plain liner show good agreement with the theory (Figs. 6.2. to 6.6.). The attitude angle is increased and both the Sommerfeld number and friction are attenuated at high eccentricity

ratios compared with a rigid bearing. The film thickness at discrete points matches well with the theoretical profiles. The pressure profiles also agree well, and show an interesting negative pressure loop (relative to atmosphere) which corresponds approximately to zero absolute pressure.

Pockets were then cut in the liner and as a result the radial clearance decreased to 158.8 μm., possibly due to relieving the hoop stress caused by the liner being an interference fit on the journal. The Elasticity factor was measured to be 2.5, the change from the plain case possibly being due to a reduced effectiveness of the bonding or an increase in unloaded (side face) area due to the presence of pockets.

For the first test (Run 1) for the pocketed case, film thickness traces showed an unexpectedly small film at the leading edge of a land, particularly at high load. This was accompanied by an oscillation in bearing friction at the highest eccentricity ratio for this test (Fig. 6.9.). The liner also came loose, slipping round the journal at the highest load causing the test to be abandoned.

The liner was therefore removed from the journal and the assembly was cleaned. The liner was replaced on the journal and adhesive was spread on the axial ends of the liner/journal. No bonding was present under the liner in this case.

It was thought that the small film thicknesses at the leading edge of a land noted in Run 1 could be caused by the land lifting due to oil being forced under it. In an attempt to avoid this, a layer of the rubber adhesive was placed on the bottom and sides of each pocket, so forming a seal between the lands and the journal. This was kept to a minimum to avoid detracting from the pocket effect.

The results for Run 2 are shown together with those for Run 1 in Figs. 6.7. to 6.9. Both runs show good agreement with the theoretical predictions, particularly with the results of method 1 for pocket pressure analysis. The variation in theoretical predictions for the two positions of the maximum film thickness (corresponding to one sixteenth of a revolution in the experiments) was reflected during the tests in an oscillation of the dependent variables, particularly of the friction and eccentricity dial indicators. In the majority of cases these oscillations were small, and a mean reading was taken, an exception being the friction reading for Run 1 where the end points of the oscillation are shown.

6.5. Test Series 2.

As the journal liner had come loose in test series 1, a new liner was bonded to the journal and ground to a diameter of 80.035 mm. giving a radial

clearance of 120.7 μm. More care was taken with both the degreasing of the journal and bonding of the liner. The Elasticity factor was measured to be 3.3.

The results for this liner shown in Figs. 6.10. to 6.12. confirm those of test series 1, agreeing with established trends for a plain elastic bearing. The attitude angle is increased at high eccentricity ratios compared with a rigid bearing. The Sommerfeld number and friction are decreased compared with a rigid bearing due to the distortion decreasing the overall film convergence and therefore pressure generation, and increasing the mean film thickness respectively.

Eight pockets were then cut in the liner, and because of the problem mentioned in test series 1 of the lands lifting a thin layer of adhesive was placed on the bottom and sides of each pocket, except for the pocket containing the pressure transducer to prevent attenuation of its reading. The radial clearance was found to have changed to 139.7 μm., and the Elasticity factor was measured to be 3.2.

The experimental results for attitude angle, Sommerfeld number, friction and maximum film pressure (Figs. 6.13. to 6.16.) follow the theoretical predictions well, in general lying between the two curves for the two maximum film thickness positions at the leading and trailing edges of a land.

The friction again oscillated at high eccentricity ratios (Fig. 6.15.), accompanied by zero

film thickness being observed for the land immediately following the pocket containing the pressure transducer. As the sealing adhesive had been left out of this pocket, this would confirm the mechanism of oil being forced under and lifting the land, although some of the oscillation must be due to the pocket-land combination passing through the region of minimum film thickness as demonstrated in the theoretical analysis.

The closeness of the Elasticity factor for the plain and pocketed cases in this test series fortunately allows a direct comparison of the two liners to be made (Figs. 6.17., 6.18.). Although the Sommerfeld number is similar for both plain and pocketed liners, the friction for the pocketed liner rises above that for the plain liner as the eccentricity ratio increases.

It is perhaps more valid to compare hydrodynamic bearings, particularly elastic ones, on the basis of a performance factor, ξ, defined as the ratio of Sommerfeld number to dimensionless bearing friction, rather than on the basis of eccentricity ratio, since a true test of bearing efficiency is the load that can be carried for a given minimum film thickness, since the friction gives an indication of the mean minimum film thickness. Sommerfeld number and friction are plotted in Fig. 6.19. for the results of this test series and for the commissioning test of Chapter 5 for a plain rigid bearing, with lines of constant ξ for reference. It is seen that the pocketed

bearing has the highest performance at low Sommerfeld numbers due to the presence of pockets reducing the overall friction. Unfortunately, this region corresponds with an eccentricity ratio for a plain rigid bearing of 0.0 to 0.4, a range which would indicate over design of a practical bearing. At higher Sommerfeld numbers the performance of the pocketed bearing flattens out, becoming less than that for both rigid and elastic plain bearings due to a larger rise in friction.

The experimental pressure profile for a pocketed liner shows a difference from the theoretical result (Fig. 6.20.). Although the profiles are not directly equivalent (the theoretical profile gives the pressure around the film at a particular instant of time, whereas the experimental profile is the pressure in a single pocket during one complete rotation of the journal), a comparison can be made by considering that the experimental curve should pass through the mid-point of the theoretical pocket pressures. In general, the peak pressure is lower but the cavitation angle is greater, so producing a similar Sommerfeld number (Fig. 6.14.). A reproduction of the earlier theoretical results for an infinitely long bearing is interesting in this respect (Fig. 6.21.). It is seen that the pressure profile for the more exact finite element distortion treatment produces a lower peak pressure and later cavitation angle than that for the simple distortion treatment. (In both cases,

however, the pressures and cavitation angle are less than that for a plain elastic bearing). It would therefore appear that a closer correlation between the experimental and theoretical pressure profiles would have been shown had a more exact treatment of distortion been used for the finite length bearing. This would suggest that the earlier theoretical explanation of the large rise in friction being caused by early cavitation is less applicable than was at first thought.

6.6. Test Series 3.

The same liner as for test series 2 was used for this series. The pocket containing the pressure transducer was filled with adhesive to avoid the problems mentioned in the last test series. The radial clearance was found to have changed to 146.1 μm. The Elasticity factor was measured to be 2.5.

The first run showed the land following the pocket containing the pressure transducer to have a non-zero film thickness. However, this time another land showed a zero film thickness at high loads. On inspection of the liner, the pocket immediately preceeding the land in question showed a crack in the sealing adhesive. The filling was therefore removed, the pocket cleaned and then refilled.

In the second run, no land exhibited a zero film thickness. However, there was a variation in mean film thickness between the eight lands, probably due to dimensional variation caused by slightly dissimilar cutting of the pockets and the irregular spread of adhesive.

It was thought that a possible explanation of the lower performance of the pocketed bearing could be that air bubbles trapped in the pockets detracted from the self pressurizing effect. In an attempt to test this, the third run was performed with two different bearing inlet pressures of 68.95 kN/m^2 and 344.75 kN/m^2. If any air was present, then it was hoped that the higher inlet pressure would 'flush' it out.

Attitude angle, Sommerfeld number and friction for the three runs are shown in Figs. 6.22. to 6.24. All the results show the same trends, including the results for the high inlet pressure so reducing the possibility of air in the pockets derating the bearing. In general, the results confirm those of series 1 and 2. Friction is again seen to oscillate at high eccentricity ratios, even without any lands exhibiting zero film thickness.

6.7. Test Series 4.

To avoid any dimensional variation in the pocketed liner, such as that mentioned in test series 3,

the liner was reground. The pocket filling was cut out of the liner used in test series 2 and 3. The journal was then cleaned, the liner bonded in place, the pockets refilled and the assembly was ground. Due to grinding, the radial clearance increased to 177.8 μm.

A different approach to the correlation of theory with experiment than that of previous tests was adopted. Formerly it had been found that the product of journal speed and film viscosity changed by small amounts during a test series. Although the tests were performed at nominally constant speeds, the electric motor speed dropped slightly under load and the film viscosity decreased with increasing load. For simplicity, however, a constant value of $U\eta$ was used in computing the Elasticity factor. In this test series a different Elasticity factor was calculated for each experimental condition. In fact the Elasticity factor varied from 1.088 to 1.209, but the effect of this on the theoretical trends was small.

Attitude angle, Sommerfeld number, friction and maximum film pressure (Figs. 6.25. to 6.28.) again show good agreement with the theoretical predictions up to an eccentricity ratio of 1.0, although the trends of low Sommerfeld number and high friction continue in the experimental results up to an eccentricity ratio of greater than 2.0. At the highest load, friction readings became impossible and the torque limiter cut out, the bearing having seized. On inspection, the

liner had twisted around the journal, breaking the bonding. Previous to this no lands had exhibited zero film thickness, and the smaller dimensional variation between lands produced by regrinding the liner allowed larger applied loads and hence greater eccentricity ratios. However, results for the theoretical analysis could not be produced for eccentricity ratios greater than approximately 1.0 due to the simple distortion treatment producing minimum film thicknesses close to the rigid case.

Comparing the experimental results for this test series with the plain rigid bearing of Chapter 5 on a performance basis (Fig. 6.29.) reveals the same trends as in test series 2. The pocketed bearing has a higher performance at low Sommerfeld numbers corresponding with plain rigid eccentricity ratios in the range 0.0 to 0.5, but at higher loads the larger friction for the pocketed bearing reduces the performance below that of the plain rigid bearing.

The discrepancy in experimental and theoretical pressure profiles is again observed (Fig. 6.30.), the lower experimental maximum pressure being reflected in Fig. 6.28. As was noted in test series 2, the early cavitation for the theoretical analysis cannot be used as a major explanation of the large rise in friction for the pocketed bearing, as the experimental pressure profile shows a larger cavitation angle. Fig. 6.31. is interesting in this respect, showing experimental film shapes for a land passing under one of the film

thickness probes. The shapes show a striking similarity with the theoretical results of the finite element distortion treatment of Chapter 3 (Fig. 3.8.), both demonstrating elastohydrodynamic type constrictions at the leading and trailing edges of a land. This small local film thickness must produce a rise in local shear stress so increasing bearing friction, the oscillation observed in Fig. 6.27. being produced by the variation in film thickness across a land and also between pocket and land. Similar film shapes were observed in all the earlier test series.

Having been satisfied as to the consistency of the experimental trends obtained and their overall agreement with the theoretical predictions, a discussion of the discrepancies of these with the original concept of bearings with pocketed elastic journal liners and with Alexandrov's earlier theoretical work is needed.

Hardness, BS^{o}	75
Specific Gravity	1.18
Tensile Strength, MN/m^{2}	5.516
Elongation At Break, %	120
Compression Set Resistance, % (22 hours at $150^{o}C$)	20
Volume Resistivity, ohm-cm	4.0
Thermal Coefficient Of Cubical Expansion	$677x10^{-6}$ $/^{o}C$

Table 6.1. Physical Properties Of Conductive Silicone Rubber, Grade X1116B.

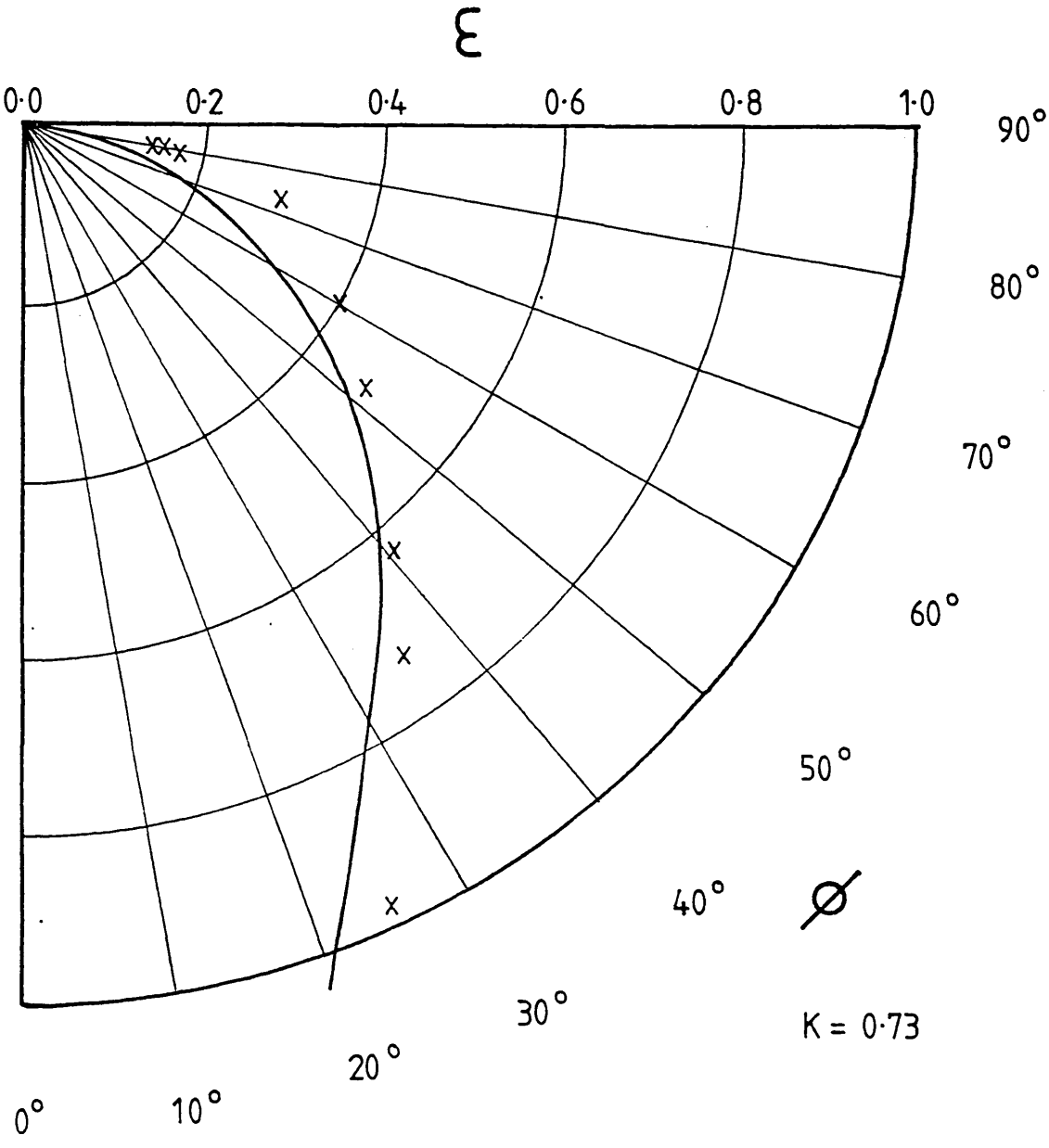


Figure 6.2. Attitude Angle For A Plain Liner.
Test Series 1.

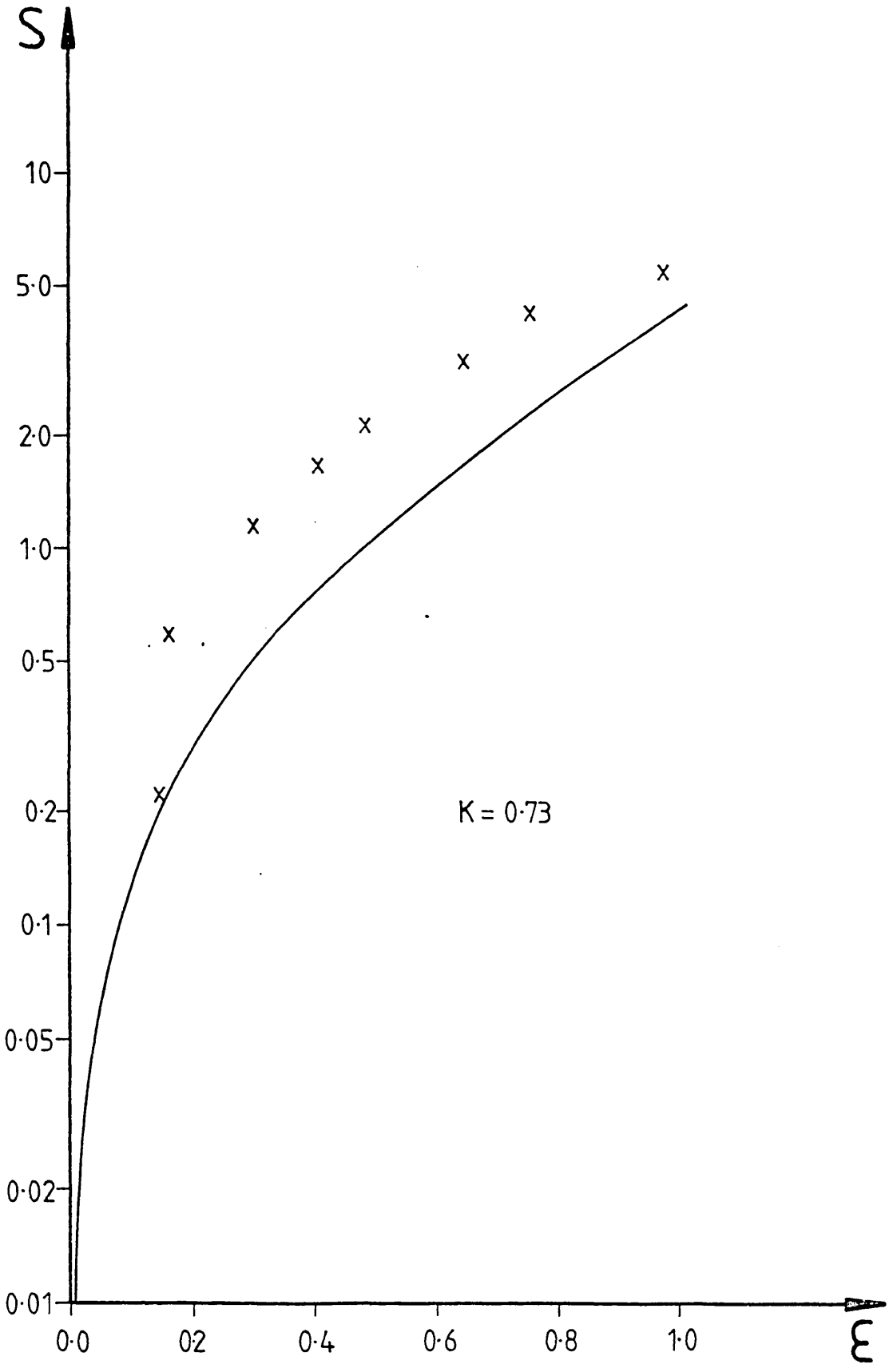


Figure 6.3. Sommerfeld Number For A Plain Liner.
Test Series 1.

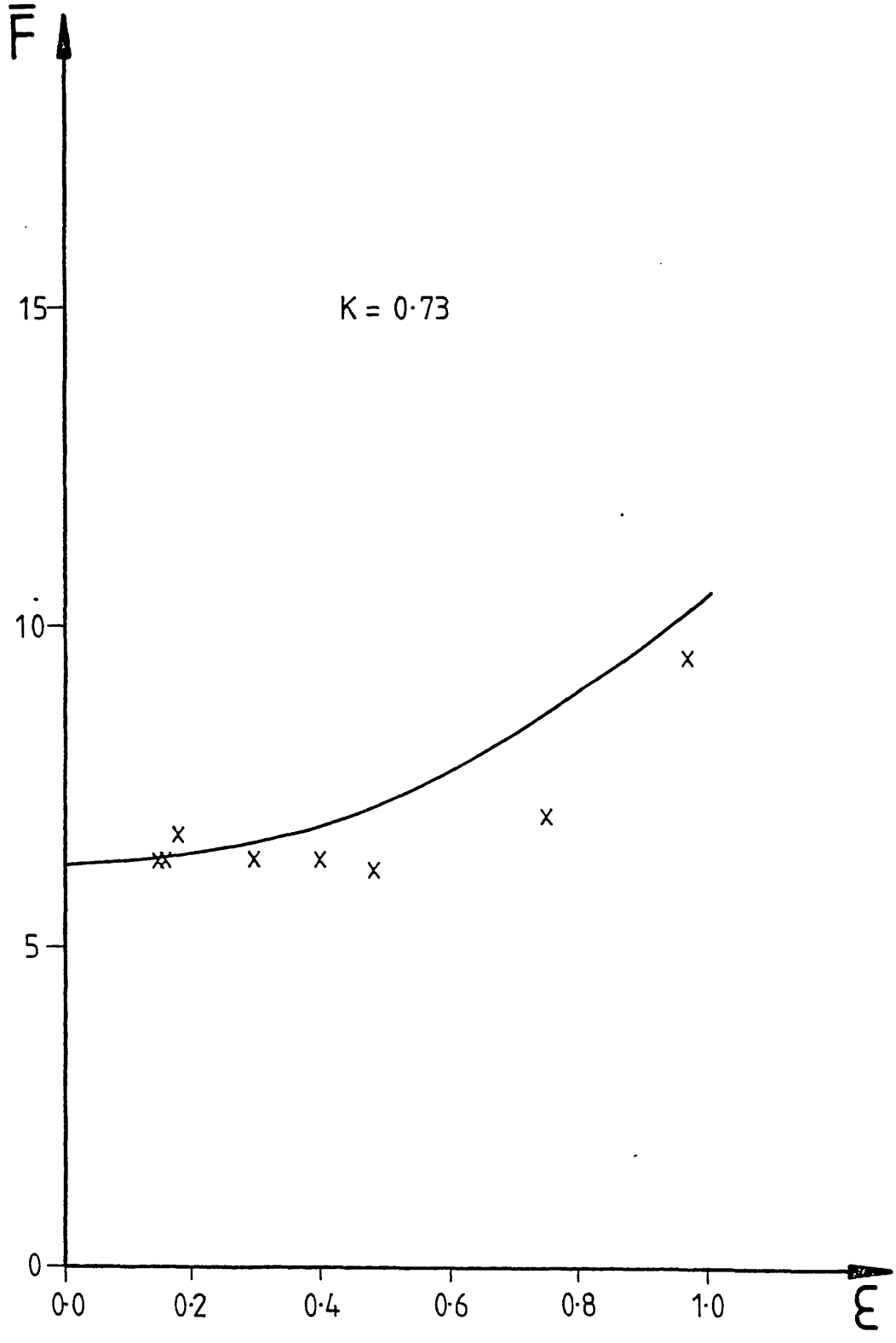


Figure 6.4. Friction For A Plain Liner.
Test Series 1.

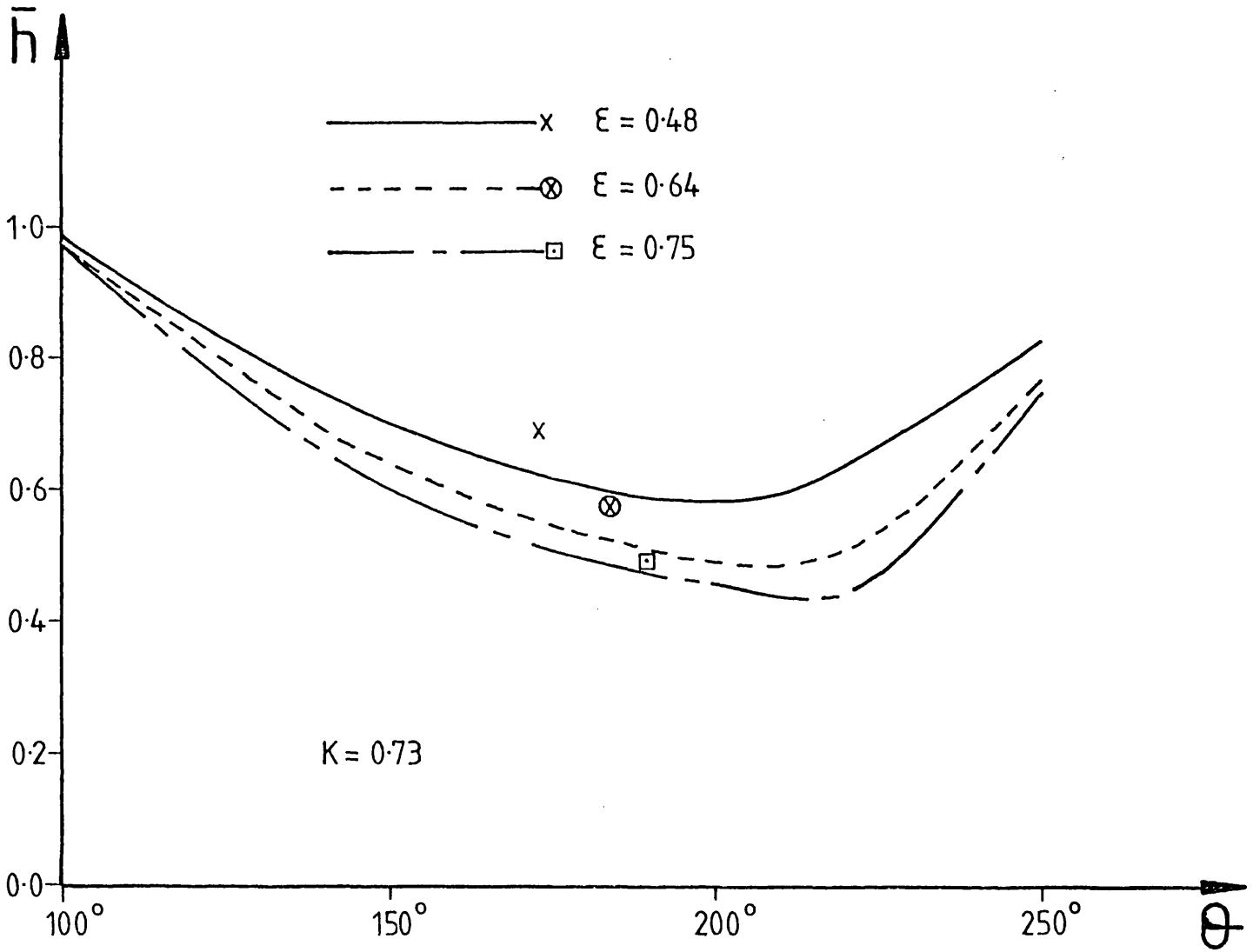


Figure 6.5. Film Thickness For A Plain Liner. Test Series 1.

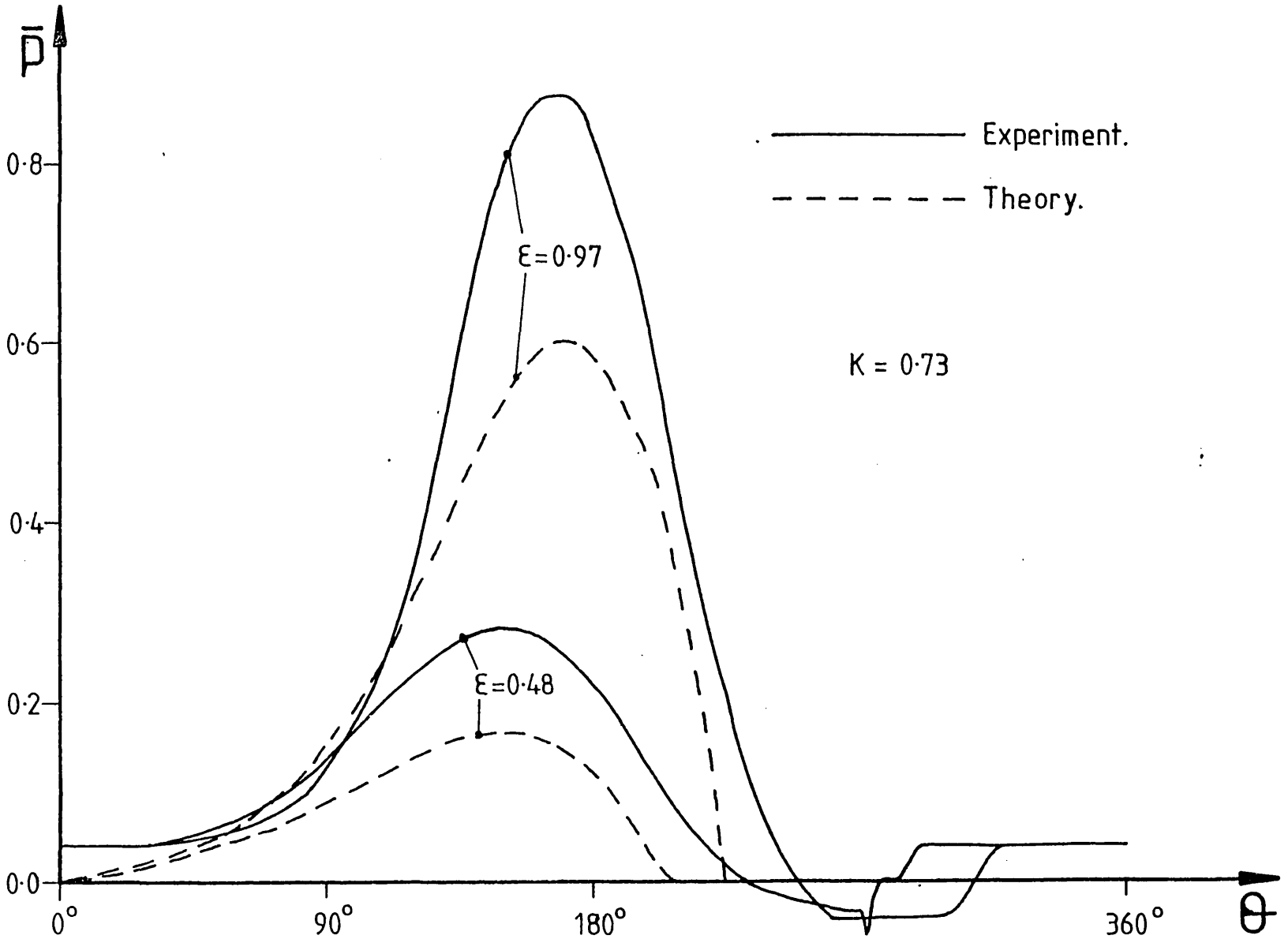


Figure 6.6. Pressure Profiles For A Plain Liner. Test Series 1.

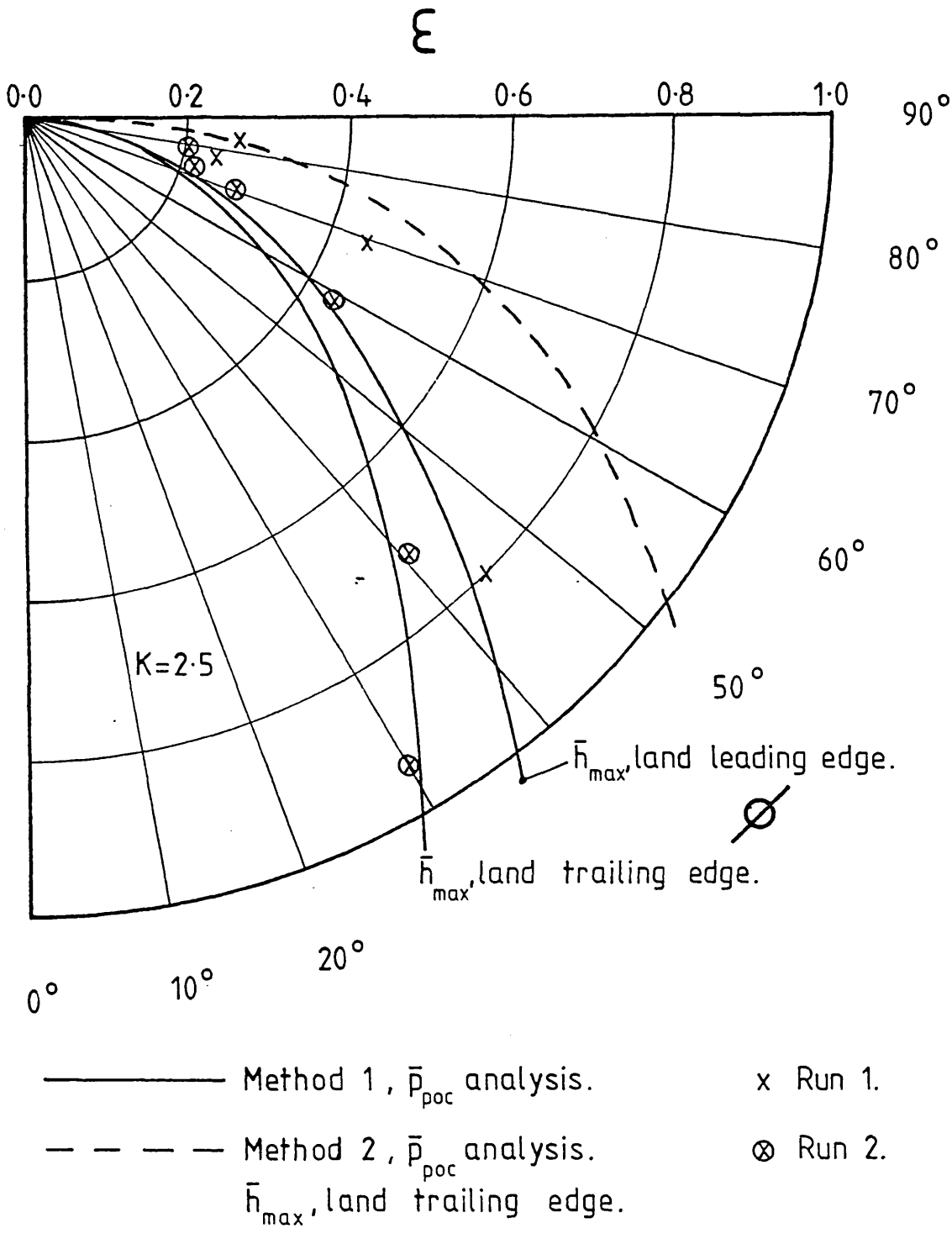


Figure 6.7. Attitude Angle For A Pocketed Liner.
Test Series 1.

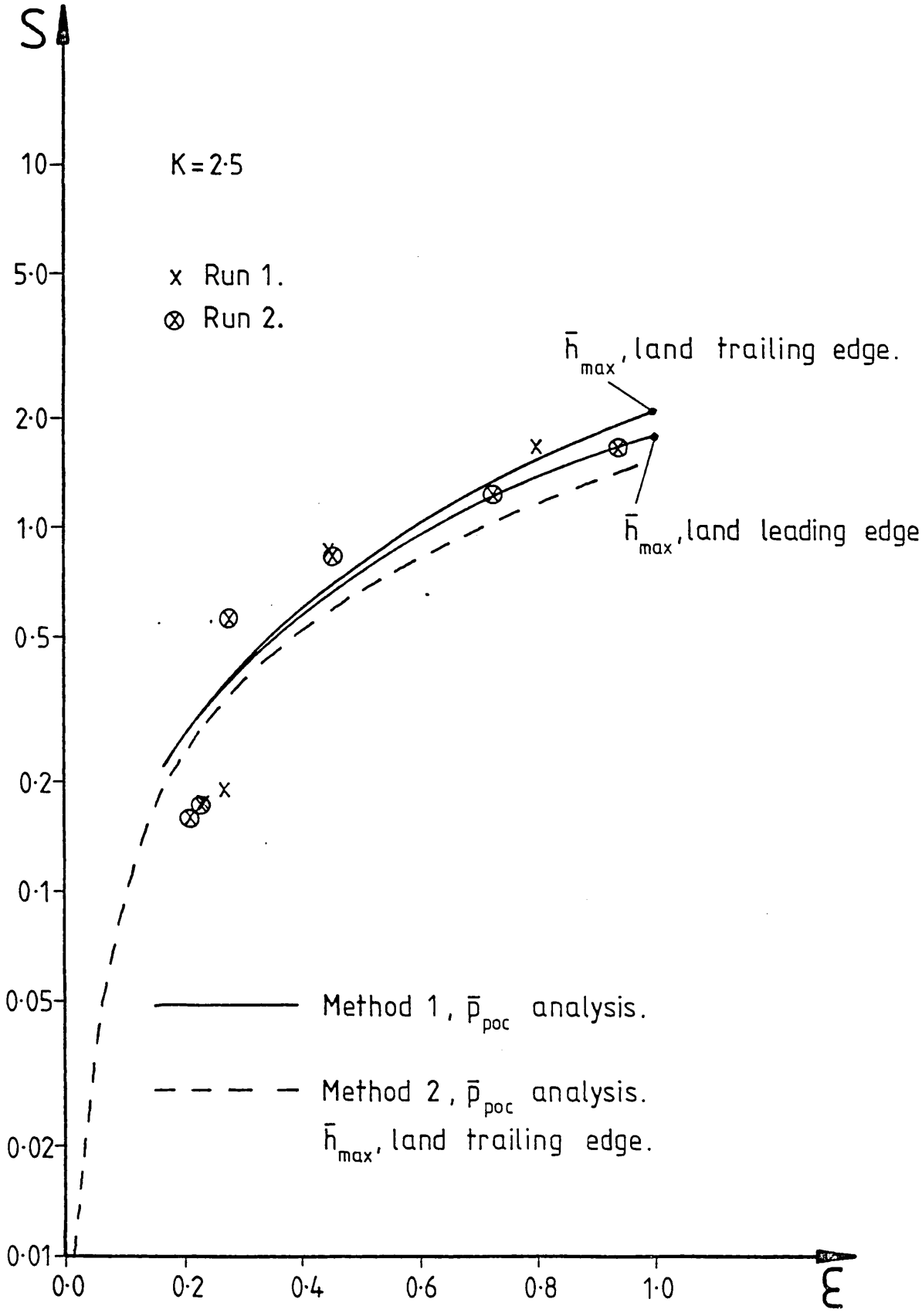


Figure 6.8. Sommerfeld Number For A Pocketed Liner. Test Series 1.

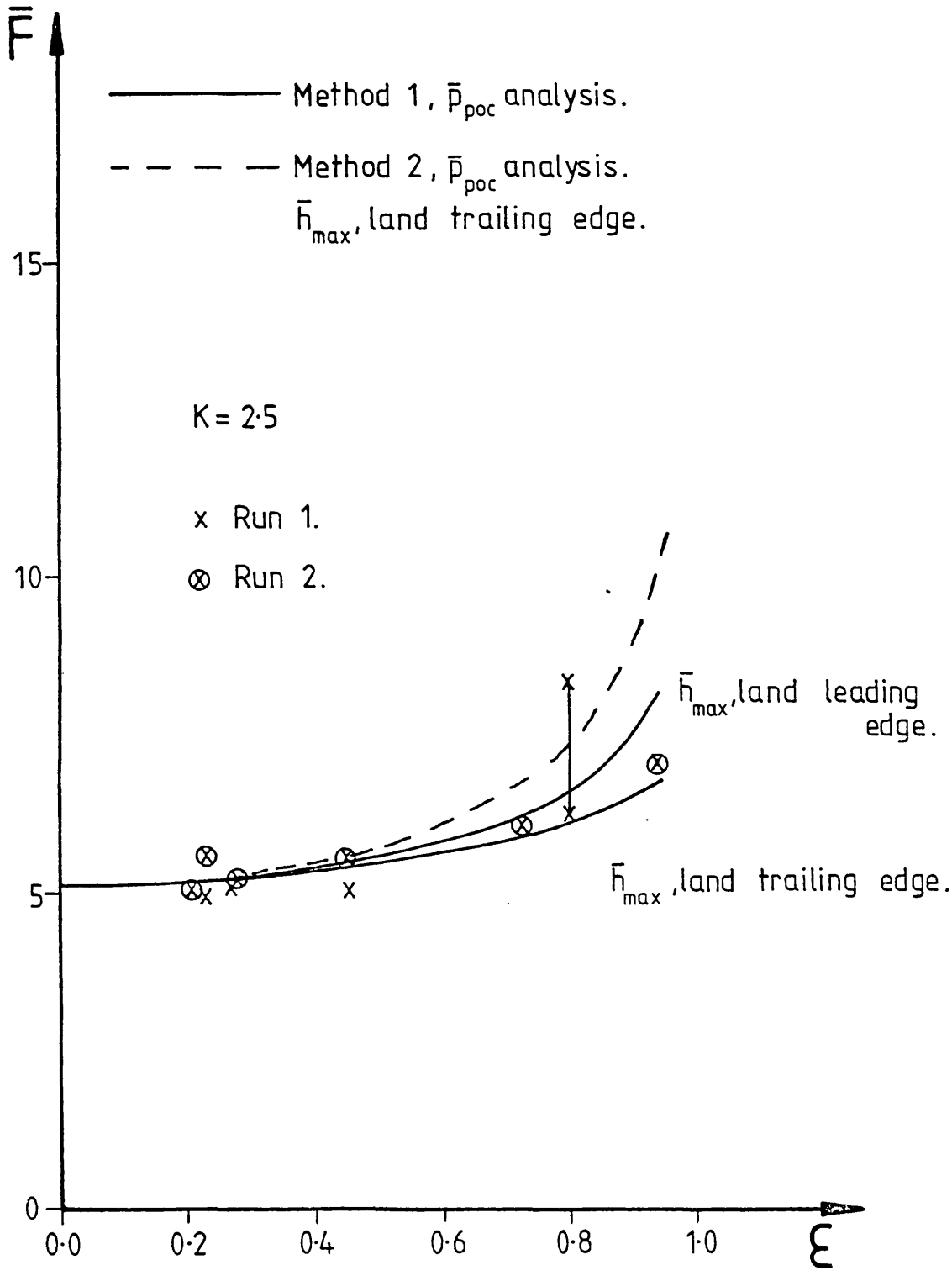


Figure 6.9. Friction For A Pocketed Liner.
Test Series 1.

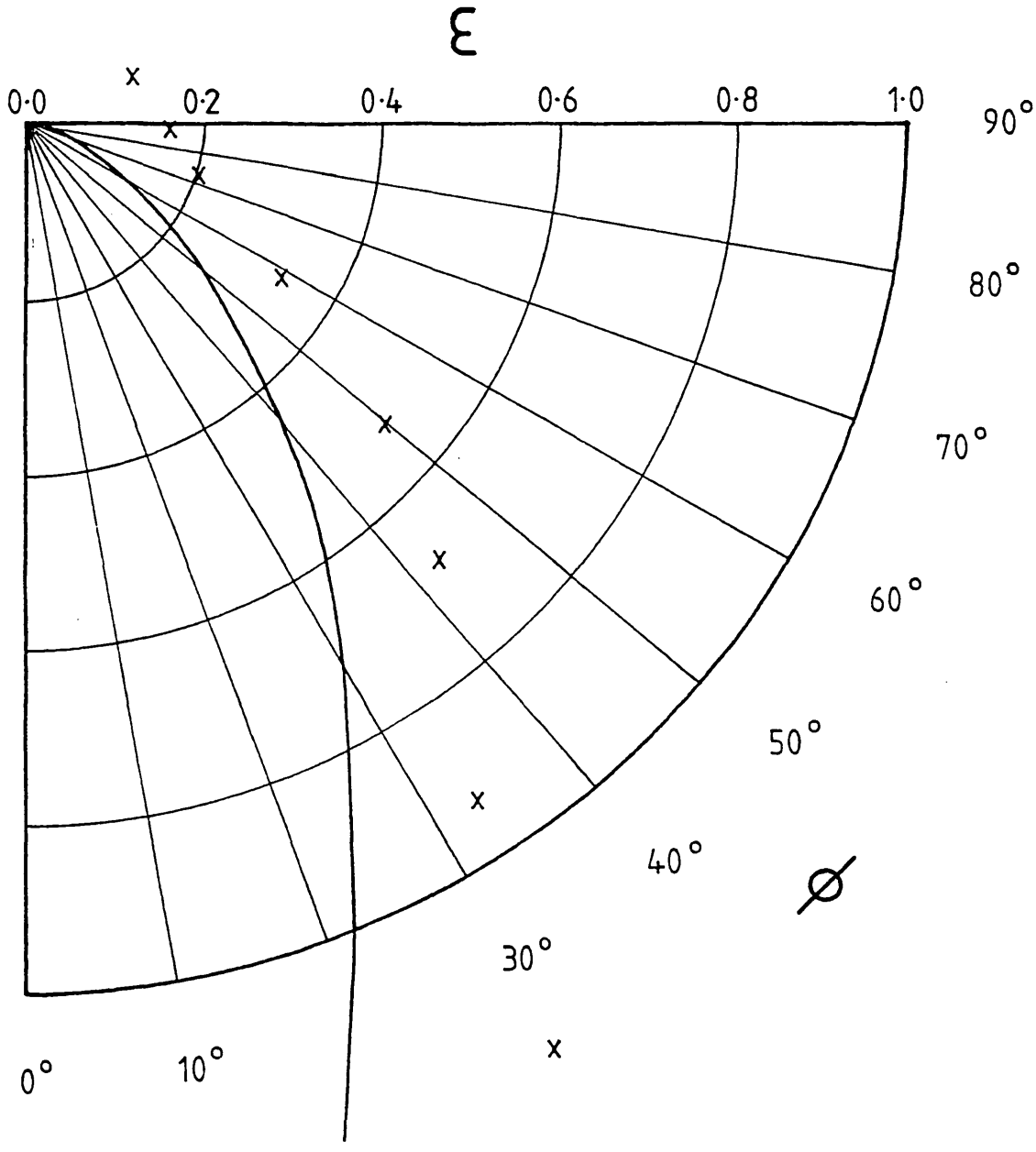


Figure 6.10. Attitude Angle For A Plain Liner.
Test Series 2.

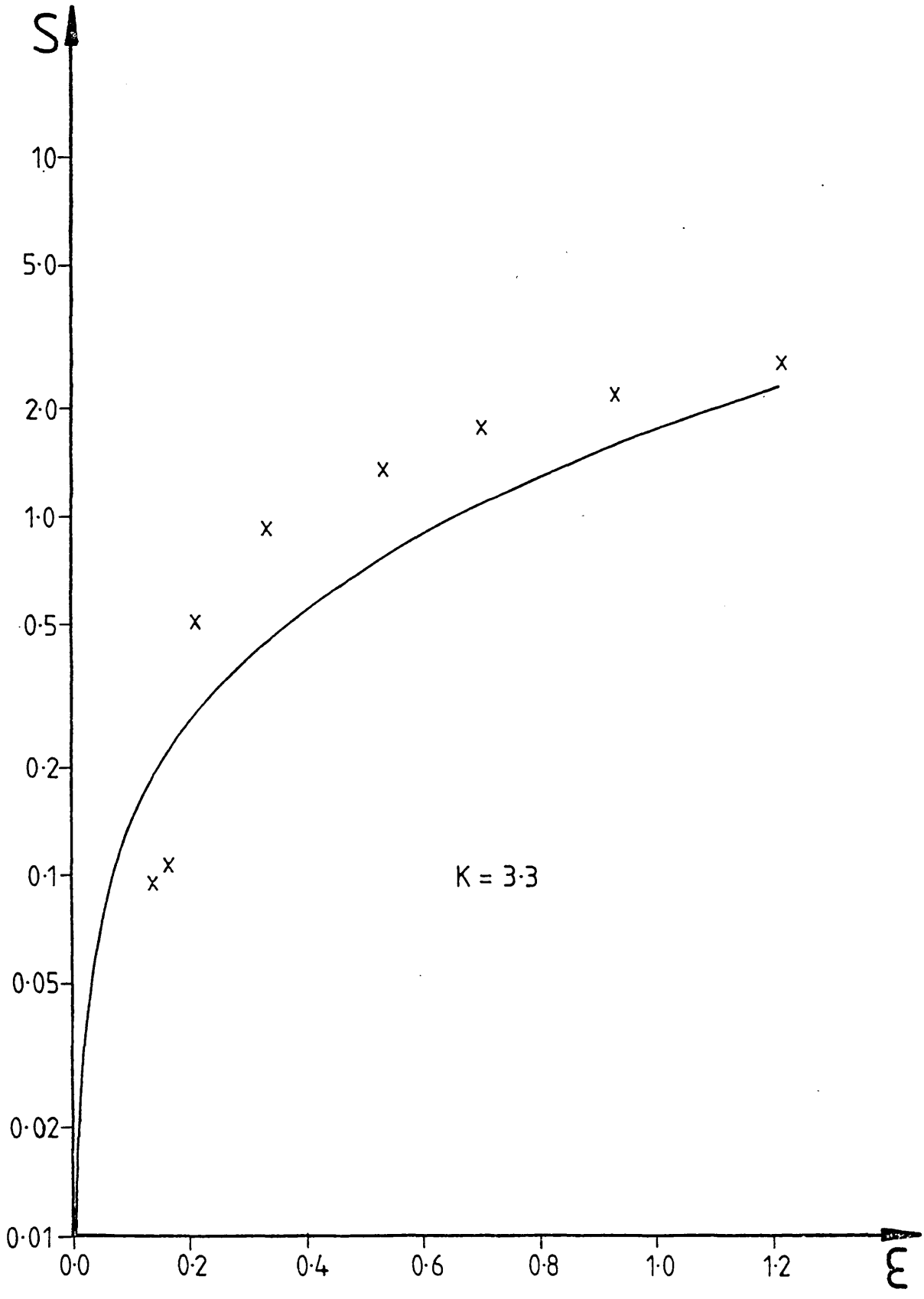


Figure 6.11. Sommerfeld Number For A Plain Liner.
Test Series 2.

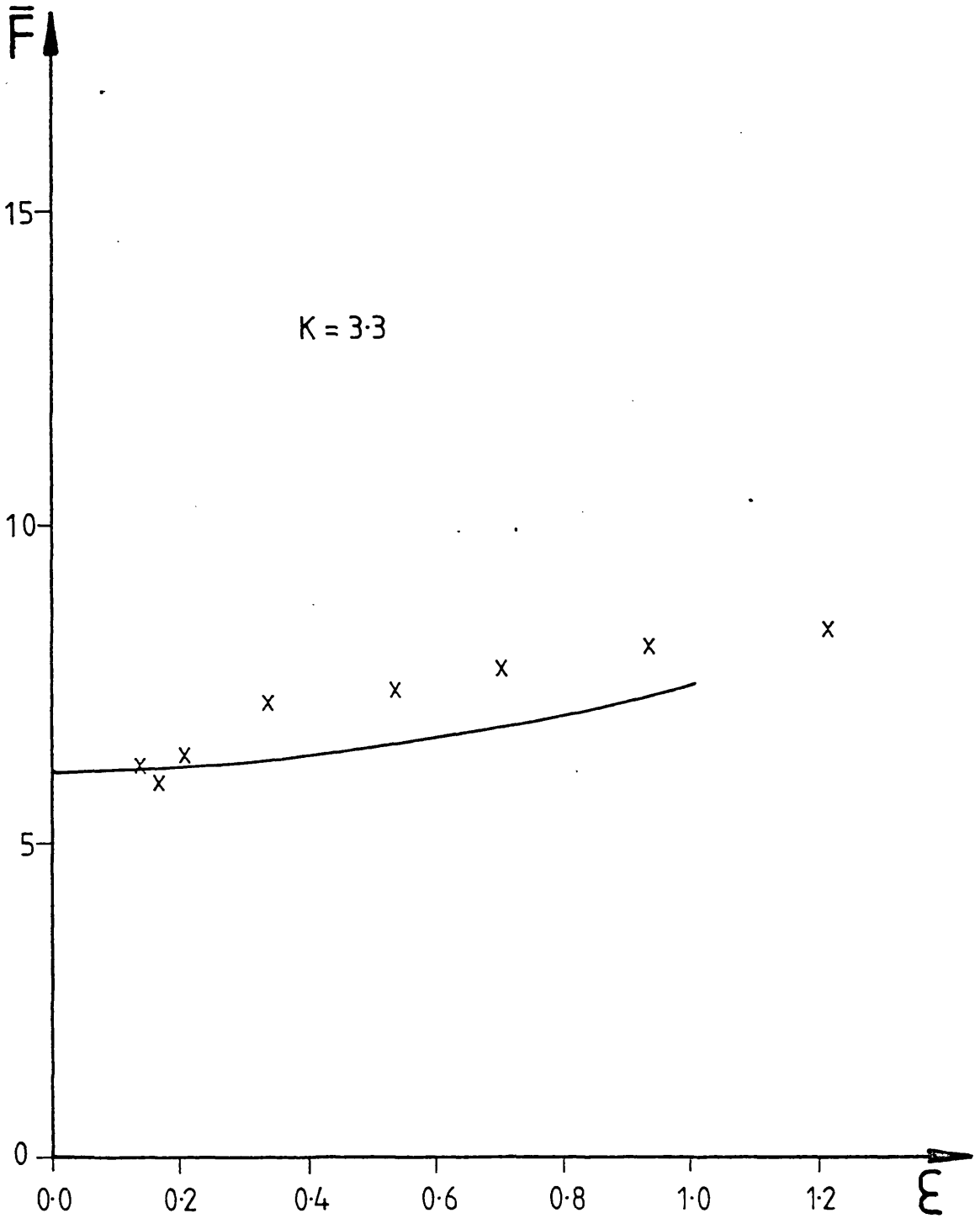


Figure 6.12. Friction For A Plain Liner.
Test Series 2.

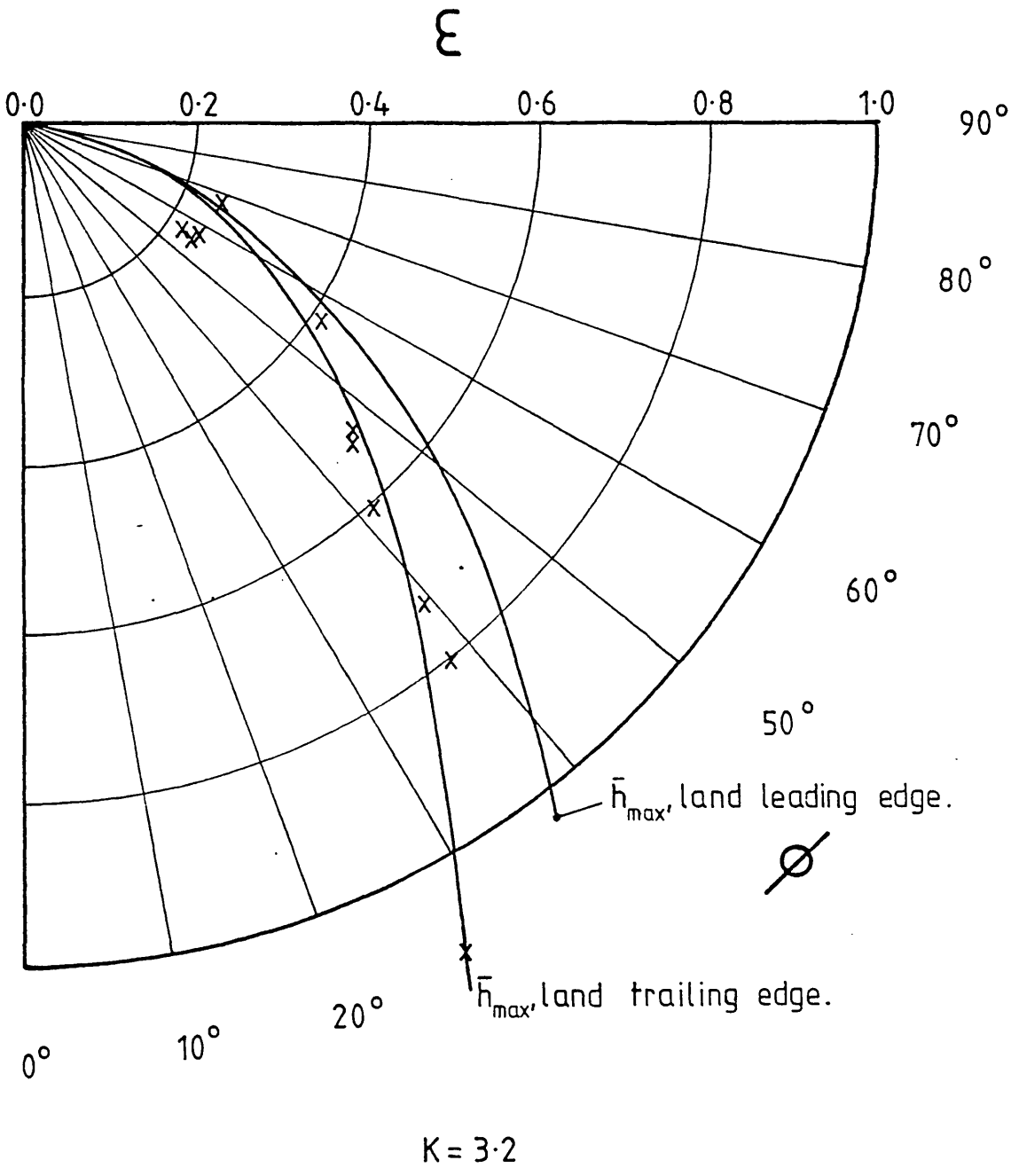


Figure 6.13. Attitude Angle For A Pocketed Liner.
Test Series 2.

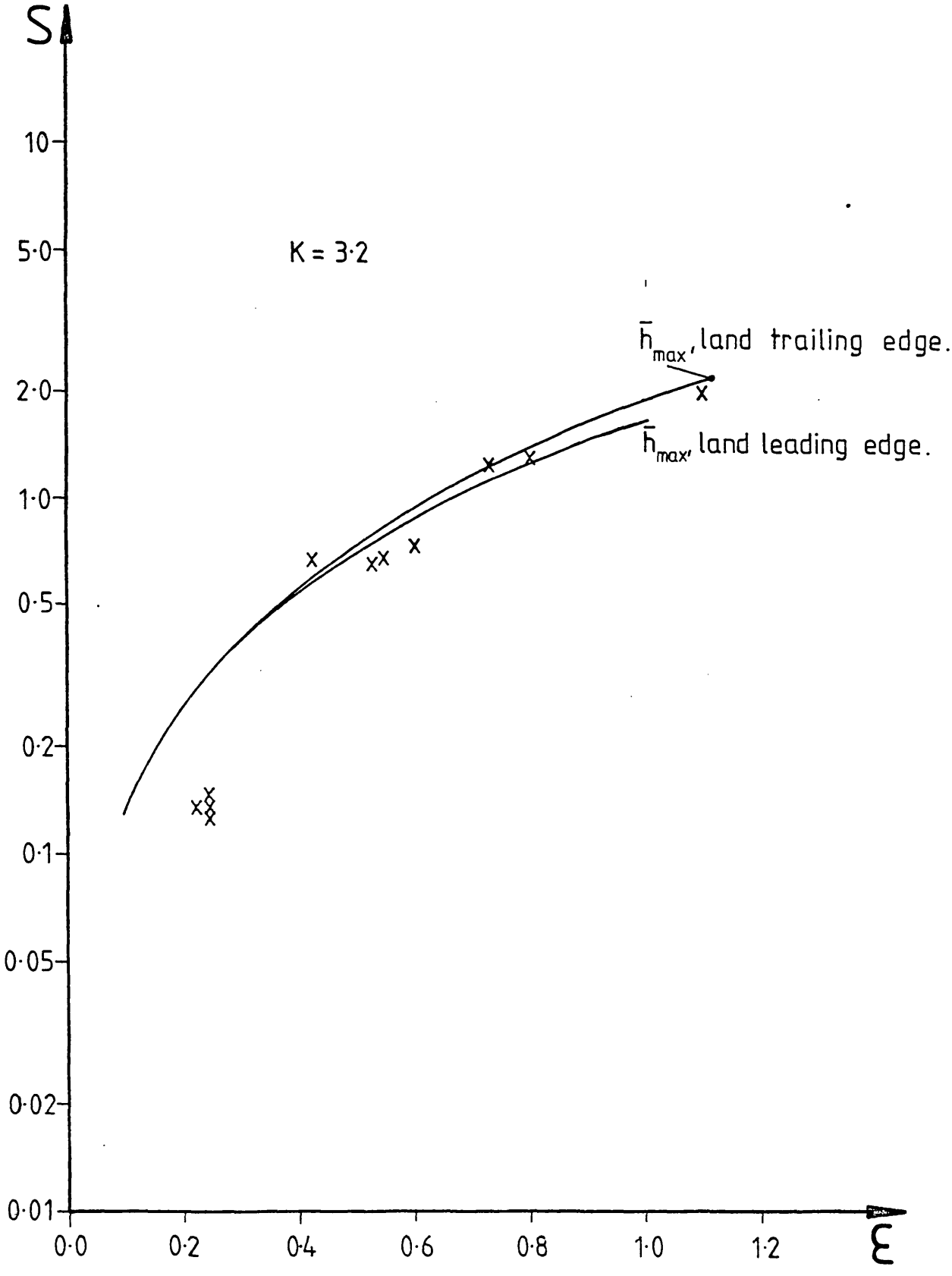


Figure 6.14. Sommerfeld Number For A Pocketed Liner. Test Series 2.

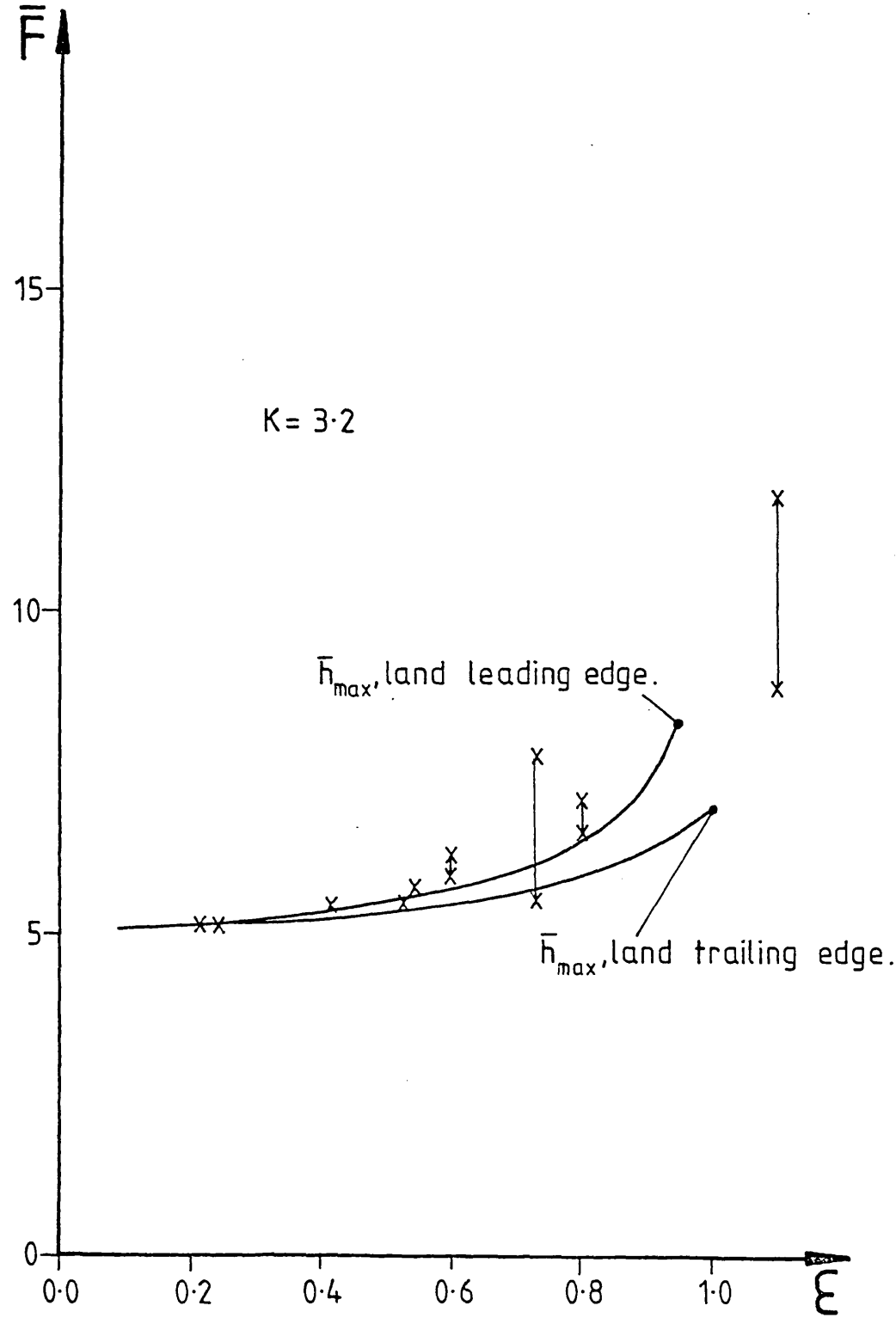


Figure 6.15. Friction For A Pocketed Liner.
Test Series 2.

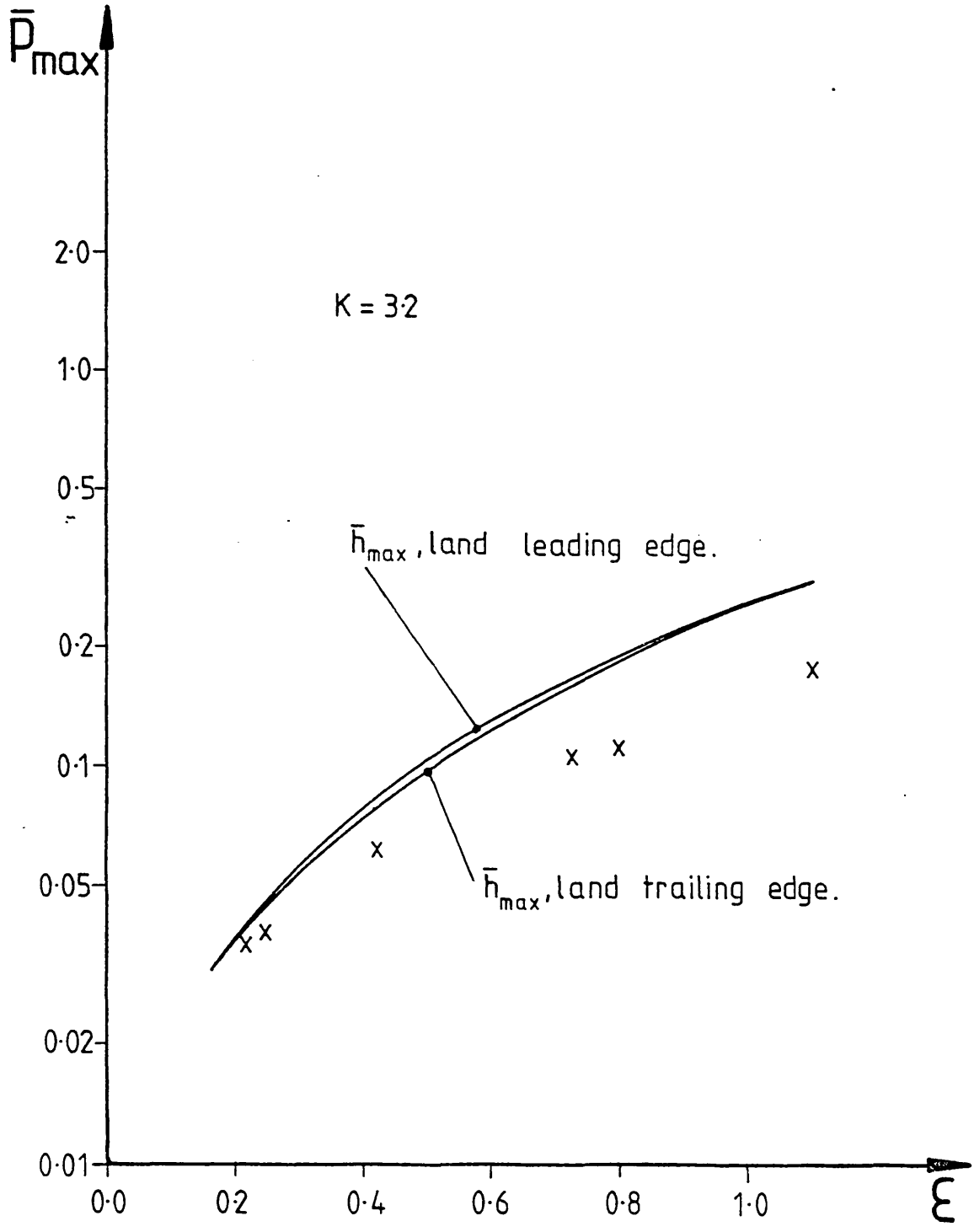


Figure 6.16. Maximum Film Pressure For A Pocketed Liner. Test Series 2.

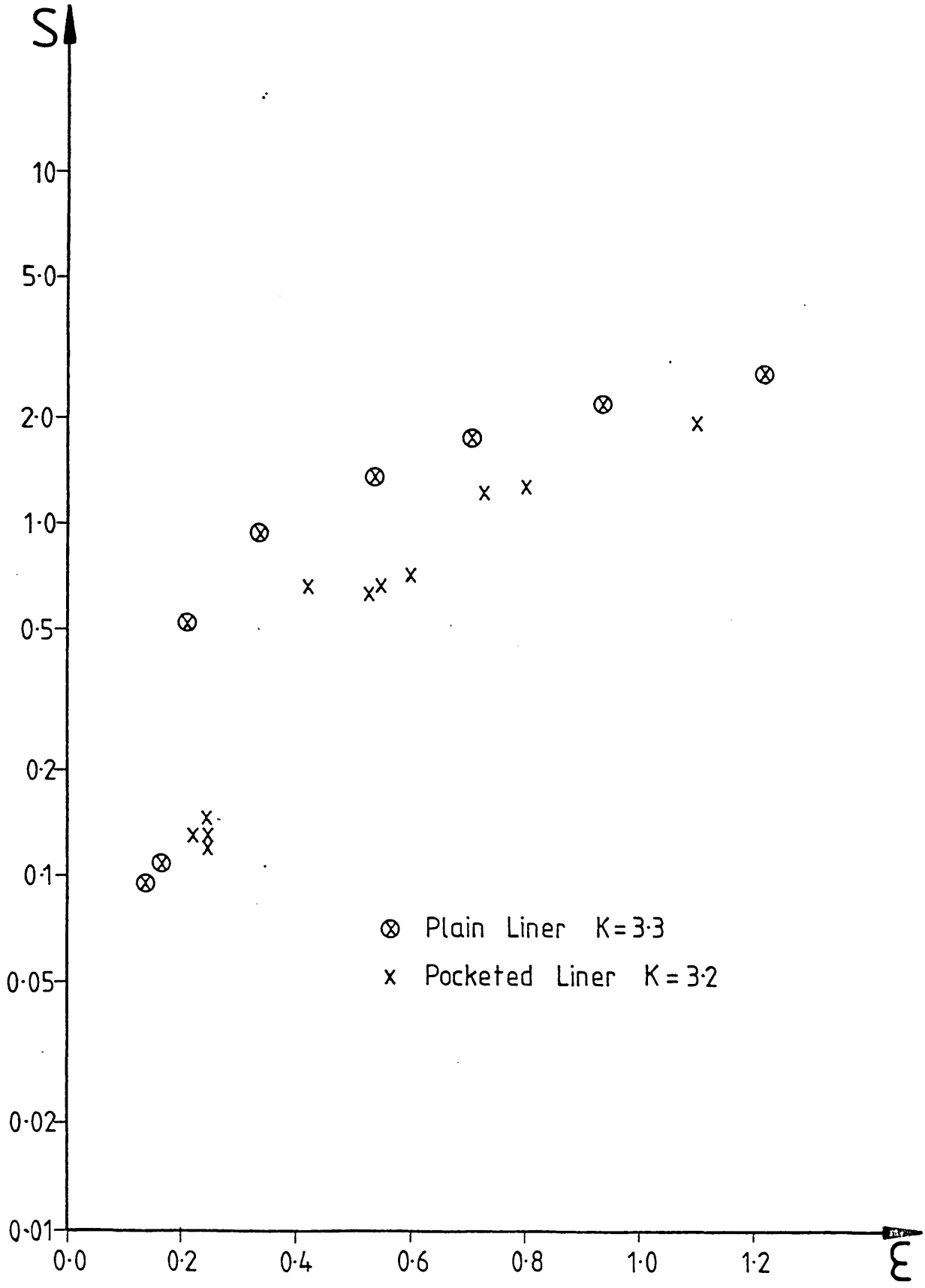


Figure 6.17. An Experimental Comparison Of Sommerfeld Number For Plain And Pocketed Liners. Test Series 2.

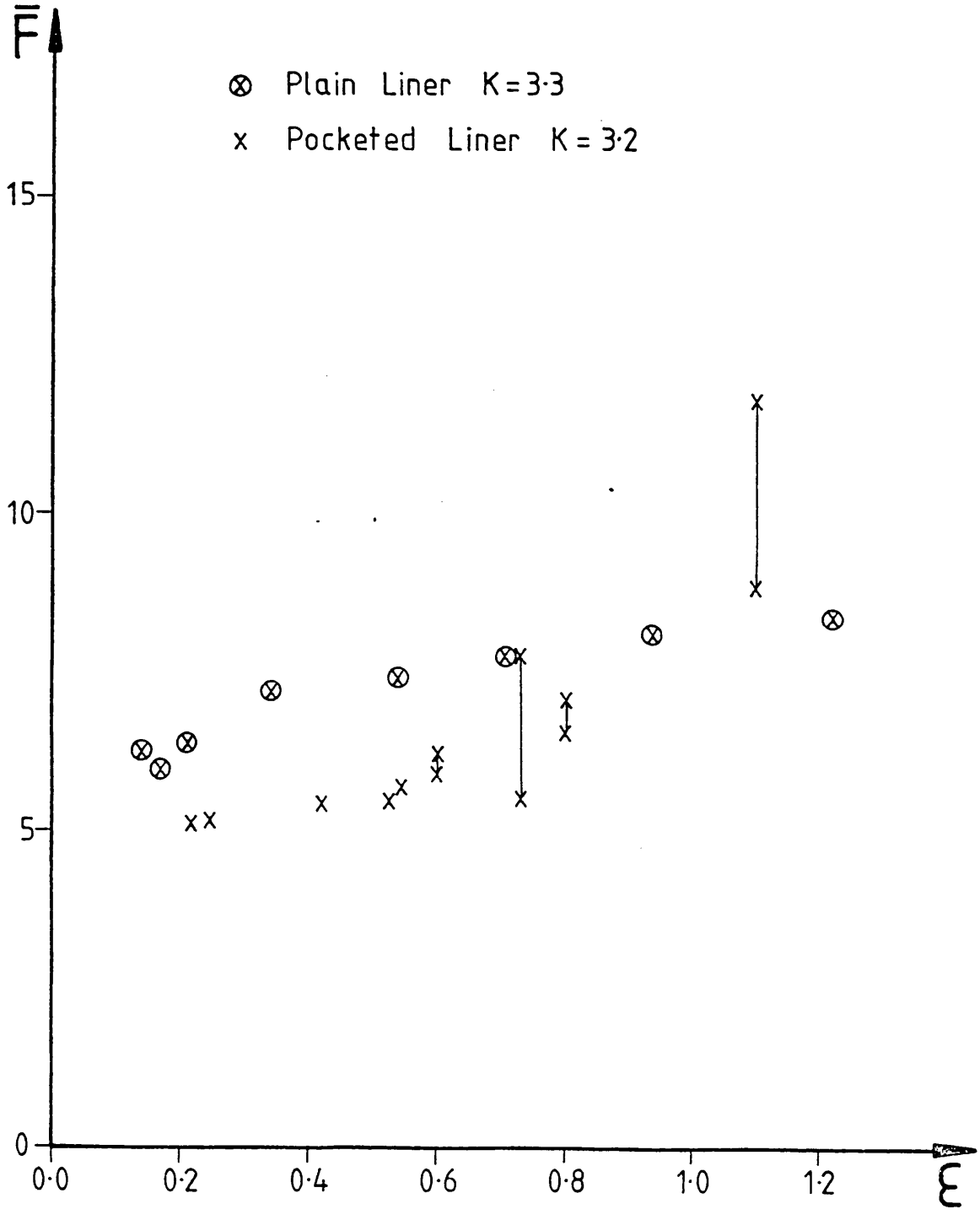


Figure 6.18. An Experimental Comparison Of Friction For Plain And Pocketed Liners. Test Series 2.

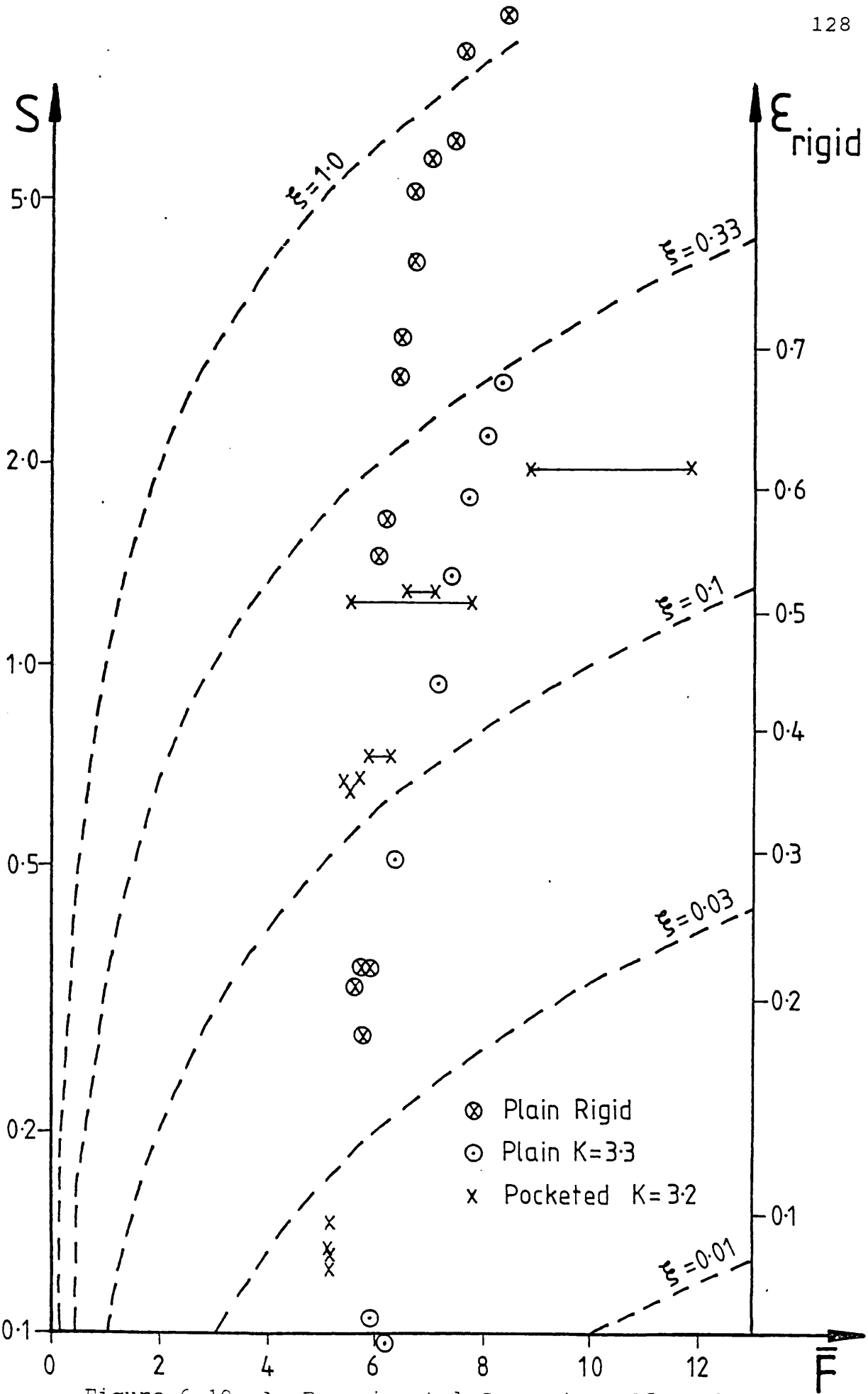


Figure 6.19. An Experimental Comparison Of Performance, ξ, For Plain Rigid And Plain And Pocketed Elastic Liners.
Test Series 2.

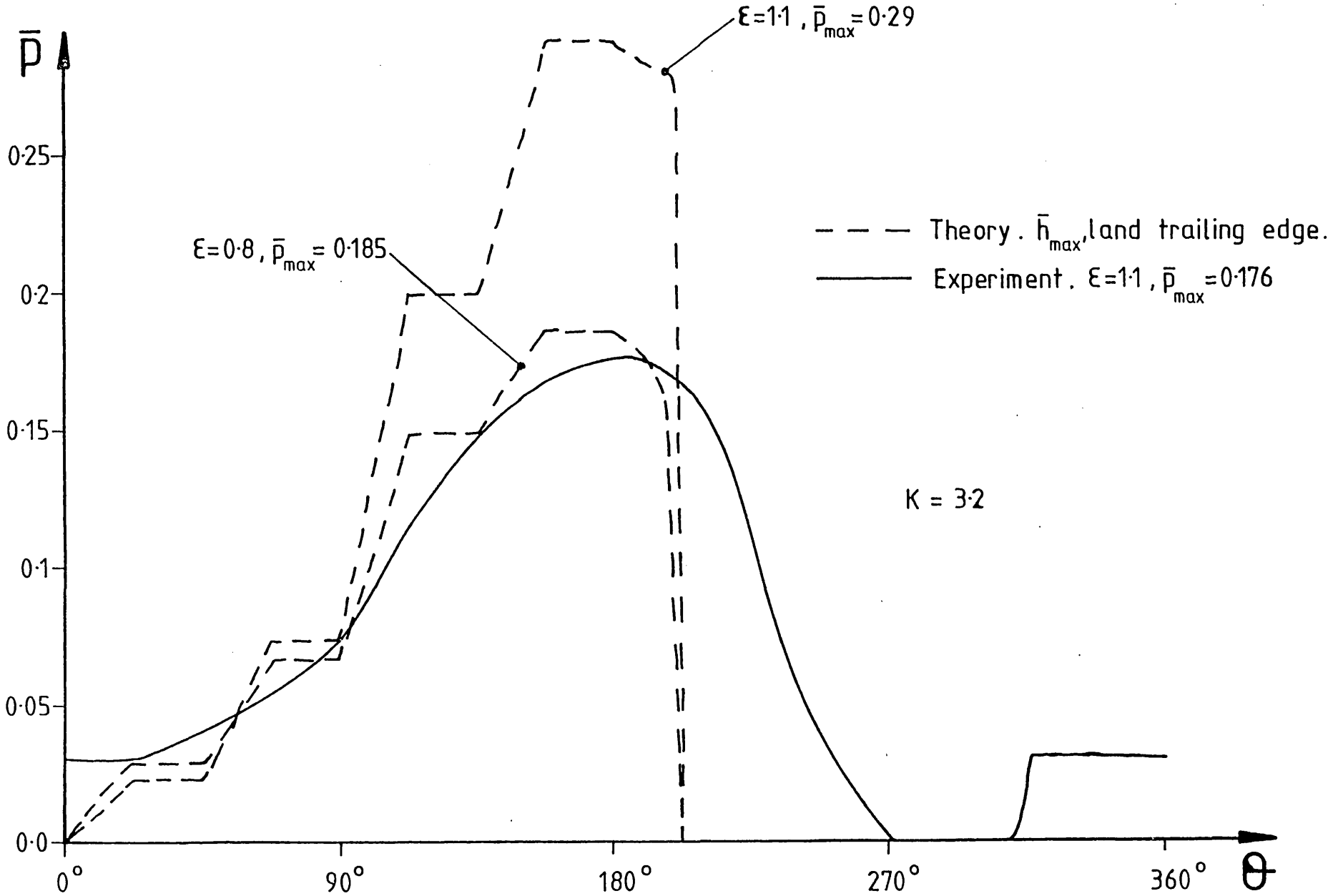


Figure 6.20. Pressure Profiles For A Pocketed Liner.
Test Series A.

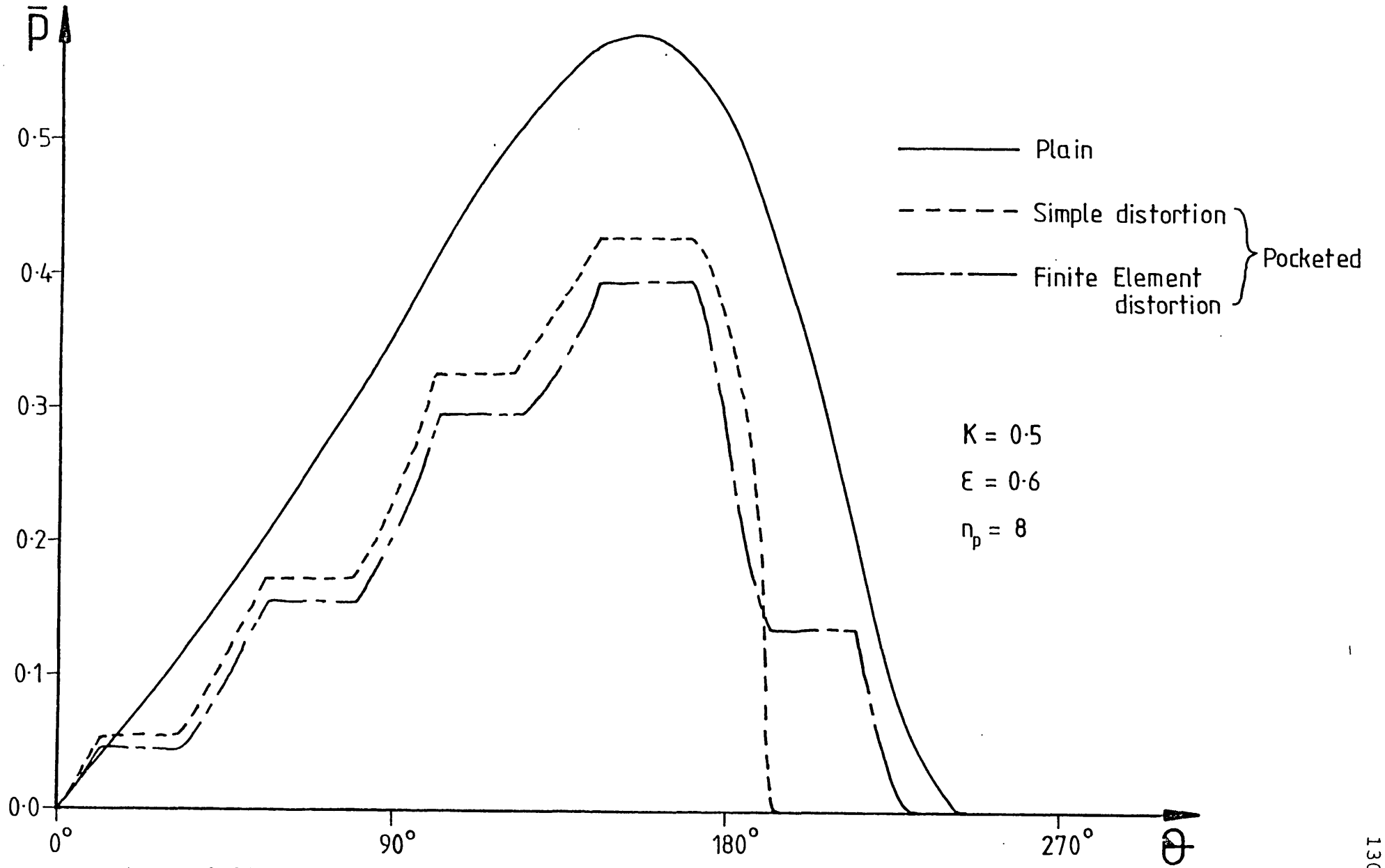


Figure 6.21. A Comparison Of Theoretical Pressure Profiles For An Infinitely Long Bearing.

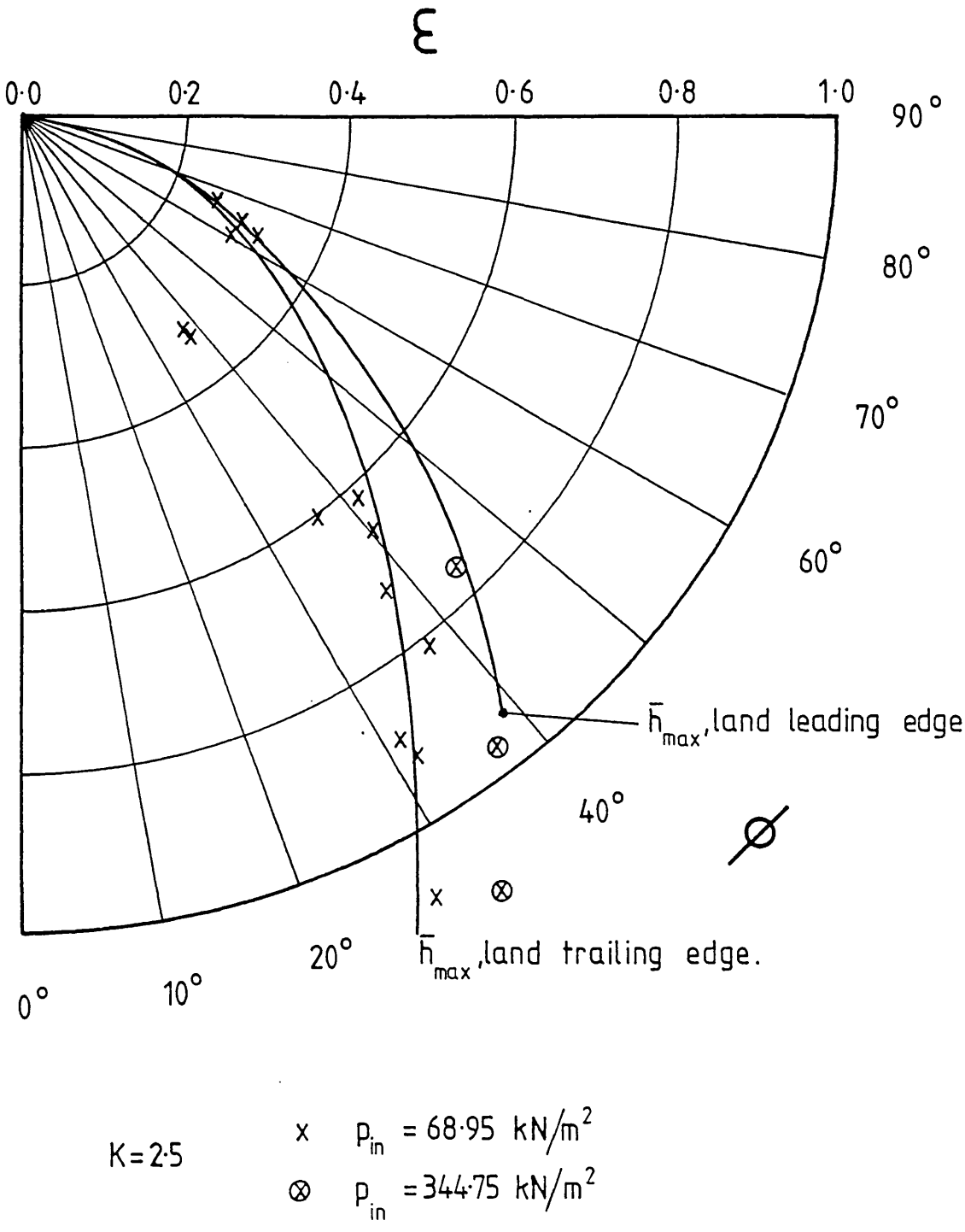


Figure 6.22. Attitude Angle For A Pocketed Liner.
Test Series 3.

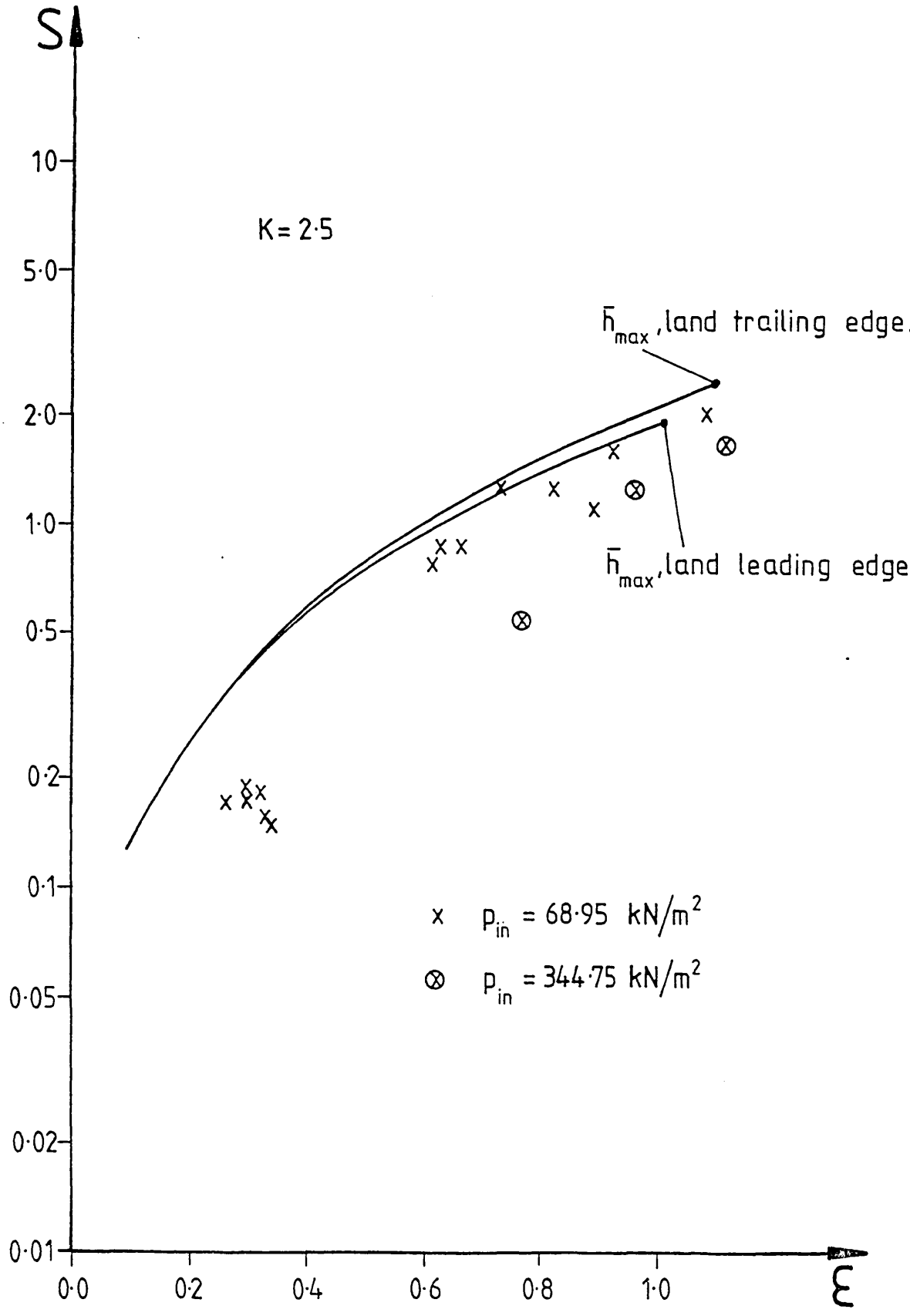


Figure 6.23. Sommerfeld Number For A Pocketed Liner. Test Series 3.

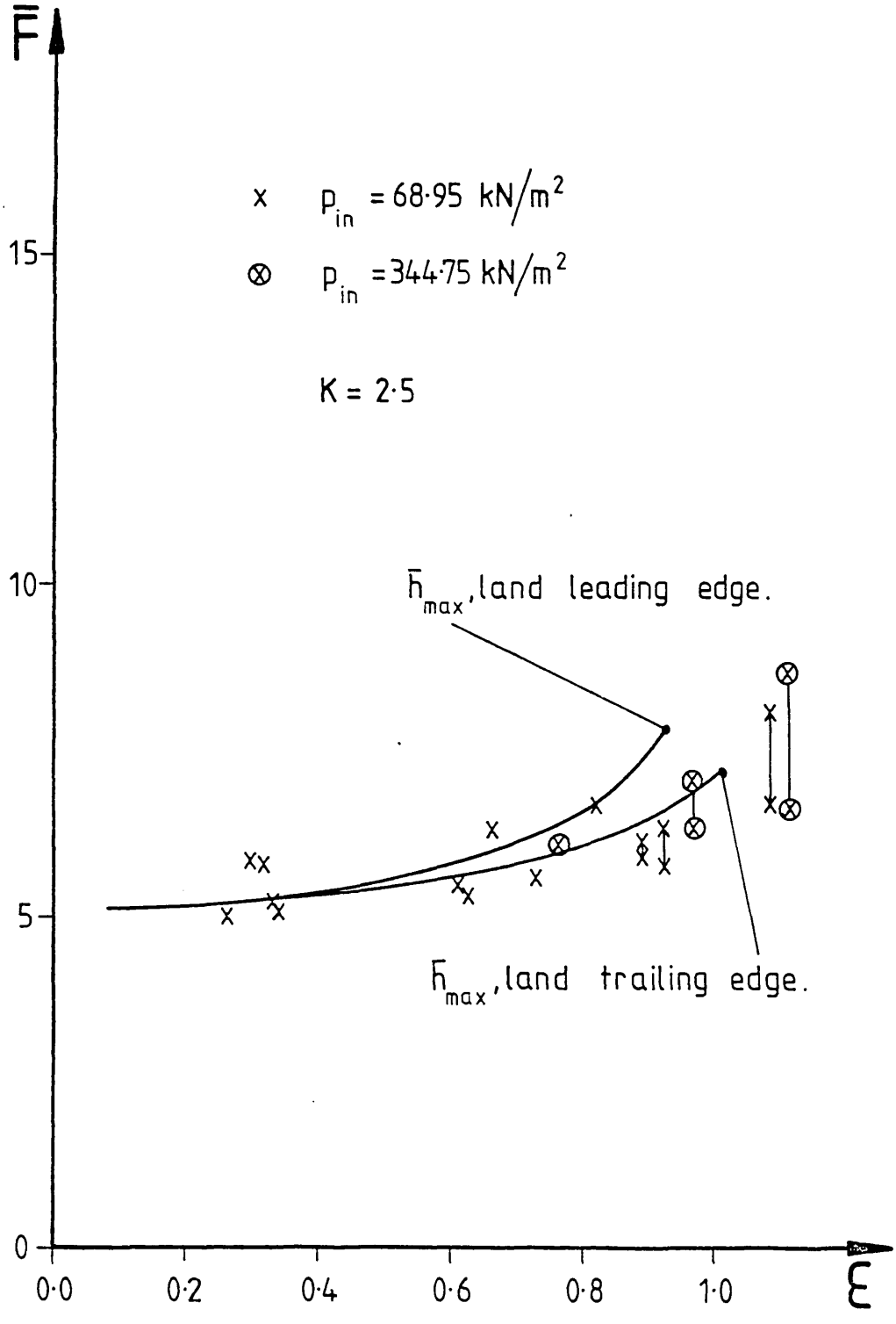


Figure 6.24. Friction For A Pocketed Liner.
Test Series 3.

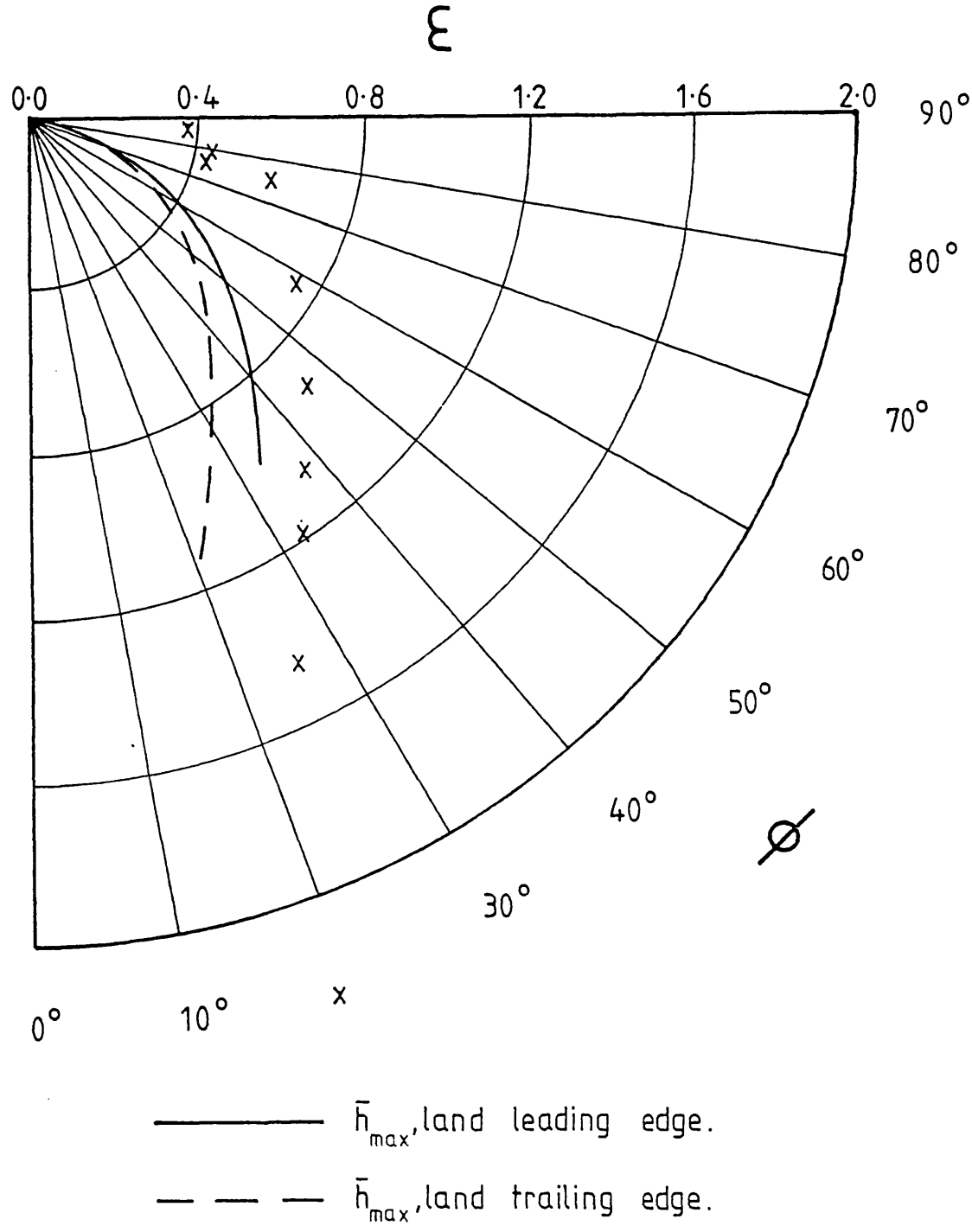


Figure 6.25. Attitude Angle For A Pocketed Liner.
Test Series 4.

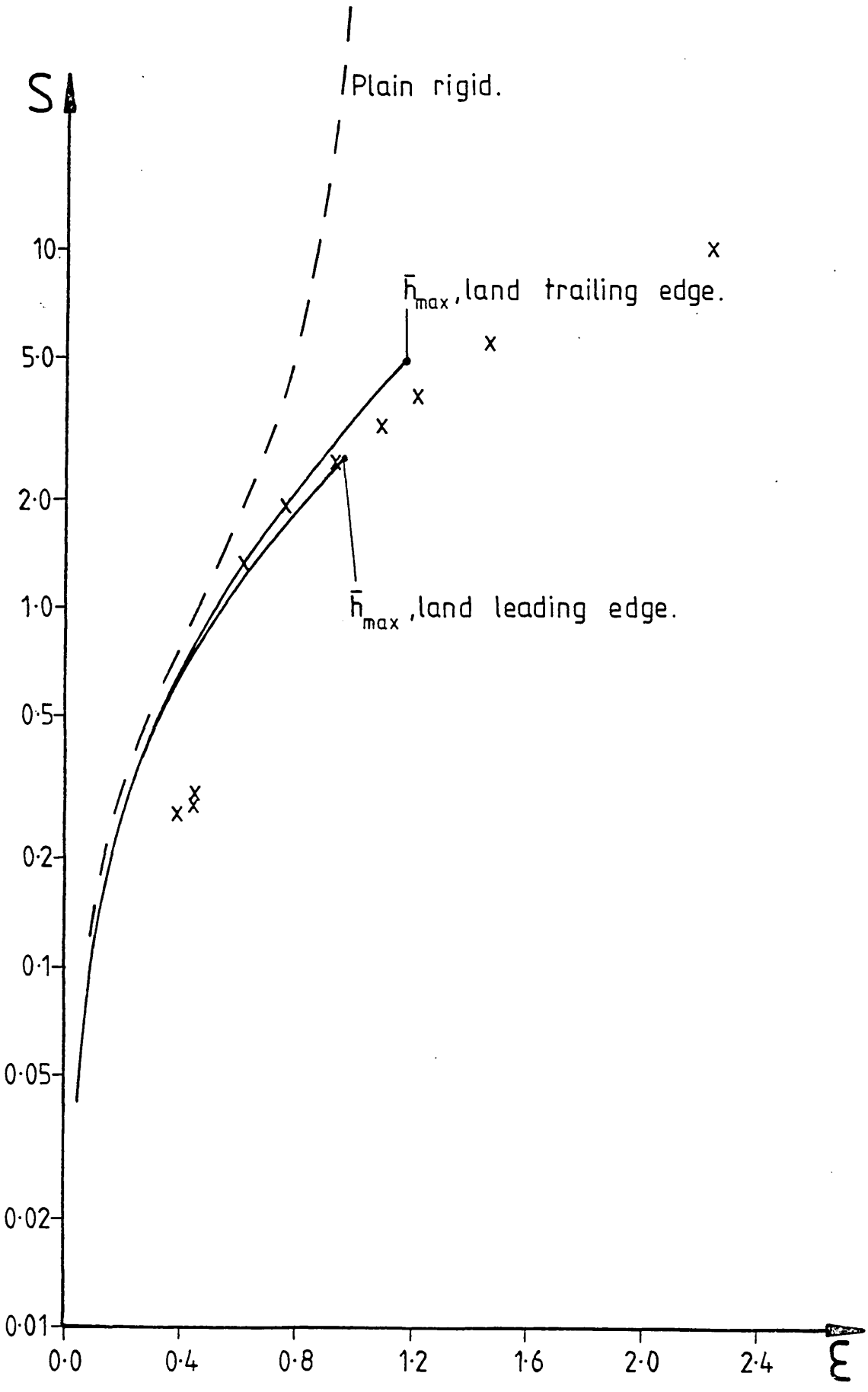


Figure 6.26. Sommerfeld Number For A Pocketed Liner.
Test Series 4.

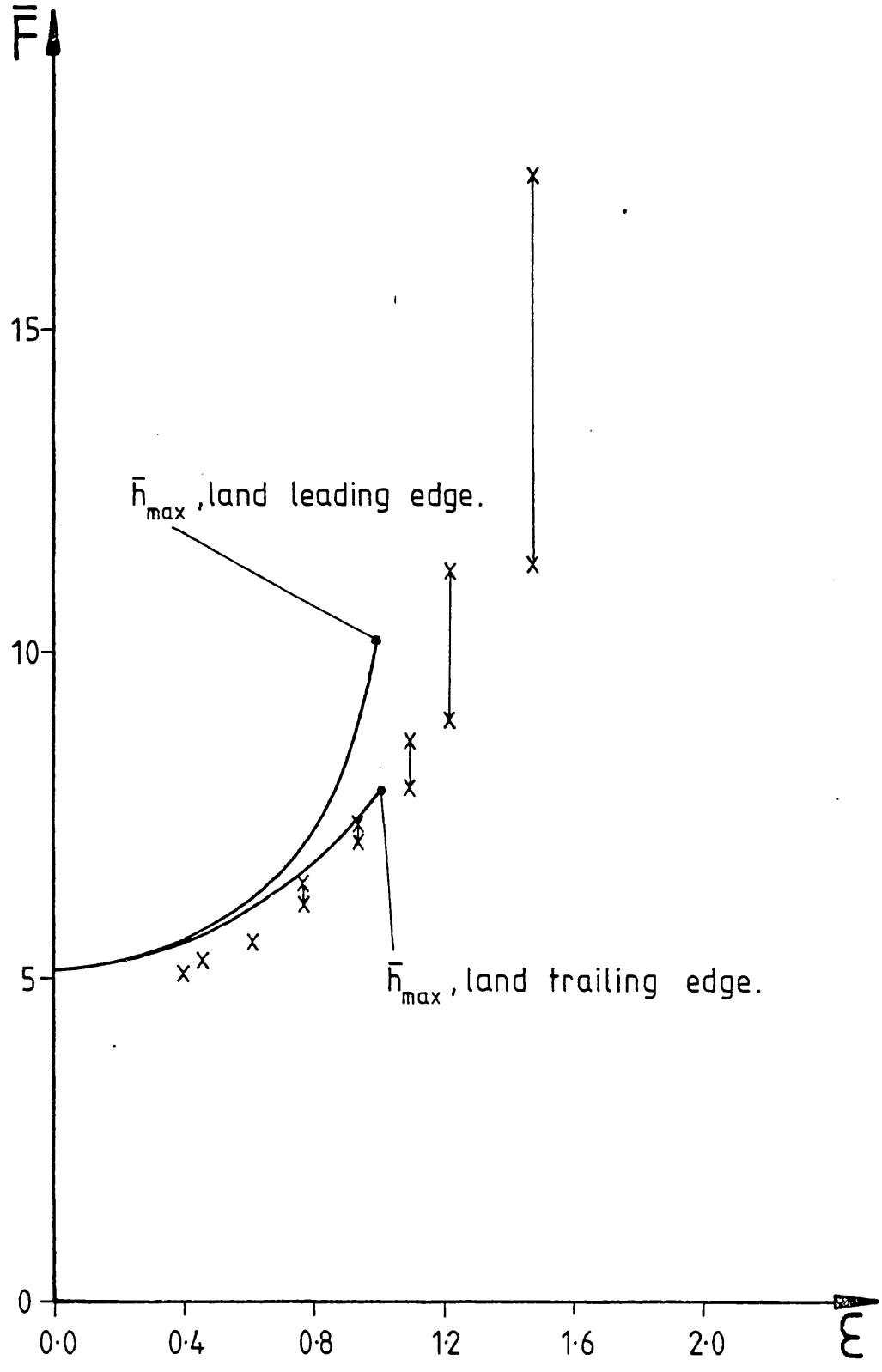


Figure 6.27. Friction For A Pocketed Liner.
Test Series 4.

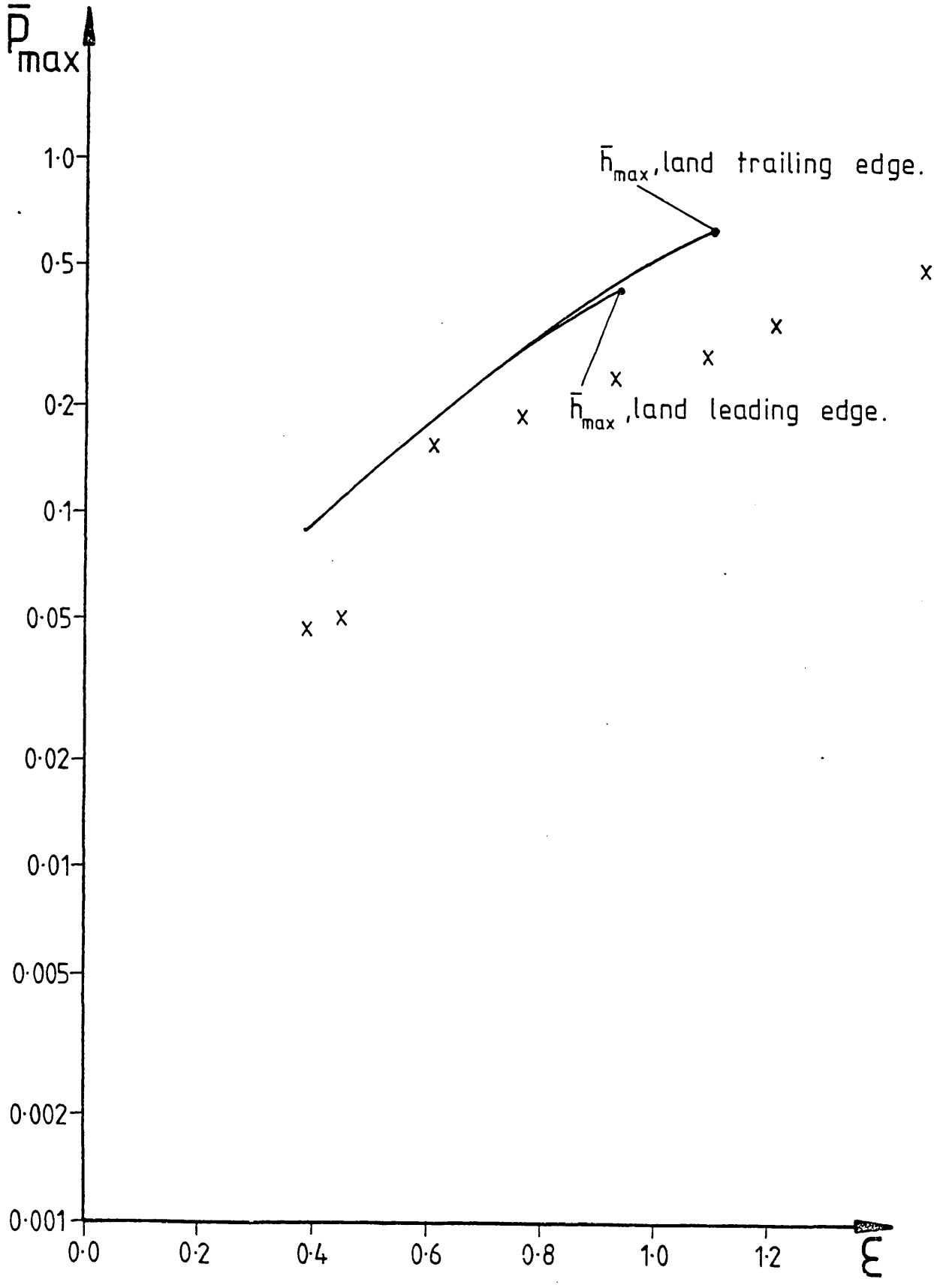


Figure 6.28. Maximum Film Pressure For A Pocketed Liner. Test Series 4.

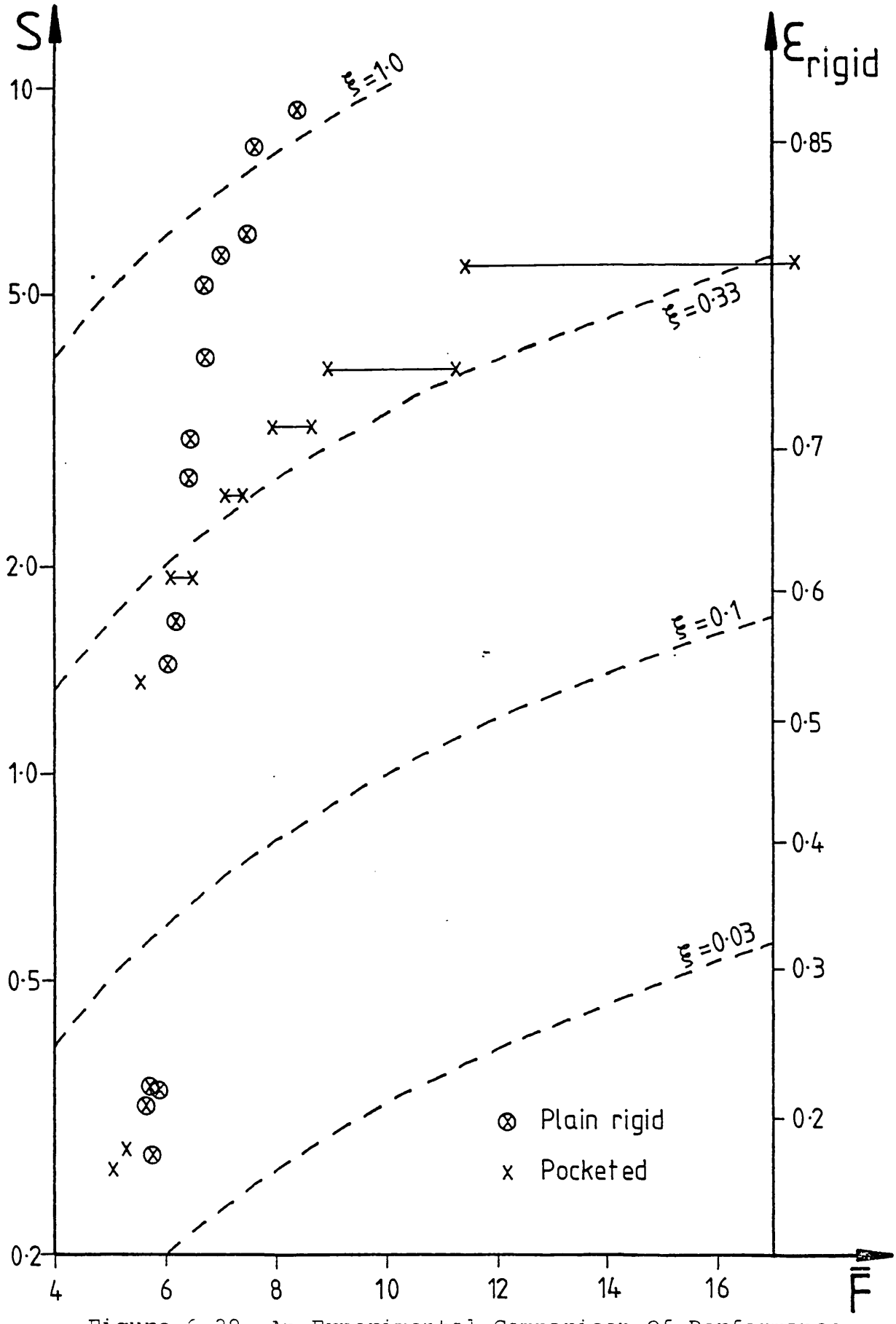


Figure 6.29. An Experimental Comparison Of Performance, ξ, For Plain Rigid And Pocketed Elastic Liners. Test Series 4.

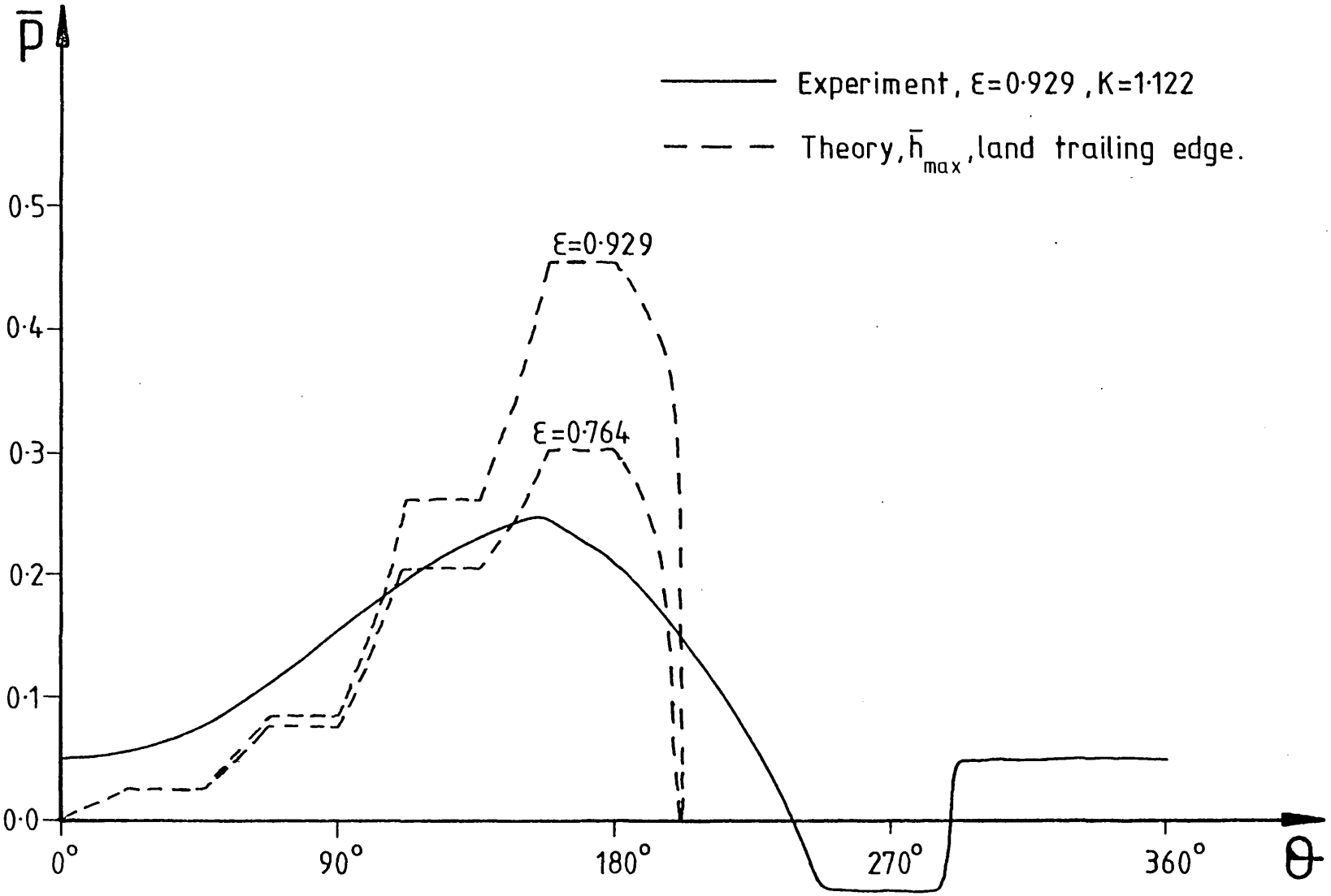


Figure 6.30. Pressure Profiles For A Pocketed Liner.
Test Series 4.

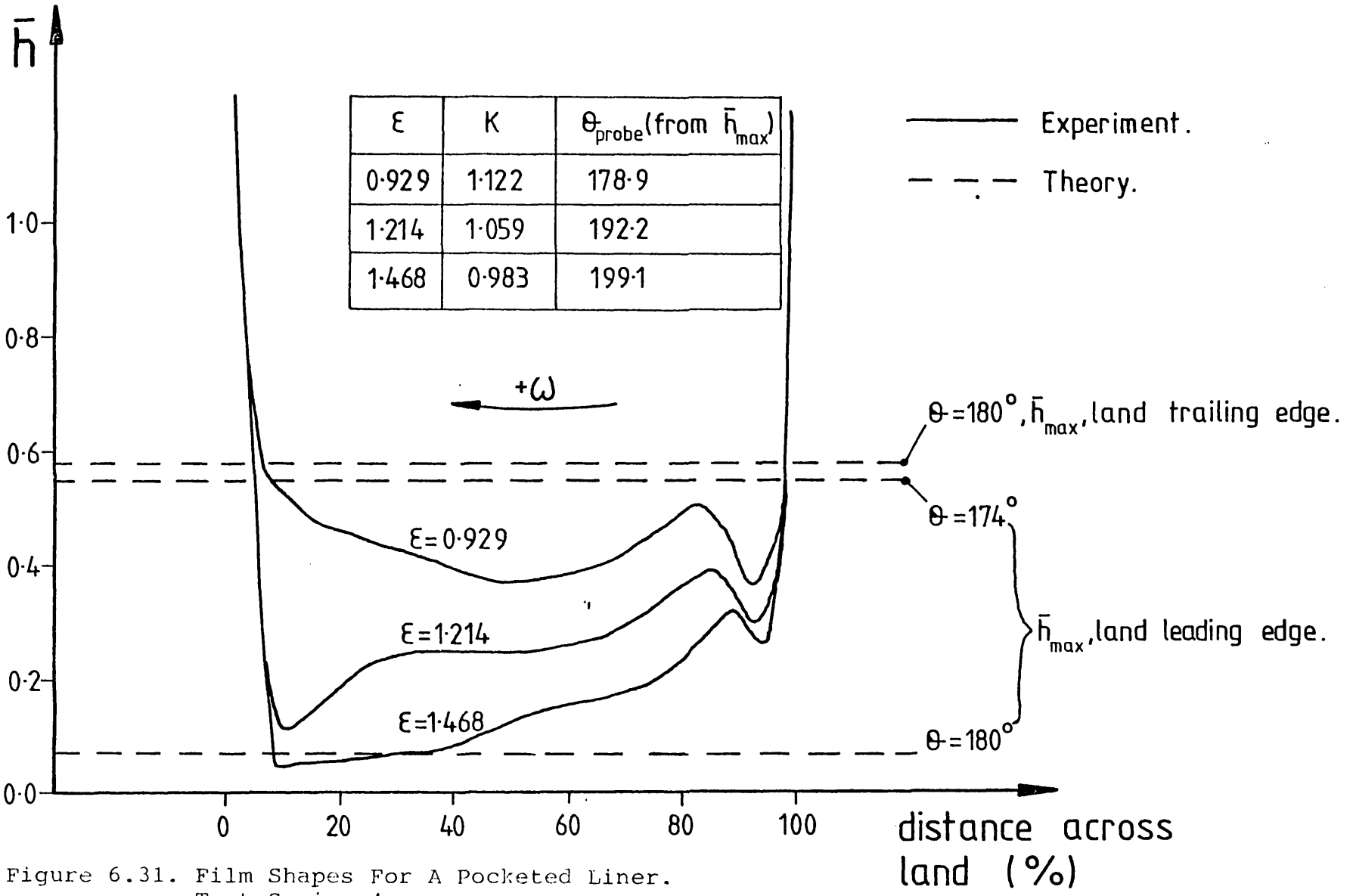


Figure 6.31. Film Shapes For A Pocketed Liner.
Test Series 4.

CHAPTER 7.

A REVIEW.

7.1. Considerations Of Oil Compressibility.

It was thought that a possible explanation of the bearing with a pocketed elastic journal liner having a lower performance than a plain bearing could be that the compressibility of the oil in the large volume pockets appreciably attenuated the volumetric flow from the pocket.

The accepted equation for the compressibility of oil is

$$C = \frac{-1}{V}\frac{dV}{dp}$$

where $$C = \left(4.35 - \frac{2.9\log_{10}\eta}{3}\right) x10^{-4} \quad m^2/MN$$

(η having the units Ns/m^2).

Using a typical value of $\eta = 0.14\ Ns/m^2$ gives

$$\frac{dV}{V} = -5.18x10^{-4}\ dp\ . \qquad (7.1.)$$

The ratio of the displaced volume from a pocket to the pocket volume is given by the ratio of the distortion at the pocket edge to the thickness of the liner, that is $\frac{dV}{V} = -\frac{\delta}{t}$. Expressing this in terms of pressure gives

$$\frac{dV}{V} = \frac{Kc\bar{p}}{t} .$$

Using typical values from test series 4 (section 6.7.) of K = 1.0, c = 177.8 μm., $\bar{p}_{max}$ = 0.3 and t = 2 mm. gives $\frac{dV}{V}$ = 2.7%.

The value of 0.3 for $\bar{p}_{max}$ corresponds to a pressure rise (relative to atmosphere) of 0.45 MN/m^2 (taking η = 0.14 Ns/m^2, ω = 35 s^{-1}, c = 177.8 μm. and R_2 = 40 mm.), and substituting this in eq. 7.1. gives $\frac{dV}{V}$ = 0.023%.

Thus, the reduction in pocket volume due to compressibility effects is of the order of 1% of the displaced pocket volume. It is therefore unlikely that the pocket pumping effect has been influenced by compressibility to any great extent in the present work. This is confirmed by the previous agreement between the experimental results and the present theory which assumes incompressible flow.

7.2. The Work Of Alexandrov.

The major problem which remained till a late stage in the present project was the difference in trends between Alexandrov's theoretical predictions and the present experimental and theoretical results. The difference was eventually found to be due to a logical error in the way Alexandrov treated the calculation of distortion and film thickness in the iteration procedure, and it is worth examining this further.

The iteration scheme for a bearing with a plain journal liner proceeds as follows.

$$\bar{\delta}_o = 0 \ , \ \bar{p}_o = 0$$

$\bar{h}_1 = \bar{h}_r$ the rigid film thickness

↓

$\bar{p}_1$

↓

First iteration

↓

$\bar{\delta}_1$

↓

$\bar{h}_2$

↓

$\bar{p}_2$

↓

Second iteration

↓

$\bar{\delta}_2$

etc.

Alexandrov adjusted the film thickness by adding the under relaxed change in distortion from one iteration to the next to the previous value of film thickness, that is

$$\bar{h}_2 = \bar{h}_r + \beta_\delta (\bar{\delta}_1 - \bar{\delta}_o) \qquad (7.2.)$$

$$\bar{h}_3 = \bar{h}_2 + \beta_\delta (\bar{\delta}_2 - \bar{\delta}_1) \qquad (7.3.)$$

.

.

.

$$\bar{h}_n = \bar{h}_{n-1} + \beta_\delta (\bar{\delta}_{n-1} - \bar{\delta}_{n-2}) \quad .$$

Substituting for $\bar{h}_2$ from eq. 7.2. into eq. 7.3. and so on gives

$$\bar{h}_n = \bar{h}_r + \sum_{1}^{n-1} \beta_\delta (\bar{\delta}_m - \bar{\delta}_{m-1}) \quad .$$

If β_δ is constant throughout the iteration procedure then

$$\bar{h}_n = \bar{h}_r + \beta_\delta \sum_{1}^{n-1} (\bar{\delta}_m - \bar{\delta}_{m-1}) \quad .$$

But if the solution has converged, then $\sum_{1}^{n-1} (\bar{\delta}_m - \bar{\delta}_{m-1})$ is the converged value of distortion, $\bar{\delta}_n$. Therefore,

$$\bar{h}_n = \bar{h}_r + \beta_\delta \bar{\delta}_n \quad .$$

This method is therefore only valid for $\beta_\delta = 1$. For values of β_δ other than 1, as in Alexandrov's case, the converged value of $\bar{h}$ (or $\bar{\delta}$) will be incorrect. This is most clearly seen in Alexandrov's results for distortion and film thickness for a plain bearing (Figs. 2.2. and 2.3. of (21)) where $\bar{\delta} = 2.0$ at $\theta = 180^\circ$ for $K = 0.55$ corresponds with a film thickness for the same conditions which is only 0.17 greater than the rigid minimum film thickness.

The consequence of using a value of β_δ other than 1 is that of modifying the Elasticity factor, and the results of Alexandrov for a plain bearing are acceptable in this light. For example, the Sommerfeld number, friction and flow in the above instance are correct for an Elasticity factor approximately equal to 0.05 (rather than 0.55).

In the present work, the new value of film thickness at each step of the iteration was found by the addition of the under relaxed value of the distortion (say $\bar{\delta}'$) to the rigid film thickness, that is

$$\bar{h}_n = \bar{h}_r + \bar{\delta}'_{n-1}$$

where $\bar{\delta}'_{n-1} = \bar{\delta}'_{n-2} + \beta_\delta(\bar{\delta}_{n-1} - \bar{\delta}'_{n-2})$.

For example,

$$\bar{h}_2 = \bar{h}_r + \bar{\delta}'_1 \qquad (7.4.)$$

$$\bar{h}_3 = \bar{h}_r + \bar{\delta}'_2 \qquad (7.5.)$$

If this is expressed in terms of the old and new values of film thickness, then eliminating $\bar{h}_r$ from eq. 7.4. and eq. 7.5. gives

$$\bar{h}_3 = \bar{h}_2 + (\bar{\delta}'_2 - \bar{\delta}'_1) \quad .$$

Thus, the correct way of updating the film thickness is by the addition of the change in the under relaxed values of distortion to the previous film thickness, rather than the addition of the under relaxed change in the value of distortion as in Alexandrov's case.

Although the results of Alexandrov for a plain bearing are acceptable, bearing in mind the modified Elasticity factor, the situation for a bearing with a pocketed elastic journal liner is more complicated. Alexandrov uses the equivalent of the unrelaxed value of distortion in calculating the volumetric flow from a pocket. Therefore, the value of the distortion used in calculating the flow from a pocket is different to the value of the distortion used in calculating the film thickness around the pocket. In the above example,

for instance, the distortion used in calculating the volumetric flow from a pocket would be approximately ten times greater than the distortion used in calculating the film thickness around the pocket. That is, the pocket flow is artificially ten times greater than the correct value for a given film thickness around the pocket (or vice-versa).

As Alexandrov's source programme was available at Imperial College, the statement concerning the updating of film thickness was changed. A subsequent run of the programme then gave comparable results to the present theoretical analysis.

The artificially boosted pocket flow in Alexandrov's case therefore fully explains the differences between his and the present work.

7.3. Conclusions.

The present work confirms previous results for plain elastic bearings when compared to plain rigid bearings.

Firstly, the Sommerfeld number for a plain elastic bearing is lower for a given eccentricity ratio due to the effect of the distortion increasing the film thickness.

Secondly, the bearing friction is also reduced due to the larger film thicknesses.

Thirdly, the peak pressure is reduced and the angle at which the film cavitates is increased,

the pressure field having a flatter profile and operating over a wider circumferential arc. This is reflected in a lower attitude angle at low eccentricity ratios and a higher attitude angle at high eccentricity ratios.

Lastly, all the above effects are increased as the Elasticity factor, K, is increased.

The introduction of pockets to the elastic journal liner is found both in the present theoretical predictions and their overall agreement with the experimental observations to produce the following effects when compared to a plain rigid bearing.

Firstly, at low values of eccentricity ratio (approximately less than 0.6), the Sommerfeld number is reduced due to the presence of pockets providing a lower hydrodynamic area. This has a major effect as the pockets are situated on the centre plane of the bearing where the pressures in plain bearings have a maximum value.

Secondly, the presence of pockets also reduces the bearing friction at low eccentricity ratios due to the smaller proportion of film being sheared.

Thirdly, for values of eccentricity ratio in the range $0.6 < \varepsilon < 1.0$ a continued reduction in the Sommerfeld number and the bearing friction is observed in contrast to the theoretical predictions of Alexandrov. The discovery of a logic error in the work of Alexandrov fully accounts for this difference.

Fourthly, at values of eccentricity ratio greater than approximately 0.6, the Sommerfeld number continues to be small in comparison to plain rigid bearings. The reason for this is probably a combination of the reduced hydrodynamic area in the presence of pockets and the elastohydrodynamic land profiles observed at the leading and trailing edges of the pockets reducing the displaced pocket volumes and hence the pumping action of the pockets. This is confirmed by the theoretical results of Chapter 4 where the side flow from the pocketed bearing is broadly similar to that of the plain rigid bearing.

Fifthly, the reduction in the Sommerfeld number at high values of eccentricity ratio is accompanied by a larger bearing friction due to the presence of small film thicknesses as a result of the elastohydrodynamic land profiles, particularly in the region of minimum film thickness. Hence, comparison on a more realistic performance basis shows no advantages of the bearing with a pocketed elastic journal liner over both rigid and elastic plain bearings.

Sixthly, following the point of maximum pressure, the pockets are seen to act as sinks in the opposite way to those acting as sources in the region of the positive pressure gradient. This induces cavitation at an earlier point than in plain bearings. As a result, the Sommerfeld number is lower due to

a lower value for the integrated pressure field, and the bearing friction is higher due to smaller film thicknesses around the point of minimum film thickness.

Lastly, the presence of pockets introduces a dynamic effect which is seen in the different theoretical predictions for different positions of the start of the film, and as an oscillation in the dependent variables in the experimental results.

The precise reasons for this particular bearing configuration not showing the expected self pressurizing effects of the original concept are probably interdependent.

The presence of air bubbles in the pockets providing a derating effect on the bearing is unlikely because of the results of test series 3 with a high inlet pressure. Similarly, an order of magnitude analysis shows that the compressibility of the oil in the pockets is small with respect to the pocket flow.

The following reasons are therefore suggested for the discrepancy between the original concept of self pressurizing effects producing an increase in performance and the above conclusions.

Firstly, at low values of eccentricity ratio the pressure which produces the change in pocket volume (and hence the self pressurizing action) also increases the local film thickness around the pocket and hence the flow from a pocket is being forced through an increased gap.

Secondly, as the eccentricity ratio is increased (to approximately 1.0 and greater), it would be expected that the mechanism show increased performance when the distortion at the land edges producing the pocket flow is comparable to and greater than the local film thickness around the pocket. In reality this does not occur due to the elastohydrodynamic land shapes detracting from the displaced pocket volume. The secondary effect of early cavitation caused by the pockets acting as sinks also reduces the performance.

7.4. Suggestions For Further Work.

It is considered unlikely that further work on the particular configuration of a pocketed elastic liner bonded to the journal, for example a more exact theoretical treatment of distortion for the finite length bearing, will show significant differences in trends to the present work.

The basic concept of Ettles (18,19,20), however, of self contained pressure sources travelling with the journal is still valid. The work of Alexandrov where a high (albeit artificial) value of pocket distortion with respect to the local film thickness around a pocket produces an increase in performance confirms this.

The main disadvantage of the present configuration would appear to be the elastohydrodynamic

land profiles which effectively reduce the displaced pocket volume. It is likely that other configurations suggested by Ettles would overcome this problem, and hence theoretical analyses together with experimental confirmation of these alternative configurations would be useful. In particular, the provision of a pocketed rigid journal liner with an elastic substrate, which in principle is similar to the 'sealed piston' device (or free ring type with back sealing) analysed by Ettles, could well show a significant increase in performance. The elastohydrodynamic effects which exist in the present configuration would not be present in this case due to the local rigidity of the liner surface.

The bearing with a pocketed elastic journal liner is just one of the methods suggested by Ettles of attempting to increase the performance of fluid film bearings, and it is conceivable that the characteristics of other suggested configurations would produce an enhancement of the operating conditions of fluid film journal bearings.

APPENDIX A1.

LITERATURE REFERENCES.

1. Tower, B.

'Friction Experiments'.

Proc. Inst. Mech. Engrs.

1st Report, Nov. 1883, p.636-66;

2nd Report, 1885, p.58-70;

3rd Report, 1888, p.173-205;

4th Report, 1891, p.111-40.

2. Reynolds, O.

'On The Theory Of Lubrication And Its Application To Mr. Beauchamp Tower's Experiments, Including An Experimental Determination Of The Viscosity Of Olive Oil'.

Phil. Trans. Roy. Soc., London, vol. 177, part I, 1886, p.157-234.

3. Motosh, N.

'Cylindrical Journal Bearings Under Constant Load, The Influence Of Temperature And Pressure On Viscosity' .

Proc. 2nd Conv. Lub. and Wear, Proc. Inst. Mech. Engrs., paper 24, 1964, p.148.

4. Higginson, G.R.
'The Theoretical Effects Of Elastic Deformation Of The Bearing Liner On Journal Bearing Performance'.
Proc. Symp. On Elastohydrodynamic Lubrication, paper 1, 1965-66, 180, 3B, p.31.

5. O'Donoghue, J.P.; Brighton, D.K. and Hooke, C.J.
'The Effect Of Elastic Distortions On Journal Bearing Performance'.
J. Lubrication Technology, Trans. A.S.M.E., 1967, 89, series F, no. 4, p.409.

6. Hooke, C.J.; Brighton, D.K. and O'Donoghue, J.P.
'The Effect Of Elastic Distortions On The Performance Of Thin Shell Bearings'.
Symp. On Journal Bearings For Reciprocating And Turbo Machinery, Proc. Inst. Mech. Engrs., paper 10, 1966-67, 181, 3B, p.63.

7. Brighton, D.K.; Hooke, C.J. and O'Donoghue, J.P.
'A Theoretical And Experimental Investigation Of The Effect Of Elastic Distortions On The Performance Of Journal Bearings'.
Tribology Conv., Proc. Inst. Mech. Engrs., paper 23, 1967-68, 182, 3N, p.192.

8. Hooke, C.J.; Koch, P.R. and O'Donoghue, J.P.
'Heavily Loaded Rubber Journal Bearings'.
Tribology Conv., Proc. Inst. Mech. Engrs.,
report paper 10, 1967-68, 182, 3N, p.269.

9. O'Donoghue, J.P.; Koch, P.R. and Hooke, C.J.
'Approximate Short Bearing Analysis And
Experimental Results Obtained Using Plastic
Bearing Liners'.
Tribology Conv., Proc. Inst. Mech. Engrs.,
report paper 2, 1969-70, 184, 3L, p.190.

10. Oh, K.P. and Heubner, K.H.
'Solution Of The Elastohydrodynamic Finite
Journal Bearing Problem'.
J. Lubrication Technology, Trans. A.S.M.E.,
1973, 95, series F, no. 3, p.342.

11. Conway, H.D. and Lee, H.C.
'The Analysis Of The Lubrication Of A
Flexible Journal Bearing'.
J. Lubrication Technology, Trans. A.S.M.E.
1975, p.599.

12. Taylor, G.I.
'The Stability Of A Viscous Liquid Contained
Between Two Rotating Cylinders'.
Trans. Roy. Soc., 1923, 223, series A, p.289.

13. Wilcock, D.F.

'Turbulence In High Speed Journal Bearings'.

Trans. A.S.M.E., 1950, 72, no. 6, p.825-34.

14. Blok, H. and Van Rossum, J.J.

'The Foil Bearing; A New Departure In Hydrodynamic Lubrication'.

Lub. Engineering, Dec. 1975, vol. 9, no. 6, p.316.

15. Patel, B.J. and Cameron, A.

'The Foil Bearing'.

Conf. On Lub. And Wear, Proc. Inst. Mech. Engrs., 1957, paper 73, p.219.

16. O'Donoghue, J.P. and Rowe, W.B.

'Hydrostatic Bearing Design'.

Tribology, Feb. 1969, p.25-71.

17. Braithwaite, E.R. (editor)

'Lubrication And Lubricants'.

Elsevier Publishing Co., 1967, p.353-4.

18. Ettles, C. and Michell Bearings Ltd.

British Patent 24685/69.

Filed 14th May 1969.

19. Ettles, C. and Michell Bearings Ltd.

U.S. Patent 3804474.

Filed 16th April 1974.

20. Ettles, C.M.M.
'The Vane Bearing - A Self-Pressurizing Journal Bearing'.
Proc. Inst. Mech. Engrs., vol. 189, 3B, 1975, p.99-106.

21. Alexandrov, V.A.
'A Study Of The Vane Bearing With A Flexible Journal Liner'.
D.I.C. Thesis, Mechanical Engineering Dept., Imperial College, 1975.

22. Alexandrov, V.A. and Ettles, C.M.M.
'Analysis Of A Journal Bearing With Self-Boosted Pressure Generation'.
J. Mech. Eng. Science, vol. 19, no. 2, 1977, p.58-64.

23. Brighton, D.K.
'Elastohydrodynamic Lubrication Of Full Journal Bearings'.
Ph.D. Thesis, University Of London, 1969.

24. Christopherson, D.G.
'A New Mathematical Method For The Solution Of Film Lubrication Problems'.
Proc. Inst. Mech. Engrs., 146, no. 3, 1942, p.126-35.

25. Sheldon, D.F.; O'Donoghue, J.P. and Hooke, C.J.
'A Hydrodynamic Pocket Journal Bearing'.
Proc. Inst. Mech. Engrs., 184, 3L, 1969/70, p.70.

26. Wordsworth, R.A. and Ettles, C.M.M.
'The Effect Of Jacking Pockets In Hydrodynamic Thrust Pads'.
Wear, 1975, 31, p.167.

27. Zienkiewicz, O.C.
'The Finite Element Method In Engineering Science'.
McGraw-Hill, London, 1971, 2nd ed., pp.57, 166-69.

28. Timoshenko, S.P. and Goodier, J.N.
'Theory Of Elasticity'.
McGraw-Hill Kogakusha Ltd., 3rd ed., 1970, p.243.

29. Ranger, A.P.; Ettles, C.M.M. and Cameron, A.
'The Solution Of The Point Contact Elastohydrodynamic Problem'.
Proc. Roy. Soc., London, series A, 346, 1975, p.227-44.

30. Robinson, C.L. and Cameron, A.
'Studies In Hydrodynamic Thrust Bearings'.
Phil. Trans. Roy. Soc., London, series A, 278, 1975, p.351-66, (fig. 9 in particular).

31. Blok, H. and Koens, H.J.
'The 'Breathing' Film Between A Flexible Seal And A Reciprocating Rod'.
Proc. Symp. On Elastohydrodynamic Lubrication, 1965-66, 180, 3B, p.221.

32. Taylor, D. and Roberts, A.D.
'Fluid Film Lubrication Of Rubber-
An Interferometric Study'.
Wear, 11, 1968, p.163.

33. Swales, P.D.
'An Investigation Of The Lubrication Of
Rolling And Sliding Contacts Involving
Materials Of Low Elastic Moduli'.
Ph.D. Thesis, Leeds University, May 1969.

34. Lindley, P.B.
'Engineering Design With Natural Rubber'.
The Malaysian Rubber Producers' Research Association,
NR Technical Bulletin, 1974, p.19.

35. Op Cit. p.33.

APPENDIX A2.

THEORETICAL ANALYSIS NEGLECTING AXIAL FIELD VARIATION.

A2.1. Film Pressure.

Reynolds' equation for an infinitely long bearing is

$$\frac{d}{dx}\left(h^3\frac{dp}{dx}\right) = 6\eta U\frac{dh}{dx} .$$

Defining the dimensionless variables $h = c\bar{h}$ and $p = \frac{6\eta U R_2 \bar{p}}{c^2}$, and substituting these and $x = R_2\theta$ gives

$$\frac{d}{d\theta}\left(\bar{h}^3\frac{d\bar{p}}{d\theta}\right) = \frac{d\bar{h}}{d\theta} .$$

Expanding;

$$\frac{d^2\bar{p}}{d\theta^2} + \frac{3}{\bar{h}}\frac{d\bar{h}}{d\theta}\frac{d\bar{p}}{d\theta} = \frac{1}{\bar{h}^3}\frac{d\bar{h}}{d\theta} .$$

Boundary conditions are;

$$\bar{p} = 0 \text{ at } \theta = 0$$

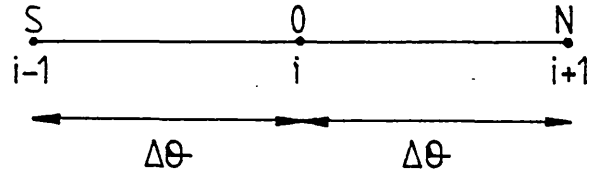
and

$$\bar{p} = \frac{d\bar{p}}{d\theta} = 0 \text{ at } \theta = \theta_{cav} .$$

Using the following finite difference approximations for the differentials,

$$\frac{d\bar{p}}{d\theta} = \frac{\bar{p}_{i+1} - \bar{p}_{i-1}}{2\Delta\theta} \quad , \quad \frac{d\bar{h}}{d\theta} = \frac{\bar{h}_{i+1} - \bar{h}_{i-1}}{2\Delta\theta} \quad ,$$

$$\frac{d^2\bar{p}}{d\theta^2} = \frac{\bar{p}_{i+1} - 2\bar{p}_i + \bar{p}_{i-1}}{\Delta\theta^2} \quad ,$$



and substituting gives

$$\frac{\bar{p}_{i+1} - 2\bar{p}_i + \bar{p}_{i-1}}{\Delta\theta^2} + \frac{3}{\bar{h}_i} \frac{(\bar{h}_{i+1} - \bar{h}_{i-1})(\bar{p}_{i+1} - \bar{p}_{i-1})}{4\Delta\theta^2}$$

$$= \frac{1}{\bar{h}_i^3} \frac{(\bar{h}_{i+1} - \bar{h}_{i-1})}{2\Delta\theta} \quad .$$

Rearranging this

$$\bar{p}_i = CN_i\bar{p}_{i+1} + CS_i\bar{p}_{i-1} + CO_i$$

where $$CN_i = \frac{1}{2} + \frac{3}{8\bar{h}_i} (\bar{h}_{i+1} - \bar{h}_{i-1})$$

$$CS_i = \frac{1}{2} - \frac{3}{8\bar{h}_i} (\bar{h}_{i+1} - \bar{h}_{i-1})$$

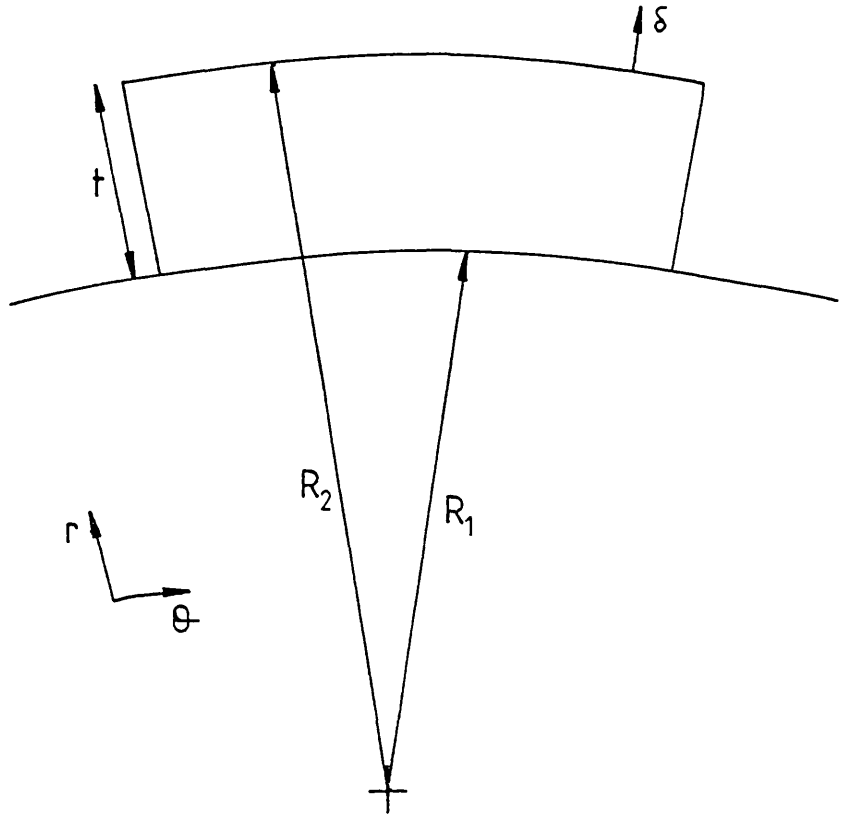
$$CO_i = \frac{-\Delta\theta}{4\bar{h}_i^3}(\bar{h}_{i+1} - \bar{h}_{i-1}) \quad .$$

$\bar{h}$ is defined at each point by

$$\bar{h}_i = 1 + \varepsilon\cos\theta - \bar{\delta}_i \quad .$$

The equation $\left[CN, CS\right]\left[\bar{p}\right] = \left[CO\right]$ is solved using Gauss-Seidel iteration including successive over relaxation in the form $\bar{p}_{new} = \bar{p}_{old} + \beta_p(\Delta\bar{p})$, where β_p is a relaxation factor $(1 < \beta_p < 2)$, and $\Delta\bar{p}$ is the change in pressure from one iteration to the next.

A2.2. Distortion.



For a linear elastic material, Hooke's law can be expressed as

$$\varepsilon_r = \frac{1}{E}\left\{\sigma_r - \nu(\sigma_\theta + \sigma_z)\right\}$$

$$\varepsilon_\theta = \frac{1}{E}\left\{\sigma_\theta - \nu(\sigma_r + \sigma_z)\right\}$$

$$\varepsilon_z = \frac{1}{E}\left\{\sigma_z - \nu(\sigma_r + \sigma_\theta)\right\} \qquad \text{(A2.1.)}$$

Assuming plane strain ($\varepsilon_z = 0$), and that the liner is bonded to the journal so that circumferential strains are negligible ($\varepsilon_\theta = 0$), then substituting for σ_θ and σ_z into eq. A2.1. gives

$$\varepsilon_r = \frac{1}{E}\left(1 - \frac{2\nu^2}{1-\nu}\right)\sigma_r \quad .$$

If we consider that σ_r is only a function of r, then at the outer surface of the land $\sigma_r = -p$ and the equation can be integrated to give

$$\delta = \frac{-t}{E}\left(1 - \frac{2\nu^2}{1-\nu}\right)p$$

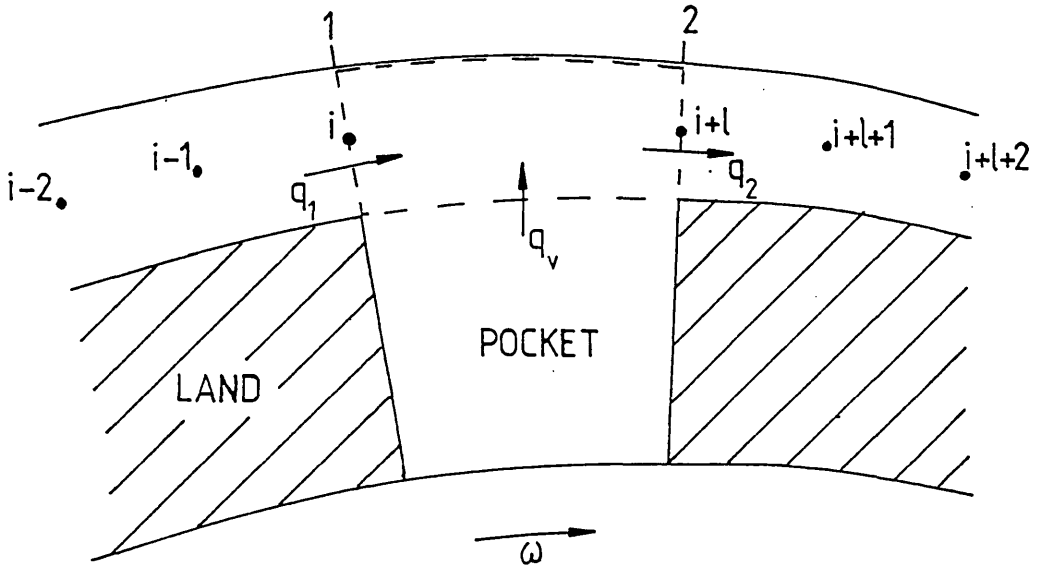
where t is the liner thickness. Substituting the dimensionless variables $\bar{\delta} = \frac{\delta}{c}$ and $\bar{p} = \frac{c^2 p}{6\eta U R_2}$,

then $\bar{\delta} = -K\bar{p}$

where $K = \dfrac{6\eta U R_2 t}{c^3 E}\left(1 - \dfrac{2\nu^2}{1-\nu}\right)$.

A2.3. Pocket Pressure.

A computing equation for pocket pressure is derived from a consideration of flow continuity.



The control volume is bounded by the bearing, the edge of the pocket and the film stations 1 and 2. Side flow is zero and so to satisfy flow continuity

$$q_v = q_2 - q_1 = q_n \qquad \text{(A2.2.)}$$

The film flows q_1 and q_2 are of the form

$$q = \frac{-h^3}{12\eta}\left(\frac{dp}{dx}\right) + \frac{Uh}{2} \quad .$$

Therefore,

$$q_1 = \frac{-h_1^3}{12\eta}\left(\frac{dp}{dx}\right) + \frac{h_1\,\omega(R_2 + \delta_1)}{2}$$

and similarly

$$q_2 = \frac{-h_2^3}{12\eta}\left(\frac{dp}{dx}\right) + \frac{h_2\,\omega(R_2 + \delta_2)}{2} \quad .$$

Substituting for the dimensionless variables $h = c\bar{h}$, $p = \frac{6\eta U R_2 \bar{p}}{c^2}$ and $x = R_2\theta$ gives

$$q_n = q_2 - q_1 = \frac{\omega c R_2}{2}\left\{\bar{h}_1^3\left(\frac{d\bar{p}}{d\theta}\right)_1 - \bar{h}_2^3\left(\frac{d\bar{p}}{d\theta}\right)_2 + \bar{h}_2\left(1 + \frac{\bar{\delta}_2 c}{R_2}\right) - \bar{h}_1\left(1 + \frac{\bar{\delta}_1 c}{R_2}\right)\right\}$$

For a uniform pocket pressure and due to the assumptions used in the distortion theory, then $\bar{\delta}_1 = \bar{\delta}_2 = \bar{\delta}_{poc}$.

Therefore,

$$\frac{2q_n}{\omega c R_2} = \bar{h}_1^3 \left(\frac{d\bar{p}}{d\bar{\theta}}\right)_1 - \bar{h}_2^3 \left(\frac{d\bar{p}}{d\bar{\theta}}\right)_2 + (\bar{h}_2 - \bar{h}_1)\left(1 + \bar{\delta}_{poc}\frac{c}{R_2}\right)$$

The flow from the pocket into the control volume is equal to the rate of change of displaced volume with respect to θ.

$$q_v = \omega \frac{dV}{d\theta} \qquad \text{(A2.4.)}$$

where the displaced volume

$$V = \frac{\Delta\theta_{poc}}{2}\left(R_2^2 - (R_2 + \delta_{poc})^2\right)$$

where $\Delta\theta_{poc}$ is the angle subtended by the pocket at the centre of the journal. Substituting $\delta = c\bar{\delta}$ and expanding gives

$$V = -\frac{\Delta\theta_{poc}}{2}\bar{\delta}_{poc}\, cR_2\left(2 + \bar{\delta}_{poc}\frac{c}{R_2}\right)$$

Substituting for V into eq. A2.4. gives

$$\frac{2q_v}{\omega c R_2} = \Delta\theta_{poc}\frac{d}{d\theta}\left(-\bar{\delta}_{poc}\left(2 + \bar{\delta}_{poc}\frac{c}{R_2}\right)\right)$$

Defining

$$\bar{V} = -\bar{\delta}_{poc}\left(2 + \bar{\delta}_{poc}\frac{c}{R_2}\right)$$

then $$\frac{2q_v}{\omega_c R_2} = \Delta\theta_{poc} \frac{d\bar{V}}{d\theta} \quad . \qquad (A2.5.)$$

Substituting for q_n from eq. A2.3. and q_v from eq. A2.5. into eq. A2.2. gives

$$\Delta\theta_{poc} \frac{d\bar{V}}{d\theta} = \bar{h}_1^3 \left(\frac{d\bar{p}}{d\theta}\right)_1 - \bar{h}_2^3 \left(\frac{d\bar{p}}{d\theta}\right)_2 + (\bar{h}_2 - \bar{h}_1)\left(1 + \bar{\delta}_{poc} \frac{c}{R_2}\right) \quad . (A2.6.)$$

At this point the question of how to approximate $\frac{d\bar{V}}{d\theta}$ arises. This was done in two ways.

i). Method 1.

This uses a coarse discretization namely

$$\frac{d\bar{V}}{d\theta} = \frac{\bar{V}^n - \bar{V}^{n-1}}{\Delta\theta_{pocl}}$$

where $\bar{V}^n$ is the displaced volume of the n^{th} pocket, and $\Delta\theta_{pocl}$ is the angle subtended by a pocket and land together at the journal centre.

Eq. A2.6. as a whole is discretized taking station 1 as node i and station 2 as node i + 1. As

the differentials $\left(\frac{d\bar{p}}{d\bar{\theta}}\right)_1$ and $\left(\frac{d\bar{p}}{d\bar{\theta}}\right)_2$ act at the edge

of a pocket, a parabolic interpolation is used.

$$\left(\frac{d\bar{p}}{d\bar{\theta}}\right)_1 = \frac{3\bar{p}_i - 4\bar{p}_{i-1} + \bar{p}_{i-2}}{2\Delta\bar{\theta}}$$

and $$\left(\frac{d\bar{p}}{d\bar{\theta}}\right)_2 = \frac{-3\bar{p}_{i+1} + 4\bar{p}_{i+1+1} - \bar{p}_{i+1+2}}{2\Delta\bar{\theta}} \quad .$$

Eq. A2.6. then gives

$$\frac{\Delta\bar{\theta}_{poc}}{\Delta\bar{\theta}_{pocl}} (\bar{v}^n - \bar{v}^{n-1}) - (\bar{h}_{i+1} - \bar{h}_i) \left(1 + \bar{\delta}_i \frac{c}{R_2}\right)$$

$$= \frac{\bar{h}_i^3}{2\Delta\bar{\theta}} (3\bar{p}_i - 4\bar{p}_{i-1} + \bar{p}_{i-2})$$

$$- \frac{\bar{h}_{i+1}^3}{2\Delta\bar{\theta}} (-3\bar{p}_{i+1} + 4\bar{p}_{i+1+1} - \bar{p}_{i+1+2}) \quad .$$

But $\bar{p}_{i+1} = \bar{p}_i$, therefore rearranging gives

$$\bar{p}_i = \frac{2\Delta\bar{\theta}}{3(\bar{h}_i^3 + \bar{h}_{i+1}^3)} \left\{ \frac{\Delta\bar{\theta}_{poc}}{\Delta\bar{\theta}_{pocl}} (\bar{v}^n - \bar{v}^{n-1}) \right.$$

$$\left. - (\bar{h}_{i+1} - \bar{h}_i) \left(1 + \bar{\delta}_i \frac{c}{R_2}\right) \right\}$$

$$+ \frac{\bar{h}_i^3(4\bar{p}_{i-1} - \bar{p}_{i-2}) + \bar{h}_{i+1}^3(4\bar{p}_{i+1+1} - \bar{p}_{i+1+2})}{3(\bar{h}_i^3 + \bar{h}_{i+1}^3)}$$

where $\bar{V} = -\bar{\delta}_i \left(2 + \bar{\delta}_i \frac{c}{R_2}\right)$

ii). Method 2.

This follows the method used by Alexandrov.

$$\frac{d\bar{V}}{d\theta} = \frac{d}{d\theta}\left\{-\bar{\delta}_{poc}\left(2 + \bar{\delta}_{poc}\frac{c}{R_2}\right)\right\} \quad .$$

As the term $\bar{\delta}_{poc}\frac{c}{R_2}$ is of the order of 10^3 less than 2

then it can be neglected.

$$\frac{d\bar{V}}{d\theta} = -2\,\frac{d(\bar{\delta}_{poc})}{d\theta} \quad .$$

But $\bar{\delta} = -K\bar{p}$, therefore

$$\frac{d\bar{V}}{d\theta} = 2K\left(\frac{d\bar{p}}{d\theta}\right)_{poc} \quad .$$

In the limit of small rotations of the journal, $\left(\frac{d\bar{p}}{d\bar{\theta}}\right)_{poc}$ is taken to be the mean of the pressure gradients at the edge of a pocket.

$$\left(\frac{d\bar{p}}{d\bar{\theta}}\right)_{poc} = \frac{\left(\frac{d\bar{p}}{d\bar{\theta}}\right)_1 + \left(\frac{d\bar{p}}{d\bar{\theta}}\right)_2}{2}$$

Therefore

$$\frac{d\bar{V}}{d\bar{\theta}} = K\left\{\left(\frac{d\bar{p}}{d\bar{\theta}}\right)_1 + \left(\frac{d\bar{p}}{d\bar{\theta}}\right)_2\right\}$$

Substituting for $\frac{d\bar{V}}{d\bar{\theta}}$ into eq. A2.6. and discretizing as before gives

$$\frac{K\Delta\bar{\theta}_{poc}}{2\Delta\bar{\theta}}\left\{(3\bar{p}_i - 4\bar{p}_{i-1} + \bar{p}_{i-2}) + (-3\bar{p}_{i+1} + 4\bar{p}_{i+1+1} - \bar{p}_{i+1+2})\right\}$$

$$= \frac{\bar{h}_i^3}{2\Delta\bar{\theta}}(3\bar{p}_i - 4\bar{p}_{i-1} + \bar{p}_{i-2})$$

$$- \frac{\bar{h}_{i+1}^3}{2\Delta\bar{\theta}}(-3\bar{p}_{i+1} + 4\bar{p}_{i+1+1} - \bar{p}_{i+1+2})$$

$$+ (\bar{h}_{i+1} - \bar{h}_i)\left(1 + \bar{\delta}_i\frac{c}{R_2}\right)$$

Putting $\bar{p}_i = \bar{p}_{i+1}$ and rearranging gives

$$\bar{p}_i = \frac{2\Delta\theta(\bar{h}_i - \bar{h}_{i+1})}{3(\bar{h}_i^3 + \bar{h}_{i+1}^3)} \left(1 + \bar{\delta}_i \frac{c}{R_2}\right)$$

$$- \frac{(\Delta\theta_{poc} K - \bar{h}_i^3)(4\bar{p}_{i-1} - \bar{p}_{i-2})}{3(\bar{h}_i^3 + \bar{h}_{i+1}^3)}$$

$$+ \frac{(\Delta\theta_{poc} K + \bar{h}_{i+1}^3)(4\bar{p}_{i+1+1} - \bar{p}_{i+1+2})}{3(\bar{h}_i^3 + \bar{h}_{i+1}^3)}$$

Both methods therefore yield an equation for the pocket pressure, $\bar{p}_i$, in terms of geometric variables and the film pressures surrounding the pocket. These computing equations can be included in the algorithm for film pressure.

A2.4. Load, Attitude Angle And Friction.

The load is found by integrating the pressure field. The two components of load per unit length, parallel and perpendicular to the line of centres, are given by

$$W_x = \frac{6\eta U R_2^2}{c^2} \int_0^{2\pi} \bar{p} \cos\theta \, d\theta = \frac{6\eta U R_2^2}{c^2} \bar{W}_x$$

$$W_y = \frac{6\eta U R_2^2}{c^2} \int_0^{2\pi} \bar{p} \sin\theta \, d\theta = \frac{6\eta U R_2^2}{c^2} \bar{W}_y$$

$\bar{W}_x$ and $\bar{W}_y$ are integrated using Simpson's rule. The Sommerfeld number

$$S = \frac{W}{LU\eta}\left(\frac{c}{R}\right)^2$$

where $$W = \sqrt{W_x^2 + W_y^2}$$

so $$W = \frac{6\eta U R_2^2}{c^2}\sqrt{\bar{W}_x^2 + \bar{W}_y^2}$$

Therefore

$$S = 6\sqrt{\bar{W}_x^2 + \bar{W}_y^2}$$

The angle between the line of centres and the load line, the attitude angle, is given by

$$\phi = \tan^{-1}\left(-\frac{\bar{W}_y}{\bar{W}_x}\right)$$

The frictional torque is found by integrating the elemental shear stresses

$$F = \int_0^{2\pi} \tau R_2 \, d\theta \qquad \text{per unit length,}$$

where $$\tau = \frac{\eta U}{h} + \frac{h}{2}\frac{dp}{dx} \quad .$$

The dimensionless friction

$$\bar{F} = \int_0^{2\pi} \frac{1}{\bar{h}} + 3\bar{h}\,\frac{d\bar{p}}{d\bar{\theta}}\; d\bar{\theta}$$

where $\bar{F} = \dfrac{Fc}{\eta U R_2}$ per unit length

$\bar{F}$ is integrated using Simpson's rule.

APPENDIX A3.

COMPUTER PROGRAMMES FOR AN INFINITELY LONG BEARING.

Variables.

ATT	Attitude angle, ϕ.
CDIVR	Clearance ratio, c/R_2.
CLEAR	Clearance, c.
DTHETA	Increment of theta, ϑ .
ELAST	Elasticity factor, K.
EPS	Eccentricity ratio, ε .
FRIC	Dimensionless friction, $\bar{F}$.
ITERD	Iteration limit for distortion.
ITERP	Iteration limit for pressure.
LADD	Number of meshes across a pocket and land.
LLAND	Number of meshes across a land.
LPOK	Number of meshes across a pocket.
NSTART	Number of nodes from the start of the first land to $\bar{h}_{max}$.
NSTEPX	Total number of meshes from $\vartheta = 0$ to $\vartheta = 2\pi$.
NUMPOK	Number of pockets, n_p.
NX	Total number of nodes from $\vartheta = 0$ to $\vartheta = 2\pi$.
OMEGA	Angular velocity of the journal, ω .
POISSN	Poisson's ratio, ν .
RDIVR	Ratio of journal to bearing radius, $\frac{R_1}{R_2} = \frac{R_2 - t}{R_2}$.

RELXD Distortion relaxation factor, β_δ.

RELXP Pressure relaxation factor, β_p.

RTWO Bearing radius, R_2.

SOMM Sommerfeld number, S.

TLINER Liner thickness, t.

VISCOS Viscosity, η.

YOUNG Young's modulus, E.

Subscripted Variables.

DEL Dimensionless distortion, $\bar{\delta}$.

H Dimensionless film thickness, $\bar{h}$.

LSKIP Matrix of flag coefficients taking the values:

-1 for pocket nodes.

0 for edge of pocket nodes.

+1 for land nodes.

P Dimensionless pressure, $\bar{p}$.

THETAN Angle from $\bar{h}_{max}$, θ.

```
      PROGRAM JB1(INPUT,OUTPUT,TAPE5=INPUT,TAPE6=OUTPUT)
C
C                     INFINITELY LONG PLAIN RIGID JOURNAL
C                     BEARING SOLUTION
C
      COMMON/CGEOM/NX,DTHETA,GEOM1,GEOM2
     1/CCOEFP/CN(103),CS(103),CC(103)
     2/CSOLVP/P(103),H(103),RELXP,ITERP,PITER(200),NMID
      DIMENSION FFX(103)
      DIMENSION THETAN(103)
C
C                     SET PROBLEM PARAMETERS
C
      PIE=3.1415926536
      READ(5,101)NSTEPX
  101 FORMAT(I5)
      WRITE(6,141)NSTEPX
  141 FORMAT(////,1HO,*NSTEPX=*,I5)
      READ(5,101)NEPS
      READ(5,102)RELXP,ITERP
  102 FORMAT(F10.5,I5)
      WRITE(6,142)RELXP,ITERP
  142 FORMAT(1HO,*RELXP=*,F10.5,5X,*ITERP=*,I5)
C
C                     CALCULATE INITIAL VALUES
C
      NX=NSTEPX+1
      DTHETA=2.*PIE/FLOAT(NSTEPX)
      GEOM1=3./8.
      GEOM2=-DTHETA/4.
      NMID=NSTEPX/3
      DO 1001 I=1,NX+1
      THETAN(I)=FLOAT(I-1)*DTHETA
      P(I)=0.
 1001 CONTINUE
C
C                     MAIN ITERATION LOOP              **********************
C
      DO 1002 N=1,NEPS
      READ(5,103)EPS
  103 FORMAT(F10.4)
      DO 1003 I=1,NX+1
      H(I)=1.+EPS*COS(THETAN(I))
 1003 CONTINUE
      CALL COEFP
      CALL CALCP
      WRITE(6,151)(PITER(M),M=1,ITERP)
  151 FORMAT(10F10.7)
C
C                     CALCULATE FINAL VALUES
C
      DO 1004 I=1,NX
      FFX(I)=P(I)*COS(THETAN(I))
 1004 CONTINUE
      CALL TRAP(FFX,1,NX,DTHETA,WX)
      DO 1005 I=1,NX
      FFX(I)=P(I)*SIN(THETAN(I))
 1005 CONTINUE
      CALL TRAP(FFX,1,NX,DTHETA,WY)
      SOMM=6.*SQRT(WX**2+WY**2)
      ATT=ATAN(-WY/WX)*180./PIE
      P(NX+1)=P(2)
      DO 1006 I=2,NX
      FFX(I)=1./H(I)+3.*H(I)*(P(I+1)-P(I-1))/DTHETA
```

```
 1006 CONTINUE
      FFX(1)=1./H(1)+3.*H(1)*(P(2)-P(NX))/DTHETA
      CALL TRAP(FFX,1,NX,DTHETA,FRIC)
C
C                    WRITE FINAL RESULTS FOR EACH VALUE OF EPS
C
      WRITE(6,152)EPS
  152 FORMAT(///,1HO,*EPS=*,F10.4)
      WRITE(6,153)SOMM,ATT
  153 FORMAT(1HO,*SOMMERFELD NUMBER=*,F10.6,5X,*ATTITUDE ANGLE=*,F10.6,
     1*DEGREES*)
      WRITE(6,154)FRIC
  154 FORMAT(1HO,*FRICTION=*,F10.6)
      WRITE(6,155)
  155 FORMAT(1HO,*FINAL PRESSURE FIELD*,/)
      WRITE(6,160) (P(I),I=1,NX)
  160 FORMAT(1H ,12F10.6)
      WRITE(6,156)
  156 FORMAT(1HO,*FINAL FILM THICKNESS FIELD*,/)
      WRITE(6,160) (H(I),I=1,NX)
 1002 CONTINUE
C
C                    END OF MAIN ITERATION LOOP     **********************
C
      STOP
      END

      SUBROUTINE COEFP
      COMMON/CGEOM/NX,DTHETA,GEOM1,GEOM2
     1/CCOEFP/CN(103),CS(103),CC(103)
     2/CSOLVP/P(103),H(103),RELXP,ITERP,PITER(200),NMID
      DO 2001 I=2,NX-1
      HMEAN=H(I+1)-H(I-1)
      CN(I)=0.5+GEOM1*HMEAN/H(I)
      CS(I)=0.5-GEOM1*HMEAN/H(I)
      CC(I)=GEOM2*HMEAN/(H(I)**3)
 2001 CONTINUE
      RETURN
      END

      SUBROUTINE CALCP
      COMMON/CGEOM/NX,DTHETA,GEOM1,GEOM2
     1/CCOEFP/CN(103),CS(103),CC(103)
     2/CSOLVP/P(103),H(103),RELXP,ITERP,PITER(200),NMID
      DO 3001 M=1,ITERP
      DO 3002 I=2,NX-1
      OLDP=P(I)
      P(I)=CN(I)*P(I+1)+CS(I)*P(I-1)+CC(I)
      P(I)=OLDP+RELXP*(P(I)-OLDP)
      IF(P(I).LT.0.)P(I)=0.
 3002 CONTINUE
      PITER(M)=P(NMID)
 3001 CONTINUE
      RETURN
      END

      SUBROUTINE TRAP(F,NA,NZ,H,AREA)
      DIMENSION F(NZ)
C
C     SUBROUTINE TO INTEGRATE A FUNCTION F USING
C     TRAPEZOIDAL RULE BETWEEN LIMITS NA AND NZ
C     WITH STEP WIDTH H AND GIVING ANSWER AREA
C
      IF((NZ-NA).EQ.1)GO TO 91
```

```
      IF((NZ-NA).EQ.0)GO TO 92
      NB=NA+1
      NY=NZ-1
      SUM=0.
      DO 9001 ITRAP=NB,NY
      SUM=SUM+F(ITRAP)
 9001 CONTINUE
      AREA=0.5*H*(F(NA)+F(NZ)+2.*SUM)
      GO TO 93
   91 AREA=0.5*H*(F(NA)+F(NZ))
      GO TO 93
   92 AREA=0.
   93 RETURN
      END
```

```
      PROGRAM JBDEL1(INPUT,OUTPUT,TAPE5=INPUT,TAPE6=OUTPUT,TAPE1,TAPE2)
C
C                     INFINITELY LONG JOURNAL BEARING WITH
C                     ELASTIC LINER
C
      COMMON/CGEOM/NX,DTHETA,GEOM1,GEOM2,EPS,THETAN(103)
     1/CCOEFP/CN(103),CS(103),CC(103)
     2/CSOLVP/P(103),H(103),RELXP,ITERP,PITER(200),NMID
     3/CDEFL/RELXD,ITERD,ELAST,DEL(103),DITER(50)
      DIMENSION FFX(103)
C
C                     SET PROBLEM PARAMETERS
C
      PIE=3.1415926536
      READ(5,101)NSTEPX,ELAST
  101 FORMAT(I5,F10.4)
      WRITE(6,102)NSTEPX,ELAST
  102 FORMAT(////,1HO,*NSTEPX=*,I5,5X,*ELAST=*,F10.5)
      READ(5,103)NEPS
  103 FORMAT(I5)
      READ(5,104)RELXP,ITERP,RELXD,ITERD
  104 FORMAT(F10.5,I5,F10.5,I5)
      WRITE(6,105)RELXP,ITERP,RELXD,ITERD
  105 FORMAT(1HO,*RELXP=*,F10.5,5X,*ITERP=*,I5,5X,
     1*RELXD=*,F10.5,5X,*ITERD=*,I5)
C
C                     CALCULATE INITIAL VALUES
C
      NX=NSTEPX+1
      DTHETA=2.*PIE/FLOAT(NSTEPX)
      GEOM1=3./8.
      GEOM2=-DTHETA/4.
      NMID=NSTEPX/3
      DO 1001 I=1,NX+1
      THETAN(I)=FLOAT(I-1)*DTHETA
 1001 CONTINUE
      READ(1)(P(I),I=1,NX+1),(DEL(I),I=1,NX+1)
C
C                     MAIN ITERATION LOOP            **********************
C
      READ(1)EPS
      DO 1002 N=1,NEPS
      READ(5,106)DEPS
  106 FORMAT(F10.4)
      EPS=EPS+DEPS
      DO 1003 NDIT=1,ITERD
      CALL COEFP
      CALL CALCP
      CALL DEFL
      DITER(NDIT)=DEL(NMID)
 1003 CONTINUE
      WRITE(6,107)
  107 FORMAT(////,1HO,*PRESSURE CONVERGANCE FOR FINAL ITERATION*)
      WRITE(6,108)(PITER(M),M=1,ITERP)
  108 FORMAT(10F10.7)
C
C                     CALCULATE FINAL VALUES
C
      DO 1004 I=1,NX
      FFX(I)=P(I)*COS(THETAN(I))
 1004 CONTINUE
      CALL SIMP(FFX,1,NX,DTHETA,WX)
      DO 1005 I=1,NX
      FFX(I)=P(I)*SIN(THETAN(I))
```

```
 1005 CONTINUE
      CALL SIMP(FFX,1,NX,DTHETA,WY)
      SOMM=6.*SQRT(WX**2+WY**2)
      ATT=ATAN(-WY/WX)*180./PIE
      P(NX+1)=P(2)
      DO 1006 I=2,NX
      FFX(I)=1./H(I)+3.*H(I)*(P(I+1)-P(I-1))/DTHETA
 1006 CONTINUE
      FFX(1)=1./H(1)+3.*H(1)*(P(2)-P(NX))/DTHETA
      CALL SIMP(FFX,1,NX,DTHETA,FRIC)
C
C                    WRITE FINAL RESULTS FOR EACH VALUE OF EPS
C
      WRITE(6,109)EPS,DEPS
  109 FORMAT(///,1HO,*EPS=*,F10.4,5X,*DEPS=*,F10.4)
      WRITE(6,110)SOMM,ATT
  110 FORMAT(1HO,*SOMMERFELD NUMBER=*,F10.6,5X,*ATTITUDE ANGLE=*,F10.6,
     1*DEGREES*)
      WRITE(6,111)FRIC
  111 FORMAT(1HO,*FRICTION=*,F10.6)
      WRITE(6,112)
  112 FORMAT(1HO,*FINAL PRESSURE FIELD*,/)
      WRITE(6,113)(P(I),I=1,NX)
  113 FORMAT(1H ,12F10.6)
      WRITE(6,114)
  114 FORMAT(1HO,*FINAL FILM THICKNESS FIELD*,/)
      WRITE(6,113)(H(I),I=1,NX)
      WRITE(6,115)
  115 FORMAT(1HO,*FINAL DISTORTION FIELD*,/)
      WRITE(6,113)(DEL(I),I=1,NX)
      WRITE(6,116)
  116 FORMAT(//,1HO,*DISTORTION CONVERGANCE*)
      WRITE(6,117)(DITER(M),M=1,ITERD)
  117 FORMAT(1HO,10F10.6)
      WRITE(2)(P(I),I=1,NX+1),(DEL(I),I=1,NX+1)
      WRITE(2)EPS
 1002 CONTINUE
C
C                    END OF MAIN ITERATION LOOP     **********************
C
      STOP
      END

      SUBROUTINE COEFP
      COMMON/CGEOM/NX,DTHETA,GEOM1,GEOM2,EPS,THETAN(103)
     1/CCOEFP/CN(103),CS(103),CC(103)
     2/CSOLVP/P(103),H(103),RELXP,ITERP,PITER(200),NMID
     3/CDEFL/RELXD,ITERD,ELAST,DEL(103),DITER(50)
      DO 2001 I=1,NX+1
      H(I)=1.+EPS*COS(THETAN(I))-DEL(I)
 2001 CONTINUE
      DO 2002 I=2,NX-1
      HMEAN=H(I+1)-H(I-1)
      CN(I)=0.5+GEOM1*HMEAN/H(I)
      CS(I)=0.5-GEOM1*HMEAN/H(I)
      CC(I)=GEOM2*HMEAN/(H(I)**3)
 2002 CONTINUE
      RETURN
      END

      SUBROUTINE CALCP
      COMMON/CGEOM/NX,DTHETA,GEOM1,GEOM2,EPS,THETAN(103)
     1/CCOEFP/CN(103),CS(103),CC(103)
     2/CSOLVP/P(103),H(103),RELXP,ITERP,PITER(200),NMID
```

```
      DO 3001 M=1,ITERP
      DO 3002 I=2,NX-1
      OLDP=P(I)
      P(I)=CN(I)*P(I+1)+CS(I)*P(I-1)+CC(I)
      P(I)=OLDP+RELXP*(P(I)-OLDP)
      IF(P(I).LT.0.)P(I)=0.
 3002 CONTINUE
      PITER(M)=P(NMID)
 3001 CONTINUE
      RETURN
      END

      SUBROUTINE DEFL
      COMMON/CGEOM/NX,DTHETA,GEOM1,GEOM2,EPS,THETAN(103)
     1/CSOLVP/P(103),H(103),RELXP,ITERP,PITER(200),NMID
     2/CDEFL/RELXD,ITERD,ELAST,DEL(103),DITER(50)
      DO 4001 I=1,NX+1
      OLDD=DEL(I)
      DEL(I)=OLDD+RELXD*(-ELAST*P(I)-OLDD)
 4001 CONTINUE
      RETURN
      END

      SUBROUTINE SIMP(F,NA,NZ,H,AREA)
      DIMENSION F(NZ)
C
C                    SUBROUTINE TO INTEGRATE A FUNCTION F USING
C                    SIMPSON RULE BETWEEN LIMITS NA AND NZ
C                    WITH STEP WIDTH H AND GIVING ANSWER AREA
C
      NB2=NA+2
      NB4=NA+1
      NY2=NZ-2
      NY4=NZ-1
      SUM2=0.
      SUM4=0.
      DO 9001 ISIMP=NB2,NY2,2
      SUM2=SUM2+F(ISIMP)
 9001 CONTINUE
      DO 9002 ISIMP=NB4,NY4,2
      SUM4=SUM4+F(ISIMP)
 9002 CONTINUE
      AREA=(H/3.)*(F(NA)+2.*SUM2+4.*SUM4+F(NZ))
      RETURN
      END
```

```
      PROGRAM VANE1A(INPUT,OUTPUT,TAPE5=INPUT,TAPE6=OUTPUT,TAPE1,TAPE2)
C
C                     INFINITELY LONG JOURNAL BEARING WITH
C                     POCKETED ELASTIC JOURNAL LINER, METHOD 1
C                     USED FOR POCKET PRESSURE ANALYSIS
C
      COMMON/CGEOM/LSKIP(203),NUMPOK,NX,LPOK,LLAND,DTHETA,PIE
     1/CCOEFP/H(203),CN(203),CS(203),CC(203),THETAN(203),CDIVR,RDIVR
     2/CSOLVP/P(203),DVOL(250),RELXP,ITERP,EPS,NMID,NXZ,NXPOK(30)
     3/CDEFL/DEL(203),RELXD,ITERD,ELAST,GEOMPK,LADD
      DIMENSION PMID(100),DELMID(100)
      DIMENSION FP(202)
      DIMENSION FF(202)
C
C           SET PROBLEM PARAMETERS
C
      PIE=3.1415926536
      READ(1)NSTEPX,NUMPOK,LPOK,LLAND,NSTART
      READ(5,101)ITERP,RELXP
  101 FORMAT(I5,F10.4)
      READ(5,102)RTWO,TLINER,CLEAR
  102 FORMAT(3F10.4)
      READ(5,103)VISCOS,OMEGA,YOUNG,POISSN
  103 FORMAT(E10.4,F10.4,E10.4,F10.4)
      READ(5,104)RELXD,ITERD
  104 FORMAT(F10.4,I5)
      READ(5,105)DEPS
  105 FORMAT(F10.4)
      WRITE(6,106)NSTEPX,NUMPOK,LPOK,LLAND,NSTART,ITERP
  106 FORMAT(/////,1HO,*NSTEPX=*,I5,5X,*NUMPOK=*,I5,5X,*LPOK=*,I5,5X,
     1*LLAND=*,I5,5X,*NSTART=*,I5,5X,*ITERP=*,I5,5X)
      WRITE(6,107)RELXP
  107 FORMAT(1HO,*RELXP=*,F10.5,5X)
      WRITE(6,108)RTWO,TLINER,CLEAR
  108 FORMAT(1HO,*RTWO=*,F10.5,5X,*TLINER=*,F10.5,5X,*CLEAR=*,F10.5,5X)
      WRITE(6,109)VISCOS,OMEGA,YOUNG,POISSN
  109 FORMAT(1HO,*VISCOS=*,E10.4,5X,*OMEGA=*,F10.4,5X,
     1*YOUNG=*,E10.4,5X,*POISSN=*,F10.4,5X)
      WRITE(6,110)RELXD,ITERD
  110 FORMAT(1HO,*RELXD=*,F10.4,5X,*ITERD=*,I5,5X)
C
C           CALCULATE PROBLEM PARAMETERS
C
      NX=NSTEPX+1
      DTHETA=2.*PIE/FLOAT(NSTEPX)
      CDIVR=CLEAR/RTWO
      RDIVR=(RTWO-TLINER)/RTWO
      EMAT=(1.-(2.*POISSN**2)/(1.-POISSN))/YOUNG
      ELAST=6.*VISCOS*OMEGA*EMAT*(1./CDIVR**3)*(1.-RDIVR)
      NMID=(NUMPOK/2)*(LPOK+LLAND)-LPOK-LLAND/2
      NXZ=NX-1
      IF(NSTART.EQ.1)NXZ=NX-LPOK-2
      IF(NSTART.GT.LLAND)NXZ=NX-NSTART+LLAND
      LADD=LPOK+LLAND
      GEOMPK=FLOAT(LPOK)/FLOAT(LADD)
      READ(1)EPS
      EPS=EPS+DEPS
      WRITE(6,111)EPS,DEPS
  111 FORMAT(1HO,*EPS=*,F10.5,5X,*DEPS=*,F10.5)
      WRITE(6,112)EMAT,ELAST
  112 FORMAT(1HO,*EMAT=*,E10.4,5X,*ELAST=*,F10.5)
      READ(1)(P(I),I=1,NX+2),(DEL(I),I=1,NX+2),(LSKIP(I),I=1,NX+2),
     1(THETAN(I),I=1,NX+2)
      DO 1001 N=1,NUMPOK+1
```

```
      IF (NSTART.GT.LLAND) GO TO 11
      LNO=LLAND-NSTART+2+(N-1)*LADD
      GO TO 12
   11 LNO=LLAND-NSTART+2+N*LADD
   12 NXPOK(N)=LNO
 1001 CONTINUE
C
C           MAIN ITERATION LOOP
C
      DO 1002 NDIT=1,ITERD
      CALL COEFP
      CALL CALCP
      CALL DEFL
      PMID(NDIT)=P(NMID)
      DELMID(NDIT)=DEL(NMID)
 1002 CONTINUE
      DO 1003 I=1,NX
      FP(I)=P(I)*COS(THETAN(I))
 1003 CONTINUE
      CALL SIMP(FP,1,NX,DTHETA,WX)
      DO 1004 I=1,NX
      FP(I)=P(I)*SIN(THETAN(I))
 1004 CONTINUE
      CALL SIMP(FP,1,NX,DTHETA,WY)
      SOMM=6.*SQRT(WX**2+WY**2)
      ATT=ATAN(-WY/WX)*180./PIE
      DO 1005 I=1,NX
      IF(LSKIP(I).NE.-1) GO TO 1005
      H(I)=1.+EPS*COS(THETAN(I))+TLINER/CLEAR
 1005 CONTINUE
      DO 1006 I=2,NX
      FF(I)=1./H(I)+3.*H(I)*(P(I+1)-P(I-1))/(2.*DTHETA)
 1006 CONTINUE
      FF(1)=1./H(1)+3.*H(1)*(P(2)-P(NX-1))/(2.*DTHETA)
      CALL SIMP(FF,1,NX,DTHETA,FRIC)
C
C           WRITE FINAL VALUES
C
      WRITE(6,113)
  113 FORMAT(//,1HO,*FINAL PRESSURE FIELD*)
      WRITE(6,114) (P(I),I=1,NX+2)
  114 FORMAT(1HO,10F10.5)
      WRITE(6,115)
  115 FORMAT(//,1HO,*FINAL DISTORTION FIELD*)
      WRITE(6,114) (DEL(I),I=1,NX+2)
      WRITE(6,116)
  116 FORMAT(//,1HO,*FINAL FILM THICKNESS FIELD*)
      WRITE(6,114) (H(I),I=1,NX+2)
      WRITE(6,117)SOMM
  117 FORMAT(//,1HO,*SOMMERFELD NUMBER=*,F10.5)
      WRITE(6,118)ATT
  118 FORMAT(//,1HO,*ATTITUDE ANGLE=*,F10.5,5X,*DEGREES*)
      WRITE(6,119)FRIC
  119 FORMAT(//,1HO,*FRICTION=*,F10.5)
      WRITE(6,120)
  120 FORMAT(//,1HO,*MAIN CONVERGANCE*,/,1HO,5X,*PMID*,5X,*DELMID*)
      WRITE(6,121) (PMID(N),DELMID(N),N=1,ITERD)
  121 FORMAT(1HO,2F10.5)
C
C           WRITE VALUES TO DATA FILE
C
      WRITE(2)NSTEPX,NUMPOK,LPOK,LLAND,NSTART
      WRITE(2)EPS
      WRITE(2) (P(I),I=1,NX+2),(DEL(I),I=1,NX+2),(LSKIP(I),I=1,NX+2),
```

```
     1(THETAN(I),I=1,NX+2)
      STOP
      END

      SUBROUTINE COEFP
      COMMON/CGEOM/LSKIP(203),NUMPOK,NX,LPOK,LLAND,DTHETA,PIE
     1/CCOEFP/H(203),CN(203),CS(203),CC(203),THETAN(203),CDIVR,RDIVR
     2/CSOLVP/P(203),DVOL(250),RELXP,ITERP,EPS,NMID,NXZ,NXPOK(30)
     3/CDEFL/DEL(203),RELXD,ITERD,ELAST,GEOMPK,LADD
      DIMENSION VOL(30)
      DO 3002 I=1,NX+2
      IF(LSKIP(I).EQ.-1)GO TO 3002
      H(I)=1.+EPS*COS(THETAN(I))-DEL(I)
3002  CONTINUE
      DO 3003 I=1,NUMPOK
      VOL(I)=-DEL(NXPOK(I))*(DEL(NXPOK(I))*CDIVR+2.)
3003  CONTINUE
      DVOL(NXPOK(1))=GEOMPK*(VOL(1)-VOL(NUMPOK))
      DO 3004 I=2,NUMPOK
      DVOL(NXPOK(I))=GEOMPK*(VOL(I)-VOL(I-1))
3004  CONTINUE
      DO 3001 I=2,NXZ
      IF(LSKIP(I))3001,32,33
   32 IF(LSKIP(I-1).EQ.-1)GO TO 3001
      HCUBP=3.*(H(I+LPOK)**3+H(I)**3)
      CN(I)=H(I+LPOK)**3/HCUBP
      CS(I)=H(I)**3/HCUBP
      CC(I)=2.*DTHETA*(DVOL(I)+H(I)*(1.+DEL(I)*CDIVR)
     1                      -H(I+LPOK)*(1.+DEL(I+LPOK)*CDIVR))/HCUBP
      GO TO 3001
   33 CN(I)=0.5+3.*(H(I+1)-H(I-1))/(8.*H(I))
      CS(I)=0.5-3.*(H(I+1)-H(I-1))/(8.*H(I))
      CC(I)=-DTHETA*(H(I+1)-H(I-1))/(4.*H(I)**3)
3001  CONTINUE
      RETURN
      END

      SUBROUTINE CALCP
      COMMON/CGEOM/LSKIP(203),NUMPOK,NX,LPOK,LLAND,DTHETA,PIE
     1/CCOEFP/H(203),CN(203),CS(203),CC(203),THETAN(203),CDIVR,RDIVR
     2/CSOLVP/P(203),DVOL(250),RELXP,ITERP,EPS,NMID,NXZ,NXPOK(30)
     3/CDEFL/DEL(203),RELXD,ITERD,ELAST,GEOMPK,LADD
      DIMENSION PMID(500)
      DO 4001 N=1,ITERP
      DO 4002 I=2,NXZ
      OLDP=P(I)
      IF(LSKIP(I))41,42,43
   41 P(I)=P(I-1)
      GO TO 4002
   42 IF(LSKIP(I-1).EQ.-1)GO TO 41
      P(I)=CN(I)*(4.*P(I+LPOK+1)-P(I+LPOK+2))
     1     +CS(I)*(4.*P(I-1)-P(I-2))+CC(I)
      GO TO 44
   43 P(I)=CN(I)*P(I+1)+CS(I)*P(I-1)+CC(I)
   44 P(I)=OLDP+RELXP*(P(I)-OLDP)
      IF(P(I).LT.0.)P(I)=0.
4002  CONTINUE
      P(NX+1)=P(2)
      P(1)=P(NX)
      PMID(N)=P(NMID)
4001  CONTINUE
      P(NX+2)=P(3)
      RETURN
      END
```

```
      SUBROUTINE DEFL
      COMMON/CGEOM/LSKIP(203),NUMPOK,NX,LPOK,LLAND,DTHETA,PIE
     1/CCOEFP/H(203),CN(203),CS(203),CC(203),THETAN(203),CDIVR,RDIVR
     2/CSOLVP/P(203),DVOL(250),RELXP,ITERP,EPS,NMID,NXZ,NXPOK(30)
     3/CDEFL/DEL(203),RELXD,ITERD,ELAST,GEOMPK,LADD
      DO 6001 I=1,NX+2
      IF(LSKIP(I).EQ.-1)GO TO 6001
      OLDD=DEL(I)
      DEL(I)=-ELAST*P(I)
      DEL(I)=OLDD+RELXD*(DEL(I)-OLDD)
 6001 CONTINUE
      RETURN
      END

      SUBROUTINE SIMP(F,NA,NZ,H,AREA)
      DIMENSION F(NZ)
C
C                    SUBROUTINE TO INTEGRATE A FUNCTION F USING
C                    SIMPSON RULE BETWEEN LIMITS NA AND NZ
C                    WITH STEP WIDTH H AND GIVING ANSWER AREA
C
      NB2=NA+2
      NB4=NA+1
      NY2=NZ-2
      NY4=NZ-1
      SUM2=0.
      SUM4=0.
      DO 9001 ISIMP=NB2,NY2,2
      SUM2=SUM2+F(ISIMP)
 9001 CONTINUE
      DO 9002 ISIMP=NB4,NY4,2
      SUM4=SUM4+F(ISIMP)
 9002 CONTINUE
      AREA=(H/3.)*(F(NA)+2.*SUM2+4.*SUM4+F(NZ))
      RETURN
      END
```

```
      PROGRAM VANE1P(INPUT,OUTPUT,TAPE5=INPUT,TAPE6=OUTPUT,TAPE1,TAPE2)
C
C                     INFINITELY LONG JOURNAL BEARING WITH
C                     POCKETED ELASTIC JOURNAL LINER, METHOD 2
C                     USED FOR POCKET PRESSURE ANALYSIS
C
      COMMON/CGEOM/LSKIP(203),NUMPOK,NX,LPOK,LLAND,DTHETA,PIE
     1/CCOEFP/H(203),CN(203),CS(203),CC(203),THETAN(203),CDIVR,RDIVR
     2/CSOLVP/P(203),RELXP,ITERP,EPS,NMID,NXZ,NXPOK(30)
     3/CDEFL/DEL(203),RELXD,ITERD,ELAST,GEOMPK,LADD
      DIMENSION PMID(100),DELMID(100)
      DIMENSION FP(202)
      DIMENSION FF(202)
C
C           SET PROBLEM PARAMETERS
C
      PIE=3.1415926536
      READ(1)NSTEPX,NUMPOK,LPOK,LLAND,NSTART
      READ(5,101)ITERP,RELXP
  101 FORMAT(I5,F10.4)
      READ(5,102)RTWO,TLINER,CLEAR
  102 FORMAT(3F10.4)
      READ(5,103)VISCOS,OMEGA,YOUNG,POISSN
  103 FORMAT(E10.4,F10.4,E10.4,F10.4)
      READ(5,104)RELXD,ITERD
  104 FORMAT(F10.4,I5)
      READ(5,105)DEPS
  105 FORMAT(F10.4)
      WRITE(6,106)NSTEPX,NUMPOK,LPOK,LLAND,NSTART,ITERP
  106 FORMAT(/////,1HO,*NSTEPX=*,I5,5X,*NUMPOK=*,I5,5X,*LPOK=*,I5,5X,
     1*LLAND=*,I5,5X,*NSTART=*,I5,5X,*ITERP=*,I5,5X)
      WRITE(6,107)RELXP
  107 FORMAT(1HO,*RELXP=*,F10.5,5X)
      WRITE(6,108)RTWO,TLINER,CLEAR
  108 FORMAT(1HO,*RTWO=*,F10.5,5X,*TLINER=*,F10.5,5X,*CLEAR=*,F10.5,5X)
      WRITE(6,109)VISCOS,OMEGA,YOUNG,POISSN
  109 FORMAT(1HO,*VISCOS=*,E10.4,5X,*OMEGA=*,F10.4,5X,
     1*YOUNG=*,E10.4,5X,*POISSN=*,F10.4,5X)
      WRITE(6,110)RELXD,ITERD
  110 FORMAT(1HO,*RELXD=*,F10.4,5X,*ITERD=*,I5,5X)
C
C           CALCULATE PROBLEM PARAMETERS
C
      NX=NSTEPX+1
      DTHETA=2.*PIE/FLOAT(NSTEPX)
      CDIVR=CLEAR/RTWO
      RDIVR=(RTWO-TLINER)/RTWO
      EMAT=(1.-(2.*POISSN**2)/(1.-POISSN))/YOUNG
      ELAST=6.*VISCOS*OMEGA*EMAT*(1./CDIVR**3)*(1.-RDIVR)
      NMID=(NUMPOK/2)*(LPOK+LLAND)-LPOK-LLAND/2
      NXZ=NX-1
      IF(NSTART.EQ.1)NXZ=NX-LPOK-2
      IF(NSTART.GT.LLAND)NXZ=NX-NSTART+LLAND
      LADD=LPOK+LLAND
      READ(1)EPS
      EPS=EPS+DEPS
      WRITE(6,111)EPS,DEPS
  111 FORMAT(1HO,*EPS=*,F10.5,5X,*DEPS=*,F10.5)
      WRITE(6,112)EMAT,ELAST
  112 FORMAT(1HO,*EMAT=*,E10.4,5X,*ELAST=*,F10.5)
      READ(1)(P(I),I=1,NX+2),(DEL(I),I=1,NX+2),(LSKIP(I),I=1,NX+2),
     1(THETAN(I),I=1,NX+2)
      DO 1001 N=1,NUMPOK+1
      IF(NSTART.GT.LLAND)GO TO 11
```

```
      LNO=LLAND-NSTART+2+(N-1)*LADD
      GO TO 12
   11 LNO=LLAND-NSTART+2+N*LADD
   12 NXPOK(N)=LNO
 1001 CONTINUE
C
C          MAIN ITERATION LOOP
C
      DO 1002 NDIT=1,ITERD
      CALL COEFP
      CALL CALCP
      CALL DEFL
      PMID(NDIT)=P(NMID)
      DELMID(NDIT)=DEL(NMID)
 1002 CONTINUE
      DO 1003 I=1,NX
      FP(I)=P(I)*COS(THETAN(I))
 1003 CONTINUE
      CALL SIMP(FP,1,NX,DTHETA,WX)
      DO 1004 I=1,NX
      FP(I)=P(I)*SIN(THETAN(I))
 1004 CONTINUE
      CALL SIMP(FP,1,NX,DTHETA,WY)
      SOMM=6.*SQRT(WX**2+WY**2)
      ATT=ATAN(-WY/WX)*180./PIE
      DO 1006 I=1,NX
      IF(LSKIP(I).NE.-1)GO TO 1006
      H(I)=1.+EPS*COS(THETAN(I))+TLINER/CLEAR
 1006 CONTINUE
      DO 1007 I=2,NX
      FF(I)=1./H(I)+3.*H(I)*(P(I+1)-P(I-1))/(2.*DTHETA)
 1007 CONTINUE
      FF(1)=1./H(1)+3.*H(1)*(P(2)-P(NX-1))/(2.*DTHETA)
      CALL SIMP(FF,1,NX,DTHETA,FRIC)
C
C          WRITE FINAL VALUES
C
      WRITE(6,113)
  113 FORMAT(//,1HO,*FINAL PRESSURE FIELD*)
      WRITE(6,114)(P(I),I=1,NX+2)
  114 FORMAT(1HO,10F10.5)
      WRITE(6,115)
  115 FORMAT(//,1HO,*FINAL DISTORTION FIELD*)
      WRITE(6,114)(DEL(I),I=1,NX+2)
      WRITE(6,116)
  116 FORMAT(//,1HO,*FINAL FILM THICKNESS FIELD*)
      WRITE(6,114)(H(I),I=1,NX+2)
      WRITE(6,117)SOMM
  117 FORMAT(//,1HO,*SOMMERFELD NUMBER=*,F10.5)
      WRITE(6,118)ATT
  118 FORMAT(//,1HO,*ATTITUDE ANGLE=*,F10.5,5X,*DEGREES*)
      WRITE(6,119)FRIC
  119 FORMAT(//,1HO,*FRICTION=*,F10.5)
      WRITE(6,120)
  120 FORMAT(//,1HO,*MAIN CONVERGANCE*,/,1HO,5X,*PMID*,5X,*DELMID*)
      WRITE(6,121)(PMID(N),DELMID(N),N=1,ITERD)
  121 FORMAT(1HO,2F10.5)
C
C          WRITE VALUES TO DATA FILE
C
      WRITE(2)NSTEPX,NUMPOK,LPOK,LLAND,NSTART
      WRITE(2)EPS
      WRITE(2)(P(I),I=1,NX+2),(DEL(I),I=1,NX+2),(LSKIP(I),I=1,NX+2),
     1(THETAN(I),I=1,NX+2)
```

```
      STOP
      END

      SUBROUTINE COEFP
      COMMON/CGEOM/LSKIP(203),NUMPOK,NX,LPOK,LLAND,DTHETA,PIE
     1/CCOEFP/H(203),CN(203),CS(203),CC(203),THETAN(203),CDIVR,RDIVR
     2/CSOLVP/P(203),RELXP,ITERP,EPS,NMID,NXZ,NXPOK(30)
     3/CDEFL/DEL(203),RELXD,ITERD,ELAST,GEOMPK,LADD
      DO 3001 I=1,NX+2
      IF(LSKIP(I).EQ.-1)GO TO 3001
      H(I)=1.+EPS*COS(THETAN(I))-DEL(I)
3001  CONTINUE
      DO 3002 I=2,NXZ
      IF(LSKIP(I))3002,31,32
   31 IF(LSKIP(I-1).EQ.-1)GO TO 3002
      HCUBP=3.*(H(I+LPOK)**3+H(I)**3)
      CN(I)=(DTHETA*FLOAT(LPOK)*ELAST+H(I+LPOK)**3)/HCUBP
      CS(I)=-(DTHETA*FLOAT(LPOK)*ELAST-H(I)**3)/HCUBP
      CC(I)=2.*DTHETA*(H(I)*(1.+DEL(I)*CDIVR)
     1                 -H(I+LPOK)*(1.+DEL(I+LPOK)*CDIVR))/HCUBP
      GO TO 3002
   32 CN(I)=0.5+3.*(H(I+1)-H(I-1))/(8.*H(I))
      CS(I)=0.5-3.*(H(I+1)-H(I-1))/(8.*H(I))
      CC(I)=-DTHETA*(H(I+1)-H(I-1))/(4.*H(I)**3)
3002  CONTINUE
      RETURN
      END

      SUBROUTINE CALCP
      COMMON/CGEOM/LSKIP(203),NUMPOK,NX,LPOK,LLAND,DTHETA,PIE
     1/CCOEFP/H(203),CN(203),CS(203),CC(203),THETAN(203),CDIVR,RDIVR
     2/CSOLVP/P(203),RELXP,ITERP,EPS,NMID,NXZ,NXPOK(30)
     3/CDEFL/DEL(203),RELXD,ITERD,ELAST,GEOMPK,LADD
      DIMENSION PMID(500)
      DO 4001 N=1,ITERP
      DO 4002 I=2,NXZ
      OLDP=P(I)
      IF(LSKIP(I))41,42,43
   41 P(I)=P(I-1)
      GO TO 4002
   42 IF(LSKIP(I-1).EQ.-1)GO TO 41
      P(I)=CN(I)*(4.*P(I+LPOK+1)-P(I+LPOK+2))
     1     +CS(I)*(4.*P(I-1)-P(I-2))+CC(I)
      GO TO 44
   43 P(I)=CN(I)*P(I+1)+CS(I)*P(I-1)+CC(I)
   44 P(I)=OLDP+RELXP*(P(I)-OLDP)
      IF(P(I).LT.0.)P(I)=0.
4002  CONTINUE
      P(NX+1)=P(2)
      P(1)=P(NX)
      PMID(N)=P(NMID)
4001  CONTINUE
      P(NX+2)=P(3)
      RETURN
      END

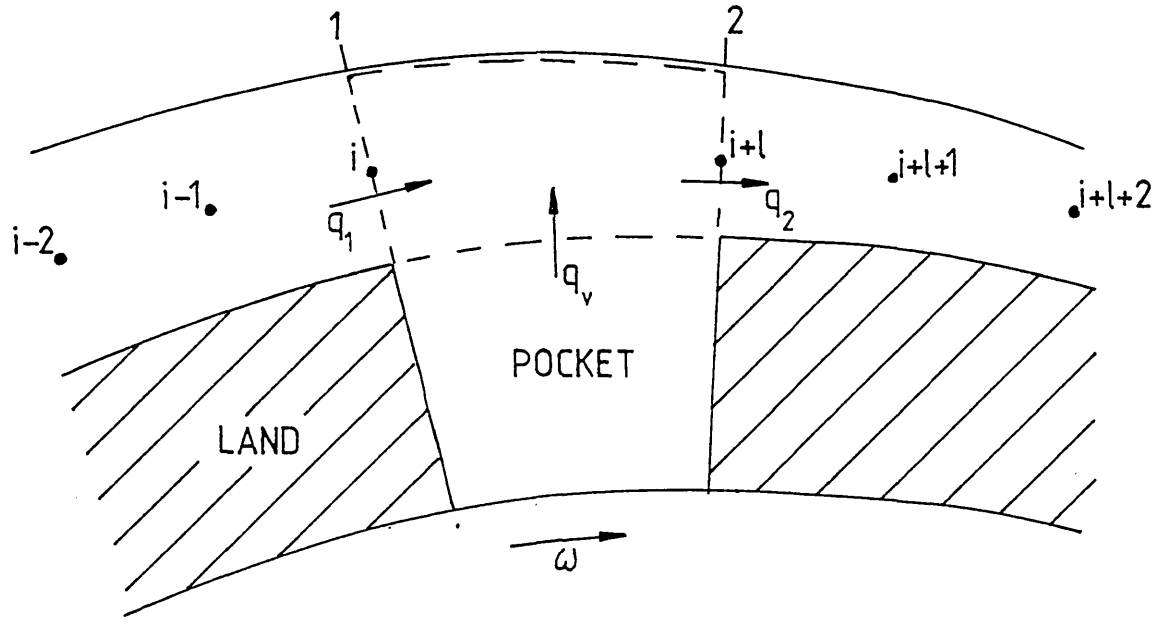
      SUBROUTINE DEFL
      COMMON/CGEOM/LSKIP(203),NUMPOK,NX,LPOK,LLAND,DTHETA,PIE
     1/CCOEFP/H(203),CN(203),CS(203),CC(203),THETAN(203),CDIVR,RDIVR
     2/CSOLVP/P(203),RELXP,ITERP,EPS,NMID,NXZ,NXPOK(30)
     3/CDEFL/DEL(203),RELXD,ITERD,ELAST,GEOMPK,LADD
      DO 6001 I=1,NX+2
      IF(LSKIP(I).EQ.-1)GO TO 6001
      OLDD=DEL(I)
```

```
      DEL(I)=-ELAST*P(I)
      DEL(I)=OLDD+RELXD*(DEL(I)-OLDD)
 6001 CONTINUE
      RETURN
      END

      SUBROUTINE SIMP(F,NA,NZ,H,AREA)
      DIMENSION F(NZ)
C
C                    SUBROUTINE TO INTEGRATE A FUNCTION F USING
C                    SIMPSON RULE BETWEEN LIMITS NA AND NZ
C                    WITH STEP WIDTH H AND GIVING ANSWER AREA
C
      NB2=NA+2
      NB4=NA+1
      NY2=NZ-2
      NY4=NZ-1
      SUM2=0.
      SUM4=0.
      DO 9001 ISIMP=NB2,NY2,2
      SUM2=SUM2+F(ISIMP)
 9001 CONTINUE
      DO 9002 ISIMP=NB4,NY4,2
      SUM4=SUM4+F(ISIMP)
 9002 CONTINUE
      AREA=(H/3.)*(F(NA)+2.*SUM2+4.*SUM4+F(NZ))
      RETURN
      END
```

APPENDIX A4.

POCKET PRESSURE ANALYSIS INCLUDING FINITE ELEMENT DISTORTIONS.



As in the simple distortion treatment, pocket pressure is found from flow continuity.

$$q_v = q_2 - q_1 = q_n \quad . \tag{A4.1.}$$

As before

$$\frac{2q_n}{\omega c R_2} = \bar{h}_1^3 \left(\frac{d\bar{p}}{d\bar{\theta}}\right)_1 - \bar{h}_2^3 \left(\frac{d\bar{p}}{d\bar{\theta}}\right)_2$$

$$+ \bar{h}_2 \left(1 + \bar{\delta}_2 \frac{c}{R_2}\right) - \bar{h}_1 \left(1 + \bar{\delta}_1 \frac{c}{R_2}\right) \tag{A4.2.}$$

and the volumetric flow due to the distortion of the top of the land is

$$\frac{2q_v^a}{\omega_c R_2} = \frac{\Delta\theta_{poc}}{\Delta\theta_{pocl}} (\bar{v}^n - \bar{v}^{n-1}) \qquad (A4.3.)$$

using Method 1 for the approximation of $\frac{d\bar{v}}{d\theta}$ (see Appendix A2.). In this case

$$\bar{v}^n = -\bar{\delta}\left(2 + \bar{\delta}\frac{c}{R_2}\right)$$

where $\bar{\delta}$ is the mean value of the distortion at both edges of the pocket.

$$\bar{\delta} = \frac{\bar{\delta}_1 + \bar{\delta}_2}{2} = \frac{\bar{\delta}_i + \bar{\delta}_{i+1}}{2} \quad .$$

To this volumetric flow must be added the contribution from the land side distortions. Defining this distortion as γ (positive in the circumferential direction), the displaced volume is then the integral of γ at each side of the pocket.

$$V' = \int_0^t \gamma_1 \, dz - \int_0^t \gamma_2 \, dz$$

Defining $\bar{\gamma} = \frac{\gamma}{c}$ and $\bar{z} = \frac{z}{t}$, then

$$V' = ct\left(\int_0^1 \bar{\gamma}_1 \, d\bar{z} - \int_0^1 \bar{\gamma}_2 \, d\bar{z} \right)$$

The added flow, $q_v^b = \frac{dV'}{d\theta}$ is given by

$$q_v^b = \frac{\omega ct}{\Delta\theta_{pocl}} (\bar{V}'^{,n} - \bar{V}'^{,n-1})$$

where $$\bar{V}'^{,n} = \int_0^1 \bar{\gamma}_1 \, d\bar{z} - \int_0^1 \bar{\gamma}_2 \, d\bar{z} \quad .$$

But $t = R_2 \left(1 - \frac{R_1}{R_2} \right)$, therefore

$$\frac{2q_v^b}{\omega c R_2} = \frac{2}{\Delta\theta_{pocl}} \left(1 - \frac{R_1}{R_2} \right) (\bar{V}'^{,n} - \bar{V}'^{,n-1}) \qquad \text{(A4.4.)}$$

and from eq. A4.3. and eq. A4.4., the total volumetric flow $q_v = q_v^a + q_v^b$, hence

$$\frac{2q_v}{\omega c R_2} = \frac{\Delta\theta_{poc}}{\Delta\theta_{pocl}} (\bar{V}^n - \bar{V}^{n-1})$$

$$+ \frac{2}{\Delta\theta_{pocl}} \left(1 - \frac{R_1}{R_2} \right) (\bar{V}'^{,n} - \bar{V}'^{,n-1})$$

Re-defining the total displaced pocket volume, $\bar{V}^n$, as

$$\bar{V}^n = -\bar{\delta}\left(2 + \bar{\delta}\frac{c}{R_2}\right) + \frac{2}{\Delta\theta_{poc}}\left(1 - \frac{R_1}{R_2}\right)\left(\int_0^1 \bar{\gamma}_1\, d\bar{z} - \int_0^1 \bar{\gamma}_2\, d\bar{z}\right) \quad \text{(A4.6.)}$$

$$\text{then} \qquad \frac{2q_v}{\omega c R_2} = \frac{\Delta\theta_{poc}}{\Delta\theta_{pocl}}\left(\bar{V}^n - \bar{V}^{n-1}\right) \quad \text{(A4.7.)}$$

Substituting from eq. A4.2. into eq. A4.1. gives

$$\frac{\Delta\theta_{poc}}{\Delta\theta_{pocl}}\left(\bar{V}^n - \bar{V}^{n-1}\right) = \bar{h}_1^3\left(\frac{d\bar{p}}{d\theta}\right)_1 - \bar{h}_2^3\left(\frac{d\bar{p}}{d\theta}\right)_2 + \bar{h}_2\left(1 + \bar{\delta}_2\frac{c}{R_2}\right) - \bar{h}_1\left(1 + \bar{\delta}_1\frac{c}{R_2}\right)$$

Using the same discretizations for the differentials as in Appendix A2 and rearranging gives

$$\bar{p}_i = \frac{2}{3(\bar{h}_i^3 + \bar{h}_{i+1}^3)}\left\{\frac{\Delta\theta_{poc}}{\Delta\theta_{pocl}}\left(\bar{V}^n - \bar{V}^{n-1}\right)\right.$$

$$+ \bar{h}_i \left(1 + \bar{\delta}_i \frac{c}{R_2}\right)$$

$$- \bar{h}_{i+1} \left(1 + \bar{\delta}_{i+1} \frac{c}{R_2}\right) \Bigg\}$$

$$+ \frac{\bar{h}_i^3 (4\bar{p}_{i-1} - \bar{p}_{i-2}) + \bar{h}_{i+1}^3 (4\bar{p}_{i+1+1} - \bar{p}_{i+1+2})}{3(\bar{h}_i^3 + \bar{h}_{i+1}^3)} \cdot$$

APPENDIX A5.

COMPUTER PROGRAMME INCLUDING FINITE ELEMENT DISTORTIONS.

Variables.

GMPKH Geometric coefficient, $\dfrac{2\left(1 - \dfrac{R_1}{R_2}\right) - }{\Delta\theta_{poc}}$.

IFLAG Flag coefficient taking the values:

-1 to exclude the effects of land side distortion.

+1 to include the effects of land side distortion.

NCASES Number of unit pressure loads.

NODESH Number of nodes at the side of a land.

NODESV Number of nodes on the top of a land.

Subscripted Variables.

DELH1 Deflection at the trailing edge side of a land.

DELH2 Deflection at the leading edge side of a land.

DINF1 Flexibility matrix for the trailing edge side.

DINF2 Flexibility matrix for the leading edge side.

DINFV	Flexibility matrix for the top of a land.
GAMMA	Distortion at the side of a land.

Other variables are as in Appendix A3.

```
      PROGRAM VANE1F(INPUT,OUTPUT,TAPE5=INPUT,TAPE6=OUTPUT,
     1TAPE1,TAPE2,TAPE3)
C
C                    INFINITELY LONG JOURNAL BEARING WITH
C                    POCKETED ELASTIC JOURNAL LINER, METHOD 1
C                    USED FOR POCKET PRESSURE ANALYSIS, DISTORTIONS
C                    CALCULATED USING AN INFLUENCE MATRIX GENERATED
C                    BY *FINEL*, A FINITE ELEMENT PROGRAM WRITTEN
C                    BY MR. D. HITCHINGS, AERO. DEPT.
C
      COMMON/CGEOM/LSKIP(203),NUMPOK,NX,LPOK,LLAND,DTHETA,PIE
     1/CCOEFP/H(203),CN(203),CS(203),CC(203),THETAN(203),CDIVR,RDIVR
     2/CSOLVP/P(203),DVOL(250),RELXP,ITERP,EPS,NMID,NXZ,NXPOK(30)
     3/CDEFL/DEL(203),RELXD,ITERD,ELAST,GEOMPK,LADD
     4/CFINEL/DINF1(10,10),DINF2(10,10),DINFV(10,10),GMPKH,
     5DELH1(10,10),DELH2(10,10),NCASES,NODESH,NODESV,NSTART,DZ,IFLAG
      DIMENSION PMID(100),DELMID(100)
      DIMENSION FP(202)
      DIMENSION FF(202)
C
C          SET PROBLEM PARAMETERS
C
      PIE=3.1415926536
      READ(1)NSTEPX,NUMPOK,LPOK,LLAND,NSTART
      READ(5,101)ITERP,RELXP
  101 FORMAT(I5,F10.4)
      READ(5,102)RTWO,TLINER,CLEAR
  102 FORMAT(3F10.4)
      READ(5,103)VISCOS,OMEGA,YOUNG,POISSN
  103 FORMAT(E10.4,F10.4,E10.4,F10.4)
      READ(5,104)RELXD,ITERD,IFLAG
  104 FORMAT(F10.4,2I5)
      READ(5,105)DEPS
  105 FORMAT(F10.4)
      WRITE(6,106)NSTEPX,NUMPOK,LPOK,LLAND,NSTART,ITERP
  106 FORMAT(/////,1HO,*NSTEPX=*,I5,5X,*NUMPOK=*,I5,5X,*LPOK=*,I5,5X,
     1*LLAND=*,I5,5X,*NSTART=*,I5,5X,*ITERP=*,I5,5X)
      WRITE(6,107)RELXP
  107 FORMAT(1HO,*RELXP=*,F10.5,5X)
      WRITE(6,108)RTWO,TLINER,CLEAR
  108 FORMAT(1HO,*RTWO=*,F10.5,5X,*TLINER=*,F10.5,5X,*CLEAR=*,F10.5,5X)
      WRITE(6,109)VISCOS,OMEGA,YOUNG,POISSN
  109 FORMAT(1HO,*VISCOS=*,E10.4,5X,*OMEGA=*,F10.4,5X,
     1*YOUNG=*,E10.4,5X,*POISSN=*,F10.4,5X)
      WRITE(6,110)RELXD,ITERD,IFLAG
  110 FORMAT(1HO,*RELXD=*,F10.4,5X,*ITERD=*,I5,5X,*IFLAG=*,I5,5X)
C
C          CALCULATE PROBLEM PARAMETERS
C
      NX=NSTEPX+1
      DTHETA=2.*PIE/FLOAT(NSTEPX)
      CDIVR=CLEAR/RTWO
      RDIVR=(RTWO-TLINER)/RTWO
      EMAT=(1.-(2.*POISSN**2)/(1.-POISSN))/YOUNG
      ELAST=6.*VISCOS*OMEGA*EMAT*(1./CDIVR**3)*(1.-RDIVR)
      NMID=(NUMPOK/2)*(LPOK+LLAND)-LPOK-LLAND/2
      NXZ=NX-1
      IF(NSTART.EQ.1)NXZ=NX-LPOK-2
      IF(NSTART.GT.LLAND)NXZ=NX-NSTART+LLAND
      LADD=LPOK+LLAND
      GEOMPK=FLOAT(LPOK)/FLOAT(LADD)
      GMPKH=2.*(1.-RDIVR)/(DTHETA*FLOAT(LPOK))
      READ(1)EPS
      EPS=EPS+DEPS
```

```
      WRITE(6,111) EPS,DEPS
  111 FORMAT(1HO,*EPS=*,F10.5,5X,*DEPS=*,F10.5)
      WRITE(6,112) EMAT,ELAST
  112 FORMAT(1HO,*EMAT=*,E10.4,5X,*ELAST=*,F10.5)
      READ(1) (P(I),I=1,NX+2),(DEL(I),I=1,NX+2),(LSKIP(I),I=1,NX+2),
     1(THETAN(I),I=1,NX+2)
      DO 1001 N=1,NUMPOK+1
      IF(NSTART.GT.LLAND) GO TO 11
      LNO=LLAND-NSTART+2+(N-1)*LADD
      GO TO 12
   11 LNO=LLAND-NSTART+2+N*LADD
   12 NXPOK(N)=LNO
 1001 CONTINUE
      READ(3) NODESH,NODESV,NCASES
      DO 1010 I=1,NODESH
      READ(3) (DINF1(I,J),J=1,NCASES)
 1010 CONTINUE
      DO 1011 I=1,NODESH
      READ(3) (DINF2(I,J),J=1,NCASES)
 1011 CONTINUE
      DO 1012 I=1,NODESV
      READ(3) (DINFV(I,J),J=1,NCASES)
 1012 CONTINUE
      DO 1013 I=1,NODESH
      DO 1014 N=1,NUMPOK
      DELH1(N,I)=0.
      DELH2(N,I)=0.
 1014 CONTINUE
 1013 CONTINUE
      DZ=1./FLOAT(NODESH)
C
C          MAIN ITERATION LOOP
C
      DO 1002 NDIT=1,ITERD
      CALL COEFP
      CALL CALCP
      CALL DEFL
      PMID(NDIT)=P(NMID)
      DELMID(NDIT)=DEL(NMID)
 1002 CONTINUE
      DO 1003 I=1,NX
      FP(I)=P(I)*COS(THETAN(I))
 1003 CONTINUE
      CALL SIMP(FP,1,NX,DTHETA,WX)
      DO 1004 I=1,NX
      FP(I)=P(I)*SIN(THETAN(I))
 1004 CONTINUE
      CALL SIMP(FP,1,NX,DTHETA,WY)
      SOMM=6.*SQRT(WX**2+WY**2)
      ATT=ATAN(-WY/WX)*180./PIE
      DO 1005 I=1,NX
      IF(LSKIP(I).NE.-1) GO TO 1005
      H(I)=1.+EPS*COS(THETAN(I))+TLINER/CLEAR
 1005 CONTINUE
      DO 1006 I=2,NX
      FF(I)=1./H(I)+3.*H(I)*(P(I+1)-P(I-1))/(2.*DTHETA)
 1006 CONTINUE
      FF(1)=1./H(1)+3.*H(1)*(P(2)-P(NX-1))/(2.*DTHETA)
      CALL SIMP(FF,1,NX,DTHETA,FRIC)
C
C          WRITE FINAL VALUES
C
      WRITE(6,113)
  113 FORMAT(//,1HO,*FINAL PRESSURE FIELD*)
```

```
      WRITE(6,114) (P(I),I=1,NX+2)
  114 FORMAT(1HO,10F10.5)
      WRITE(6,115)
  115 FORMAT(//,1HO,*FINAL DISTORTION FIELD*)
      WRITE(6,114) (DEL(I),I=1,NX+2)
      WRITE(6,116)
  116 FORMAT(//,1HO,*FINAL FILM THICKNESS FIELD*)
      WRITE(6,114) (H(I),I=1,NX+2)
      WRITE(6,117)SOMM
  117 FORMAT(//,1HO,*SOMMERFELD NUMBER=*,F10.5)
      WRITE(6,118)ATT
  118 FORMAT(//,1HO,*ATTITUDE ANGLE=*,F10.5,5X,*DEGREES*)
      WRITE(6,119)FRIC
  119 FORMAT(//,1HO,*FRICTION=*,F10.5)
      WRITE(6,120)
  120 FORMAT(//,1HO,*MAIN CONVERGANCE*,/,1HO,5X,*PMID*,5X,*DELMID*)
      WRITE(6,121) (PMID(N),DELMID(N),N=1,ITERD)
  121 FORMAT(1HO,2F10.5)
      WRITE(6,122)
  122 FORMAT(1HO,*DEFLECTIONS AT SIDES OF LANDS*,////,5X,
     1*STATION ONE IS THE LEADING EDGE OF A LAND*,//,5X,
     2*STATION TWO IS THE TRAILING EDGE OF A LAND*,//,5X,
     3*DEFLECTIONS ARE POSITIVE IN THE THETA DIRECTION*,//////)
      DO 1020 N=1,NUMPOK
      WRITE(6,123)N
  123 FORMAT(1HO,*LAND NUMBER*,I5,/,5X,*DELH1*,10X,*DELH2*,/)
      WRITE(6,124) (DELH1(N,M),DELH2(N,M),M=1,NODESH)
  124 FORMAT(1HO,F10.5,5X,F10.5)
 1020 CONTINUE
C
C          WRITE VALUES TO DATA FILE
C
      WRITE(2)NSTEPX,NUMPOK,LPOK,LLAND,NSTART
      WRITE(2)EPS
      WRITE(2) (P(I),I=1,NX+2),(DEL(I),I=1,NX+2),(LSKIP(I),I=1,NX+2),
     1(THETAN(I),I=1,NX+2)
      STOP
      END

      SUBROUTINE COEFP
      COMMON/CGEOM/LSKIP(203),NUMPOK,NX,LPOK,LLAND,DTHETA,PIE
     1/CCOEFP/H(203),CN(203),CS(203),CC(203),THETAN(203),CDIVR,RDIVR
     2/CSOLVP/P(203),DVOL(250),RELXP,ITERP,EPS,NMID,NXZ,NXPOK(30)
     3/CDEFL/DEL(203),RELXD,ITERD,ELAST,GEOMPK,LADD
     4/CFINEL/DINF1(10,10),DINF2(10,10),DINFV(10,10),GMPKH,
     5DELH1(10,10),DELH2(10,10),NCASES,NODESH,NODESV,NSTART,DZ,IFLAG
      DIMENSION VOL(30),GAMMA(10)
      DO 3002 I=1,NX+2
      IF(LSKIP(I).EQ.-1)GO TO 3002
      H(I)=1.+EPS*COS(THETAN(I))-DEL(I)
 3002 CONTINUE
      DO 3003 I=1,NUMPOK
      DP=(DEL(NXPOK(I))+DEL(NXPOK(I)+LPOK))/2.
      VOL(I)=-DP*(DP*CDIVR+2.)
 3003 CONTINUE
      IF(IFLAG.LT.0)GO TO 34
      DO 3005 N=1,NUMPOK-1
      DO 3006 M=1,NODESH
      GAMMA(M)=DELH1(N+1,M)
 3006 CONTINUE
      CALL SIMP(GAMMA,1,NODESH,DZ,V1H)
      VOL(N)=VOL(N)-V1H*GMPKH
 3005 CONTINUE
      DO 3007 M=1,NODESH
```

```
      GAMMA(M)=DELH1(1,M)
3007  CONTINUE
      CALL SIMP(GAMMA,1,NODESH,DZ,V1H)
      VOL(NUMPOK)=VOL(NUMPOK)-V1H*GMPKH
      DO 3008 N=1,NUMPOK
      DO 3009 M=1,NODESH
      GAMMA(M)=DELH2(N,M)
3009  CONTINUE
      CALL SIMP(GAMMA,1,NODESH,DZ,V2H)
      VOL(N)=VOL(N)+V2H*GMPKH
3008  CONTINUE
   34 CONTINUE
      DVOL(NXPOK(1))=GEOMPK*(VOL(1)-VOL(NUMPOK))
      DO 3004 I=2,NUMPOK
      DVOL(NXPOK(I))=GEOMPK*(VOL(I)-VOL(I-1))
3004  CONTINUE
      DO 3001 I=2,NXZ
      IF(LSKIP(I))3001,32,33
   32 IF(LSKIP(I-1).EQ.-1)GO TO 3001
      HCUBP=3.*(H(I+LPOK)**3+H(I)**3)
      CN(I)=H(I+LPOK)**3/HCUBP
      CS(I)=H(I)**3/HCUBP
      CC(I)=2.*DTHETA*(DVOL(I)+H(I)*(1.+DEL(I)*CDIVR)
     1                        -H(I+LPOK)*(1.+DEL(I+LPOK)*CDIVR))/HCUBP
      GO TO 3001
   33 CN(I)=0.5+3.*(H(I+1)-H(I-1))/(8.*H(I))
      CS(I)=0.5-3.*(H(I+1)-H(I-1))/(8.*H(I))
      CC(I)=-DTHETA*(H(I+1)-H(I-1))/(4.*H(I)**3)
3001  CONTINUE
      RETURN
      END

      SUBROUTINE CALCP
      COMMON/CGEOM/LSKIP(203),NUMPOK,NX,LPOK,LLAND,DTHETA,PIE
     1/CCOEFP/H(203),CN(203),CS(203),CC(203),THETAN(203),CDIVR,RDIVR
     2/CSOLVP/P(203),DVOL(250),RELXP,ITERP,EPS,NMID,NXZ,NXPOK(30)
     3/CDEFL/DEL(203),RELXD,ITERD,ELAST,GEOMPK,LADD
      DIMENSION PMID(500)
      DO 4001 N=1,ITERP
      DO 4002 I=2,NXZ
      OLDP=P(I)
      IF(LSKIP(I))41,42,43
   41 P(I)=P(I-1)
      GO TO 4002
   42 IF(LSKIP(I-1).EQ.-1)GO TO 41
      P(I)=CN(I)*(4.*P(I+LPOK+1)-P(I+LPOK+2))
     1      +CS(I)*(4.*P(I-1)-P(I-2))+CC(I)
      GO TO 44
   43 P(I)=CN(I)*P(I+1)+CS(I)*P(I-1)+CC(I)
   44 P(I)=OLDP+RELXP*(P(I)-OLDP)
      IF(P(I).LT.0.)P(I)=0.
4002  CONTINUE
      P(NX+1)=P(2)
      P(1)=P(NX)
      PMID(N)=P(NMID)
4001  CONTINUE
      P(NX+2)=P(3)
      RETURN
      END

      SUBROUTINE DEFL
      COMMON/CGEOM/LSKIP(203),NUMPOK,NX,LPOK,LLAND,DTHETA,PIE
     1/CCOEFP/H(203),CN(203),CS(203),CC(203),THETAN(203),CDIVR,RDIVR
     2/CSOLVP/P(203),DVOL(250),RELXP,ITERP,EPS,NMID,NXZ,NXPOK(30)
```

```
     3/CDEFL/DEL(203),RELXD,ITERD,ELAST,GEOMPK,LADD
     4/CFINEL/DINF1(10,10),DINF2(10,10),DINFV(10,10),GMPKH,
     5DELH1(10,10),DELH2(10,10),NCASES,NODESH,NODESV,NSTART,DZ,IFLAG
      DIMENSION PX(10)
      DO 6001 N=1,NUMPOK
      NXP=NXPOK(N)-LLAND-1
      IF(N.EQ.1.AND.NSTART.LE.LLAND)GO TO 61
      DO 6002 L=2,NCASES-1
      PX(L)=P(NXP+L-1)
 6002 CONTINUE
      PX(1)=P(NXP+1)
      PX(NCASES)=P(NXP+LLAND+1)
      DO 6005 M=1,NODESV
      DSUM=0.
      DO 6006 INF=1,NCASES
      DSUM=DSUM+DINFV(M,INF)*PX(INF)
 6006 CONTINUE
      OLDD=DEL(NXP+M)
      DEL(NXP+M)=OLDD+RELXD*(DSUM-OLDD)
 6005 CONTINUE
      GO TO 62
   61 DO 6003 L=1,NSTART+1
      PX(L)=0.
 6003 CONTINUE
      DO 6004 L=NSTART+2,NCASES-1
      PX(L)=P(L-NSTART)
 6004 CONTINUE
      PX(NCASES)=P(NCASES-1-NSTART)
      DO 6009 M=1,NSTART
      DSUM=0.
      DO 6010 INF=1,NCASES
      DSUM=DSUM+DINFV(M,INF)*PX(INF)
 6010 CONTINUE
      OLDD=DEL(NX+NXP-1+M)
      DEL(NX+NXP-1+M)=OLDD+RELXD*(DSUM-OLDD)
 6009 CONTINUE
      DO 6011 M=NSTART,NODESV
      DSUM=0.
      DO 6012 INF=1,NCASES
      DSUM=DSUM+DINFV(M,INF)*PX(INF)
 6012 CONTINUE
      OLDD=DEL(NXP+M)
      DEL(NXP+M)=OLDD+RELXD*(DSUM-OLDD)
 6011 CONTINUE
   62 DEL(NX+1)=DEL(2)
      DEL(NX+2)=DEL(3)
      DO 6007 M=1,NODESH
      DSUM1=0.
      DSUM2=0.
      DO 6008 INF=1,NCASES
      DSUM1=DSUM1+DINF1(M,INF)*PX(INF)
      DSUM2=DSUM2+DINF2(M,INF)*PX(INF)
 6008 CONTINUE
      OLDD=DELH1(N,M)
      DELH1(N,M)=OLDD+RELXD*(DSUM1-OLDD)
      OLDD=DELH2(N,M)
      DELH2(N,M)=OLDD+RELXD*(DSUM2-OLDD)
 6007 CONTINUE
 6001 CONTINUE
      RETURN
      END

      SUBROUTINE SIMP(F,NA,NZ,H,AREA)
      DIMENSION F(NZ)
```

```
C
C                    SUBROUTINE TO INTEGRATE A FUNCTION F USING
C                    SIMPSON RULE BETWEEN LIMITS NA AND NZ
C                    WITH STEP WIDTH H AND GIVING ANSWER AREA
C
      NB2=NA+2
      NB4=NA+1
      NY2=NZ-2
      NY4=NZ-1
      SUM2=0.
      SUM4=0.
      DO 9001 ISIMP=NB2,NY2,2
      SUM2=SUM2+F(ISIMP)
 9001 CONTINUE
      DO 9002 ISIMP=NB4,NY4,2
      SUM4=SUM4+F(ISIMP)
 9002 CONTINUE
      AREA=(H/3.)*(F(NA)+2.*SUM2+4.*SUM4+F(NZ))
      RETURN
      END
```

APPENDIX A6.

THEORETICAL ANALYSIS INCLUDING AXIAL FIELD VARIATION.

A6.1. Film Pressure.

Reynolds' equation for two dimensional, steady, incompressible, isoviscous flow is

$$\frac{\partial}{\partial x}\left(h^3 \frac{\partial p}{\partial x}\right) + \frac{\partial}{\partial y}\left(h^3 \frac{\partial p}{\partial y}\right) = 6\eta U \frac{\partial h}{\partial x}$$

Substituting for the dimensionless variables $h = c\bar{h}$, $y = \frac{L\bar{y}}{2}$, $p = \frac{6\eta U R_2 \bar{p}}{c^2}$ and $x = R_2\theta$ gives

$$\frac{\partial}{\partial \theta}\left(\bar{h}^3 \frac{\partial \bar{p}}{\partial \theta}\right) + \left(\frac{D}{L}\right)^2 \frac{\partial}{\partial \bar{y}}\left(\bar{h}^3 \frac{\partial \bar{p}}{\partial \bar{y}}\right) = \frac{\partial \bar{h}}{\partial \theta}$$

where $D = 2R_2$. Putting $\lambda = \left(\frac{D}{L}\right)^2$ and expanding,

$$\frac{\partial^2 \bar{p}}{\partial \theta^2} + \lambda \frac{\partial^2 \bar{p}}{\partial \bar{y}^2} + \frac{3}{\bar{h}} \frac{\partial \bar{h}}{\partial \theta} \frac{\partial \bar{p}}{\partial \theta} + \frac{3\lambda}{\bar{h}} \frac{\partial \bar{h}}{\partial \bar{y}} \frac{\partial \bar{p}}{\partial \bar{y}} = \frac{1}{\bar{h}^3} \frac{\partial \bar{h}}{\partial \theta} \qquad \text{(A6.1.)}$$

The boundary conditions are,

$$\bar{p} = 0 \text{ at } \bar{\theta} = 0$$

$$\bar{p} = \frac{\partial \bar{p}}{\partial \bar{\theta}} = 0 \text{ at } \bar{\theta} = \bar{\theta}_{cav}$$

and $$\frac{\partial \bar{p}}{\partial \bar{y}} = 0 \text{ at } \bar{y} = 0$$

Using the following finite difference approximations for the differentials,

$$\frac{\partial \bar{p}}{\partial \bar{\theta}} = \frac{\bar{p}_{i+1,j} - \bar{p}_{i-1,j}}{2\Delta\bar{\theta}} ,$$

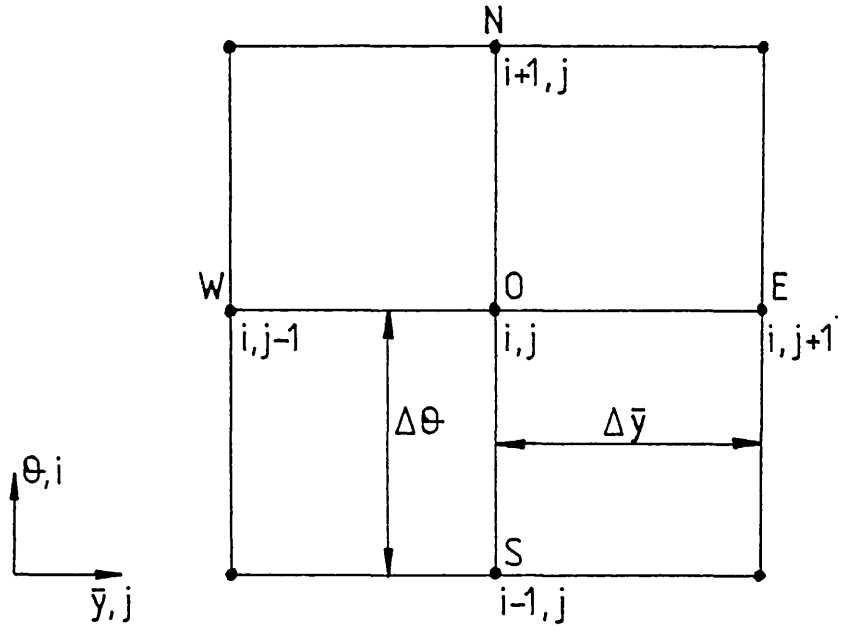
$$\frac{\partial \bar{h}}{\partial \bar{\theta}} = \frac{\bar{h}_{i+1,j} - \bar{h}_{i-1,j}}{2\Delta\bar{\theta}} ,$$

$$\frac{\partial \bar{p}}{\partial \bar{y}} = \frac{\bar{p}_{i,j+1} - \bar{p}_{i,j-1}}{2\Delta\bar{y}} ,$$

$$\frac{\partial \bar{h}}{\partial \bar{y}} = \frac{\bar{h}_{i,j+1} - \bar{h}_{i,j-1}}{2\Delta\bar{y}} ,$$

$$\frac{\partial^2 \bar{p}}{\partial \bar{\theta}^2} = \frac{\bar{p}_{i+1,j} + \bar{p}_{i-1,j} - 2\bar{p}_{i,j}}{\Delta\bar{\theta}^2} ,$$

$$\frac{\partial^2 \bar{p}}{\partial \bar{y}^2} = \frac{\bar{p}_{i,j+1} + \bar{p}_{i,j-1} - 2\bar{p}_{i,j}}{\Delta \bar{y}^2} \quad .$$



and substituting in eq. A6.1. gives

$$\frac{\bar{p}_{i+1,j} + \bar{p}_{i-1,j} - 2\bar{p}_{i,j}}{\Delta\theta^2} + \frac{\lambda(\bar{p}_{i,j+1} + \bar{p}_{i,j-1} - 2\bar{p}_{i,j})}{\Delta \bar{y}^2}$$

$$+ \frac{3(\bar{h}_{i+1,j} - \bar{h}_{i-1,j})(\bar{p}_{i+1,j} - \bar{p}_{i-1,j})}{4\bar{h}_{i,j}\Delta\theta^2}$$

$$+ \frac{3\lambda(\bar{h}_{i,j+1} - \bar{h}_{i,j-1})(\bar{p}_{i,j+1} - \bar{p}_{i,j-1})}{4\bar{h}_{i,j}\Delta \bar{y}^2}$$

$$= \frac{(\bar{h}_{i+1,j} - \bar{h}_{i-1,j})}{2\bar{h}^3_{i,j}\Delta\theta}$$

Rearranging this gives

$$\bar{p}_{i,j} = CN_{i,j}\bar{p}_{i+1,j} + CS_{i,j}\bar{p}_{i-1,j}$$

$$+ CE_{i,j}\bar{p}_{i,j+1} + CW_{i,j}\bar{p}_{i,j-1} + C0_{i,j}$$

where

$$CN_{i,j} = \frac{0.5}{\left(1 + \frac{\lambda\Delta\theta^2}{\Delta\bar{y}^2}\right)}\left(1 + \frac{3}{4\bar{h}_{i,j}}(\bar{h}_{i+1,j} - \bar{h}_{i-1,j})\right)$$

$$CS_{i,j} = \frac{0.5}{\left(1 + \frac{\lambda\Delta\theta^2}{\Delta\bar{y}^2}\right)}\left(1 - \frac{3}{4\bar{h}_{i,j}}(\bar{h}_{i+1,j} - \bar{h}_{i-1,j})\right)$$

$$CE_{i,j} = \frac{0.5}{\left(1 + \frac{\Delta\bar{y}^2}{\lambda\Delta\theta^2}\right)}\left(1 + \frac{3}{4\bar{h}_{i,j}}(\bar{h}_{i,j+1} - \bar{h}_{i,j-1})\right)$$

$$CW_{i,j} = \frac{0.5}{\left(1 + \frac{\Delta\bar{y}^2}{\lambda\Delta\theta^2}\right)}\left(1 - \frac{3}{4\bar{h}_{i,j}}(\bar{h}_{i,j+1} - \bar{h}_{i,j-1})\right)$$

$$C0_{i,j} = \frac{-0.25\Delta\theta}{\left(1 + \frac{\lambda\Delta\theta^2}{\Delta\bar{y}^2}\right)}\left(\frac{\bar{h}_{i+1,j} - \bar{h}_{i-1,j}}{\bar{h}^3_{i,j}}\right)$$

$\bar{h}$ is defined at each point by

$$\bar{h}_{i,j} = 1 + \varepsilon\cos\theta - \bar{\delta}_{i,j}$$

where, as in the simple distortion treatment,

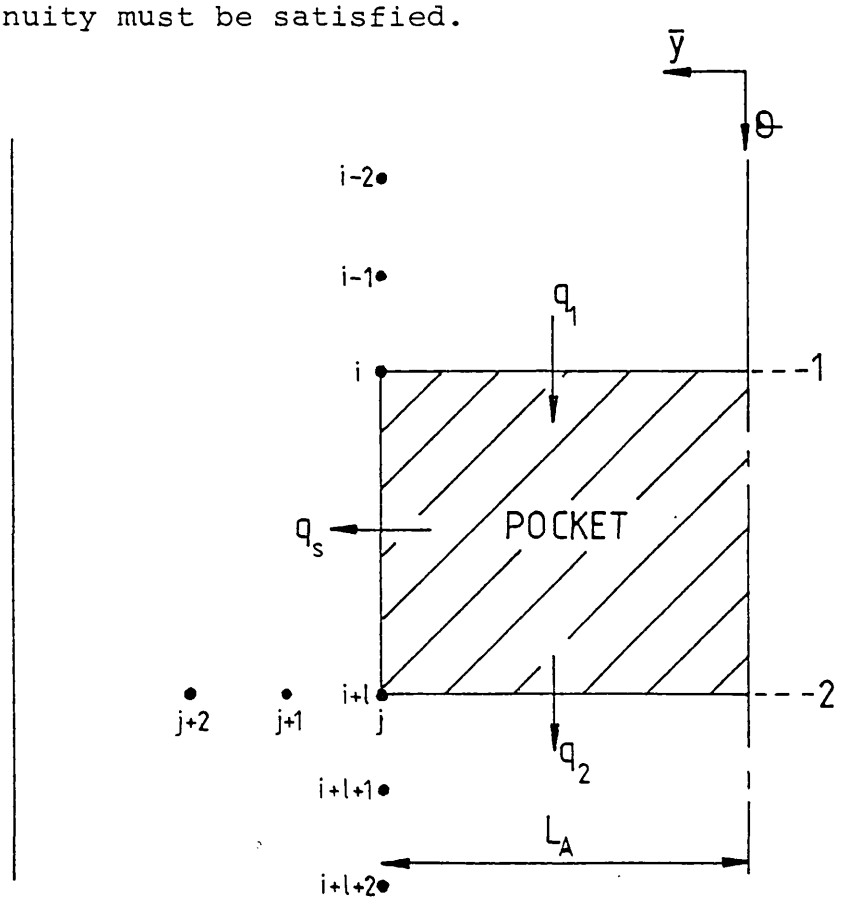
$$\bar{\delta} = -K\bar{p}$$

and $$K = \frac{6\eta U R_2 t}{c^3 E}\left(1 - \frac{2\nu^2}{1-\nu}\right)$$

The equation $\left[CN, CS, CE, CW\right]\left[\bar{p}\right] = \left[C0\right]$ is solved using Gauss-Seidel iteration, including successive over relaxation in the form $\bar{p}_{new} = \bar{p}_{old} + \beta_p(\Delta\bar{p})$, where β_p is a relaxation factor $(1<\beta_p<2)$, and $\Delta\bar{p}$ is the change in pressure from one iteration to the next.

A6.2. Pocket Pressure.

Considering the flows around a half pocket, continuity must be satisfied.



$$q_v = q_2 - q_1 + q_s = q_n \qquad \text{(A6.2.)}$$

where q_s, the sill flow, arises from the axial pressure distribution. As pressure is a function of both θ and $\bar{y}$, then the film flows q_1, q_2 and q_s are found by integration along the pocket edge. That is

$$q_1 = \int_0^{L_A} \frac{-h_1^3}{12\eta}\left(\frac{\partial p}{\partial x}\right)_1 + \frac{h_1\omega(R_2 + \delta_1)}{2}\, dy$$

$$q_2 = \int_0^{L_A} \frac{-h_2^3}{12\eta}\left(\frac{\partial p}{\partial x}\right)_2 + \frac{h_2\omega(R_2 + \delta_2)}{2}\, dy$$

$$q_s = \int_1^2 \frac{-h_s^3}{12\eta}\left(\frac{\partial p}{\partial y}\right)_s dx$$

Substituting for the dimensionless variables $h = c\bar{h}$, $\delta = c\bar{\delta}$, $y = \frac{L\bar{y}}{2}$, $p = \frac{6\eta U R_2 \bar{p}}{c^2}$ and $x = R_2\theta$ gives

$$q_n = q_2 - q_1 + q_s = \frac{\omega c R_2 L}{4}\left\{I_2 - I_1 + \left(\frac{D}{L}\right)^2 I_s\right\} \qquad \text{(A6.3.)}$$

where

$$I_1 = \int_0^{\frac{2L_A}{L}} -\bar{h}_1^3\left(\frac{\partial \bar{p}}{\partial \theta}\right)_1 + \bar{h}_1\left(1 + \frac{\bar{\delta}_1 c}{R_2}\right) d\bar{y} \qquad \text{(A6.4.)}$$

$$I_2 = \int_0^{\frac{2L_A}{L}} -\bar{h}_2^3\left(\frac{\partial \bar{p}}{\partial \theta}\right)_2 + \bar{h}_2\left(1 + \frac{\bar{\delta}_2 c}{R_2}\right) d\bar{y} \qquad \text{(A6.5.)}$$

and $$I_s = \int_1^2 -\bar{h}_s^3 \left(\frac{\partial \bar{p}}{\partial \bar{y}}\right)_s \, d\bar{\theta} \qquad \text{(A6.6.)}$$

The nett film flow is equal to the flow from the pocket into the control volume.

$$q_n = q_v = \omega \frac{\partial V}{\partial \bar{\theta}} \qquad \text{(A6.7.)}$$

where the displaced pocket volume

$$V = \frac{\Delta\bar{\theta}_{poc} L_A \left(R_2^2 - (R_2 + \delta_{poc})^2\right)}{2}$$

δ_{poc} is constant for a given pocket due to the assumptions of a uniform pocket pressure and the elasticity theory. Substituting $\delta = c\bar{\delta}$ and expanding gives

$$V = \frac{\Delta\bar{\theta}_{poc} L_A c R_2 \, \bar{V}}{2}$$

where $$\bar{V} = -\bar{\delta}_{poc}\left(2 + \bar{\delta}_{poc}\frac{c}{R_2}\right)$$

Substituting for V in eq. A6.7. gives

$$q_v = \frac{\omega c R_2}{2}\left\{\Delta\bar{\theta}_{poc} L_A \frac{\partial \bar{V}}{\partial \bar{\theta}}\right\} \qquad \text{(A6.8.)}$$

Therefore, from eqs. A6.2., A6.3. and A6.8.

$$I_2 - I_1 + \left(\frac{D}{L}\right)^2 I_s = \frac{2L_A}{L} \Delta\theta_{poc} \frac{\partial \bar{v}}{\partial \theta} \qquad \text{(A6.9.)}$$

I_1, I_2 and I_s are discretized and expanded taking station 1 as node i, station 2 as node i + 1, and the side of the pocket as node j. Parabolic interpolation is used for the differential terms, that is

$$\left(\frac{\partial \bar{p}}{\partial \theta}\right)_1 = \frac{3\bar{p}_i - 4\bar{p}_{i-1} + \bar{p}_{i-2}}{2\Delta\theta}$$

$$\left(\frac{\partial \bar{p}}{\partial \theta}\right)_2 = \frac{-3\bar{p}_{i+1} + 4\bar{p}_{i+1+1} - \bar{p}_{i+1+2}}{2\Delta\theta}$$

and

$$\left(\frac{\partial \bar{p}}{\partial \bar{y}}\right)_s = \frac{-3\bar{p}_j + 4\bar{p}_{j+1} - \bar{p}_{j+2}}{2\Delta\bar{y}}$$

Then from eqs. A6.4. and A6.5.,

$$I_2 - I_1 = \int_0^j \frac{\bar{h}_i^3}{2\Delta\theta}(3\bar{p}_i - 4\bar{p}_{i-1} + \bar{p}_{i-2}) \, d\bar{y}$$

$$- \int_0^j \frac{\bar{h}_{i+1}^3}{2\Delta\theta}(-3\bar{p}_{i+1} + 4\bar{p}_{i+1+1} - \bar{p}_{i+1+2}) \, d\bar{y}$$

$$+ \int_0^j \bar{h}_{i+1}\left(1 + \frac{\bar{\delta}_{i+1} c}{R_2}\right) - \bar{h}_i\left(1 + \frac{\bar{\delta}_i c}{R_2}\right) \, d\bar{y}$$

and $$I_s = \int_i^{i+1} \frac{-\bar{h}_i^3}{2\Delta\bar{y}} (-3\bar{p}_j + 4\bar{p}_{j+1} - \bar{p}_{j+2})$$

For a uniform pocket pressure and due to the assumptions used in the distortion theory, then $\bar{p}_i = \bar{p}_{i+1} = \bar{p}_j$, and $\bar{\delta}_i = \bar{\delta}_{i+1}$. Also $\bar{p}_i$ and $\bar{\delta}_i$ are not functions of $\bar{y}$ and $\bar{\theta}$, and $\bar{h}_i$ and $\bar{h}_{i+1}$ are not functions of $\bar{y}$ for a given pocket. Therefore,

$$I_2 - I_1 + \left(\frac{D}{L}\right)^2 I_s$$

$$= \frac{3\bar{p}_i}{2\Delta\bar{\theta}} \left(\frac{2L_A}{L}\right) (\bar{h}_i^3 + \bar{h}_{i+1}^3)$$

$$+ \frac{\bar{h}_i^3}{2\Delta\bar{\theta}} \int_0^j (-4\bar{p}_{i-1} + \bar{p}_{i-2}) \, d\bar{y}$$

$$- \frac{\bar{h}_{i+1}^3}{2\Delta\bar{\theta}} \int_0^j (4\bar{p}_{i+1+1} - \bar{p}_{i+1+2}) \, d\bar{y}$$

$$+ \left(\frac{2L_A}{L}\right) (\bar{h}_{i+1} - \bar{h}_i) \left(1 + \bar{\delta}_i \frac{c}{R_2}\right)$$

$$+ \left(\frac{D}{L}\right)^2 \frac{1}{2\Delta\bar{y}} \left\{ 3\bar{p}_i \int_i^{i+1} \bar{h}_j^3 \, d\bar{\theta} \right.$$

$$\left. - \int_i^{i+1} \bar{h}_j^3 (4\bar{p}_{j+1} - \bar{p}_{j+2}) \, d\bar{\theta} \right\}$$

But $$\bar{h}_j = (1 - \bar{\delta}_i) + \xi\cos\theta$$

and $$\int_i^{i+1} \bar{h}_j^3 \, d\theta = \int_i^{i+1} \left\{ (1 - \bar{\delta}_i)^3 + 3(1 - \bar{\delta}_i)^2 \xi\cos\theta + 3(1 - \bar{\delta}_i)\xi^2\cos^2\theta + \xi^3\cos^3\theta \right\} d\theta$$

Now $$\int \cos\theta \, d\theta = \sin\theta$$

$$\int \cos^2\theta \, d\theta = \frac{1}{4}(2\theta + \sin 2\theta)$$

and $$\int \cos^3\theta \, d\theta = \frac{1}{4}\left(3\sin\theta + \frac{\sin 3\theta}{3}\right)$$

So $$\int_i^{i+1} \bar{h}_j^3 \, d\theta = A_\delta + A_\xi$$

where $$A_\delta = \Delta\theta_{poc}\left((1 - \bar{\delta}_i)^3 - \frac{3\bar{\delta}_i\xi^2}{2}\right) + 3\xi(\sin\theta_{i+1} - \sin\theta_i)(1 - \bar{\delta}_i)^2 - \frac{3\xi^2\bar{\delta}_i}{4}(\sin 2\theta_{i+1} - \sin 2\theta_i)$$

and $$A_\xi = \frac{\xi^3}{12}(\sin 3\theta_{i+1} - \sin 3\theta_i) + \frac{3\xi^2}{4}(2\Delta\theta_{poc} + \sin 2\theta_{i+1} - \sin 2\theta_i) + \frac{3\xi^3}{4}(\sin\theta_{i+1} - \sin\theta_i)$$

A_δ contains all the terms which include $\bar{\delta}_i$. Thus, A_ε can be calculated once for each pocket for a given value of ε, but A_δ must be recalculated each time the distortion field is calculated in the iteration scheme.

Therefore, from eq. A6.9.

$$\frac{2L_A \Delta\theta_{poc}}{L} \frac{\partial \bar{v}}{\partial \theta}$$

$$= \bar{p}_i \left\{ \frac{3}{2\Delta\theta} \left(\frac{2L_A}{L} \right) (\bar{h}_i^3 + \bar{h}_{i+1}^3) \right.$$

$$\left. + \frac{3}{2\Delta\bar{y}} \left(\frac{D}{L} \right)^2 (A_\delta + A_\varepsilon) \right\}$$

$$+ \frac{\bar{h}_i^3}{2\Delta\theta} \int_0^j (-4\bar{p}_{i-1} + \bar{p}_{i-2}) \, d\bar{y}$$

$$- \frac{\bar{h}_{i+1}^3}{2\Delta\theta} \int_0^j (4\bar{p}_{i+1+1} - \bar{p}_{i+1+2}) \, d\bar{y}$$

$$- \left(\frac{D}{L} \right)^2 \frac{1}{2\Delta\bar{y}} \int_i^{i+1} \bar{h}_j^3 (4\bar{p}_{j+1} - \bar{p}_{j+2}) \, d\theta$$

$$+ \left(\frac{2L_A}{L} \right) (\bar{h}_{i+1} - \bar{h}_i) \left(1 + \bar{\delta}_i \frac{c}{R_2} \right) \qquad \text{(A6.10.)}$$

The approximation of $\frac{\partial \bar{v}}{\partial \theta}$ was again performed in two ways following the methods of Chapter 2.

i). Method 1.

This uses the approximation,

$$\frac{\partial \bar{v}}{\partial \bar{\theta}} = \frac{\bar{v}^n - \bar{v}^{n-1}}{\Delta\bar{\theta}_{pocl}}$$

Therefore, from eq. A6.10.,

$$\bar{p}_i \left\{ \frac{3}{2\Delta\bar{\theta}} \left(\frac{2L_A}{L} \right) (\bar{h}_i^3 + \bar{h}_{i+1}^3) + \frac{3}{2\Delta\bar{y}} \left(\frac{D}{L} \right)^2 (A_\delta + A_\varepsilon) \right\}$$

$$= \left(\frac{2L_A}{L} \right) \left\{ \frac{\Delta\bar{\theta}_{poc}}{\Delta\bar{\theta}_{pocl}} (\bar{v}^n - \bar{v}^{n-1}) \right.$$

$$\left. - (\bar{h}_{i+1} - \bar{h}_i) \left(1 + \bar{\delta}_i \frac{c}{R_2} \right) \right\}$$

$$+ \frac{\bar{h}_i^3}{2\Delta\bar{\theta}} \int_0^j (4\bar{p}_{i-1} - \bar{p}_{i-2}) \, d\bar{y}$$

$$+ \frac{\bar{h}_{i+1}^3}{2\Delta\bar{\theta}} \int_0^j (4\bar{p}_{i+1+1} - \bar{p}_{i+1+2}) \, d\bar{y}$$

$$+ \left(\frac{D}{L} \right)^2 \frac{1}{2\Delta\bar{y}} \int_i^{i+1} \bar{h}_j^3 (4\bar{p}_{j+1} - \bar{p}_{j+2}) \, d\bar{\theta} \qquad \text{(A6.11.)}$$

where $$\bar{v}^n = -\bar{\delta}_i \left(2 + \bar{\delta}_i \frac{c}{R_2} \right)$$

ii). Method 2.

This follows the method used by Alexandrov.

$$\frac{\partial \bar{V}}{\partial \theta} = \frac{\partial}{\partial \theta}\left\{-2\bar{\delta}_{poc} - \bar{\delta}^2_{poc}\,\frac{c}{R_2}\right\}$$

$$\frac{\partial \bar{V}}{\partial \theta} = -\left\{2\left(\frac{\partial \bar{\delta}}{\partial \theta}\right)_{poc} + \frac{c}{R_2}\,2\bar{\delta}_{poc}\left(\frac{\partial \bar{\delta}}{\partial \theta}\right)_{poc}\right\}$$

Putting $\bar{\delta} = -K\bar{p}$,

$$\frac{\partial \bar{V}}{\partial \theta} = 2K\left(1 + \bar{\delta}_{poc}\,\frac{c}{R_2}\right)\left(\frac{\partial \bar{p}}{\partial \theta}\right)_{poc}$$

$\left(\frac{\partial \bar{p}}{\partial \theta}\right)_{poc}$ in the limit of small rotations of the journal, is taken to be the mean of the pressure gradients at the edge of a pocket.

$$\left(\frac{\partial \bar{p}}{\partial \theta}\right)_{poc} = \frac{\frac{1}{L_A}\int_0^{\frac{2L_A}{L}}\left(\frac{\partial \bar{p}}{\partial \theta}\right)_1 d\bar{y} + \frac{1}{L_A}\int_0^{\frac{2L_A}{L}}\left(\frac{\partial \bar{p}}{\partial \theta}\right)_2 d\bar{y}}{2}$$

Discretizing as before, and using a parabolic interpolation for the pressure gradients gives,

$$\frac{\partial \bar{v}}{\partial \bar{\theta}} = \frac{K}{2L_A \Delta \bar{\theta}} \left(1 + \frac{\bar{\delta}_i c}{R_2}\right) \left\{ \int_0^j (3\bar{p}_i - 4\bar{p}_{i-1} + \bar{p}_{i-2})\, d\bar{y} + \int_0^j (-3\bar{p}_i + 4\bar{p}_{i+1+1} - \bar{p}_{i+1+2})\, d\bar{y} \right\}$$

$$\frac{\partial \bar{v}}{\partial \bar{\theta}} = \frac{K}{2L_A \Delta \bar{\theta}} \left(1 + \frac{\bar{\delta}_i c}{R_2}\right) \left\{ \int_0^j (-4\bar{p}_{i-1} + \bar{p}_{i-2})\, d\bar{y} + \int_0^j (4\bar{p}_{i+1+1} - \bar{p}_{i+1+2})\, d\bar{y} \right\}$$

Substituting for $\frac{\partial \bar{v}}{\partial \bar{\theta}}$ in eq. A6.10. gives,

$$\bar{p}_i \left\{ \frac{3}{2\Delta \bar{\theta}} \left(\frac{2L_A}{L}\right) (\bar{h}_i^3 + \bar{h}_{i+1}^3) + \frac{3}{2\Delta \bar{y}} \left(\frac{D}{L}\right)^2 (A_\delta + A_\varepsilon) \right\}$$

$$= - \left(\frac{2L_A}{L}\right) (\bar{h}_{i+1} - \bar{h}_i) \left(1 + \frac{\bar{\delta}_i\, c}{R_2}\right)$$

$$+ \left\{ \frac{\bar{h}_i^3}{2\Delta \bar{\theta}} - \frac{K \Delta \bar{\theta}_{poc}}{2L_A \Delta \bar{\theta}} \left(\frac{2L_A}{L}\right) \left(1 + \frac{\bar{\delta}_i\, c}{R_2}\right) \right\} \int_0^j (4\bar{p}_{i-1} - \bar{p}_{i-2})\, d\bar{y}$$

$$+ \left\{ \frac{\bar{h}_{i+1}^3}{2\Delta \bar{\theta}} + \frac{K \Delta \bar{\theta}_{poc}}{2L_A \Delta \bar{\theta}} \left(\frac{2L_A}{L}\right)^0 \left(1 + \frac{\bar{\delta}_i\, c}{R_2}\right) \right\} \int_0^j (4\bar{p}_{i+1+1} - \bar{p}_{i+1+2})\, d\bar{y}$$

$$+ \left(\frac{D}{L}\right)^2 \frac{1}{2\Delta\bar{y}} \int_i^{i+1} \bar{h}_j^3 (4\bar{p}_{j+1} - \bar{p}_{j+2}) \, d\bar{\theta} \qquad \text{(A6.12.)}$$

Both methods therefore yield an equation for the pocket pressure, $\bar{p}_i$, in terms of geometric variables and integrals of pressure and film thickness surrounding the pocket. The integrations were performed using Simpson's rule.

A6.3. Load, Attitude Angle, Friction And Flow.

The load is found by integrating the pressure field. The two components of load, parallel and perpendicular to the line of centres, are given by

$$W_x = \frac{6\eta U R_2^2 L}{c^2} \int_0^1 \int_0^{2\pi} \bar{p} \sin\bar{\theta} \, d\bar{\theta} \, d\bar{y} = 6\eta U L \left(\frac{R_2}{c}\right)^2 \bar{W}_x$$

$$W_y = \frac{6\eta U R_2^2 L}{c^2} \int_0^1 \int_0^{2\pi} \bar{p} \cos\bar{\theta} \, d\bar{\theta} \, d\bar{y} = 6\eta U L \left(\frac{R_2}{c}\right)^2 \bar{W}_y$$

$\bar{W}_x$ and $\bar{W}_y$ are integrated using Simpson's rule. The Sommerfeld number, $S = \dfrac{W}{LU\eta} \left(\dfrac{c}{R_2}\right)^2$

where $\quad W = \sqrt{W_x^2 + W_y^2}$

so $\quad W = 6\eta U \left(\dfrac{R_2}{c}\right)^2 \sqrt{\bar{W}_x^2 + \bar{W}_y^2}$

Therefore

$$S = 6\sqrt{\bar{W}_x^2 + \bar{W}_y^2}$$

The angle between the line of centres and the load line, the attitude angle, is given by

$$\phi = \tan^{-1}\left(\frac{-\bar{W}_y}{\bar{W}_x}\right)$$

The frictional torque is found by integrating the elemental shear stresses.

$$F = 2\int_0^{\frac{L}{2}}\int_0^{2\pi} \tau R_2 \, d\theta \, dy$$

where $$\tau = \frac{\eta U}{h} + \frac{h}{2}\frac{\partial p}{\partial x}$$

The dimensionless friction,

$$\bar{F} = \int_0^1\int_0^{2\pi}\left(\frac{1}{\bar{h}} + 3\bar{h}\frac{\partial \bar{p}}{\partial \theta}\right) d\theta \, d\bar{y}$$

where $$\bar{F} = \frac{c}{\eta U R_2 L} F$$

The axial pressure gradient introduces side flow from the two edges of the bearing.

$$Q = -2\int_0^{2\pi} \frac{h^3}{12\eta}\left(\frac{\partial p}{\partial y}\right)_s R_2 \, d\theta$$

The dimensionless flow,

$$\bar{Q} = \int_0^{2\pi} \bar{h}^3 \left(\frac{\partial \bar{p}}{\partial \bar{y}}\right)_s d\theta$$

where $\bar{Q} = \dfrac{-L \; Q}{2UcR_2^2}$

$\bar{F}$ and $\bar{Q}$ are integrated using Simpson's rule.

APPENDIX A7.

COMPUTER PROGRAMMES FOR A FINITE LENGTH BEARING.

Variables.

ADEL — Geometric variable, A_δ.

ALPHA — LOVERD inverse squared, $\lambda = \left(\frac{D}{L}\right)^2$.

DTHETA — Increment of theta, $\Delta\theta$.

DTHPOK — Angle subtended by a pocket, $\Delta\theta_{poc}$.

DY — Increment of axial length, $\Delta\bar{y}$.

FLOW — Dimensionless flow, $\bar{Q}$.

LLANDX — Number of meshes across a land in the circumferential direction.

LLANDY — Number of meshes across a land in the axial direction.

LOVERD — Length to diameter ratio, $\frac{L}{D}$.

LPOKX — Number of meshes across a pocket in the circumferential direction.

LPOKY — Number of meshes across a pocket in the axial direction.

NSTEPX — Total number of meshes from $\theta = 0$ to $\theta = 2\pi$.

NSTEPY — Total number of meshes from $\bar{y} = 0$ to $\bar{y} = 1$.

NX Total number of nodes from $\theta = 0$ to $\theta = 2\pi$.

NY Total number of nodes from $\bar{y} = -\Delta\bar{y}$ to $\bar{y} = 1$.

Subscripted Variable.

EPSSIN Geometric variable for each pocket, A_ε.

Other variables are the same as Appendix A3.

```
      PROGRAM JB2(INPUT,OUTPUT,TAPE5=INPUT,TAPE6=OUTPUT)
C
C                     FINITE LENGTH RIGID JOURNAL
C                     BEARING SOLUTION
C
      COMMON/CGEOM/NX,NY,DTHETA,DY,GEOM1,GEOM2,GEOM3
     1/CCOEFP/CN(103,12),CS(103,12),CE(103,12),CW(103,12),CC(103,12)
     2/CSOLVP/P(103,12),H(103,12),RELXP,ITERP,PITER(200),NMID
      DIMENSION FFX(103),FFY(12)
      DIMENSION THETAN(103)
      REAL LOVERD
C
C                     SET PROBLEM PARAMETERS
C
      PIE=3.1415926536
      READ(5,101)NSTEPX,NSTEPY,LOVERD
  101 FORMAT(2I5,F10.4)
      WRITE(6,141)NSTEPX,NSTEPY,LOVERD
  141 FORMAT(////,1HO,*NSTEPX=*,I5,5X,*NSTEPY=*,I5,5X,*LOVERD=*,F10.6,/)
      READ(5,102)NEPS
  102 FORMAT(I5)
      READ(5,103)RELXP,ITERP
  103 FORMAT(F10.5,I5)
      WRITE(6,142)RELXP,ITERP
  142 FORMAT(1HO,*RELXP=*,F10.5,5X,*ITERP=*,I5,/)
C
C                     CALCULATE INITIAL VALUES
C
      NX=NSTEPX+1
      NY=NSTEPY+2
      DTHETA=2.*PIE/FLOAT(NSTEPX)
      DY=1./FLOAT(NSTEPY)
      ALPHA=1./LOVERD**2
      GEOM1=1./(2.*(1.+ALPHA*DTHETA**2/DY**2))
      GEOM2=1./(2.*(1.+DY**2/(ALPHA*DTHETA**2)))
      GEOM3=-DTHETA*GEOM1/2.
      NMID=NSTEPX/3
      DO 1001 I=1,NX+1
      THETAN(I)=FLOAT(I-1)*DTHETA
      DO 1002 J=1,NY
      P(I,J)=0.
 1002 CONTINUE
 1001 CONTINUE
C
C                     MAIN ITERATION LOOP            **********************
C
      DO 1003 N=1,NEPS
      READ(5,104)EPS
  104 FORMAT(F10.4)
      DO 1004 I=1,NX+1
      HI=1.+EPS*COS(THETAN(I))
      DO 1005 J=1,NY
      H(I,J)=HI
 1005 CONTINUE
 1004 CONTINUE
      CALL COEFP
      CALL CALCP
      WRITE(6,151)(PITER(M),M=1,ITERP)
  151 FORMAT(10F10.7)
C
C                     CALCULATE FINAL VALUES
C
      DO 1006 I=1,NX
      COSX=COS(THETAN(I))
```

```
      DO 1007 J=2,NY
      FFY(J)=P(I,J)*COSX
 1007 CONTINUE
      CALL TRAP(FFY,2,NY,DY,AREA)
      FFX(I)=AREA
 1006 CONTINUE
      CALL TRAP(FFX,1,NX,DTHETA,WX)
      DO 1008 I=1,NX
      SINX=SIN(THETAN(I))
      DO 1009 J=2,NY
      FFY(J)=P(I,J)*SINX
 1009 CONTINUE
      CALL TRAP(FFY,2,NY,DY,AREA)
      FFX(I)=AREA
 1008 CONTINUE
      CALL TRAP(FFX,1,NX,DTHETA,WY)
      SOMM=6.*SQRT(WX**2+WY**2)
      ATT=ATAN(-WY/WX)*180./PIE
      DO 1010 J=2,NY
      P(NX+1,J)=P(2,J)
      DO 1011 I=2,NX
      FFX(I)=1./H(I,J)+3.*H(I,J)*(P(I+1,J)-P(I-1,J))/DTHETA
 1011 CONTINUE
      FFX(1)=1./H(1,J)+3.*H(1,J)*(P(2,J)-P(NX,J))/DTHETA
      CALL TRAP(FFX,1,NX,DTHETA,AREA)
      FFY(J)=AREA
 1010 CONTINUE
      CALL TRAP(FFY,2,NY,DY,FRIC)
      DO 1012 I=1,NX
      FFX(I)=H(I,NY)**3*(3.*P(I,NY)-4.*P(I,NY-1)+P(I,NY-2))/(2.*DY)
 1012 CONTINUE
      CALL TRAP(FFX,1,NX,DTHETA,FLOW)
C
C                    WRITE FINAL RESULTS FOR EACH VALUE OF EPS
C
      WRITE(6,152)EPS
  152 FORMAT(///,1HO,*EPS=*,F10.4)
      WRITE(6,153)SOMM,ATT
  153 FORMAT(1HO,*SOMMERFELD NUMBER=*,F10.6,5X,*ATTITUDE ANGLE=*,F10.6,
     1*DEGREES*)
      WRITE(6,154)FRIC,FLOW
  154 FORMAT(1HO,*FRICTION=*,F10.6,5X,*FLOW=*,F10.6)
      WRITE(6,155)
  155 FORMAT(1HO,*FINAL PRESSURE FIELD*,/)
      DO 1013 I=1,NX
      WRITE(6,160)(P(I,J),J=1,NY)
  160 FORMAT(1H ,12F10.6)
 1013 CONTINUE
      WRITE(6,156)
  156 FORMAT(1HO,*FINAL FILM THICKNESS FIELD*,/)
      DO 1014 I=1,NX
      WRITE(6,160)(H(I,J),J=1,NY)
 1014 CONTINUE
 1003 CONTINUE
C
C                    END OF MAIN ITERATION LOOP    **********************
C
      STOP
      END

      SUBROUTINE COEFP
      COMMON/CGEOM/NX,NY,DTHETA,DY,GEOM1,GEOM2,GEOM3
     1/CCOEFP/CN(103,12),CS(103,12),CE(103,12),CW(103,12),CC(103,12)
     2/CSOLVP/P(103,12),H(103,12),RELXP,ITERP,PITER(200),NMID
```

```
      DO 2001 I=2,NX-1
      DO 2002 J=2,NY-1
      CN(I,J)=GEOM1*(1.+3.*(H(I+1,J)-H(I-1,J))/(4.*H(I,J)))
      CS(I,J)=GEOM1*(1.-3.*(H(I+1,J)-H(I-1,J))/(4.*H(I,J)))
      CE(I,J)=GEOM2*(1.+3.*(H(I,J+1)-H(I,J-1))/(4.*H(I,J)))
      CW(I,J)=GEOM2*(1.-3.*(H(I,J+1)-H(I,J-1))/(4.*H(I,J)))
      CC(I,J)=GEOM3*(H(I+1,J)-H(I-1,J))/H(I,J)**3
 2002 CONTINUE
 2001 CONTINUE
      RETURN
      END

      SUBROUTINE CALCP
      COMMON/CGEOM/NX,NY,DTHETA,DY,GEOM1,GEOM2,GEOM3
     1/CCOEFP/CN(103,12),CS(103,12),CE(103,12),CW(103,12),CC(103,12)
     2/CSOLVP/P(103,12),H(103,12),RELXP,ITERP,PITER(200),NMID
      DO 3001 M=1,ITERP
      DO 3002 I=2,NX-1
      DO 3003 J=2,NY-1
      OLDP=P(I,J)
      P(I,J)=CN(I,J)*P(I+1,J)+CS(I,J)*P(I-1,J)
     1       +CE(I,J)*P(I,J+1)+CW(I,J)*P(I,J-1)+CC(I,J)
      P(I,J)=OLDP+RELXP*(P(I,J)-OLDP)
      IF(P(I,J).LT.0.)P(I,J)=0.
 3003 CONTINUE
 3002 CONTINUE
      PITER(M)=P(NMID,2)
      DO 3004 I=2,NX-1
      P(I,1)=P(I,3)
 3004 CONTINUE
 3001 CONTINUE
      RETURN
      END

      SUBROUTINE TRAP(F,NA,NZ,H,AREA)
      DIMENSION F(NZ)
C
C     SUBROUTINE TO INTEGRATE A FUNCTION F USING
C     TRAPEZOIDAL RULE BETWEEN LIMITS NA AND NZ
C     WITH STEP WIDTH H AND GIVING ANSWER AREA
C
      IF((NZ-NA).EQ.1)GO TO 91
      IF((NZ-NA).EQ.0)GO TO 92
      NB=NA+1
      NY=NZ-1
      SUM=0.
      DO 9001 ITRAP=NB,NY
      SUM=SUM+F(ITRAP)
 9001 CONTINUE
      AREA=0.5*H*(F(NA)+F(NZ)+2.*SUM)
      GO TO 93
   91 AREA=0.5*H*(F(NA)+F(NZ))
      GO TO 93
   92 AREA=0.
   93 RETURN
      END
```

```
      PROGRAM JBDEL2(INPUT,OUTPUT,TAPE5=INPUT,TAPE6=OUTPUT,TAPE1,TAPE2)
C
C                     FINITE LENGTH JOURNAL BEARING WITH
C                     ELASTIC LINER
C
      COMMON/CGEOM/NX,NY,DTHETA,DY,GEOM1,GEOM2,GEOM3,EPS,THETAN(103)
     1/CCOEFP/CN(103,12),CS(103,12),CE(103,12),CW(103,12),CC(103,12)
     2/CSOLVP/P(103,12),H(103,12),RELXP,ITERP,PITER(200),NMID
     3/CDEFL/RELXD,ITERD,ELAST,DEL(103,12),DITER(50)
      DIMENSION FFX(103),FFY(12)
      DIMENSION HMEAN(103)
      REAL LOVERD
C
C                     SET PROBLEM PARAMETERS
C
      PIE=3.1415926536
      READ(5,101)NSTEPX,NSTEPY,LOVERD,ELAST
  101 FORMAT(2I5,2F10.4)
      WRITE(6,102)NSTEPX,NSTEPY,LOVERD,ELAST
  102 FORMAT(////,1HO,*NSTEPX=*,I5,5X,*NSTEPY=*,I5,5X,
     1*LOVERD=*,F10.6,5X,*ELAST=*,F10.6,/)
      READ(5,103)NEPS
  103 FORMAT(I5)
      READ(5,104)RELXP,ITERP,RELXD,ITERD
  104 FORMAT(F10.5,I5,F10.5,I5)
      WRITE(6,105)RELXP,ITERP,RELXD,ITERD
  105 FORMAT(1HO,*RELXP=*,F10.5,5X,*ITERP=*,I5,5X,
     1*RELXD=*,F10.5,5X,*ITERD=*,I5,/)
C
C                     CALCULATE INITIAL VALUES
C
      NX=NSTEPX+1
      NY=NSTEPY+2
      DTHETA=2.*PIE/FLOAT(NSTEPX)
      DY=1./FLOAT(NSTEPY)
      ALPHA=1./LOVERD**2
      GEOM1=1./(2.*(1.+ALPHA*DTHETA**2/DY**2))
      GEOM2=1./(2.*(1.+DY**2/(ALPHA*DTHETA**2)))
      GEOM3=-DTHETA*GEOM1/2.
      NMID=NSTEPX/3
      DO 1001 I=1,NX+1
      THETAN(I)=FLOAT(I-1)*DTHETA
 1001 CONTINUE
      DO 1002 J=1,NY
      READ(1)(P(I,J),I=1,NX+1),(DEL(I,J),I=1,NX+1)
 1002 CONTINUE
C
C                     MAIN ITERATION LOOP            **********************
C
      READ(1)EPS
      DO 1003 N=1,NEPS
      READ(5,106)DEPS
  106 FORMAT(F10.4)
      EPS=EPS+DEPS
      DO 1004 NDIT=1,ITERD
      CALL COEFP
      CALL CALCP
      CALL DEFL
      DITER(NDIT)=DEL(NMID,2)
 1004 CONTINUE
      WRITE(6,107)
  107 FORMAT(////,1HO,*PRESSURE CONVERGANCE FOR FINAL ITERATION*)
      WRITE(6,108)(PITER(M),M=1,ITERP)
  108 FORMAT(10F10.7)
```

```
C
C                    CALCULATE FINAL VALUES
C
      DO 1005 I=1,NX
      COSX=COS(THETAN(I))
      DO 1006 J=2,NY
      FFY(J)=P(I,J)*COSX
 1006 CONTINUE
      CALL SIMP(FFY,2,NY,DY,AREA)
      FFX(I)=AREA
 1005 CONTINUE
      CALL SIMP(FFX,1,NX,DTHETA,WX)
      DO 1007 I=1,NX
      SINX=SIN(THETAN(I))
      DO 1008 J=2,NY
      FFY(J)=P(I,J)*SINX
 1008 CONTINUE
      CALL SIMP(FFY,2,NY,DY,AREA)
      FFX(I)=AREA
 1007 CONTINUE
      CALL SIMP(FFX,1,NX,DTHETA,WY)
      SOMM=6.*SQRT(WX**2+WY**2)
      ATT=ATAN(-WY/WX)*180./PIE
      DO 1009 J=2,NY
      P(NX+1,J)=P(2,J)
      DO 1010 I=2,NX
      FFX(I)=1./H(I,J)+3.*H(I,J)*(P(I+1,J)-P(I-1,J))/DTHETA
 1010 CONTINUE
      FFX(1)=1./H(1,J)+3.*H(1,J)*(P(2,J)-P(NX,J))/DTHETA
      CALL SIMP(FFX,1,NX,DTHETA,AREA)
      FFY(J)=AREA
 1009 CONTINUE
      CALL SIMP(FFY,2,NY,DY,FRIC)
      DO 1011 I=1,NX
      FFX(I)=H(I,NY)**3*(3.*P(I,NY)-4.*P(I,NY-1)+P(I,NY-2))/(2.*DY)
 1011 CONTINUE
      CALL SIMP(FFX,1,NX,DTHETA,FLOW)
      DO 1012 I=1,NX
      DO 1013 J=2,NY
      FFY(J)=H(I,J)
 1013 CONTINUE
      CALL SIMP(FFY,2,NY,DY,HINT)
      HMEAN(I)=HINT
 1012 CONTINUE
C
C                    WRITE FINAL RESULTS FOR EACH VALUE OF EPS
C
      WRITE(6,109)EPS,DEPS
  109 FORMAT(///,1HO,*EPS=*,F10.4,5X,*DEPS=*,F10.4)
      WRITE(6,110)SOMM,ATT
  110 FORMAT(1HO,*SOMMERFELD NUMBER=*,F10.6,5X,
     1*ATTITUDE ANGLE=*,F10.6,*DEGREES*)
      WRITE(6,111)FRIC,FLOW
  111 FORMAT(1HO,*FRICTION=*,F10.6,5X,*FLOW=*,F10.6)
      WRITE(6,112)
  112 FORMAT(1HO,*FINAL PRESSURE FIELD*,/)
      DO 1014 I=1,NX
      WRITE(6,113)(P(I,J),J=1,NY)
  113 FORMAT(1H ,12F10.6)
 1014 CONTINUE
      WRITE(6,114)
  114 FORMAT(1HO,*FINAL FILM THICKNESS FIELD*,/)
      DO 1015 I=1,NX
      WRITE(6,113)(H(I,J),J=1,NY)
```

```
 1015 CONTINUE
      WRITE(6,115)
  115 FORMAT(1HO,*FINAL DISTORTION FIELD*)
      DO 1016 I=1,NX
      WRITE(6,113) (DEL(I,J),J=1,NY)
 1016 CONTINUE
      WRITE(6,116)
  116 FORMAT(1HO,*MEAN FILM THICKNESS ALONG EACH AXIAL LINE*)
      WRITE(6,117) (HMEAN(I),I=1,NX)
  117 FORMAT(1HO,10F10.7)
      WRITE(6,118)
  118 FORMAT(1HO,*DISTORTION CONVERGANCE*)
      WRITE(6,119) (DITER(L),L=1,ITERD)
  119 FORMAT(1HO,10F10.6)
      DO 1017 J=1,NY
      WRITE(2) (P(I,J),I=1,NX+1),(DEL(I,J),I=1,NX+1)
 1017 CONTINUE
      WRITE(2)EPS
 1003 CONTINUE
C
C                    END OF MAIN ITERATION LOOP    **********************
C
      STOP
      END

      SUBROUTINE COEFP
      COMMON/CGEOM/NX,NY,DTHETA,DY,GEOM1,GEOM2,GEOM3,EPS,THETAN(103)
     1/CCOEFP/CN(103,12),CS(103,12),CE(103,12),CW(103,12),CC(103,12)
     2/CSOLVP/P(103,12),H(103,12),RELXP,ITERP,PITER(200),NMID
     3/CDEFL/RELXD,ITERD,ELAST,DEL(103,12),DITER(50)
      DO 2001 I=1,NX+1
      HI=1.+EPS*COS(THETAN(I))
      DO 2002 J=1,NY
      H(I,J)=HI-DEL(I,J)
 2002 CONTINUE
 2001 CONTINUE
      DO 2003 I=2,NX-1
      DO 2004 J=2,NY-1
      CN(I,J)=GEOM1*(1.+3.*(H(I+1,J)-H(I-1,J))/(4.*H(I,J)))
      CS(I,J)=GEOM1*(1.-3.*(H(I+1,J)-H(I-1,J))/(4.*H(I,J)))
      CE(I,J)=GEOM2*(1.+3.*(H(I,J+1)-H(I,J-1))/(4.*H(I,J)))
      CW(I,J)=GEOM2*(1.-3.*(H(I,J+1)-H(I,J-1))/(4.*H(I,J)))
      CC(I,J)=GEOM3*(H(I+1,J)-H(I-1,J))/H(I,J)**3
 2004 CONTINUE
 2003 CONTINUE
      RETURN
      END

      SUBROUTINE CALCP
      COMMON/CGEOM/NX,NY,DTHETA,DY,GEOM1,GEOM2,GEOM3,EPS,THETAN(103)
     1/CCOEFP/CN(103,12),CS(103,12),CE(103,12),CW(103,12),CC(103,12)
     2/CSOLVP/P(103,12),H(103,12),RELXP,ITERP,PITER(200),NMID
      DO 3001 M=1,ITERP
      DO 3002 I=2,NX-1
      DO 3003 J=2,NY-1
      OLDP=P(I,J)
      P(I,J)=CN(I,J)*P(I+1,J)+CS(I,J)*P(I-1,J)
     1      +CE(I,J)*P(I,J+1)+CW(I,J)*P(I,J-1)+CC(I,J)
      P(I,J)=OLDP+RELXP*(P(I,J)-OLDP)
      IF(P(I,J).LT.0.)P(I,J)=0.
 3003 CONTINUE
 3002 CONTINUE
      PITER(M)=P(NMID,2)
      DO 3004 I=2,NX-1
```

```
      P(I,1)=P(I,3)
 3004 CONTINUE
 3001 CONTINUE
      RETURN
      END

      SUBROUTINE DEFL
      COMMON/CGEOM/NX,NY,DTHETA,DY,GEOM1,GEOM2,GEOM3,EPS,THETAN(103)
     1/CSOLVP/P(103,12),H(103,12),RELXP,ITERP,PITER(200),NMID
     2/CDEFL/RELXD,ITERD,ELAST,DEL(103,12),DITER(50)
      DO 4001 I=1,NX+1
      DO 4002 J=1,NY
      OLDD=DEL(I,J)
      DEL(I,J)=OLDD+RELXD*(-ELAST*P(I,J)-OLDD)
 4002 CONTINUE
 4001 CONTINUE
      RETURN
      END

      SUBROUTINE SIMP(F,NA,NZ,H,AREA)
      DIMENSION F(NZ)
C
C                    SUBROUTINE TO INTEGRATE A FUNCTION F USING
C                    SIMPSON RULE BETWEEN LIMITS NA AND NZ
C                    WITH STEP WIDTH H AND GIVING ANSWER AREA
C
      NB2=NA+2
      NB4=NA+1
      NY2=NZ-2
      NY4=NZ-1
      SUM2=0.
      SUM4=0.
      DO 9001 ISIMP=NB2,NY2,2
      SUM2=SUM2+F(ISIMP)
 9001 CONTINUE
      DO 9002 ISIMP=NB4,NY4,2
      SUM4=SUM4+F(ISIMP)
 9002 CONTINUE
      AREA=(H/3.)*(F(NA)+2.*SUM2+4.*SUM4+F(NZ))
      RETURN
      END
```

```
      PROGRAM VANE2A(INPUT,OUTPUT,TAPE5=INPUT,TAPE6=OUTPUT,TAPE1,TAPE2)
C
C                     FINITE LENGTH JOURNAL BEARING WITH
C                     POCKETED ELASTIC JOURNAL LINER, METHOD 1
C                     USED FOR POCKET PRESSURE ANALYSIS
C
      COMMON/CGEOM/NX,NY,LPOKX,LPOKY,DY,DTHETA,LOVERD,CDIVR,NMID,EPS,
     1GEOMPX,GEOMPY,GEOM1,GEOM2,GEOM3,NUMPOK,ADEL1,ADEL2(103),ADEL3(103)
     2/CCOEFP/P(103,12),DEL(103,12),H(103,12),DVOL(103),AS,DTHPOK,
     3CN(103,12),CS(103,12),CE(103,12),CW(103,12),CC(103,12),
     4LSKIP(103),THETAN(103),APOK(103),EPSSIN(103),FN(103),NXPOK(21)
     5/CSOLVP/ITERP,RELXP,PMID(100),NXZ
     6/CDEFL/ELAST,RELXD,DELMID(25)
      DIMENSION FNN(103)
      DIMENSION HMEAN(103)
      REAL LOVERD
C
C           SET PROBLEM PARAMATERS
C
      PIE=3.1415926536
      READ(1)NSTEPX,NSTEPY,LPOKX,LLANDX,LPOKY,LLANDY,NUMPOK,NSTART
      READ(5,101)ITERP,RELXP
  101 FORMAT(I5,F10.4)
      READ(5,102)RTWO,TLINER,CLEAR,LOVERD
  102 FORMAT(4F10.4)
      READ(5,103)VISCOS,YOUNG,POISSN,OMEGA
  103 FORMAT(2E10.4,2F10.4)
      READ(5,104)ITERD,RELXD
  104 FORMAT(I5,F10.4)
      READ(5,105)DEPS
  105 FORMAT(F10.4)
      WRITE(6,110)NSTEPX,NSTEPY,LPOKX,LLANDX,LPOKY,LLANDY,NUMPOK,NSTART
  110 FORMAT(/////,1HO,*NSTEPX=*,I5,5X,*NSTEPY=*,I5,5X,*LPOKX=*,I5,5X,
     1*LLANDX=*,I5,5X,*LPOKY=*,I5,5X,*LLANDY=*,I5,5X,
     2/,1HO,*NUMPOK=*,I5,5X,*NSTART=*,I5)
      WRITE(6,111)ITERP,RELXP
  111 FORMAT(1HO,*ITERP=*,I5,5X,*RELXP=*,F10.4)
      WRITE(6,112)RTWO,TLINER,CLEAR,LOVERD
  112 FORMAT(1HO,*RTWO=*,F10.5,5X,*TLINER=*,F10.5,5X,*CLEAR=*,F10.4,5X,
     1*LOVERD=*,F10.5)
      WRITE(6,113)VISCOS,YOUNG,POISSN,OMEGA
  113 FORMAT(1HO,*VISCOS=*,E10.4,5X,*YOUNG=*,E10.4,5X,
     1*POISSN=*,F10.5,5X,*OMEGA=*,F10.5)
      WRITE(6,114)ITERD,RELXD
  114 FORMAT(1HO,*ITERD=*,I5,5X,*RELXD=*,F10.5)
C
C           CALCULATE PROBLEM PARAMETERS
C
      NX=NSTEPX+1
      NY=NSTEPY+1
      NXZ=NX-1
      IF(NSTART.EQ.1)NXZ=NX-LPOKX-1
      IF(NSTART.GT.LLANDX)NXZ=NX-NSTART+LLANDX
      DTHETA=2.*PIE/FLOAT(NSTEPX)
      DY=1./FLOAT(NSTEPY)
      CDIVR=CLEAR/RTWO
      RDIVR=(RTWO-TLINER)/RTWO
      EMAT=(1.-(2.*POISSN**2)/(1.-POISSN))/YOUNG
      ELAST=6.*VISCOS*OMEGA*EMAT*(1./CDIVR**3)*(1.-RDIVR)
      LADDX=LPOKX+LLANDX
      LADDY=LPOKY+LLANDY
      NMID=(NUMPOK/2)*LADDX-LPOKX-LLANDX/2
      GEOMPX=FLOAT(LPOKX)/FLOAT(LADDX)
      GEOMPY=FLOAT(LPOKY)/FLOAT(LADDY)
```

```
      GEOM1=1./(2.*(1.+DTHETA**2/(LOVERD*DY)**2))
      GEOM2=1./(2.*(1.+(LOVERD*DY)**2/DTHETA**2))
      GEOM3=-DTHETA*GEOM1/2.
      DTHPOK=FLOAT(LPOKX)*DTHETA
      AS=1./(2.*DY*LOVERD**2)
C
C           READ VALUES FROM DATA FILE
C
      READ(1)EPS
      EPS=EPS+DEPS
      WRITE(6,115)EPS,DEPS
  115 FORMAT(1HO,*EPS=*,F10.5,5X,*DEPS=*,F10.5)
      WRITE(6,116)EMAT,ELAST
  116 FORMAT(1HO,*EMAT=*,E10.4,5X,*ELAST=*,F10.5)
      DO 1001 J=1,NY+1
      READ(1)(P(I,J),I=1,NX+2),(DEL(I,J),I=1,NX+2)
 1001 CONTINUE
      READ(1)(THETAN(I),I=1,NX+2),(LSKIP(I),I=1,NX+2)
C
C           CALCULATE ARRAYS NXPOK AND EPSSIN
C
      DO 1002 N=1,NUMPOK+1
      IF(NSTART.GT.LLANDX)GO TO 10
      LNO=LLANDX-NSTART+2+(N-1)*LADDX
      GO TO 11
   10 LNO=LLANDX-NSTART+2+N*LADDX
   11 NXPOK(N)=LNO
 1002 CONTINUE
      ADEL1=-DTHPOK*1.5*EPS**2
      DO 1003 I=2,NX-1
      IF(LSKIP(I))1003,12,1003
   12 IF(LSKIP(I-1).EQ.-1)GO TO 1003
      ADEL2(I)=3.*EPS*(SIN(THETAN(I+LPOKX))-SIN(THETAN(I)))
      ADEL3(I)=-0.75*EPS**2*(SIN(2.*THETAN(I+LPOKX))-SIN(2.*THETAN(I)
      EPSSIN(I)=(EPS**3/12.)*(SIN(3.*THETAN(I+LPOKX))-SIN(3.*THETAN(I
     1           +0.75*EPS**2*(SIN(2.*THETAN(I+LPOKX))-SIN(2.*THETAN(I
     2                        +2.*DTHPOK)
     3           +0.75*EPS**3*(SIN(THETAN(I+LPOKX))-SIN(THETAN(I)))
 1003 CONTINUE
C
C **********  MAIN ITERATION LOOP  **********************************
C
      DO 1004 NDIT=1,ITERD
      CALL COEFP
      CALL CALCP
      CALL DEFL
      PMID(NDIT)=P(NMID,2)
      DELMID(NDIT)=DEL(NMID,2)
 1004 CONTINUE
C
C **********  END OF MAIN ITERATION LOOP  ***************************
C
C
C           CALCULATE LOAD AND ATTITUDE ANGLE
C
      DO 1005 I=1,NX
      COSX=COS(THETAN(I))
      DO 1006 J=2,NY+1
      FNN(J)=P(I,J)*COSX
 1006 CONTINUE
      CALL SIMP(FNN,2,NY+1,DY,FNJ)
      FN(I)=FNJ
 1005 CONTINUE
      CALL SIMP(FN,1,NX,DTHETA,WX
```

```
      DO 1007 I=1,NX
      SINX=SIN(THETAN(I))
      DO 1008 J=2,NY+1
      FNN(J)=P(I,J)*SINX
 1008 CONTINUE
      CALL SIMP(FNN,2,NY+1,DY,FNJ)
      FN(I)=FNJ
 1007 CONTINUE
      CALL SIMP(FN,1,NX,DTHETA,WY)
      SOMM=6.*SQRT(WX**2+WY**2)
      ATT=ATAN(-WY/WX)*180./PIE
C
C           CALCULATE FRICTION
C
      DO 1009 I=1,NX
      IF(LSKIP(I).NE.-1)GO TO 1009
      HPOK=1.+EPS*COS(THETAN(I))+TLINER/CLEAR
      DO 1010 J=1,LPOKY+1
      H(I,J)=HPOK
 1010 CONTINUE
 1009 CONTINUE
      DO 1011 I=2,NX
      DO 1012 J=3,NY+1
      FNN(J)=1./H(I,J)+3.*H(I,J)*(P(I+1,J)-P(I-1,J))/(2.*DTHETA)
 1012 CONTINUE
      FNN(2)=1./H(I,2)
      CALL SIMP(FNN,2,NY+1,DY,FNJ)
      FN(I)=FNJ
 1011 CONTINUE
      DO 1013 J=3,NY+1
      FNN(J)=1./H(1,J)+3.*H(1,J)*(P(2,J)-P(1,J))/DTHETA
 1013 CONTINUE
      FNN(2)=1./H(1,2)
      CALL SIMP(FNN,2,NY+1,DY,FNJ)
      FN(1)=FNJ
      CALL SIMP(FN,1,NX,DTHETA,FRIC)
C
C           CALCULATE SIDE FLOW
C
      DO 1014 I=1,NX
      FN(I)=H(I,NY+1)**3*(3.*P(I,NY+1)-4.*P(I,NY)+P(I,NY-1))/(2.*DY)
 1014 CONTINUE
      CALL SIMP(FN,1,NX,DTHETA,FLOW)
      DO 1020 I=1,NX
      DO 1021 J=2,NY+1
      FNN(J)=H(I,J)
 1021 CONTINUE
      CALL SIMP(FNN,2,NY+1,DY,HINT)
      HMEAN(I)=HINT
 1020 CONTINUE
C
C           WRITE FINAL VALUES
C
      WRITE(6,120)
  120 FORMAT(//,1HO,*FINAL PRESSURE FIELD*)
      DO 1015 I=1,NX
      WRITE(6,121)(P(I,J),J=1,NY+1)
  121 FORMAT(1HO,13F10.5)
 1015 CONTINUE
      WRITE(6,122)
  122 FORMAT(//,1HO,*FINAL DISTORTION FIELD*)
      DO 1016 I=1,NX
      WRITE(6,121)(DEL(I,J),J=1,NY+1)
 1016 CONTINUE
```

```
      WRITE(6,123)
  123 FORMAT(//,1HO,*FINAL FILM THICKNESS FIELD*)
      DO 1017 I=1,NX
      WRITE(6,121) (H(I,J),J=1,NY+1)
 1017 CONTINUE
      WRITE(6,124) SOMM
  124 FORMAT(//,1HO,*SOMMERFELD NUMBER = *,F10.5)
      WRITE(6,125) ATT
  125 FORMAT(//,1HO,*ATTITUDE ANGLE = *,F10.5,5X,*DEGREES*)
      WRITE(6,126) FRIC
  126 FORMAT(//,1HO,*FRICTION = *,F10.5)
      WRITE(6,127) FLOW
  127 FORMAT(//,1HO,*FLOW = *,F10.5)
      WRITE(6,128)
  128 FORMAT(//,1HO,*MAIN CONVERGANCE*,/,1HO,5X,*PMID*,5X,*DELMID*)
      WRITE(6,129) (PMID(N),DELMID(N),N=1,ITERD)
  129 FORMAT(1HO,2F10.5)
      WRITE(6,130)
  130 FORMAT(1HO,*MEAN FILM THICKNESS ALONG EACH AXIAL LINE*)
      WRITE(6,131) (HMEAN(I),I=1,NX)
  131 FORMAT(1HO,10F10.5)
C
C           WRITE VALUES TO DATA FILE
C
      WRITE(2) NSTEPX,NSTEPY,LPOKX,LLANDX,LPOKY,LLANDY,NUMPOK,NSTART
      WRITE(2) EPS
      DO 1018 J=1,NY+1
      WRITE(2) (P(I,J),I=1,NX+2),(DEL(I,J),I=1,NX+2)
 1018 CONTINUE
      WRITE(2) (THETAN(I),I=1,NX+2),(LSKIP(I),I=1,NX+2)
      STOP
      END

      SUBROUTINE COEFP
      COMMON/CGEOM/NX,NY,LPOKX,LPOKY,DY,DTHETA,LOVERD,CDIVR,NMID,EPS,
     1GEOMPX,GEOMPY,GEOM1,GEOM2,GEOM3,NUMPOK,ADEL1,ADEL2(103),ADEL3(103)
     2/CCOEFP/P(103,12),DEL(103,12),H(103,12),DVOL(103),AS,DTHPOK,
     3CN(103,12),CS(103,12),CE(103,12),CW(103,12),CC(103,12),
     4LSKIP(103),THETAN(103),APOK(103),EPSSIN(103),FN(103),NXPOK(21)
      DIMENSION VOL(21)
      REAL LOVERD
C
C           UPDATE FILM THICKNESS FIELD
C
      DO 3001 I=1,NX+2
      IF(LSKIP(I))31,32,32
   31 DO 3002 J=LPOKY+2,NY+1
      H(I,J)=1.+EPS*COS(THETAN(I))-DEL(I,J)
 3002 CONTINUE
      GO TO 3001
   32 DO 3003 J=1,NY+1
      H(I,J)=1.+EPS*COS(THETAN(I))-DEL(I,J)
 3003 CONTINUE
 3001 CONTINUE
C
C           CALCULATE DVOL FOR EACH POCKET
C
      DO 3004 N=1,NUMPOK
      VOL(N)=-DEL(NXPOK(N),2)*(DEL(NXPOK(N),2)*CDIVR+2.)
 3004 CONTINUE
      DVOL(NXPOK(1))=VOL(1)-VOL(NUMPOK)
      DO 3005 N=2,NUMPOK
      DVOL(NXPOK(N))=VOL(N)-VOL(N-1)
 3005 CONTINUE
```

```
      DO 3006 I=2,NX-1
      IF(LSKIP(I))33,34,35
   34 IF(LSKIP(I-1).EQ.-1)GO TO 33
C
C           CALCULATE COEFFICIENT FOR LEADING EDGE OF POCKET
C
      ADEL=DTHPOK*(1.-DEL(I,2))**3+(ADEL1+ADEL3(I))*DEL(I,2)
     1      +ADEL2(I)*(1.-DEL(I,2))**2
      APOK(I)=3.*AS*(ADEL+EPSSIN(I))
     1         +1.5*GEOMPY*(H(I,2)**3+H(I+LPOKX,2)**3)/DTHETA
      GO TO 33
C
C           CALCULATE COEFFICIENTS FOR LANDS
C
   35 DO 3007 J=2,LPOKY+2
      HDIFF=3.*(H(I+1,J)-H(I-1,J))/(4.*H(I,J))
      CN(I,J)=GEOM1*(1.+HDIFF)
      CS(I,J)=GEOM1*(1.-HDIFF)
      HDIFF=3.*(H(I,J+1)-H(I,J-1))/(4.*H(I,J))
      CE(I,J)=GEOM2*(1.+HDIFF)
      CW(I,J)=GEOM2*(1.-HDIFF)
      CC(I,J)=GEOM3*(H(I+1,J)-H(I-1,J))/H(I,J)**3
 3007 CONTINUE
   33 DO 3008 J=LPOKY+3,NY
      HDIFF=3.*(H(I+1,J)-H(I-1,J))/(4.*H(I,J))
      CN(I,J)=GEOM1*(1.+HDIFF)
      CS(I,J)=GEOM1*(1.-HDIFF)
      HDIFF=3.*(H(I,J+1)-H(I,J-1))/(4.*H(I,J))
      CE(I,J)=GEOM2*(1.+HDIFF)
      CW(I,J)=GEOM2*(1.-HDIFF)
      CC(I,J)=GEOM3*(H(I+1,J)-H(I-1,J))/H(I,J)**3
 3008 CONTINUE
 3006 CONTINUE
      RETURN
      END

      SUBROUTINE CALCP
      COMMON/CGEOM/NX,NY,LPOKX,LPOKY,DY,DTHETA,LOVERD,CDIVR,NMID,EPS,
     1GEOMPX,GEOMPY,GEOM1,GEOM2,GEOM3,NUMPOK,ADEL1,ADEL2(103),ADEL3(103)
     2/CCOEFP/P(103,12),DEL(103,12),H(103,12),DVOL(103),AS,DTHPOK,
     3CN(103,12),CS(103,12),CE(103,12),CW(103,12),CC(103,12),
     4LSKIP(103),THETAN(103),APOK(103),EPSSIN(103),FN(103),NXPOK(21)
     5/CSOLVP/ITERP,RELXP,PMID(100),NXZ
      REAL LOVERD
      DO 5001 N=1,ITERP
      DO 5002 I=2,NXZ
      IF(LSKIP(I))51,53,54
   51 P(I,2)=P(I-1,2)
   52 DO 5003 J=3,LPOKY+2
      P(I,J)=P(I,J-1)
 5003 CONTINUE
      GO TO 55
   53 IF(LSKIP(I-1).EQ.-1)GO TO 51
      A3=GEOMPY*(GEOMPX*DVOL(I)-(H(I+LPOKX,2)-H(I,2))
     1                          *(1.+DEL(I,2)*CDIVR))
      DO 5004 INT=I,I+LPOKX
      FN(INT)=H(INT,LPOKY+2)**3*(4.*P(INT,LPOKY+3)-P(INT,LPOKY+4))
 5004 CONTINUE
      CALL SIMP(FN,I,I+LPOKX,DTHETA,PS)
      DO 5005 JINT=2,LPOKY+2
      FN(JINT)=4.*P(I-1,JINT)-P(I-2,JINT)
 5005 CONTINUE
      CALL SIMP(FN,2,LPOKY+2,DY,P1)
      DO 5006 JINT=2,LPOKY+2
```

```
      FN(JINT)=4.*P(I+LP0KX+1,JINT)-P(I+LP0KX+2,JINT)
 5006 CONTINUE
      CALL SIMP(FN,2,LP0KY+2,DY,P2)
      0LDP=P(I,2)
      P(I,2)=0LDP+RELXP*((A3+AS*PS+H(I,2)**3*P1/(2.*DTHETA)
     1                   +H(I+LP0KX,2)**3*P2/(2.*DTHETA))/AP0K(I)-0LDP)
      IF(P(I,2).LT.0.)P(I,2)=0.
      G0 T0 52
   54 D0 5007 J=2,LP0KY+2
      0LDP=P(I,J)
      P(I,J)=0LDP+RELXP*(CN(I,J)*P(I+1,J)+CS(I,J)*P(I-1,J)
     1                  +CE(I,J)*P(I,J+1)+CW(I,J)*P(I,J-1)
     2                  +CC(I,J)-0LDP)
      IF(P(I,J).LT.0.)P(I,J)=0.
 5007 CONTINUE
   55 D0 5008 J=LP0KY+3,NY
      0LDP=P(I,J)
      P(I,J)=0LDP+RELXP*(CN(I,J)*P(I+1,J)+CS(I,J)*P(I-1,J)
     1                  +CE(I,J)*P(I,J+1)+CW(I,J)*P(I,J-1)
     2                  +CC(I,J)-0LDP)
      IF(P(I,J).LT.0.)P(I,J)=0.
 5008 CONTINUE
 5002 CONTINUE
      D0 5009 I=2,NX-1
      P(I,1)=P(I,3)
 5009 CONTINUE
      D0 5010 J=1,NY
      P(NX+1,J)=P(2,J)
 5010 CONTINUE
 5001 CONTINUE
      D0 5011 J=1,NY
      P(NX+2,J)=P(3,J)
 5011 CONTINUE
      RETURN
      END

      SUBR0UTINE DEFL
      C0MM0N/CGE0M/NX,NY,LP0KX,LP0KY,DY,DTHETA,L0VERD,CDIVR,NMID,EPS,
     1GE0MPX,GE0MPY,GE0M1,GE0M2,GE0M3,NUMP0K,ADEL1,ADEL2(103),ADEL3(103)
     2/CC0EFP/P(103,12),DEL(103,12),H(103,12),DV0L(103),AS,DTHP0K,
     3CN(103,12),CS(103,12),CE(103,12),CW(103,12),CC(103,12),
     4LSKIP(103),THETAN(103),AP0K(103),EPSSIN(103),FN(103),NXP0K(21)
     6/CDEFL/ELAST,RELXD,DELMID(25)
      REAL L0VERD
      D0 7001 I=1,NX+2
      IF(LSKIP(I))71,72,72
   71 D0 7002 J=LP0KY+2,NY
      0LDD=DEL(I,J)
      DEL(I,J)=0LDD+RELXD*(-ELAST*P(I,J)-0LDD)
 7002 CONTINUE
      G0 T0 7001
   72 D0 7003 J=1,NY
      0LDD=DEL(I,J)
      DEL(I,J)=0LDD+RELXD*(-ELAST*P(I,J)-0LDD)
 7003 CONTINUE
 7001 CONTINUE
      RETURN
      END

      SUBR0UTINE SIMP(F,NA,NZ,H,AREA)
      DIMENSI0N F(NZ)
C
C                    SUBR0UTINE T0 INTEGRATE A FUNCTI0N F USING
C                    SIMPS0N RULE BETWEEN LIMITS NA AND NZ
```

```
C                    WITH STEP WIDTH H AND GIVING ANSWER AREA
C
      NB2=NA+2
      NB4=NA+1
      NY2=NZ-2
      NY4=NZ-1
      SUM2=0.
      SUM4=0.
      DO 9001 ISIMP=NB2,NY2,2
      SUM2=SUM2+F(ISIMP)
 9001 CONTINUE
      DO 9002 ISIMP=NB4,NY4,2
      SUM4=SUM4+F(ISIMP)
 9002 CONTINUE
      AREA=(H/3.)*(F(NA)+2.*SUM2+4.*SUM4+F(NZ))
      RETURN
      END
```

```
      PROGRAM VANE2P(INPUT,OUTPUT,TAPE5=INPUT,TAPE6=OUTPUT,TAPE1,TAPE2)
C
C                    FINITE LENGTH JOURNAL BEARING WITH
C                    POCKETED ELASTIC JOURNAL LINER, METHOD 2
C                    USED FOR POCKET PRESSURE ANALYSIS
C
      COMMON/CGEOM/NX,NY,LPOKX,LPOKY,DY,DTHETA,LOVERD,CDIVR,NMID,EPS,
     1GEOMPX,GEOMPY,GEOM1,GEOM2,GEOM3,NUMPOK,ADEL1,ADEL2(103),ADEL3(103)
     2/CCOEFP/P(103,12),DEL(103,12),H(103,12),AS,DTHPOK,A12C,
     3CN(103,12),CS(103,12),CE(103,12),CW(103,12),CC(103,12),
     4LSKIP(103),THETAN(103),APOK(103),EPSSIN(103),FN(103),NXPOK(50)
     5/CSOLVP/ITERP,RELXP,PMID(100),NXZ
     6/CDEFL/ELAST,RELXD,DELMID(100)
      DIMENSION FNN(103)
      DIMENSION HMEAN(103)
      REAL LOVERD
C
C           SET PROBLEM PARAMATERS
C
      PIE=3.1415926536
      READ(1)NSTEPX,NSTEPY,LPOKX,LLANDX,LPOKY,LLANDY,NUMPOK,NSTART
      READ(5,101)ITERP,RELXP
  101 FORMAT(I5,F10.4)
      READ(5,102)RTWO,TLINER,CLEAR,LOVERD
  102 FORMAT(4F10.4)
      READ(5,103)VISCOS,YOUNG,POISSN,OMEGA
  103 FORMAT(2E10.4,2F10.4)
      READ(5,104)ITERD,RELXD
  104 FORMAT(I5,F10.4)
      READ(5,105)DEPS
  105 FORMAT(F10.4)
      WRITE(6,110)NSTEPX,NSTEPY,LPOKX,LLANDX,LPOKY,LLANDY,NUMPOK,NSTART
  110 FORMAT(/////,1HO,*NSTEPX=*,I5,5X,*NSTEPY=*,I5,5X,*LPOKX=*,I5,5X,
     1*LLANDX=*,I5,5X,*LPOKY=*,I5,5X,*LLANDY=*,I5,5X,
     2/,1HO,*NUMPOK=*,I5,5X,*NSTART=*,I5)
      WRITE(6,111)ITERP,RELXP
  111 FORMAT(1HO,*ITERP=*,I5,5X,*RELXP=*,F10.4)
      WRITE(6,112)RTWO,TLINER,CLEAR,LOVERD
  112 FORMAT(1HO,*RTWO=*,F10.5,5X,*TLINER=*,F10.5,5X,*CLEAR=*,F10.4,5X,
     1*LOVERD=*,F10.5)
      WRITE(6,113)VISCOS,YOUNG,POISSN,OMEGA
  113 FORMAT(1HO,*VISCOS=*,E10.4,5X,*YOUNG=*,E10.4,5X,
     1*POISSN=*,F10.5,5X,*OMEGA=*,F10.5)
      WRITE(6,114)ITERD,RELXD
  114 FORMAT(1HO,*ITERD=*,I5,5X,*RELXD=*,F10.5)
C
C           CALCULATE PROBLEM PARAMETERS
C
      NX=NSTEPX+1
      NY=NSTEPY+1
      NXZ=NX-1
      IF(NSTART.EQ.1)NXZ=NX-LPOKX-1
      IF(NSTART.GT.LLANDX)NXZ=NX-NSTART+LLANDX
      DTHETA=2.*PIE/FLOAT(NSTEPX)
      DY=1./FLOAT(NSTEPY)
      CDIVR=CLEAR/RTWO
      RDIVR=(RTWO-TLINER)/RTWO
      EMAT=(1.-(2.*POISSN**2)/(1.-POISSN))/YOUNG
      ELAST=6.*VISCOS*OMEGA*EMAT*(1./CDIVR**3)*(1.-RDIVR)
      LADDX=LPOKX+LLANDX
      LADDY=LPOKY+LLANDY
      NMID=(NUMPOK/2)*LADDX-LPOKX-LLANDX/2
      GEOMPX=FLOAT(LPOKX)/(2.*FLOAT(LADDX))
      GEOMPY=FLOAT(LPOKY)/FLOAT(LADDY)
```

```
      GEOM1=1./(2.*(1.+DTHETA**2/(LOVERD*DY)**2))
      GEOM2=1./(2.*(1.+(LOVERD*DY)**2/DTHETA**2))
      GEOM3=-DTHETA*GEOM1/2.
      DTHPOK=FLOAT(LPOKX)*DTHETA
      AS=1./(2.*DY*LOVERD**2)
      A12C=GEOMPY*ELAST*FLOAT(LPOKX)/(FLOAT(LPOKY)*DY*2.)
C
C           READ VALUES FROM DATA FILE
C
      READ(1)EPS
      EPS=EPS+DEPS
      WRITE(6,115)EPS,DEPS
  115 FORMAT(1HO,*EPS=*,F10.5,5X,*DEPS=*,F10.5)
      WRITE(6,116)EMAT,ELAST
  116 FORMAT(1HO,*EMAT=*,E10.4,5X,*ELAST=*,F10.5)
      DO 1001 J=1,NY+1
      READ(1)(P(I,J),I=1,NX+2),(DEL(I,J),I=1,NX+2)
 1001 CONTINUE
      READ(1)(THETAN(I),I=1,NX+2),(LSKIP(I),I=1,NX+2)
C
C           CALCULATE ARRAYS NXPOK AND EPSSIN
C
      DO 1002 N=1,NUMPOK+1
      IF(NSTART.GT.LLANDX)GO TO 10
      LNO=LLANDX-NSTART+2+(N-1)*LADDX
      GO TO 11
   10 LNO=LLANDX-NSTART+2+N*LADDX
   11 NXPOK(N)=LNO
 1002 CONTINUE
      ADEL1=-DTHPOK*1.5*EPS**2
      DO 1003 I=2,NX-1
      IF(LSKIP(I))1003,12,1003
   12 IF(LSKIP(I-1).EQ.-1)GO TO 1003
      ADEL2(I)=3.*EPS*(SIN(THETAN(I+LPOKX))-SIN(THETAN(I)))
      ADEL3(I)=-0.75*EPS**2*(SIN(2.*THETAN(I+LPOKX))-SIN(2.*THETAN(I))
      EPSSIN(I)=(EPS**3/12.)*(SIN(3.*THETAN(I+LPOKX))-SIN(3.*THETAN(I)
     1          +0.75*EPS**2*(SIN(2.*THETAN(I+LPOKX))-SIN(2.*THETAN(I)
     2                        +2.*DTHPOK)
     3          +0.75*EPS**3*(SIN(THETAN(I+LPOKX))-SIN(THETAN(I))))
 1003 CONTINUE
C
C **********  MAIN ITERATION LOOP  **************************************
C
      DO 1004 NDIT=1,ITERD
      CALL COEFP
      CALL CALCP
      CALL DEFL
      PMID(NDIT)=P(NMID,2)
      DELMID(NDIT)=DEL(NMID,2)
 1004 CONTINUE
C
C **********  END OF MAIN ITERATION LOOP  *******************************
C
C
C           CALCULATE LOAD AND ATTITUDE ANGLE
C
      DO 1005 I=1,NX
      COSX=COS(THETAN(I))
      DO 1006 J=2,NY+1
      FNN(J)=P(I,J)*COSX
 1006 CONTINUE
      CALL SIMP(FNN,2,NY+1,DY,FNJ)
      FN(I)=FNJ
 1005 CONTINUE
```

```
      CALL SIMP(FN,1,NX,DTHETA,WX)
      DO 1007 I=1,NX
      SINX=SIN(THETAN(I))
      DO 1008 J=2,NY+1
      FNN(J)=P(I,J)*SINX
 1008 CONTINUE
      CALL SIMP(FNN,2,NY+1,DY,FNJ)
      FN(I)=FNJ
 1007 CONTINUE
      CALL SIMP(FN,1,NX,DTHETA,WY)
      SOMM=6.*SQRT(WX**2+WY**2)
      ATT=ATAN(-WY/WX)*180./PIE
C
C           CALCULATE FRICTION
C
      DO 1009 I=1,NX
      IF(LSKIP(I).NE.-1)GO TO 1009
      HPOK=1.+EPS*COS(THETAN(I))+TLINER/CLEAR
      DO 1010 J=1,LPOKY+1
      H(I,J)=HPOK
 1010 CONTINUE
 1009 CONTINUE
      DO 1011 I=2,NX
      DO 1012 J=3,NY+1
      FNN(J)=1./H(I,J)+3.*H(I,J)*(P(I+1,J)-P(I-1,J))/(2.*DTHETA)
 1012 CONTINUE
      FNN(2)=1./H(I,2)
      CALL SIMP(FNN,2,NY+1,DY,FNJ)
      FN(I)=FNJ
 1011 CONTINUE
      DO 1013 J=3,NY+1
      FNN(J)=1./H(1,J)+3.*H(1,J)*(P(2,J)-P(1,J))/DTHETA
 1013 CONTINUE
      FNN(2)=1./H(1,2)
      CALL SIMP(FNN,2,NY+1,DY,FNJ)
      FN(1)=FNJ
      CALL SIMP(FN,1,NX,DTHETA,FRIC)
C
C           CALCULATE SIDE FLOW
C
      DO 1014 I=1,NX
      FN(I)=H(I,NY+1)**3*(3.*P(I,NY+1)-4.*P(I,NY)+P(I,NY-1))/(2.*DY)
 1014 CONTINUE
      CALL SIMP(FN,1,NX,DTHETA,FLOW)
      DO 1020 I=1,NX
      DO 1021 J=2,NY+1
      FNN(J)=H(I,J)
 1021 CONTINUE
      CALL SIMP(FNN,2,NY+1,DY,HINT)
      HMEAN(I)=HINT
 1020 CONTINUE
C
C           WRITE FINAL VALUES
C
      WRITE(6,120)
  120 FORMAT(//,1HO,*FINAL PRESSURE FIELD*)
      DO 1015 I=1,NX
      WRITE(6,121)(P(I,J),J=1,NY+1)
  121 FORMAT(1HO,13F10.5)
 1015 CONTINUE
      WRITE(6,122)
  122 FORMAT(//,1HO,*FINAL DISTORTION FIELD*)
      DO 1016 I=1,NX
      WRITE(6,121)(DEL(I,J),J=1,NY+1)
```

```
 1016 CONTINUE
      WRITE(6,123)
  123 FORMAT(//,1HO,*FINAL FILM THICKNESS FIELD*)
      DO 1017 I=1,NX
      WRITE(6,121) (H(I,J),J=1,NY+1)
 1017 CONTINUE
      WRITE(6,124) SOMM
  124 FORMAT(//,1HO,*SOMMERFELD NUMBER = *,F10.5)
      WRITE(6,125) ATT
  125 FORMAT(//,1HO,*ATTITUDE ANGLE = *,F10.5,5X,*DEGREES*)
      WRITE(6,126) FRIC
  126 FORMAT(//,1HO,*FRICTION = *,F10.5)
      WRITE(6,127) FLOW
  127 FORMAT(//,1HO,*FLOW = *,F10.5)
      WRITE(6,128)
  128 FORMAT(//,1HO,*MAIN CONVERGANCE*,/,1HO,5X,*PMID*,5X,*DELMID*)
      WRITE(6,129) (PMID(N),DELMID(N),N=1,ITERD)
  129 FORMAT(1HO,2F10.5)
      WRITE(6,130)
  130 FORMAT(1HO,*MEAN FILM THICKNESS ALONG EACH AXIAL LINE*)
      WRITE(6,131) (HMEAN(I),I=1,NX)
  131 FORMAT(1HO,10F10.5)
C
C           WRITE VALUES TO DATA FILE
C
      WRITE(2) NSTEPX,NSTEPY,LPOKX,LLANDX,LPOKY,LLANDY,NUMPOK,NSTART
      WRITE(2) EPS
      DO 1018 J=1,NY+1
      WRITE(2) (P(I,J),I=1,NX+2),(DEL(I,J),I=1,NX+2)
 1018 CONTINUE
      WRITE(2) (THETAN(I),I=1,NX+2),(LSKIP(I),I=1,NX+2)
      STOP
      END

      SUBROUTINE COEFP
      COMMON/CGEOM/NX,NY,LPOKX,LPOKY,DY,DTHETA,LOVERD,CDIVR,NMID,EPS,
     1GEOMPX,GEOMPY,GEOM1,GEOM2,GEOM3,NUMPOK,ADEL1,ADEL2(103),ADEL3(103)
     2/CCOEFP/P(103,12),DEL(103,12),H(103,12),AS,DTHPOK,A12C,
     3CN(103,12),CS(103,12),CE(103,12),CW(103,12),CC(103,12),
     4LSKIP(103),THETAN(103),APOK(103),EPSSIN(103),FN(103),NXPOK(50)
      REAL LOVERD
C
C           UPDATE FILM THICKNESS FIELD
C
      DO 3001 I=1,NX+2
      IF(LSKIP(I))31,32,32
   31 DO 3002 J=LPOKY+2,NY+1
      H(I,J)=1.+EPS*COS(THETAN(I))-DEL(I,J)
 3002 CONTINUE
      GO TO 3001
   32 DO 3003 J=1,NY+1
      H(I,J)=1.+EPS*COS(THETAN(I))-DEL(I,J)
 3003 CONTINUE
 3001 CONTINUE
      DO 3004 I=2,NX-1
      IF(LSKIP(I))33,34,35
   34 IF(LSKIP(I-1).EQ.-1)GO TO 33
C
C           CALCULATE COEFFICIENT FOR LEADING EDGE OF POCKET
C
      ADEL=DTHPOK*(1.-DEL(I,2))**3+(ADEL1+ADEL3(I))*DEL(I,2)
     1      +ADEL2(I)*(1.-DEL(I,2))**2
      APOK(I)=3.*AS*(ADEL+EPSSIN(I))
     1         +1.5*GEOMPY*(H(I,2)**3+H(I+LPOKX,2)**3)/DTHETA
```

```
      GO TO 33
C
C           CALCULATE COEFFICIENTS FOR LANDS
C
   35 DO 3005 J=2,LPOKY+2
      HDIFF=3.*(H(I+1,J)-H(I-1,J))/(4.*H(I,J))
      CN(I,J)=GEOM1*(1.+HDIFF)
      CS(I,J)=GEOM1*(1.-HDIFF)
      HDIFF=3.*(H(I,J+1)-H(I,J-1))/(4.*H(I,J))
      CE(I,J)=GEOM2*(1.+HDIFF)
      CW(I,J)=GEOM2*(1.-HDIFF)
      CC(I,J)=GEOM3*(H(I+1,J)-H(I-1,J))/H(I,J)**3
 3005 CONTINUE
   33 DO 3006 J=LPOKY+3,NY
      HDIFF=3.*(H(I+1,J)-H(I-1,J))/(4.*H(I,J))
      CN(I,J)=GEOM1*(1.+HDIFF)
      CS(I,J)=GEOM1*(1.-HDIFF)
      HDIFF=3.*(H(I,J+1)-H(I,J-1))/(4.*H(I,J))
      CE(I,J)=GEOM2*(1.+HDIFF)
      CW(I,J)=GEOM2*(1.-HDIFF)
      CC(I,J)=GEOM3*(H(I+1,J)-H(I-1,J))/H(I,J)**3
 3006 CONTINUE
 3004 CONTINUE
      RETURN
      END

      SUBROUTINE CALCP
      COMMON/CGEOM/NX,NY,LPOKX,LPOKY,DY,DTHETA,LOVERD,CDIVR,NMID,EPS,
     1GEOMPX,GEOMPY,GEOM1,GEOM2,GEOM3,NUMPOK,ADEL1,ADEL2(103),ADEL3(103
     2/CCOEFP/P(103,12),DEL(103,12),H(103,12),AS,DTHPOK,A12C,
     3CN(103,12),CS(103,12),CE(103,12),CW(103,12),CC(103,12),
     4LSKIP(103),THETAN(103),APOK(103),EPSSIN(103),FN(103),NXPOK(50)
     5/CSOLVP/ITERP,RELXP,PMID(100),NXZ
     6/CDEFL/ELAST,RELXD,DELMID(100)
      REAL LOVERD
      DO 5001 N=1,ITERP
      DO 5002 I=2,NXZ
      IF(LSKIP(I))51,53,54
   51 P(I,2)=P(I-1,2)
   52 DO 5003 J=3,LPOKY+2
      P(I,J)=P(I,J-1)
 5003 CONTINUE
      GO TO 55
   53 IF(LSKIP(I-1).EQ.-1)GO TO 51
      A3=-GEOMPY*(H(I+LPOKX,2)-H(I,2))*(1.+DEL(I,2)*CDIVR)
      DO 5004 INT=I,I+LPOKX
      FN(INT)=H(INT,LPOKY+2)**3*(4.*P(INT,LPOKY+3)-P(INT,LPOKY+4))
 5004 CONTINUE
      CALL SIMP(FN,I,I+LPOKX,DTHETA,PS)
      DO 5005 JINT=2,LPOKY+2
      FN(JINT)=4.*P(I-1,JINT)-P(I-2,JINT)
 5005 CONTINUE
      CALL SIMP(FN,2,LPOKY+2,DY,P1)
      DO 5006 JINT=2,LPOKY+2
      FN(JINT)=4.*P(I+LPOKX+1,JINT)-P(I+LPOKX+2,JINT)
 5006 CONTINUE
      CALL SIMP(FN,2,LPOKY+2,DY,P2)
      OLDP=P(I,2)
      P(I,2)=OLDP+RELXP*((A3+AS*PS
     1                    +(H(I,2)**3/(2.*DTHETA)
     2                      -A12C*(1.+DEL(I,2)*CDIVR))*P1
     3                    +(H(I+LPOKX,2)**3/(2.*DTHETA)
     4                      +A12C*(1.+DEL(I,2)*CDIVR))*P2
     5                    )/APOK(I)-OLDP)
```

```
      IF (P(I,2) .LT.0.) P(I,2) =0.
      GO TO 52
   54 DO 5007 J=2,LPOKY+2
      OLDP=P(I,J)
      P(I,J) =OLDP+RELXP*(CN(I,J) *P(I+1,J) +CS(I,J) *P(I-1,J)
     1                    +CE(I,J) *P(I,J+1) +CW(I,J) *P(I,J-1)
     2                    +CC(I,J) -OLDP)
      IF (P(I,J) .LT.0.) P(I,J) =0.
 5007 CONTINUE
   55 DO 5008 J=LPOKY+3,NY
      OLDP=P(I,J)
      P(I,J) =OLDP+RELXP*(CN(I,J) *P(I+1,J) +CS(I,J) *P(I-1,J)
     1                    +CE(I,J) *P(I,J+1) +CW(I,J) *P(I,J-1)
     2                    +CC(I,J) -OLDP)
      IF (P(I,J) .LT.0.) P(I,J) =0.
 5008 CONTINUE
 5002 CONTINUE
      DO 5009 I=2,NX-1
      P(I,1) =P(I,3)
 5009 CONTINUE
      DO 5010 J=1,NY
      P(NX+1,J) =P(2,J)
 5010 CONTINUE
 5001 CONTINUE
      DO 5011 J=1,NY
      P(NX+2,J) =P(3,J)
 5011 CONTINUE
      RETURN
      END

      SUBROUTINE DEFL
      COMMON/CGEOM/NX,NY,LPOKX,LPOKY,DY,DTHETA,LOVERD,CDIVR,NMID,EPS,
     1GEOMPX,GEOMPY,GEOM1,GEOM2,GEOM3,NUMPOK,ADEL1,ADEL2(103),ADEL3(103
     2/CCOEFP/P(103,12),DEL(103,12),H(103,12),AS,DTHPOK,A12C,
     3CN(103,12),CS(103,12),CE(103,12),CW(103,12),CC(103,12),
     4LSKIP(103),THETAN(103),APOK(103),EPSSIN(103),FN(103),NXPOK(50)
     6/CDEFL/ELAST,RELXD,DELMID(100)
      REAL LOVERD
      DO 7001 I=1,NX+2
      IF (LSKIP(I)) 71,72,72
   71 DO 7002 J=LPOKY+2,NY
      OLDD=DEL(I,J)
      DEL(I,J) =OLDD+RELXD*(-ELAST*P(I,J) -OLDD)
 7002 CONTINUE
      GO TO 7001
   72 DO 7003 J=1,NY
      OLDD=DEL(I,J)
      DEL(I,J) =OLDD+RELXD*(-ELAST*P(I,J) -OLDD)
 7003 CONTINUE
 7001 CONTINUE
      RETURN
      END

      SUBROUTINE SIMP(F,NA,NZ,H,AREA)
      DIMENSION F(NZ)
C
C                    SUBROUTINE TO INTEGRATE A FUNCTION F USING
C                    SIMPSON RULE BETWEEN LIMITS NA AND NZ
C                    WITH STEP WIDTH H AND GIVING ANSWER AREA
C
      NB2=NA+2
      NB4=NA+1
      NY2=NZ-2
      NY4=NZ-1
```

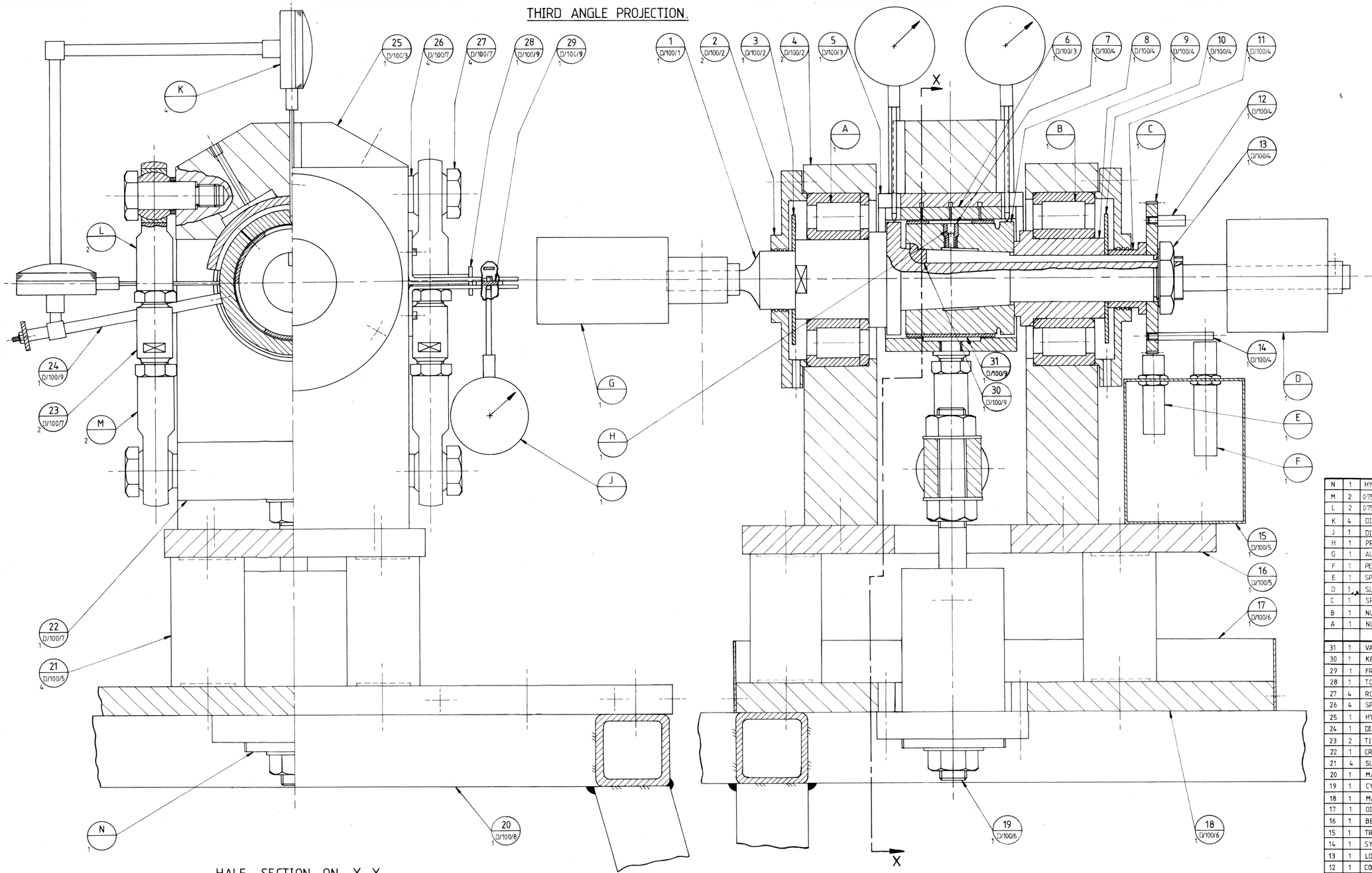
```
      SUM2=0.
      SUM4=0.
      DO 9001 ISIMP=NB2,NY2,2
      SUM2=SUM2+F(ISIMP)
 9001 CONTINUE
      DO 9002 ISIMP=NB4,NY4,2
      SUM4=SUM4+F(ISIMP)
 9002 CONTINUE
      AREA=(H/3.)*(F(NA)+2.*SUM2+4.*SUM4+F(NZ))
      RETURN
      END
```

APPENDIX A8.

DETAIL ASSEMBLY DRAWING OF THE EXPERIMENTAL APPARATUS.

DRAWING NUMBER TC/E100/5

THIRD ANGLE PROJECTION.



HALF - SECTION ON X-X

N	1	HYDRAULIC CYLINDER RCH-12IA	ENERPAC
M	2	0·75 in. B.S.F.(R.H.) ROD END	ROSE BEARINGS
L	2	0·75 in. B.S.F.(L.H.) ROD END	ROSE BEARINGS
K	4	DIAL INDICATOR DC2-4L	MOORE & WRIGHT LTD.
J	1	DIAL INDICATOR 2416	MITUTOYO MFG CO.
H	1	PRESSURE TRANSDUCER	SENSOTEC INC.
G	1	AUTOGAURD 201/AF/1	GIB PRECISION LTD.
F	1	PERCEPTION HEAD EMP9/1	SMITHS IND. LTD.
E	1	SPEED TRANSDUCER 11-0054	AIRPAX ELECTRONICS
D	1	SLIP RINGS PS 20-8	D.J. MOULDINGS LTD.
C	1	SPUR GEAR WHEEL	MUFFET
B	1	NU 2311E	FAG BEARING CO.
A	1	NUP 2311E	FAG BEARING CO.
			SOURCE
31	1	VANE LINER	POLYMER
30	1	KEY	MILD STEEL
29	1	FRICTION CANTILEVER	SPRING STEEL
28	1	TORQUE ARM	MILD STEEL
27	4	ROD END BOLT	EN 24V
26	4	SPACER WASHER	MILD STEEL
25	1	HYDROSTATIC BEARING	MILD STEEL
24	1	DIAL GAUGE FRAME	MILD STEEL
23	2	TIE ROD	EN 24V
22	1	CROSS BEAM	MILD STEEL
21	4	SUPPORT PILLAR	MILD STEEL
20	1	MAIN FRAME	R.H.S.
19	1	CYLINDER ROD	EN 24V
18	1	MAIN BASEPLATE	MILD STEEL
17	1	OIL COLLECTOR	16 S.W.G. SHEET
16	1	BEARING BASEPLATE	MILD STEEL
15	1	TRANSDUCER FRAME	16 S.W.G. SHEET
14	1	SYNCHRONISATION ROD	MILD STEEL
13	1	LOCKNUT	MILD STEEL
12	1	COUNTERWEIGHT	MILD STEEL
11	1	SPACER SLEEVE	MILD STEEL
10	1	2nd OIL FLINGER	MILD STEEL
9	1	RACEWAY SLEEVE	EN 24T
8	1	TRANSDUCER SLEEVE	MILD STEEL
7	1	PRESSURE TRANSDUCER BOLT	MILD STEEL
6	1	TEST JOURNAL BEARING	MILD STEEL
5	1	BEARING COVER CAP	LEAD-BRONZE
4	2	SLAVE B'G HOUSING	MILD STEEL
3	1	1st OIL FLINGER	MILD STEEL
2	2	SLAVE B'G COVER PLATE	MILD STEEL
1	1	SHAFT	EN24T
PART NO.	NO. OFF	DESCRIPTION	MATERIAL

MECHANICAL ENGINEERING DEPARTMENT,
IMPERIAL COLLEGE,
LONDON SW7 2BX.

DRAWN	T.J. Coates	SCALE 1:1
APPROVED	T.J. Coates	
TRACED	T.J. Coates	DATE DEC 1979
CHECKED	T.J. Coates	

TITLE: VANE BEARING TEST MACHINE : DETAIL ASSEMBLY

AMENDMENTS

DRAWING NUMBER: TC/E100/5

NAME: T.J. COATES